UNIVERSITY OF SOUTHAMPTON

FACULTY OF NATURAL AND ENVIRONMENTAL SCIENCES

Ocean and Earth Science

CHARCOAL, FORESTS, AND EARTH'S PALAEOZOIC GEOCHEMICAL OXYGEN CYCLE

by

David Kevin Carpenter

Thesis submitted in partial fulfilment of the requirements

for the degree of Doctor of Philosophy

September 2016

UNIVERSITY OF SOUTHAMPTON

ABSTRACT

FACULTY OF NATURAL AND ENVIRONMENTAL SCIENCES

Ocean and Earth Sciences

Thesis submitted in partial fulfilment of the requirements

for the degree of Doctor of Philosophy

CHARCOAL, FORESTS AND EARTH'S PALAEOZOIC GEOCHEMICAL OXYGEN CYCLE

By David Kevin Carpenter

It is widely assumed that the Devonian transition to a forested planet, and subsequent massive expansion of coal-swamp environments during the Carboniferous, significantly increased the production and retention of atmospheric oxygen by fuelling increased organic carbon burial, fundamentally altering the biotic regulation of Earth's long-term oxygen cycle. Modelling approaches to the reconstruction of Phanerozoic pO_2 are hampered by the unavoidable complexity of the models, and the difficulty in testing their inherent assumptions. This has led to a wide variety of predictions for atmospheric O_2 during this critical 120 million-year interval. The abundance of microscopic charcoal ('inertinite') in coals has previously been used as the basis for a direct pO_2 reconstruction, on the assumption that fire activity correlates with oxygen supply; however, coals are scarce prior to the Viséan. A high-resolution Devonian–Carboniferous dataset charting inertinite abundance in dispersed organic matter indicates that O_2 could not have fallen below c. 16.5% vol. at any stage, and that a previously identified Mid-Devonian 'charcoal gap' is most likely an artefact of low sampling density. Thus, models predicting intervals of profound hypoxia cannot be correct, and the hypothesis that the Tournaisian tetrapod diversity crisis ('Romer's Gap') was the result of global hypoxia is not supported. Both coal and DOM charcoal records indicate gently declining fire activity during the Mississippian, followed by a sharp rise in the Mid-Pennsylvanian; this is consistent with the GEOCARBSULF palaeoatmosphere model, and suggests a substantial lag between afforestation and pO_2 increase. This is turn suggests it was not the rise of forests *per se* but the formation of very large wetland basins, which was tectonically driven, that led to enhanced coal formation and a late Palaeozoic oxygen pulse. An interesting corollary of this interpretation is that high pO_2 was not the main driver of arthropod gigantism during the Palaeozoic.

Table of Contents

List of tables ..... **vii**

List of figures ..... **ix**

List of supplementary information ..... **xvii**

DECLARATION OF AUTHORSHIP ..... **xix**

Acknowledgements ..... **xxi**

List of definitions and abbreviations ..... **xxiii**

1. Introduction **1**

1.1: The evolution of atmospheric O_2 through geological time 3

1.2: Modelling Phanerozoic O_2 7

1.3: Atmospheric O_2 and wildfire activity 10

1.4: Is all inertinite charcoal? 18

1.5: Testing the models: establishing a new Silurian–Carboniferous charcoal dataset 28

2. Identifying and quantifying charcoal in the fossil record: materials, methods, and rationale **30**

2.1: Sample preparation and analysis 30

2.2: Data analysis 34

2.3: Relationship between fusinite and total inertinite 45

2.4: Reflectance, fire intensity, and pO_2 48

2.5: Maceral oxidation 49

2.6: Taphonomic considerations 54

2.7: Summary 59

3. The Devonian charcoal gap **61**

3.1: The Catskill Delta complex in New York and Pennsylvania 63

3.2: Sampling localities – Devonian, USA 67

3.3: Sampling localities – Silurian, USA 109

3.4: The Catskill Delta complex in eastern Canada 112

3.5: The Devonian in Gondwana: the Malvinokaffric realm 116

3.6: Results 123

3.7: Discussion 131

3.8: Summary 134

4. Atmospheric O_2 during Romer's Gap **135**

4.1: Sampling localities – Northumberland, Fife, and the Scottish Borders 139

4.2: Sampling localities – Central East Greenland 147

4.3: Sampling localities – Spitsbergen 150
4.4: Results 154
4.5: Discussion 158
4.6: Summary 160
4.7: Tetrapod World: early evolution and diversification 161
5. Late Palaezoic hyperoxia 176
5.1: Sampling localities 179
5.2: Results 187
5.3: Discussion 192
5.4: Summary 196
6. Conclusions 197
7. Appendix 1: high-vitrinite samples 203
7.1: Tynemouth (DOM) 203
7.2: Tynemouth (coals) 205
7.3: Willie's Hole (DOM) 207
7.4: Fife (DOM) 209
7.5: Fife (coals) 211
7.6: Fife (carbonaceous shales) 213
8. Appendix 2 – keys for sedimentary logs 215
9. References 217

List of Tables

Table 1.1: Past (Taylor) and current (ICCP) nomenclature for inertinite-group macerals.

Table 1.2: Summary of ICCP (2001) descriptions of the inertinite macerals.

Table 2.1: Correlation coefficients for inertinite/fusinite abundance data. r, Pearson's Correlation; R_s, Spearman Correlation; P, P-value.

Table 2.2: Phytoclast reflectance data for shale sample F14_72; subsamples exposed to nitric acid for 300, 600, and 1200 seconds.

Table 2.3: Spearman rank correlation coefficients for exposure time with overall mean phytoclast reflectance, R_v, R_i, and relative abundance of inertinite as estimated by normalmixEM.

Table 3.1: Significant differences identified by pairwise comparison of Kruskal-Wallis ANOVA results (Dunn's method) for Euramerican time-series data.

Table 3.2: Pairwise comparison of Kruskal-Wallis ANOVA results (Dunn's method) for inertinite abundance in marine, transitional, and terrestrial environments (all data).

Table 3.3: Pairwise comparison of Kruskal-Wallis ANOVA results (Dunn's method), combined Euramerica/Gondwana time series.

Table 3.4: sample density for this study, compared to that of Glasspool *et al*. (2015) for the Devonian.

Table 4.1: Comparison of mean relative inertinite abundance in coals reported in this study and by previous workers.

Table 5.1: Significant differences in DOM-inertinite identified by pairwise Kruskal-Wallis ANOVA.

List of Figures

Figure 1.1: Box model summarising main carbon and sulphur cycle controls on atmospheric pO_2.

Figure 1.2: Geochemical constraints on atmospheric O_2 through geological time.

Figure 1.3: Comparison of model predictions for atmospheric O_2 (% vol.), and extent of the 'fire window'.

Figure 1.4: Stages of combustion, as seen in a burning log.

Figure 1.5: Famennian macroscopic charcoal (dark fragments) from the Cressler Plant Bed, Red Hill, Pennsylvania, USA.

Figure 1.6: Charcoal fragments and coalified wood (left), and spores (centre/right) as seen using transmitted light microscopy. Scale bar = 1 mm. Reproduced from Scott (2010, fig. 17a) with permission from Elsevier.

Figure 1.7: Inertinite and pyrite (p), as seen using incident light microscopy. Scale bar = 80 µm. Reproduced from Hower *et al*. (1998, slide 23-7).

Figure 1.8: Inertinite-group macerals. A, fusinite; B, semifusinite; C, funginite, derived from fungal spores (Sp) and sclerotiae (Sc); D, secretinite; E, macrinite; F, micrinite; G, inertodetrinite. Scale bars = 75 µm. Reproduced from Hower *et al*. (2001; figs. 1, 3, 5, 7, 8, 10, 11) with permission from Elsevier.

Figure 1.9: Coalification tracks of selected macerals and maceral groups. A, Rmax/Rmin of fusinite and vitrinite, and Rmean of exinite, plotted against volatile yield (ind. increasing thermal rank). Modified after Alpern and Lemos de Susa (1970, figs. 1, 3). B, relationship between $R_i$max, $R_v$max and $R_e$max at increasing thermal rank, with speculative inertinite/vitrinite convergence point. Modified after Teichmüller (1989, fig. 1).

Figure 1.10: Effect of heating time on charcoal reflectance. Reproduced from Guo and Bustin (1998, fig. 1) with permission from Elsevier.

Figure 1.11: Examples of funginite in close association with other macerals of lower reflectance. A, reproduced from Belkin *et al*. (2009, fig. 3A); B, reproduced from Hower *et al*. (2009, fig. 4). With permission from Elsevier.

Figure 1.12: Incident light photomicrograph of polished charcoal pellet, showing varied levels of reflectance (= fusinization) at the sub-mm scale in a fragment of modern, artificially produced charcoal. Scale bar = 32.5 µm.

Figure 2.1: Reflectogram showing phytoclast reflectance profile for coal sample T15_13 (Bottom Hutton Coal, Tynemouth, Westphalian B). Black bar indicates separation, judged by eye, between vitrinite and inertinite.

Figure 2.2: Reflectogram showing phytoclast reflectance profile for DOM extracted from shale sample Sten_8 (Stensiö Bjerg, Famennian). Strongly overlapping maceral reflectance profiles result in a mixture distribution.

Figure 2.3: Comparison of inertinite abundance estimates provided by normalmixEM function (A) and reflectogram shape (B), for shale sample F14_36 (Fife, Viséan). Red/green curves (A) indicate density plot output of normalmixEM; position of black bar (B) is subjective, based on reflectogram shape.

Figure 2.4: Phytoclast and vitrinite reflectograms for sample NYS14_71, superimposed, showing complete overlap of inertinite and vitrinite reflectance profiles.

Figure 2.5: Output of normalmixEM function for sample NYS14_71 (New York State, Givetian).

Figure 2.6: Comparison of normalmixEM prediction for R_v with measured values, showing linear regression line. Pearson r = 0.893. For raw data and list of samples, see SI 2.2.

Figure 2.7: Incident light photomicrograph, showing densely clustered DOM on polished slide. 58% of grid squares cover empty space between macerals. Scale bar = 30 µm.

Figure 2.8: Maceral settling pattern and reflectance, mapped out on standard coverslip.

Figure 2.9: Trends in fusinite and semifusinite abundance through geological time, reproduced from Robinson (1991, fig.3) with permission from Elsevier.

Figure 2.10: Scatter plots comparing Fusinite and total inertinite relative abundance and showing linear regression lines for high-vitrinite samples from Carboniferous successions in East Fife, Tynemouth, and Chirnside. For geological and biostratigraphical context for localities see sections 4.1 and 5.1. A, Fife carbonaceous shales; B, Fife DOM; C, Fife Coals; D, Tynemouth coals; E, Tynemouth DOM; F, Willie's Hole DOM.

Figure 2.11: Response of phytoclast reflectance distribution to nitric acid exposure of varying duration, sample F14_72. White bars, mean; black bars, median; whiskers, $10^{th}/90^{th}$ percentile; dots, all outliers.

Figure 2.12: F14_72 reflectograms. A, 0 seconds (control); B, 300 seconds; C, 600 seconds; D, 1200 seconds.

Figure 2.13: Maceral size distribution (A) and reflectogram (B) for shale sample EH_6, Burnmouth Shore, Tournaisian. A: Red bars, mean; black bars, median; whiskers, $10^{th}/90^{th}$ percentile; dots, all outliers. B: red bar separates inertinite (right of bar) from other macerals (left of bar).

Figure 3.1: The 'charcoal gap', as originally defined by Scott and Glasspool (2006). Modified after Scott and Glasspool (2006, fig. 1).

Figure 3.2: Stratigraphic overview of the Catskill Delta Complex in New York and Pennsylvania. Dotted lines indicate uncertain boundaries; grey shading indicates unnamed/undifferentiated units. Sources: Rickard 1975, 1989; Woodrow and Sevon 1985; Ver Straeten 2007; Ver Straeten *et al*. 2011.

Figure 3.3: Sampled localities in New York and Pennsylvania. 1, Stevens Mountain Quarry; 2, Grand Gorge Road Section; 3, B-1 Borehole; 4, South Mountain Quarry; 5, Cairo Quarry; 6, NY 8 Road Section; 7, Sidney Mountain Quarry; 8, Skytop Lane Quarry; 9, Dunshee Hill Quarry #2 and #4/5; 10, CR 27 Road Section; 11, NY 23 Road Sections A–D; 12, NY 23 Road Sections E–I; 13, US 209 Road Section; 14, Bluestone Wild Forest Quarry; 15, NY 28 composite section; 16, Kaaterskill Clove (Kaaterskill Creek and NY 23A sections); 17, Plattenkill Clove (Plattekill Creek and Plattekill Creek Road sections); 18, Blue Trail; 19, Red Hill, 20, US 11 roadcut; 21, Watsontown Brick Company Quarry.

Figure 3.4: Correlation of Devonian biostratigraphic schemes, and sample coverage from Euramerica (green) and Gondwana (purple). Sources: Williams *et al*. 2000; Melo and Loboziak 2003; Grahn 2005; Kermandji *et al*. 2008; Becker *et al*. 2016.

Figure 3.5: Sedimentary log of Steven's Mountain Quarry. Modified after Bridge and Willis 1991. For key see Appendix 3.

Figure 3.6: Sedimentary log of Grand Gorge road section; gaps indicate outcrop covered by vegetation. Modified after Bridge and Willis (1991). For key see Appendix 3.

Figure 3.7: Hardenburgh Falls access point.

Figure 3.8: Formations intersected by the B1 borehole. Diamonds indicate sample points.

Figure 3.9: Oneonta Fm. exposure at South Mountain Quarry.

Figure 3.10: Sampled interval between quarry floor palaeosol and fluvial sandstone unit, Cairo Quarry.

Figure 3.11: Quarry floor palaeosol, with *Archaeopteris* root impressions.

Figure 3.12: Sedimentary log of NY 8 road section. For key see Appendix 3.

Figure 3.13: Sedimentary log of Sidney Mountain Quarry. Modified after Bishuk *et al*. (2003). For key see Appendix 3.

Figure 3.14: Unidentified fossil plant debris, Sidney Mountain Quarry.

Figure 3.15: Sedimentary log of Skytop Lane Quarry. Modified after Bishuk *et al*. (2003). For key see Appendix 3.

Figure 3.16: Exposure of undifferentiated Sonyea Group units in Dunshee Hill Quarry # 4/5, assigned to the 'Pbms' and 'Hb-I' facies of Bishuk *et al*. (2003). For key see Appendix 3.

Figure 3.17: The brachiopod *Camarotoechia*, Mount Marion Fm., NY23-A outcrop.

Figure 3.18: Plattekill Fm. red-beds at NY23-B.

Figure 3.19: Plattekill Fm. exposure at NY23-C.

Figure 3.20: Plattekill Fm. outcrop at NY23-D; lower mudrock unit of Ver Straeten (2009).

Figure 3.21: Manorkill Fm. terrestrial red-beds at NY23-E.

Figure 3.22: Interbedded mudstones, sandstones, and palaeosols of the Manorkill Fm. at NY23-F.

Figure 3.23: Manorkill Fm. roadcut NY23-G. Samples collected from prominent shale bed (B).

Figure 3.24: Charcoal-rich bed, Manorkill Fm., lower part of NY23-G road cut. 20p coin c. 2 cm.

Figure 3.25: A, Manorkill Fm. exposure at NY 23-H; B, mottled mudstone (female *Plathemis Lydia*, c. 4cm, for scale).

Figure 3.26: Manorkill Fm. roadcut NY 23-I.

Figure 3.27: Sedimentary log of US 209 road cut. Modified after Bartholomew *et al*. (2009). For key see Appendix 3.

Figure 3.28: Uppermost Mount Marion Fm., Bluestone Wild Forest quarry. With John Marshall (left) and Chuck Ver Straeten (right).

Figure 3.29: Ashokan/?Mt. Marion Fm. exposure, NY 28 section. A, channel sandstone; B, interbedded unit.

Figure 3.30: NY 28 road section.

Figure 3.31: Red mudstones at Kaaterskill Creek, with mud cracks.

Figure 3.32: Palaeosol unit, Oneonta Fm., Plattekill Creek road section. With Chuck Ver Straeten.

Figure 3.33: Sand-dominated Lower Walton Fm. exposure, Blue Trail.

Figure 3.34: Outcrop at Red Hill, Pennsylvania. A, main section; B, sampling point, showing Cressler Plant Bed (C. P. B.). White lines indicate bed boundaries.

Figure 3.35: Sedimentary log of Red Hill. Modified after Cressler (2006). For key see Appendix 3.

Figure 3.36: Macroscopic charcoal specimen from Cressler Plant Bed, Red Hill.

Figure 3.37: US 11 road cut. A, interbedded unit, Rose Hill Fm.; B, highly oxidised red-beds, Bloomsburg Fm.; C, dark shale representing marine transgression, Mifflintown Fm.; D, sedimentary log of US 11 road cut, modified after Nickelsen and Cotter (1983). For key see Appendix 3.

Figure 3.38: Location of coastal sections, Gaspé Peninsular, Québec.

Figure 3.39: Sedimentary log of McGregor section TW, Gaspé Peninsular, with sampling points; GA_31: L'Anse-à-Brilliant Coal. Modified after McGregor (1973). For key see Appendix 3.

Figure 3.40: Port North coastal section, West Falkland.

Figure 3.41: Sampling localities in central Bolivia.

Figure 3.42: Correlated sedimentary logs for Bolivia and West Falkland. Modified after Troth (2006), Troth *et al*. (2011) and Marshall (2016).

Figure 3.43: Devonian inertinite abundance in Euramerica and Gondwana. A: box-plot comparing all data for each palaeocontinent. Black bars, median; white bars, mean; whiskers, $10^{th}/90^{th}$ percentile. B, time series comparison through Early, Mid- and Late Devonian.

Figure 3.44: Inertinite abundance compared by palaeoenvironment. Black bars, median; white bars, mean; whiskers, $10^{th}/95^{th}$ percentile.

Figure 3.45: Inertinite abundance through Bermejo section, Bolivia. Known large-scale environmental perturbances (Kačák and Taghanic events) and regional 'Phytoclast Dominated Interval' (PDI) of Troth *et al*. (2011) indicated by grey shading.

Figure 3.46: A, comparison of DOM inertinite data and coal sample GA_31 (this study) with coal-inertinite data of Glasspool *et al*. (2015) for the Devonian, spanning the

'charcoal gap' (grey shading). Error bars indicate standard error. B, spread of DOM inertinite data: black bars, median; red bars, mean; whiskers, 10th/90th percentiles.

Figure 3.47: SEM image of Givetian charcoal sample collected from locality NY 23-G. Scale bars = 500 µm (A) and 100 µm (B).

Figure 4.1: International and regional stage names, lithological and biostratigraphical context for UK localities discussed in sections 5.1 and 6.1. Spore biozones of Neves *et al*. (1973), Clayton *et al*. (1977), Owens *et al*. (1977), Higgs *et al*. (1988). Additional sources: Browne *et al*. (1999), Waters *et al*. (2007), Gradstein *et al*. (2012).

Figure 4.2: Sampling localities, northern UK.

Figure 4.3: Sedimentary logs and correlation for Burnmouth Shore, the Norham Borehole, and Willie's Hole. Logs courtesy of Carys Bennett and Tim Kearsey.

Figure 4.4: Composite sedimentary log of east Fife coastal sections. Modified after Forsythe and Chisholm (1977).

Figure 4.5: Sampling localities, East Greenland.

Figure 4.6: Correlated sedimentary logs for east Greenland Celsius Bjerg Group. Courtesy of J. Marshall.

Figure 4.7: Location of Triungen, Spitsbergen.

Figure 4.8: Sedimentary log, showing Hørbyebreen Fm. succession at Triungen. Courtesy J. Marshall.

Figure 4.9: Results. A, inertinite abundance compared by age; B, palaeolatitude; C, Ballagan Fm. locality. Black bars, median; red bars, mean; whiskers, 10th/90th percentiles.

Figure 4.10: Relative inertinite abundance data for the Ballagan Fm., Burnmouth Shore section (left) and Norham core (right).

Figure 4.11: Incident-light photomicrograph of fusinized wood from the Ballagan Formation at Burnmouth Shore. Scale bar = 32.5 µm.

Figure 4.12: Comparison of inertinite abundance results for Tournaisian and Viséan coals, as determined by Glasspool et al. (2015), Diessel (2010) and this study. Black bars, median; red bars mean; whiskers, $10^{th}/90^{th}$ percentile.

Figure 5.1: Range of model predictions for atmospheric pO_2 (grey shading), and O_2 curve of Glasspool and Scott (2010)/Glasspool *et al*. (2015). Vertical shaded area indicates approximate span of arthropod gigantism during the Palaeozoic.

Figure 5.2: Location of Joppa Shore, Scotland.

Figure 5.3: Joppa Shore stratigraphy and inertinite abundance results. 1, Seven Foot Coal; 2, Pinkie Four Foot Coal; 3, Fifteen Foot Coal; 4, Nine Foot Coal; 5, Salters Coal; 6, Glass Coal. Modified after Tulloch and Walton (1958) and Mitchell *et al*. (1962). For key see Appendix 3.

Figure 5.4: Upper Limestone Fm. at Joppa Shore.

Figure 5.5: Scottish Lower Coal Measures Fm. at Joppa Shore.

Figure 5.6: Coastal sections between Tynemouth and Seaton Sluice, Northumberland. 1, Tynemouth to Table Rocks; 2, St. Mary's Island to Crag Point; 3, Crag Point to Seaton Sluice. For key see Appendix 3.

Figure 5.7: Westphalian B coastal section between Tynemouth and Seaton Sluice, with inertinite abundance results.

Figure 5.8: Inertinite levels compared by age (A) and palaeoenvironment (B). A: 1, Upper Limestone Fm. (n = 7); 2, Passage Fm. (n = 12); 3, Scottish Lower Coal Measures Fm. (n = 1); 4, Pennine Middle Coal Measures Fm. (n = 18). B: 1, transitional (n = 19); 2, terrestrial (n = 18). Black bars, median; red bars, mean; whiskers, $10^{th}/90^{th}$ percentile.

Figure 5.9: Comparison of Serpukhovian and Bashkirian coal data (this study) with that of Glasspool *et al*. (2015). Black bars, median; red bars, mean; whiskers, $10^{th}/90^{th}$ percentile.

Figure 5.10: Combined data, showing Lochkovian–Bashkirian coal and DOM-inertinite abundance binned to 10Ma (this study) compared with Emsian–Kasimovian coal data of Glasspool *et al*. (2015), and output of GEOCARBSULF O_2 model (Berner 2009). Error bars represent standard error.

List of Supplementary Information

SI 2.1: Example R code for normalmixEM function.

SI 2.2: NormalmixEM function test – raw data and statistical analyses.

SI 2.3: Maceral settling behaviour – raw reflectance and maceral distribution data.

SI 2.4: Comparison of fusinite and total inertinite abundance – raw data and statistical analyses.

SI 2.5: Maceral oxidation tests – raw data and statistical analyses.

SI 2.6: Maceral size distribution study and counting method comparison – raw data and statistical analyses.

SI 3.1: Locality information and results summary – chapter 3.

SI 3.2: Detailed results – chapter 3.

SI 3.3: Statistical analyses of results – chapter 3.

SI 3.4: Raw reflectance data and normalmixEM outputs – chapter 3.

SI 3.5: Sample correlation table, Gaspé.

SI 4.1: Locality information and results summary – chapter 4.

SI 4.2: Detailed results – chapter 4.

SI 4.3: Statistical analyses of results – chapter 4.

SI 4.4: Macroscopic charcoal reflectance data.

SI 4.5: Statistical analyses of Tournaisian and Viséan coal inertinite data, and comparison with equivalent data in Glasspool *et al*. (2015) and Diessel (2010).

SI 4.6: Raw reflectance data and normalmixEM outputs – chapter 4.

SI 5.1: Serpukhovian–Bashkirian locality information and results summary.

SI 5.2: Detailed Serpukhovian–Bashkirian results.

SI 5.3: Statistical analyses of Serpukhovian–Bashkirian DOM inertinite data.

SI 5.4: Statistical analyses of Bashkirian–Serpukhovian coal inertinite data; comparison with equivalent data in Glasspool *et al*. (2015).

SI 5.5: Statistical analyses of complete Lochkovian–Bashkirian DOM inertinite dataset.

SI 5.6: Statistical comparison of complete DOM (this study) and coal (Glasspool *et al*. 2015) datasets.

SI 5.7: Statistical comparison of complete coal datasets, this study and Glasspool *et al*. (2015).

SI 5.8: Raw Serpukhovian–Bashkirian reflectance data and normalmixEM outputs.

Declaration of Authorship

I, ...[please print name]

declare that this thesis and the work presented in it are my own and has been generated by me as the result of my own original research.

[title of thesis] .....

.....

I confirm that:

1. This work was done wholly or mainly while in candidature for a research degree at this University;
2. Where any part of this thesis has previously been submitted for a degree or any other qualification at this University or any other institution, this has been clearly stated;
3. Where I have consulted the published work of others, this is always clearly attributed;
4. Where I have quoted from the work of others, the source is always given. With the exception of such quotations, this thesis is entirely my own work;
5. I have acknowledged all main sources of help;
6. Where the thesis is based on work done by myself jointly with others, I have made clear exactly what was done by others and what I have contributed myself;
7. [Delete as appropriate] None of this work has been published before submission [or] Parts of this work have been published as: [please list references below]:

Signed: .....

Date:.....

Acknowledgements

This PhD studentship was funded by the Natural Environment Research Council standard grant NE/J007471/1 (*Evolutionary rise of deep rooting forests and enhanced chemical weathering: Quantitative investigations into the current paradigm)* and consortium grant NE/J021091/1 (*The mid-Palaeozoic biotic crisis: setting the trajectory of tetrapod evolution*). Travel to the 2014 European Palaeobotany-Palynology Conference, Padua, was funded by a small grant from the International Federation of Palynological Societies. I thank my PhD supervisors John Marshall, Ian Harding, Charles Wellman and David Beerling for their advice and support. I gratefully acknowledge the assistance of Shir Akbari (palynological processing), Kate Davies and Barry Marsh (photography), Charles Ver Straeten, Doug Rowe, Jenny Morris and Daniel Bishuk (fieldwork, New York State and Pennsylvania), Jon Lakin (fieldwork, Bolivia), Emma Reeves (fieldwork, Fife coast, and palynological processing of Ballagan Formation material), all members of the TW:eed project team, Josh Barron (Norham core borehole sample analysis), Richard Pierce (SEM), John Ford, Bob Jones and Dan Doran (slide production, charcoal mounting), Martin Wood (modern charcoal specimen), Sam Patel (nitric acid processing) and finally Ryan Gallacher, Tim Hughes, and Giang Tran for their constructive criticism of my conference posters and presentations.

List of definitions and abbreviations

ASTM: American Society for Testing and Materials

BNG: British National Grid

C_{org}: organic carbon

CPB: Cressler Plant Bed

DOC: dissolved organic carbon

DOM: dispersed organic matter

EDME: End-Devonian Mass Extinction

ICCP: International Committee for Coal and Organic Petrology

NYSPA: New York State Power Authority

PAL: Present atmospheric level

PDI: Phytoclast Dominated Interval

PMF: Panther Mountain Formation

pO_2: partial pressure of atmospheric O_2

POC: particulate organic carbon

R_i: random reflectance of inertinite in oil

$R_i$max: maximum inertinite reflectance in oil

Rmax: maximum reflectance in oil

Rmin: minimum reflectance in oil

R_v: random reflectance of vitrinite in oil

$R_v$max: maximum vitrinite reflectance in oil

TOM: terrestrial organic matter

1. Introduction

It has long been recognised that the Earth's primordial atmosphere contained only trace amounts of free oxygen, and that the persistence of this highly reactive substance in the modern ocean-atmosphere system is only possible through its continual replenishment by photosynthesis (Urey 1952; Berkner and Marshall 1965). The transition to, and stability of, an oxygenated atmosphere has, for obvious reasons, been the subject of great interest and study over many decades (e.g. Berkner and Marshall 1965; Watson *et al*. 1978; Berner 1989, 1999; Kasting 1993; Lenton 2001; Berner *et al*. 2003; Canfield 2005; Canfield *et al*. 2007; Kump 2008; Lyons *et al*. 2014); nevertheless, despite the fact that the fundamental biogeochemical controls on pO_2 were first described over 170 years ago (Ebelmen 1845), a true appreciation of the dynamic nature of the Earth's ocean-atmosphere system through the Phanerozoic was slow in coming. In part this is because Ebelmen's ground-breaking work was not widely disseminated at the time and ultimately forgotten, leading to a 130-year hiatus before the same equations were independently reformulated (Garrels and Perry 1974; Holland 1978; Garrels and Lerman 1984; Eq. 1–2):

$$CO_2 + H_2O \leftrightarrow CH_2O + O_2 \qquad [1]$$

$$2Fe_2O_3 + 8SO_4^{--} + 16H^+ \leftrightarrow 15O_2 + 4FeS_2 + 8H_2O \qquad [2]$$

Equation 1, which is quantitatively the most important (Berner 1989), describes net photosynthesis (left to right) and the oxidation of organic carbon (C_{org}) (right to left). Net photosynthesis occurs when organic matter is buried before it can undergo oxidative decay; oxidative weathering or thermal decomposition of ancient deposits supplies the inverse reaction. Equation 2 represents several reactions involved in sedimentary pyrite formation via microbial sulphate reduction (left to right), and the inverse oxidation reaction, which is similarly supplied by the weathering or thermal decomposition of pyrite. Thus, atmospheric pO_2 is primarily regulated by the long-term biogeochemical carbon and sulphur cycles (Fig. 1.1). Based on these equations and estimates of pyrite and C_{org} burial/weathering rates, O_2 residence time in the atmosphere-ocean-biosphere (i.e. short-term) system is approximately 3.2 million years (Lenton 2001).

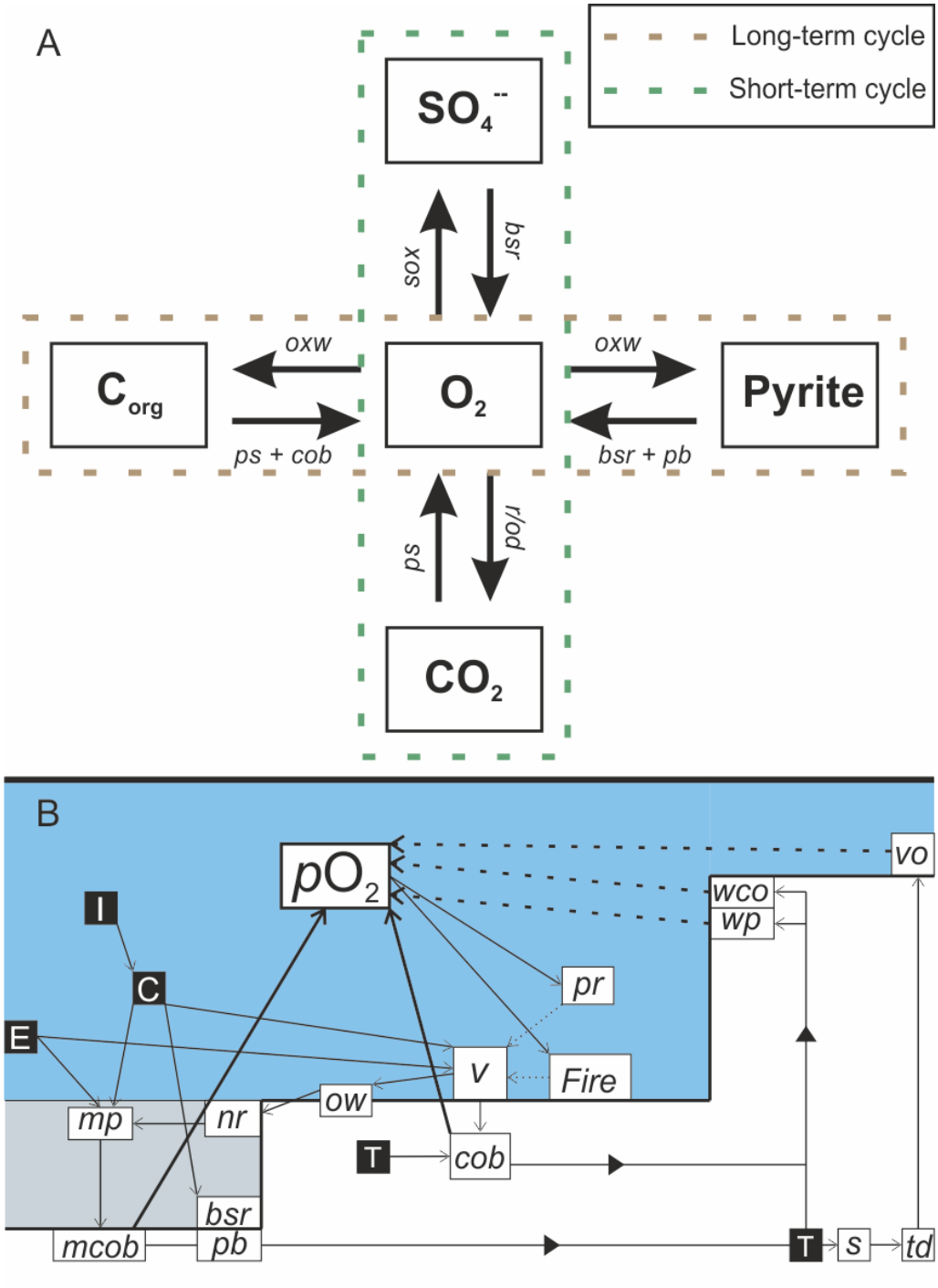

Figure 1.1: Main controls, feedbacks and forcings for atmospheric pO_2. A, simplified box model for short- and long-term biogeochemical O_2 cycles. *bsr*, bacterial sulphate reduction; *cob*, C_{org} burial; *oxw*, oxidative weathering; *pb*, pyrite burial; *ps*, photosynthesis; *sox*, sulphate oxidation. B, potential forcings (black boxes) and feedback mechanisms (linked white boxes) affecting these cycles. Solid arrows indicate positive effect (e.g. increased nutrient runoff causes increased marine productivity) and dotted arrows indicate negative effect (e.g. increased fires reduce terrestrial vegetation cover). Solid lines from forcings indicate either effect is possible. Solid

arrows to pO_2 indicate increase, dotted arrows indicate decrease. C, climate; E, Evolutionary change; I, insolation; T, tectonism; *bsr*, bacterial sulphate reduction; *cob*, C_{org} burial; *mcob*, marine C_{org} burial; *mp*, marine productivity; *nr*, nutrient runoff; *ow*, organic weathering; *pb*, pyrite burial; *pr*, photorespiration (reduces efficiency of photosynthesis under high pO_2); *s*, subduction; *td*, thermal dissociation; *v*, terrestrial vegetation; *vo*, volcanic outgassing; *wco*, C_{org} weathering; *wp*, pyrite weathering.

1.1 The evolution of atmospheric O_2 through geological time

Direct samples of the ancient atmosphere are not available for most of Earth's geological past. The oldest ice-cores, which retain air trapped at the time of ice formation, are only c. 800 kyr old (Lüthi *et al*. 2008); gases trapped in amber provide a more extensive record, with samples reported from as far back as the Late Cretaceous (c. 75–95 Ma; Berner and Landis 1988), but an intense debate over whether amber provides an effective long-term seal (Hopfenberg *et al*. 1988; Beck 1988; Chave and Smith 1988; Horibe and Craig, 1988; Landis and Berner 1988; Landis and Snell 1991) has never been resolved. Fortunately, a number of indirect geochemical markers exist which place broad constraints on pO_2 at certain points in Earth's history, allowing several general stages of atmospheric evolution to be recognised.

The steam atmosphere

The Earth's atmosphere is considered to be 'secondary', in that it was initially created by impact degassing during planetary accretion rather than captured gravitationally from the solar nebula (Zahnle *et al*. 2010). Thus, during the Hadean (4.55–4.0 Ga) atmospheric composition reflected the chemical makeup of impacting bodies and was likely dominated by volatiles such as CH_4, H_2, H_2O, N_2, NH_3, CO, and CO_2 (Schaefer and Fegley 2007; Zahnle *et al*. 2010). Molecular O_2 was generated only by abiotic processes (principally photodissociation of H_2O and CO_2) and would have been rapidly removed by reactions with reduced gasses, so is unlikely to have exceeded 10^{-13} of its present atmospheric level (PAL) at ground level (Kasting 1993; Kasting and Caitling 2003). This is often referred to as a 'steam atmosphere' (Zahnle *et al*. 2010); as temperatures fell, H_2O began to condense and the first oceans are believed to have formed by 4.4 Ga (Wilde *et al*. 2001).

The hydrocarbon haze

Mass-independent fractionation of sulphur isotopes (S-MIF) in sedimentary rocks constrains atmospheric pO_2 to < 10^{-5} PAL during the Archean (4.0–2.5 Ga) (Farquhar *et al*. 2000; Pavlov and Kasting 2002). Under such conditions, substantial concentrations of volcanogenic and (from c. 3.5 Ga), biogenic methane were able to accumulate in the atmosphere; in combination with abundant CO_2, this provided a strong greenhouse effect, allowing liquid water to exist on the Earth's surface despite the fact that the sun was significantly less luminous than today (Pavlov *et al*. 2000, 2001; Ueno *et al*. 2006). It has been calculated that such high concentrations of methane would have produced a 'hydrocarbon haze' of organic aerosols, similar to that observed today on Saturn's moon, Titan (Pavlov *et al*. 2001; Trainer *et al*. 2006; Domagal-Goldman *et al*. 2008; Zerkle *et al*. 2012). The widespread occurrence of iron oxide-rich banded iron formations (BIFs) provides further evidence for low Archean pO_2; these indicate abundant dissolved Fe(II) in the oceans, which would not have been possible under oxidising conditions and suggests atmospheric O_2 could not have exceeded 0.1% of PAL (Canfield 2005). Fe oxidation may have been bacterially mediated and would not necessarily have required an increase in dissolved oceanic O_2 (Konhauser *et al*. 2002; Lyons *et al*. 2014); alternatively, BIFs may mark a much earlier appearance of photosynthesising organisms than is generally supposed (Rosing and Frei 2004). In this model, the Fe(II) acts as a sink for O_2, preventing it from accumulating in the atmosphere.

The Great Oxygenation Event

The 'Great Oxygenation Event' (GOE) at c. 2.45–2.32 Ga marks the point at which, following the evolution of photosynthetic cyanobacteria some 200–300 Ma earlier (Knoll 2003; see however Rosing and Frei 2004), geological oxygen sinks became increasingly saturated and free oxygen began to accumulate in the atmosphere (Kopp *et al*. 2005). The cessation of S-MIF and the widespread occurrence of iron oxide in palaeosols together indicate atmospheric $O_2 \geq 1\%$ PAL (i.e. 0.21% vol.; Farquhar *et al*. 2000; Kump 2008); the persistence of deep-ocean anoxia sets an upper limit of 40% PAL (8.36% vol.; Canfield 2005). One effect of increased pO_2 would have been the enhanced removal of methane from the atmosphere; thus, it has been suggested that the 2.3–2.2 Ga Huronian 'Snowball

Earth' glaciation was a direct result of increased atmospheric oxygenation (Kopp *et al*. 2005).

BIFs reappeared between 2.0 and 1.8 Ga (Canfield 2005), indicating that pO_2 was quite variable during the Proterozoic; nevertheless, trace metal and isotopic analyses (Canfield *et al*. 2007; Sahoo *et al*. 2012; Partin *et al*. 2013) suggest that oxygenation of the oceans was well underway by 635 Ma, and essentially complete by 580 Ma, from which it can be inferred that atmospheric pO_2 exceeded 15% PAL, or 3.14% vol. This approximately coincides with the appearance of metazoans in the fossil record during the Ediacaran Period, and is well in excess of estimates for their minimum O_2 requirements (0.4–3% PAL; Runnegar 1991; Sperling *et al*. 2013a); increased oxygen availability is generally assumed to have been a driver of their evolution (e.g. Canfield *et al*. 2007), though this has been questioned by Mills *et al*. (2014), who argue, first, that fossil and molecular evidence suggests a somewhat earlier origin and second, that experiments on modern demosponges indicate greater tolerance for hypoxia than previously supposed.

The Phanerozoic

As with the Ediacaran, a further increase in atmospheric pO_2 has been proposed as an explanation for the 541–521 Ma 'Cambrian explosion' (Cloud 1968; Rhoades and Morse 1971; Knoll and Carroll 1999), during which the majority of modern animal phyla appear in the fossil record for the first time (Sperling *et al*. 2013b). Certainly, the oxygen requirements of typical early Cambrian faunas are likely to have been higher than their Ediacaran counterparts, with estimates ranging from 12–24% PAL (= 2.5–5.0% vol.; Holland 1984). Geochemical proxies have not identified any significant change in oceanic redox conditions at this time, however (Partin *et al*. 2013; Sperling *et al*. 2015), which may indicate either that the preceding Ediacaran pO_2 increase was larger than generally supposed, or simply that oceanic redox conditions are a poor guide to pO_2 changes above 15% PAL.

By the upper Silurian (c. 420 Ma), evidence of terrestrial wildfires begins to appear in the form of fossil charcoal (e.g. Glasspool *et al*. 2004). The link between wildfire activity and atmospheric O_2 derives from the very basic principle that combustion requires three fundamental components to occur, namely heat (ignition source), an oxidising agent, and

fuel; this principle is often expressed as a 'fire triangle' (e.g. Scott *et al*. 2014). Experimental studies (Belcher and McElwain 2008; Belcher *et al*. 2010) have shown that although short-lived combustion will occur at the ignition point at 15% vol. O_2, *self-sustaining* combustion is impossible below an absolute minimum of 16% vol. even at very low moisture levels. The distinction is important, because if combustion is not self-sustaining a fire cannot spread. Belcher *et al.* (2010) also noted that a more realistic minimum in natural environments (i.e. assuming some moisture is present) is 16.5%. This establishes a level of atmospheric O_2 below which global fire activity would be 'switched off'. Measurements of fire spread-rate and temperature at incrementally increasing levels of O_2 have revealed a region of high sensitivity between 19 and 21% vol. O_2 over which combustion likelihood and spread-rate climb rapidly, before reaching a plateau at c. 22% (Belcher *et al*. 2010; Lenton 2013). As O_2 continues to climb, increasingly moisture-laden plant material will burn; beyond 35% vol., moisture saturation levels which are only attained during intense rain would be required to prevent combustion (Wildman *et al*. 2004). It is reasonable to assume that by this stage plant communities worldwide would already have been severely curtailed, but the precise point at which damage to plant life would prevent any further increase in O_2 (by reducing net photosynthesis) depends on climate (e.g. humidity, weather patterns) and the strength of plant evolutionary responses to increased fire frequency; a figure of 25–35% vol. is commonly cited (Lenton and Watson 2000; Lenton 2013; Scott *et al*. 2014). Thus, the appearance of charcoal in the fossil record marks the latest possible onset of a period of relative stability which has continued to the present day, during which pO_2 has likely remained at 80–170% PAL, and many authors have postulated that the relationship between atmospheric pO_2 and global wildfire activity implies a feedback mechanism which stabilises O_2 over geological time (Lovelock 1979, 1988; Lenton and Watson 2000; Bergman *et al*. 2004; Lenton 2013).

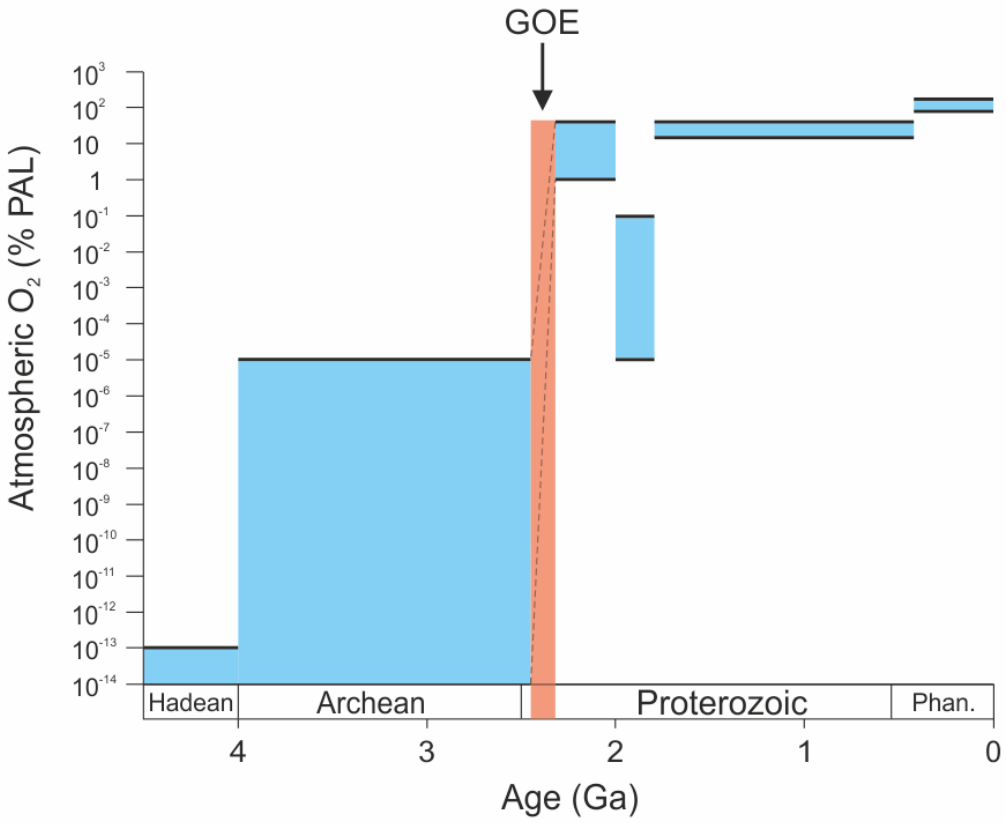

Figure 1.2: Geochemical constraints on atmospheric O_2 through geological time. GOE, great oxygenation event. Compiled from: Kasting 1993; Farquhar *et al*. 2000; Pavlov and Kasting 2002; Kasting and Caitling 2003; Glasspool *et al*. 2004; Canfield 2005; Canfield *et al*. 2007; Kump 2008; Belcher *et al*. 2010; Sahoo *et al*. 2012; Lenton 2013; Partin *et al*. 2013; Sperling *et al*. 2015.

1.2 Modelling Phanerozoic O_2

Given that pO_2 is regulated primarily by the long-term biogeochemical carbon and sulphur cycles (Fig. 1.1), an obvious question is whether and to what extent it has departed from PAL (20.9% vol.) during the Phanerozoic, in response to major biological innovations and upheavals. For example, the evolution of woody plants and the rise of the first forests during the Devonian and Carboniferous represented a massive perturbation, as large quantities of refractory organic carbon were buried and transferred from the short to the long-term carbon cycle (Berner *et al*. 2003; Berner 2006); based on Eq. 1 this implies a corresponding rise in pO_2. Proponents of the Gaia hypothesis, however (e.g. Lovelock 1972; Watson *et al*. 1978) have long argued that the continued presence of life on Earth

requires strong feedback mechanisms that resist significant change. The question is important, because though trivial in comparison to the changes that occurred during the Precambrian, Phanerozoic variations could still have had a profound effect on the biosphere; for example, a fall from 20.9% to 15% vol. O_2 would be equivalent, in terms of oxygen availability, to an altitude increase of c. 2.5 km (Graham *et al*. 1995). The physical properties of the air would also be affected, principally by a 13% reduction in density but also in terms of thermal conductivity and specific heat capacity; lower air density would alter the mechanical requirements for, and efficiency of, animal flight (Graham *et al*. 1995; Dudley 1998).

The direct geochemical proxies described above place upper and lower limits on pO_2, but cannot provide information on variation between those limits. Attention has therefore turned to model-based reconstructions, which attempt to infer atmospheric O_2 flux from the behaviour of other related biogeochemical cycles. Early models focused exclusively on either the carbon (Junge *et al*. 1975) or sulphur (Holland 1973) cycles, using $^{13}C/^{12}C$ and $^{34}S/^{32}S$ isotope data to track the flux of these elements between reduced and oxidised reservoirs; derivation of O_2 flux was based on mass-balance calculations utilising Eqs. 1 and 2. These were quickly superseded by combined carbon/sulphur models (e.g. Schidlowski *et al*. 1977; Schidlowski and Junge 1981; Kump and Garrels 1986). The isotope mass-balance approach exploits the fact that biological processes tend to preferentially utilise lighter isotopes; the isotopic composition of inorganic marine carbonates and sulphates therefore provides information on the rate of net photosynthesis or pyrite formation, which remove isotopically light carbon and sulphur from the ocean-atmosphere system (Berner *et al*. 2003). Models of this kind have evolved steadily in complexity over the last 45 years (Berner 1987, 2001, 2006, 2009; Hansen and Wallmann 2003; Fig. 1.3), and include the highly influential 'GEOCARBSULF' model (Berner 2009). An alternative approach was introduced by Berner and Canfield (1989), in which carbon and sulphur flux were calculated from estimates of global burial and weathering rates of C_{org} and pyrite rather than isotopic data. This study was the first to demonstrate that feedbacks such as 'rapid recycling' (the preferential weathering of younger rocks), are required to avoid physically impossible results (e.g. negative pO_2).

Rather than focusing exclusively on C_{org} and pyrite, a novel approach introduced by Lenton and Watson (2000) is to assume that nutrient supply is the limiting factor for biological productivity (and hence net photosynthesis/pyrite burial); in this model, pO_2 is inferred from the cycling of nutrients (principally phosphorous) to and from the oceans. Finally, models such as COPSE (Bergman *et al*. 2004) and MAGic (Arvidson *et al*. 2006) have attempted to combine elements of both approaches into a single, highly complex biogeochemical framework.

Returning to the Devonian question, early models indicated that significant pO_2 variation had indeed occurred (e.g. Schidlowski *et al*. 1977; Berner 1987; Berner and Canfield 1989), but, as noted above, also established that feedback mechanisms are essential (Berner 2001); disagreement over how to incorporate these into the models in a realistic way has led to widely diverging outputs that are difficult to reconcile (Fig. 1.3; see also review by Berner *et al*. 2003). In spite of this, many models recognise the same basic trend during the mid and late Palaeozoic: some degree of hypoxia during the Mid- to Late Devonian is followed by a sustained increase throughout the Carboniferous, with pO_2 reaching an all-time high during the Permian before crashing at the Permo-Triassic boundary.

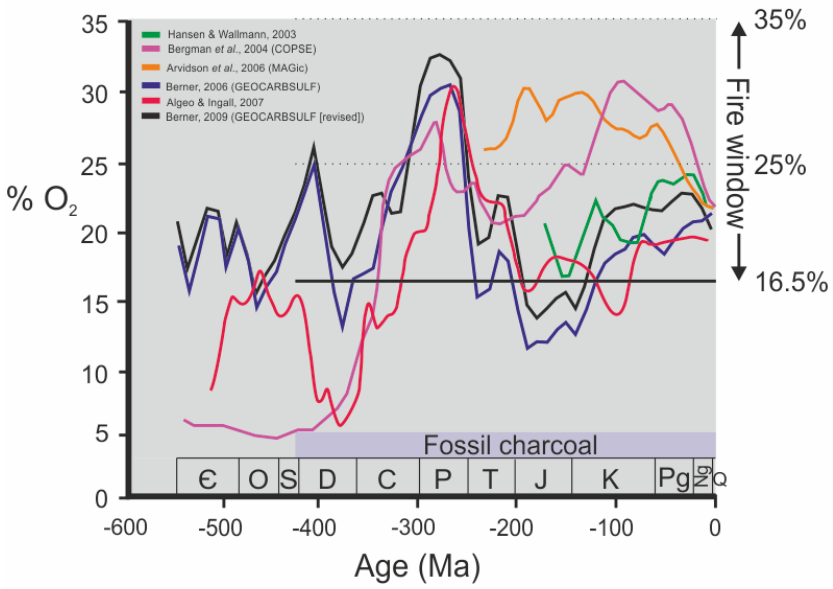

Figure 1.3: Comparison of model predictions for atmospheric O_2 (% vol.), and extent of the 'fire window'.

1.3 Atmospheric O_2 and wildfire activity

As previously noted, the rate at which combustion proceeds is positively correlated with oxygen supply as determined by ambient pO_2 (Watson *et al*. 1978; Belcher *et al*. 2010; Watson and Lovelock 2013) provided that fuel and heat are present. The frequency of lightning strikes (the most common source of ignition for modern wildfires) is unlikely to have changed significantly over the Phanerozoic (Pyne *et al*. 1996; Glasspool and Scott 2010) and colonisation of the land by plants had begun by no later than the Mid Ordovician (Rubinstein *et al*. 2010). Thus, sources of potential fuel and ignition have been continuously present since that time, and changes in fire activity can theoretically identify any significant changes in atmospheric pO_2 which have occurred over the last 470 million years.

Charcoal in the fossil record

Combustion is a two-stage process; an initial endothermic stage, pyrolysis, in which volatile compounds are released when organic material is heated above approximately 150°C (Chen *et al*. 2011), and an exothermic stage in which these volatiles and/or the remaining pyrolised material (char) are oxidised (Rein 2013). At any given time organic material undergoing combustion will exist either as unburned fuel, charcoal or inorganic mineral ash, which means that when a fire is extinguished a variety of products are left behind (Fig. 1.4). Being primarily composed of carbon which has been aromatised by the effects of heat, charcoal is chemically inert; as a result, fossil charcoal (traditionally referred to as ‘fusain’) is a common minor component of clastic sedimentary rocks and sometimes a major component of coals (Scott *et al*. 2014).

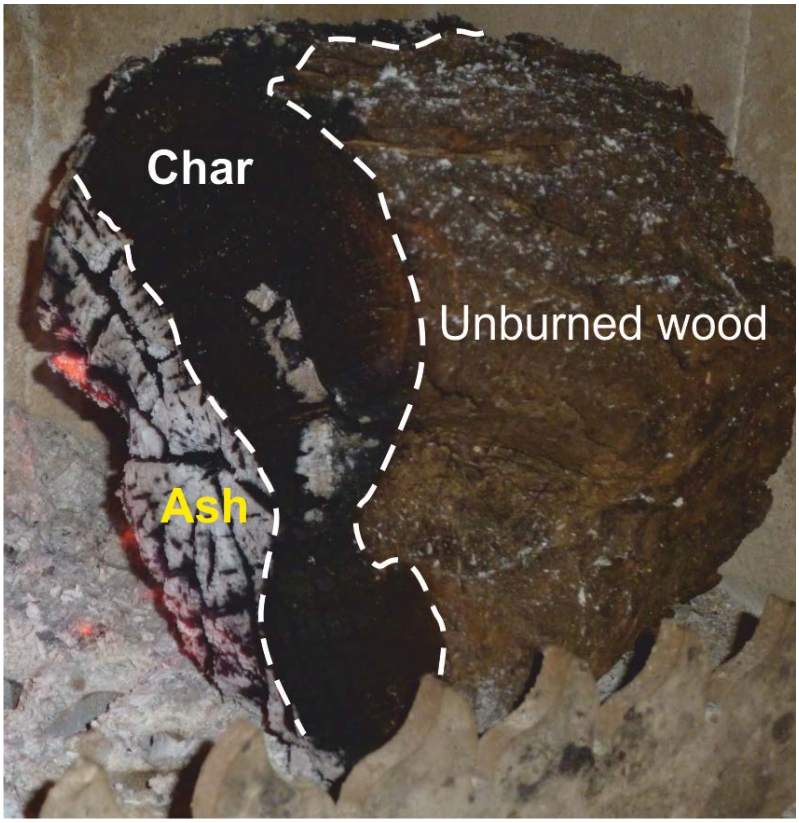

Figure 1.4: Stages of combustion, as seen in a burning log.

The earliest direct evidence of fire use by hominins (cave deposits containing burned bones and plant material) dates to approximately 1 Ma (Berna *et al*. 2012); phylogenetic and physiological studies on modern primates suggest adoption of a diet of cooked food by at least 1.9 Ma (Wrangham 2009; Organ *et al*. 2011). Prior to this, charcoal in the fossil record is assumed to be the product of natural wildfires or, more rarely, volcanic activity (Scott and Glasspool 2005).

The first attempt to use charcoal occurrence to constrain atmospheric pO_2 through geological time was that of Cope and Chaloner (1980). At that time, the oldest known specimens were of latest Devonian or Early Mississippian age (Warg and Traverse 1973); following the logic of the fire window (see above), they inferred that O_2 had not fallen below 12.8% vol. during the last c. 365 million years (their minimum value being based on the older work of Coward and Jones 1952). Robinson (1991) provided the first quantitative study, in which he compared the abundance of inertinite (= microscopic charcoal; see below) in Carboniferous–Pleistocene coals against the palaeoatmosphere model of Berner and Canfield (1989) and found “some correspondence…but also some

notable departures" between the two (Robinson, *ibid*, pp. 56). Much of the data used in that study had been collected some decades previously (e.g. Cook and Taylor 1963; George 1975), and our understanding of which microscopic components of coal ('macerals') constitute charcoal has changed quite significantly since that time (see section 1.4). In particular, a precipitous drop over the last c. 50 million years to unprecedented low levels was difficult to explain. More recently, a largely qualitative study of charcoal abundance through the Phanerozoic (Scott & Glasspool 2006) showed broad agreement with some O_2 models (e.g. Berner *et al*. 2003; Berner 2006), and examination of the inertinite content of Devonian–Tertiary coals has provided quantitative data (Glasspool and Scott 2010; Glasspool *et al*. 2015; Rimmer *et al*. 2015) that support these conclusions. Of particular note was their identification of a 'charcoal gap' during the mid-Devonian, which appears to coincide with a major dip in pO_2 predicted by many palaeoatmosphere models. Glasspool and Scott (2010) were also the first to attempt to establish an absolute rather than relative wildfire-based O_2 reconstruction, by measuring the charcoal content of recent (pre-industrial) wetland peats for use as a calibration point.

Charcoal in the fossil record 2: identification and quantification techniques

Macroscopic charcoal (Fig. 1.5) is fibrous, highly friable and black in colour, with a silky lustre and black streak (Scott 2010), and can thus be readily identified; unfortunately, it is rarely abundant enough for quantitative studies. In contrast, microscopic charcoal, though more difficult to identify, is a common minor component of the dispersed organic matter (DOM) in clastic sedimentary rocks, and is also present in varying proportions in coals, as the organic 'maceral' inertinite. The term maceral was introduced by Stopes (1935) to describe the microscopic constituents of coal in the same sense that 'mineral' describes the components of inorganic rocks; they differ from minerals, however, in that their chemical composition and physical properties are not fixed (Stach *et al*. 1982). Various methods have been suggested by which microscopic charcoal can be identified and quantified, all of which have certain drawbacks and complicating factors; some of these have not been investigated in detail, whereas others have been studied at length over several decades but yielded contradictory results. These uncertainties will be briefly introduced here, and discussed in more detail in Chapter 2.

Figure 1.5: Famennian macroscopic charcoal (dark fragments) from the Cressler Plant Bed, Red Hill, Pennsylvania, USA.

Transmitted light microscopy

Studies of DOM charcoal have tended to favour transmitted light microscopy (e.g. Marlon *et al*. 2008; Power *et al*. 2008; Power 2013; Crawford and Belcher 2014) because demineralised organic concentrates can be quickly and easily mounted on slides for this purpose (Fig. 1.6; see also Chapter 2). Correct identification is the major weakness of this approach (Winkler 1985; Patterson *et al*. 1987; Tyson 1995; Rhodes 1998; Batten 2002); charcoal particles seen in transmitted light are black, completely opaque, and quite variable in their morphology (Fig. 1.6). As a result, there has traditionally been a tendency to treat *any* opaque, black, angular particles as charcoal (e.g. Swain 1973; Clark 1988; Edney *et al*. 1990; Tinner and Hu 2003), despite the fact that this also describes some forms of pyrite (Rhodes 1998) and that some forms of charcoal are not angular (see e.g. ICCP 2001). Unlike most other mineral groups, sulphides such as pyrite are resistant to standard palynological demineralisation techniques (Wood *et al*. 1996); although partial removal of pyrite is possible by treatment with an oxidising acid (e.g. fuming nitric), organic matter is also vulnerable to such acids, and their effects on charcoal are not fully understood. Singh *et al*. (1981) reported that sediment samples treated with nitric acid

during palynological processing were consistently depleted in charcoal compared to control samples, suggesting some charcoal destruction had occurred (Patterson *et al*. 1987; see *acid digestion*, below). Recognition of charcoal can also be hampered by high thermal maturity, which can darken palynological material considerably (Taylor *et al*. 1998). Although more recent work has improved our understanding of the *controls* on charcoal morphology, which are related to its precursor materials and taphonomic history (e.g. Enache and Cumming 2005; Crawford and Belcher 2014), these problems persist.

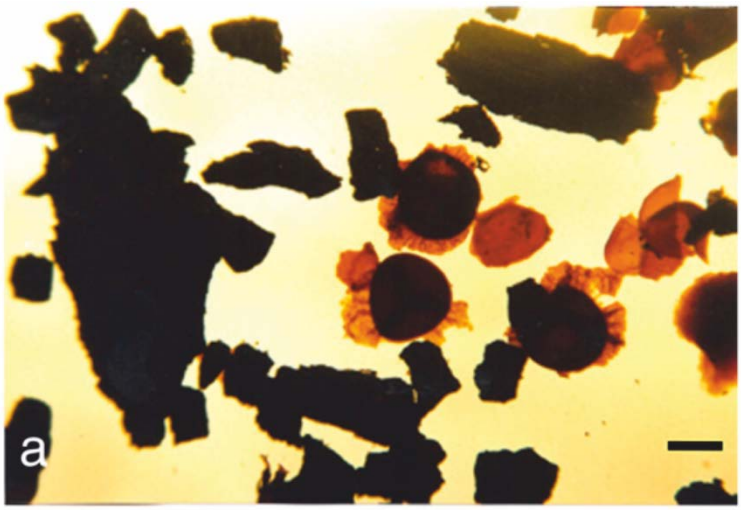

Figure 1.6: Charcoal fragments and coalified wood (left), and spores (centre/right) as seen using transmitted light microscopy. Scale bar = 1 mm. Reproduced from Scott (2010, fig. 17a) with permission from Elsevier.

Incident light microscopy

Incident light microscopy using an oil-immersed objective is the industry-standard procedure for petrological examination of coals (ASTM 2014) but can also be applied to DOM via the production of polished slides (see Chapter 2), which is useful for thermal maturity studies (e.g. Marshall *et al*. 1994a). The inertinite group, which comprises several macerals characterised by a relatively high reflectance under incident light (ICCP 2001; Tables 1.1–1.2) is believed to be at least partly synonymous with fossil charcoal (Scott and Glasspool 2007; see also section 1.4). The term 'inertinite' was originally intended to describe macerals which were non-reactive (and hence did not soften) during coking, though this was subsequently found not to true in all cases (see Taylor *et al*. 1998 and references therein). When viewed under incident light there is no possibility of

confusing charcoal and pyrite, and identification of charcoal is not dependent on shape (Fig. 1.7); an attached microphotometer system allows maceral reflectance to be measured with a high degree of precision. However, problems arise in distinguishing high reflectance caused by pyrolysis from that caused by high thermal maturity, and there are elements of circularity in the current ICCP definitions of some macerals (see section 1.4). The equipment required is also more specialist in nature, and hence less widely available.

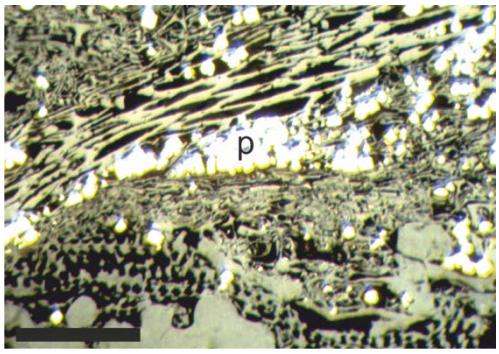

Figure 1.7: Inertinite and pyrite (p), as seen using incident light microscopy. Scale bar = 80 µm. Reproduced from Hower *et al*. (1999, slide 23-7).

Fourier Transform Infrared Spectroscopy (FTIR)

Fourier Transform Infrared spectroscopy (FTIR) is a chemical characterisation technique based on infrared absorption or transmission spectra, which has been widely employed in studies of coal structure (Solomon *et al*. 1982; Painter *et al*. 1985) and thermal maturity (Rouxhet and Robin 1978; Ganz and Kalkreuth 1987; Christy *et al*. 1989). The technique has also been applied to charcoal by Guo and Bustin (1998) and Bustin and Guo (1999), who compared the composition of modern charcoal with inertinite and funginite in coals. Earlier studies were restricted to bulk analysis of polished coals or pellet-mounted maceral concentrates, because technological limitations precluded the analysis of objects smaller than c. 2 cm^2; the development of Micro-FTIR systems have allowed progressively smaller objects to be investigated such that, from the 1990s onwards, it became possible to analyse individual macerals in-situ (Lin and Ritz 1993; Iglesias *et al*. 1995). The current generation of Micro-FTIR spectrometers can scan objects as small as 20 µm, or 3–5 µm when employing a synchrotron radiation source (Chen *et al*. 2015), and in recent years a sustained effort has been made to better characterise organic macerals in chemical terms (Chen *et al*. 2012, 2013, 2014).

The studies listed above involve investigation of the chemical composition of known macerals (i.e. the macerals are identified first by some other means); identification of unknown macerals by chemical analysis requires a standard composition against which to compare the results. Obtaining a 'baseline' for organic macerals is challenging, because their chemical composition is not fixed, and minor impurities can significantly alter the spectra produced, as can small variations in sample polishing introduced during preparation (Chen *et al*. 2015). Therefore, some subjective judgement is required when deciding what to classify as inertinite, leading to the risk of circular reasoning. Thus far, only the inertinite-group macerals fusinite, semifusinite and funginite have been characterised using FTIR spectroscopy (Chen *et al*. 2012, 2013).

Acid digestion

It is widely recognised (e.g. Tyson 1995; Taylor *et al*. 1998; Batten 2002) that charcoal is relatively inert compared to other forms of organic matter, and therefore more resistant to the destructive effects of oxidation. Several authors have examined the potential use of oxidising acids in isolating charcoal (Swain 1973; Robinson 1984; Winkler 1985; Jones *et al*. 1987); prolonged exposure to nitric acid (c. 1–2 hours) was found to be quite effective in preferentially destroying other organic matter, leaving behind a charcoal concentrate which could then be quantified relative to the original sample. These studies were conducted on Holocene peats, lake and bog sediments, and were ultimately abandoned due to the difficulty of distinguishing natural and anthropogenic charcoal, particularly with respect to modern industrial emissions (Rhodes 1998); thus, the application of this approach to thermally altered lithological material containing charcoal remains untested.

Polycyclic aromatic hydrocarbons (PAH)

PAHs are an array of compounds produced by the combustion of organic biomass, diagenesis of sedimentary organic material (i.e. formation of fossil fuels) or direct synthesis by certain microbes and plants (Belcher *et al*. 2003; Ravindra *et al*. 2008). Pyrolytic PAHs have been widely accepted as effective geochemical markers for fire activity in the fossil record (Venkatesan and Dahl 1989; Killops and Massoud 1992; Kruge *et al*. 1994; Jiang *et al*. 1998; Finkelstein *et al*. 2005; Marynowski and Simoneit 2009).

Their use was questioned by Belcher *et al*. (2003), however, who noted that at least one PAH commonly attributed to fire activity (retene) can also be produced during diagenesis of organic matter. More recently, Marynowski *et al*. (2011) discovered that the PAH considered to be the most effective indicator of fire activity, benzo[α]pyrene, was rapidly degraded during weathering to the point of complete destruction; subsequent work (Marynowski *et al*. 2015) revealed similar destruction during thermal maturation, such that it was largely removed at thermal maturities > 0.9% R_v. Thus, while PAHs may be quite effective in studies of recent or sub-recent sediments, their application in lithological specimens is questionable.

Nuclear Magnetic Resonance (NMR), Scanning Electron Microscopy (SEM), and electron spin resonance have all been used to investigate the structure and chemistry of modern and fossil charcoal, particularly with regard to the changes that occur at progressively higher temperatures (see review of Scott 2010 and references therein). However, the time, cost, and specialist equipment required for such analyses make them impractical for large-scale quantitative studies such as this one, in which 500 macerals *per sample* must be identified.

Dispersed organic matter, and the limitations of coal-based inertinite data

As discussed above, inertinite occurs both in coals and as a component of dispersed organic matter in clastic sedimentary rocks. In charting inertinite through the Phanerozoic, Glasspool and Scott (2010) chose to focus on coal partly because it was possible to compile almost all of the required data from the literature, avoiding time consuming lab-based analyses of coal samples. Restricting the study to coals also offered a degree of environmental and climatic control, in that a peat-forming environment is, by definition, permanently wet (Taylor 1998); this is an important consideration, if changes in fire activity are to be ascribed to changes in atmospheric pO_2. The principal drawback of this approach is that coals are relatively scarce during the Devonian and Early Mississippian, raising the possibility that the 'charcoal gap' is merely an artefact of low sampling density; another potential issue is that coals are mostly formed in-situ (Stach *et al*. 1982), and inertinite content may therefore be strongly affected by local fire activity. In contrast, sedimentary rocks containing DOM are commonplace, providing ample

material for study even when coals are rare; furthermore, DOM is largely river-transported, and thus represents a combination of fresh and re-worked organic material accumulated from across an entire drainage basin (Blair and Aller 2012). Although it is assumed that a time-averaged, regional signal is less likely to be distorted by local fire events, the possible effects of very old, reworked lithogenic material must be considered; this is discussed in more detail in section 2.6.

1.4. Is all inertinite charcoal?

It has long been suspected (see e.g. Stopes 1919) and, since the work of Austen *et al*. (1966), widely accepted that some inertinite group macerals are pyrogenic. Until relatively recently, however, the orthodox view (Stach *et al*. 1982; Falcon and Snyman 1986; Taylor *et al*. 1998; ICCP 2001) has been that charring is only one of a number of processes by which inertinite can be produced. Other supposed origins include fungal attack (by mould, dry rot etc.), dehydration/oxidation (during weathering or humification), high primary reflectance of precursor materials, or as a secondary product of coalification (Teichmüller 1987b, 1989). This has repeatedly been challenged (Scott, 1989; Winston 1993; Guo and Bustin 1998; Scott and Glasspool 2007) and most workers now agree that at least fusinite is synonymous with fossil charcoal (e.g. Scott 2000; Falcon-Lang 2000; Glasspool 2000; Batten 2002; Rimmer *et al*. 2015). By discarding the division of fusinite into primary, rank, degrado- and pyro-fusinite, this is a position which the International Committee for Coal and Organic Petrology (ICCP) implicitly accepts (ICCP 2001; Table 1.1), though they note that disagreement still exists. The assumption that *all* inertinite is pyrogenic, which is integral to recent charcoal-based reconstructions of atmospheric pO_2 (Scott and Glasspool 2006; Glasspool and Scott 2010, Glasspool *et al*. 2015), is more controversial; the ICCP (2001) maintains that some inertinite-group macerals are generated by processes other than fire, and that for others, fire does not play a significant role. More recently, Hower *et al*. (2009, 2011) have argued that the high reflectances of macrinite and funginite are the result of fungal degradation and high primary reflectance, respectively. In this section, each maceral subject to uncertainty will be considered; past and current inertinite-group nomenclature is summarised in Table 1.1, and the important attributes of each maceral are summarised in Table 1.2.

Taylor *et al.* (1998)		ICCP (2001)
Maceral	**Type**	**Maceral**
Fusinite	Pyrofusinite	Fusinite
	Degrado-fusinite/oxyfusinite	
	Primary fusinite	
	Rank fusinite	
Semifusinite	Pyrosemifusinite	Semifusinite
	Degrado-semifusinite/oxysemifusinite	
	Primary semifusinite	
	Rank semifusinite	
Sclerotinite	-	Funginite
	-	Secretinite
Macrinite	-	Macrinite
Micrinite	-	Micrinite
Inertodetrinite	-	Inertodetrinite

Table 1.1: Past (Taylor) and current (ICCP) nomenclature for inertinite-group macerals.

Maceral	Reflectance	Colour	Structure	Precursor material
Fusinite	'Relatively high'	Greyish or yellowish white	Cellular or 'bogen' (= arc-shaped fragments of cells)	Ligno-cellulosic cell walls
Semifusinite	Intermediate between that of co-occurring vitrinite and fusinite	Grey to white	Intermediate between co-occurring vitrinite and fusinite	Ligno-cellulosic xylem and parenchymatous tissues of herbaceous plants
Funginite	Highly variable; mainly 'high', but as low as 0.4% in low-rank coals; surpassed by vitrinite at 1.6% R_v	Pale grey to white	May retain fungal structure (spores, sclerotiae, mycelia, etc.) or appear similar to fusinite/semifusinite.	Variety of fungal tissues
Secretinite	Highly variable; encompasses reflectance range of all other inertinite macerals	Pale grey to yellowish white	Subspherical/oblate	Uncertain; possibly resin
Macrinite	Variable; higher than co-occurring vitrinite	Grey to white, sometimes yellowish	Amorphous	Uncertain; suggestions include flocculated humic matter, metabolic product of fungi/bacteria, and coprolites
Micrinite	Difficult to measure due to small size. Higher than co-occurring vitrinite until surpassed at 1.4% R_v	Pale grey to white	Rounded, very small (≤ 2µm)	Fragmentation of other inertinite macerals
Inertodetrinite	Highly variable	Highly variable; encompasses all other inertinite macerals	Variable; often angular	Fragmentation of other inertinite macerals

Table 1.2: Summary of ICCP (2001) descriptions of the inertinite macerals.

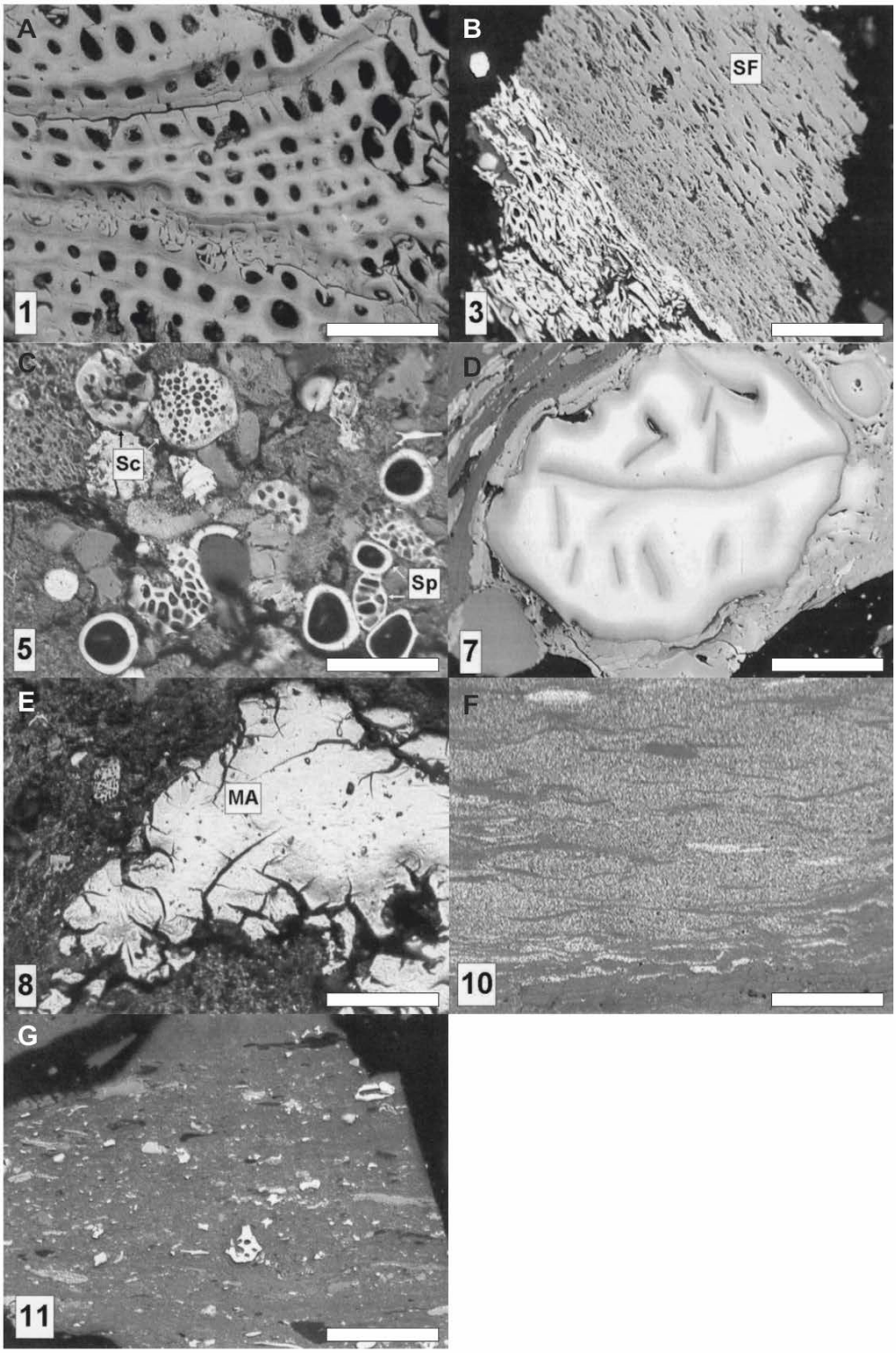

Figure 1.8: Inertinite-group macerals. A, fusinite; B, semifusinite; C, funginite, derived from fungal spores (Sp) and sclerotiae (Sc); D, secretinite; E, macrinite; F, micrinite; G, inertodetrinite. Scale bars = 75 µm. Reproduced from Hower *et al*. (2001; figs. 1, 3, 5, 7, 8, 10, 11) with permission from Elsevier.

Semifusinite (Fig. 1.8B) was identified by Stach *et al*. (1982), Teichmüller (1987b, 1989), and Taylor *et al*. (1998) as the product of incomplete fusinization; since they divided fusinite into four different types representing supposed different origins (Table 1.1), semifusinite is also divided by default. Winston (1993) demonstrated convincingly that there is scant evidence to support the existence of degrado- or primary fusinite, and his arguments apply equally to the corresponding varieties of semifusinite. The ICCP (2001) define semifusinite as a maceral which is intermediate in reflectance and structure between fusinite and vitrinite in the same rock and, while acknowledging that a wildfire origin is possible, assert that it is primarily formed in peat by humification processes, though no supporting evidence is provided. In contrast, several lines of evidence support a pyrogenic origin; the reflectance range of semifusinite falls within that observed in charcoal produced in a modern, natural wildfire (0.13–6.22%; Scott *et al*. 2000), and plant fossils have been discovered showing vitrinite-semifusinite-fusinite transitions similar to those seen in experimentally charred modern wood (Jones *et al*. 1993). The chemical properties of semifusinite, when investigated using micro-FTIR spectroscopy, have also been found to be similar to those of naturally occurring and artificially produced low-temperature charcoals (Guo and Bustin 1998).

One argument which has been advanced in support of a non-pyrogenic origin for some forms of inertinite is that very high levels are observed in some coals, seemingly at odds with the environment in which they were formed. For example, the Triassic coals of Australia were deposited in a sub-arctic climate characterised by tundra and permafrost, environments in which fires are uncommon (Scott *et al*. 2014), yet some contain > 80% inertinite (Smyth 1980); in comparison, Pleistocene peats deposited in a similar climate contain ≤ 2.0% (Koch 1969). In fact, this reflects a more general tendency for inertinite to be relatively scarce in peats and lignites compared to coals of higher thermal rank, irrespective of climate (Teichmüller 1989). Because of the dominance of peats and low-rank coals in Pleistocene–recent successions, taking the inertinite record at face value implies falling atmospheric pO_2 over the last 30–50 Ma (e.g. Robinson 1991; Glasspool and Scott 2010, Glasspool *et al*. 2015) and a consequent reduction in fire activity. If correct, the modern world is undergoing an O_2 low more profound than any seen since at least the Middle Devonian (Fig. 1.3).

A more likely explanation can be found by considering the progressive physical and chemical alterations which occur during coalification (the process of thermal maturation by which degraded organic material is transformed into DOM or coal). These have been extensively studied in the context of coal geology (Alpern and Lemos de Susa 1970; Smith and Cook 1980; Stach *et al*. 1982; Teichmüller 1987a, 1989; Taylor 1998), and found to be reliable indicators of thermal rank; the changes can be expressed as 'coalification tracks', and are different for each maceral/maceral group (Fig. 1.9).

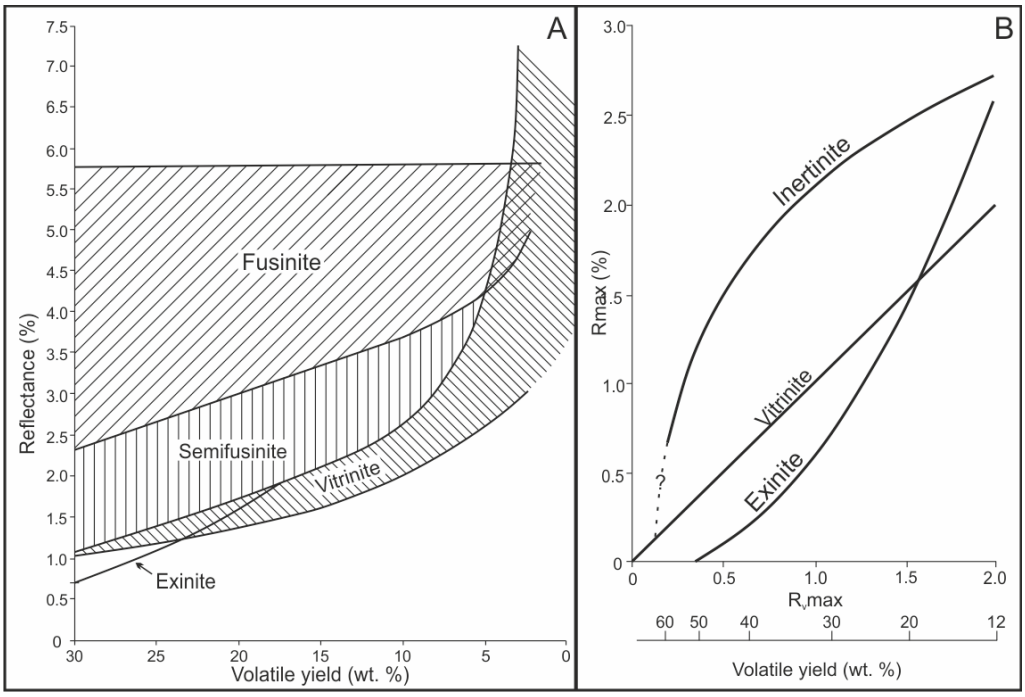

Figure 1.9: Coalification tracks of selected macerals and maceral groups. A, Rmax/Rmin of fusinite and vitrinite, and Rmean of exinite, plotted against volatile yield (ind. increasing thermal rank). Modified after Alpern and Lemos de Susa (1970, figs. 1, 3). B, relationship between $R_i$max, $R_v$max and $R_e$max at increasing thermal rank, with speculative inertinite/vitrinite convergence point. Modified after Teichmüller (1989, fig. 1).

In a study of the coalification tracks of the three main maceral groups, Smith and Cook (1980) determined that as $R_v$max increases from 0.2 to 0.9%, $R_i$max increases rapidly in response, from 0.7 to 2.0%. Although the behaviour of inertinite at the earliest stages of coalification (i.e. < 0.7% $R_i$max) was not addressed by the authors, the apparent scarcity of recent inertinite is consistent with a rapid increase in R_i during low-rank coalification; by following an initially much steeper coalification track than that of vitrinite, initially low-reflecting inertinite (not distinguishable from vitrinite under incident light) should

become much easier to identify as thermal maturity increases. Given that R_i values as low as 0.1% have been recorded in charcoals produced by modern wildfires (Scott and Glasspool 2007), it seems quite plausible that much of the inertinite in modern peats has simply gone unrecorded.

Proponents of 'rank fusinite/semifusinite' (e.g. Stach *et al*. 1982; Taylor *et al*. 1998) explain the steep initial coalification track of inertinite by invoking a hypothetical precursor material which responds particularly strongly to increasing temperature, and thus attains a higher reflectance than co-occurring vitrinite at low and intermediate thermal rank. While this is difficult to disprove, the assumption that the role could not be fulfilled by charcoal is unfounded; reflectance values and IR spectral characteristics of artificially produced charcoal both undergo rapid increase/change as a function of time as well as temperature (Guo and Bustin 1998; Scott and Glasspool 2005, 2007; Fig. 1.10). Given that the length of exposure to high temperatures during wildfires can vary from a few minutes to several hours (Scott and Glasspool 2007), it is reasonable to assume that charcoal, once buried, may undergo substantial further change in response to depth-related temperature increase.

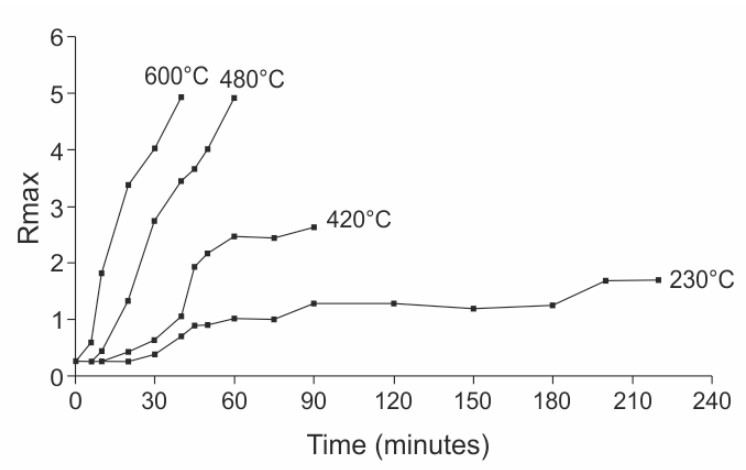

Figure 1.10: Effect of heating time on charcoal reflectance. Reproduced from Guo and Bustin (1998, fig. 1) with permission from Elsevier.

Funginite (Fig. 1.8C) is derived from fungal remains and has a higher reflectance than vitrinite in low and medium rank coals (≤1.6% R_v); beyond this point, the difference in reflectance disappears (ICCP 2001). It has been suggested that funginite is an example of

‘primary inertinite’ i.e. precursor fungal bodies were inherently highly reflecting, even before coalification, due to their high melanin content (Teichmüller 1989). Modern examples of fungi which produce black (i.e. melanin-rich) sclerotiae and spores are known (Teichmüller 1989) but as their reflectance has not been measured, the link between melanin and high reflectance is speculative; indeed, it is unclear how the reflectance of modern fungal material *could* be measured. The presence of funginite surrounded by vitrinite (Fig. 1.11A) or in close association with other macerals (Fig. 1.11B) has been invoked as an argument against charring (Belkin *et al*. 2009; Hower *et al*. 2009), on the assumption that fire would have affected the surrounding plant tissues as well. However, this presupposes that the fungi are preserved in-situ, and that the reflectance of the surrounding macerals is not also anomalously high; Hower *et al*. (2009) admit that the latter is often the case. Furthermore, the heating effect of fire on plant tissues is often uneven, resulting in sub-millimetre scale differences in reflectance, even within individual macerals (Fig. 1.12). Hower *et al*. (2009) also argued that because funginite does not universally attain high reflectance, it is “clearly different from other inertinite macerals” (p.135). This is incorrect, because most other inertinite-group macerals also exhibit a wide range of reflectance (ICCP 2001), exactly as expected if a maceral group is fire derived (see *semifusinite*, above).

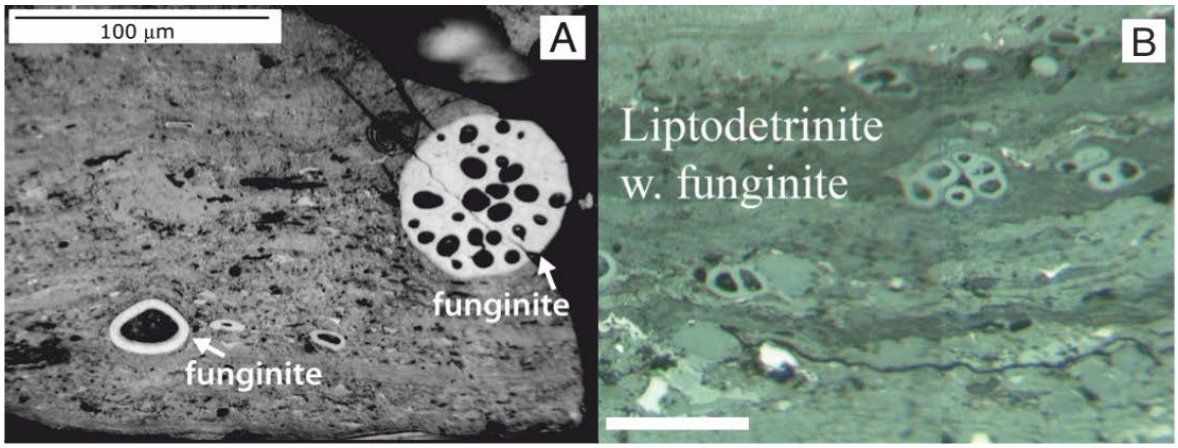

Figure 1.11: Examples of funginite in close association with other macerals of lower reflectance. A, reproduced from Belkin *et al*. (2009, fig. 3A); B, reproduced from Hower *et al*. (2009, fig. 4). With permission from Elsevier.

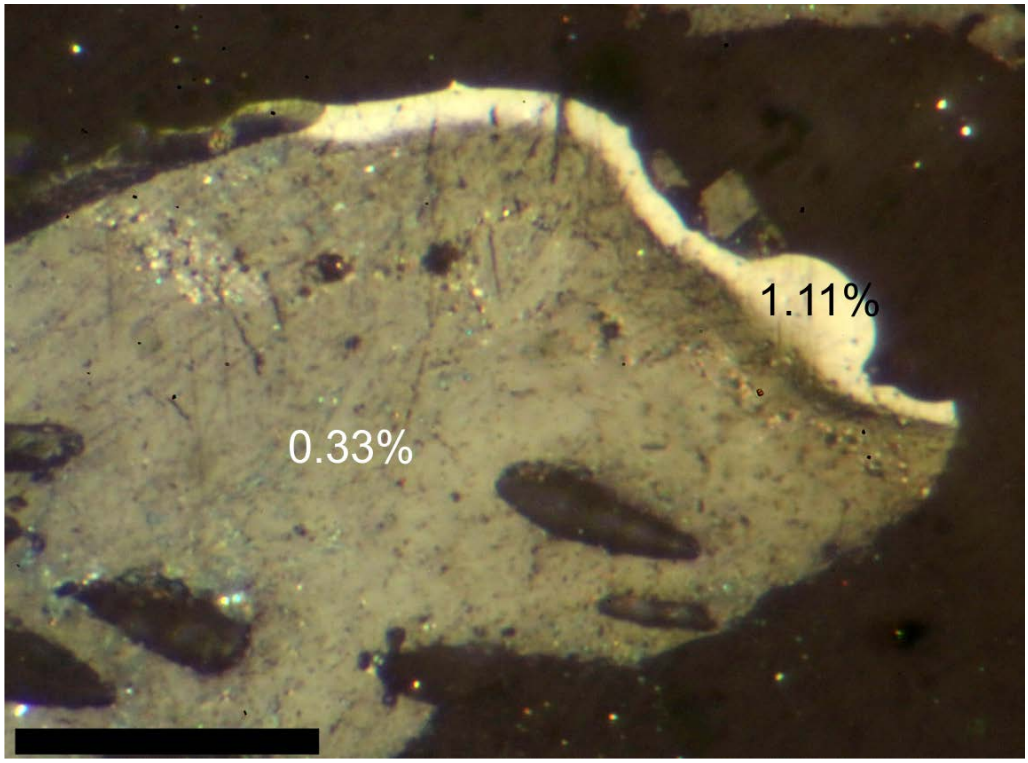

Figure 1.12: Incident light photomicrograph of the surface of a polished charcoal pellet, showing varied levels of reflectance (= fusinization) at the sub-mm scale in a fragment of modern, artificially produced charcoal. Scale bar = 32.5 µm.

Secretinite (Fig. 1.8D) was also formerly included within sclerotinite (Taylor *et al*. 1998); its properties are similar to those of funginite, but it lacks clear fungal-body morphology (ICCP 2001). The origin of this maceral is uncertain; it may derive from resin 'rodlets' (Kosanke and Harrison 1957, or as a secretion of medullosan seed ferns (Lyons *et al*. 1982, 1986; Lyons 2000). Secretinite has the widest range of reflectance of any inertinite-group maceral, at its lowest only slightly higher than vitrinite and at its highest exceeding that of fusinite (ICCP 2001). It is assumed that this indicates varying levels of inertinization (transformation of the precursor material into inertinite), and the maceral is often associated with the macrolithotype fusite (Kosanke and Harrison 1957; Lyons 2000). The assumption that this is the result of oxidation/degradation, rather than fire activity, is incorrectly attributed by the ICCP (2001) to Kosanke and Harrison (1957), who noted variable inertinization but did not address the question of how this came about. Lyons *et al*. (1986) also did not address the issue, but Lyons (2000) speculated, due to the common association with fusite, that the maceral might be of wildfire origin. Thus there is

currently no evidence that oxidation/degradation plays a part in the formation of this maceral.

Macrinite (Fig. 1.8E) is possibly the least well understood inertinite-group maceral in terms of its origins, and has been variously identified as an oxidation product of early-stage peat, a metabolic product of fungi and bacteria or derived from coprolites (Stach *et al*. 1982; Goodarzi 1985; Hower *et al*., 2011). Much of the discussion has focused on identifying its precursor(s), rather than the means by which inertinization occurred; the idea that macrinite derives from oxidative decay rather than pyrolysis appears to have originated with Timofeev and Bogoliubova (1964), though they referred to it as 'gelofusinito-collinite' and did not provide illustrations. Goodarzi (1985) reported a gelinite–macrinite transition in the Hat Creek coal deposits, corresponding to an increase in rank from lignite to subbituminous coal. The distinction was made based on reflectance, but at every rank examined the reflectance of the gelinite/macrinite was higher than the corresponding vitrinite. On this basis, under the ICCP (2001) definition all of this material would be classed as macrinite, with a wide range of reflectance as expected for that maceral. Even if gelinite is accepted as a precursor to macrinite, this does not in itself provide any information on the cause of inertinization. The assumption that the macrinite in that example formed through oxidation (Goodarzi 1985) rather than pyrolysis was based on its supposed association with 'oxyfusinite' (= degrado-fusinite) – now understood to be standard, pyrogenic fusinite. As it stands, there is no evidence to support a non-pyrogenic origin for macrinite.

Micrinite (Fig. 1.8F) is identified as inertinite based on its reflectance, but is actually a collective term for very small (≤ 2µm) particles with a variety of origins (Stach *et al*. 1982; Teichmüller 1987b; Taylor and Liu 1989; Taylor *et al*. 1998). Although some is likely fragmented inertinite (Taylor and Liu 1989; ICCP 2001), Transmitted Electron Microscopy (TEM) analysis suggests that the high reflectance is the result of interference effects caused by the very small particle size (Taylor and Liu 1989; Taylor *et al*. 1998). Although not wholly pyrogenic, the extremely small size of this maceral excludes it from this analysis (see Materials and Methods) and it will not be considered further here.

Inertodetrinite (Fig. 1.8G) is composed of the fragmented remains of other inertinite-group macerals, chiefly fusinite and semifusinite (ICCP 2001). As such, the preceding arguments apply equally to this maceral and a non-pyrogenic origin can be therefore be discounted.

1.5 Testing the models: establishing a new Silurian–Carboniferous charcoal dataset

This thesis is the result of a NERC-funded PhD studentship, tied to a NERC standard grant, *Evolutionary rise of deep rooting forests and enhanced chemical weathering: Quantitative investigations into the current paradigm*. The primary studentship research hypothesis is that:

"The spread of forests significantly increased the production and retention of atmospheric oxygen by fuelling increasing organic carbon burial to fundamentally alter biotic regulation of Earth's O_2 concentration and that this is recorded in the abundance of fossil charcoal."

In order to create a new, high-resolution Silurian–Carboniferous charcoal time-series with which to validate existing palaeoatmosphere models and test this hypothesis, organic concentrates and unprocessed shale samples from the palynological collections of the Universities of Southampton and Sheffield were supplemented with new material collected during field expeditions to central Bolivia, New York State and Pennsylvania, USA, and east Fife and Northumbria, UK; additional material was provided on loan by the New York State Museum, Albany. The use of DOM from clastic sedimentary rocks allowed previously under-sampled intervals, such as the Middle Devonian, to be examined in greater detail; opportunistic collection of Carboniferous coals from Northumbria and east Fife also allowed a comparison between DOM and coal inertinite records, and with parts of the existing coal-based charcoal time-series of Glasspool *et al*. (2015).

Thesis outline

This thesis is divided into four main chapters. Following this introduction, Chapter 2, *Identifying and quantifying charcoal in the fossil record: materials, methods, and rationale* provides a discussion of the problems associated with quantitative charcoal analysis, an

evaluation of existing approaches, and a detailed description and rationale for the methods adopted in this study. Chapters 3–5 examine wildfire activity as recorded by DOM inertinite during the Devonian, Early to Mid-Mississippian, and Late Mississippian to Early Pennsylvanian, respectively, each addressing a chapter-specific hypothesis:

Chapter 3: *that a 'charcoal gap' exists from the late Emsian to the early Famennian, indicating that wildfire activity was significantly supressed by a reduction of atmospheric* pO_2.

Chapter 4: *that 'Romer's Gap' represents a genuine bottleneck in tetrapod diversity caused by global hypoxia following the End Devonian Mass Extinction (EDME), resulting in a significant reduction in wildfire activity during the Tournaisian.*

Chapter 5: *that there was a progressive increase in* pO_2 *during the Carboniferous which is reflected by a corresponding increase in wildfire activity and is associated with arthropod gigantism.*

This is followed by an analysis, in chapter 5, of the dataset in its entirety: comparisons are made with the coal inertinite data of Glasspool *et al*. (2015) and O_2 model predictions, and the implications of the observed fire history for the primary research hypothesis are discussed.

2. Identifying and quantifying charcoal in the fossil record: materials, methods, and rationale

In the previous chapter the main methods used to identify charcoal in coals and clastic sedimentary rocks were outlined, and some of the known advantages and drawbacks of each method were discussed. An important methodological choice, made at the planning stage (i.e. before commencement of the studentship) was whether to use transmitted or incident light microscopy; the decision to opt for incident light was in part pragmatic, because suitable facilities were available at Southampton, but was also logical in that it followed the methodology of the most relevant prior work (at that time, Glasspool and Scott 2010). It was also felt that charcoal could be more reliably and quickly identified by following the well-established protocols used in standard coal petrology.

In attempting to apply these methods to DOM rather than coal, standard preparation methods and counting protocols were found to be inappropriate and had to be modified. As the work progressed it was gradually realised that in many ways inertinite is poorly defined, and that the complex factors affecting maceral reflectance are not all well understood; these issues were investigated where possible. In addition to describing the materials and methods used, this chapter details those modifications and investigations, and provides a rationale for the approach that was ultimately adopted.

2.1 Sample preparation and analysis

Extraction of DOM

After manual crushing to a coarse powder, between 5 and 10 g of each shale sample was treated for 24 hours with 37% hydrochloric acid solution (HCl), neutralised, and then for 48 hours with 60% hydrofluoric acid solution (HF) to remove carbonate and silicate minerals, respectively. Although particle size of the crushed material was not controlled, bias due to differential fragmentation of the constituents is considered highly unlikely due to the very small size of the macerals (i.e. c. 20 µm). After neutralisation of the HF, the resulting organic residue was wet-sieved using a 15 µm nylon mesh and decanted into a glass beaker. Secondary fluorides were removed by boiling for approximately 60 seconds

in 37% HCl solution, following which the resulting organic residue was sieved for a second time and finally decanted into vials. This extraction procedure follows standard palynological demineralization techniques (see e.g. Wood *et al*. 1996) except that oxidation is not employed; the use of shales is standard in studies of DOM, since they typically contain a higher proportion of organic matter than other sedimentary rocks (Tucker 2001).

Assessment of thermal maturity

Because of the complicating effects of high thermal maturity on maceral reflectance (and hence inertinite identification; see section 2.2, below), test samples (typically the stratigraphically lowest, middle, and highest sample from each section) were mounted on transmitted light slides so that each locality could be assessed for thermal maturity before samples were prepared for incident light microscopy. Samples were transferred by pipette as an aqueous suspension (using de-ionised water) to standard 22 x 22 mm glass coverslips, and left to dry overnight. The coverslips were then affixed face-down to standard glass microscope slides using an acrylic resin, Elvacite; after another 24 hours, the slides were ready for examination using a standard palynological microscope. Samples scoring 9 or higher on the Spore Colour Index (i.e. dark brown to black; Collins 1990), indicating $R_v \geq 2.0\%$ (Marshall and Yule 1999) were rejected for analysis.

Mounting of organic residues for incident light microscopy

Production of polished slides followed the approach of Hillier and Marshall (1988), with some modifications. An 18 x 18 mm glass coverslip was coated on one side with Electrolube PTFE spray, and left to dry for around 45 minutes. The sample was then transferred by pipette as an aqueous suspension (using de-ionised water) to the coated side and left to dry overnight. Once dry, the coverslip was affixed to a frosted 1.0–1.2 mm thick glass slide using Fastglas epoxy resin; the frosted surface strengthens the bond between resin and glass, and reduces the likelihood that the cover slip will detach from the slide during polishing. After 90 minutes, while the resin is still slightly soft, the coverslip was carefully removed using a razor, leaving most of the sample embedded in the resin. After 24 hours, once the resin had hardened fully, the surface was cut down by hand using Buehler silicon carbide grinding paper (grade P2500), then polished by means

of a Kemet Forcipol 300 L lapping machine using successively finer Buehler aluminium oxide powder ('coarse', 9.5 µm; 'medium', 3.0 µm; 'fine', 0.05 µm). Polishing time was 20 seconds (grinding paper), 120 seconds (coarse powder), and 80 seconds (medium and fine powder), split evenly between clockwise and anti-clockwise motion. Finally, the slide was washed thoroughly using de-ionised water.

Preparation of coal samples for incident light microscopy

Coal samples were crushed and passed through a 2 mm sieve; the resulting < 2 mm powder was mixed with Fastglas epoxy resin to produce coal pellets 2 cm in diameter and c. 1 cm thick. Polishing was by hand using grinding paper and powder as for polished slides, but without water as this was found to cause swelling and cracking of the coal particles.

Preparation of charcoal samples for incident light microscopy

The preparation procedure for charcoal specimens was identical to that of coal, except that Epoflow epoxy resin was used instead of Fastglas. Epoflow is a less viscous, higher quality resin which has superior penetrative abilities.

Measurement of maceral random reflectance in oil (R_r)

In petrographic terms, 'random' reflectance is measured randomly with respect to bireflectance, which correlates with thermal rank; macerals of higher rank have been buried more deeply, experienced greater load pressure, and hence are more anisotropic (Teichmüller 1987b). Rotation of the microscope stage under polarized light allows the Rmin and Rmax to be determined, and Rmax values are routinely quoted in older literature; the use of Rr is significantly less time consuming, less subjective, and is favoured by the International Committee of Coal and organic Petrology (see e.g. ICCP 1998, 2001). Reflectance values quoted in the present study are random in this sense, unless otherwise stated.

Reflectance measurement was by means of a Zeiss UMSP 50 Microspectrophotometer, housed in the School of Ocean and Earth Science, National Oceanography Centre Southampton, University of Southampton Waterfront Campus. Measurements were

made under standard conditions as defined by the International Committee for Coal Petrology (ASTM, 2014): measured light wavelength was 546 nm and an oil-immersion objective was used (Zeiss EPIPLAN 40/0.85 Pol with Zeiss immersion oil, n_e = 1.518 ± 0.0004 at 23°C). A halogen light-source (Hal 100, 12V, 100W; run at 11.8V to extend bulb life) regulated by a Farnell Stabilised Power Supply unit provided incident light; a Zeiss epi-condenser II P with a pin-hole field diaphragm limited the effect of stray light on measurements. Slides were mounted on a motorised stage equipped with a digital position monitor precise to 0.25 µm. The grating monochrometer utilised a standard H-Pl-Pol (Zeiss) reflected light prism set at 547 nm. The intensity of reflected light was determined by means of a photomultiplier tube (HTV R 928), run from a stabilised power source and equipped with a low drift amplifier. A photometer attachment translates the radiant flux from the photomultiplier into electrical signals; these are then interpreted by the MPC64 Control unit which also controls the various shutters, filters, and diaphragms in the microscope. Communication with the MPC unit was via an Olivetti M250E computer running MS-DOS 3.30a, using the reflectance measurement programme 'CHIT', written by S. J. Hillier and John Marshall in GW-BASIC 3.22 programming language. The photometer system was calibrated using a diamond standard, of reflectance 5.227%. Incident-light photomicrographs and standard photographs were by means of a Canon SLR, with Zeiss microscope camera adaptor as required; composite images were compiled using Helicon Focus v. 6.6.1. Figures were produced using Adobe Photoshop CS5 and CorelDraw X6.

Phytoclast selection

Slides were traversed horizontally at vertical intervals of 500 µm until 500 reflectance measurements had been made. All phytoclasts within the field of view (200 µm) were measured on each traverse. Where the volume of palynological material was low and < 500 phytoclasts were encountered, a second slide was produced; if < 250 were encountered the sample was deemed unproductive and disregarded.

2.2 Data analysis

Recognising inertinite under incident light

The International Committee for Coal and Organic Petrology (ICCP) currently defines inertinite as "a maceral group that comprises macerals whose reflectance in low- and medium-rank coals and in sedimentary rocks of corresponding rank is higher in comparison to the macerals of the vitrinite and liptinite groups." (ICCP 2001; p. 459). Thus, identification is only possible with reference to vitrinite or liptinite-group macerals in the same sample. Unfortunately, the ICCP defines *vitrinite* as "a group of macerals whose colour is grey and whose reflectance is generally between that of the associated darker liptinites and lighter inertinites over the rank range in which the three respective maceral groups can be readily recognized." (ICCP 1998, p. 350). These definitions are therefore circular with regard to reflectance, which is why, although it is possible to measure the reflectance of a target maceral with a high degree of precision, inertinite cannot be identified with reference to an absolute reflectance value unless the thermal rank (and hence expected vitrinite reflectance (R_v) of the sample) is known. The ICCP is silent on the matter of high-rank coals; because the vitrinite group follows a steeper coalification track than inertinite, R_v surpasses R_i between 3.25 and 5.25% R_v (Teichmüller 1987a). This means that, strictly speaking, the two maceral groups swap places when coalification reaches the meta-anthracite stage, which is clearly not the intent of the ICCP definitions.

Identifying inertinite on morphological grounds is equally problematic. While some inertinite-group macerals (e.g. fusinite, semifusinite, and funginite; Fig. 1.8A–C) have a distinctive form, others (e.g. macrinite, micrinite, and inertodetrinite; Fig. 1.8E–G) do not. Adopting a more restricted definition of inertinite in which only easily recognisable maceral types are included would not be appropriate, because micrinite and inertodetrinite are believed to originate at least partly from the fragmentation of other inertinite macerals (Stach *et al*. 1982; ICCP 2001), which is assumed to increase as a function of transport distance (see section 2.6).

Phytoclast reflectograms

Because inertinite cannot be identified with reference to an absolute reflectance value, several authors have investigated the use of relative reflectance to differentiate the three major maceral groups (exinite, vitrinite, and inertinite; McCartney *et al*. 1971; Spackman *et al*. 1973; Kojima *et al*. 1974; Davis 1975; Hoover *et al*. 1976; Hoover and Davis 1979, 1980). In this method the reflectance of all phytoclasts in a specimen (or rather, a representative subsample) is measured, and presented as a reflectogram (e.g. Fig. 2.1); peaks on the reflectogram are identified, either by eye or using curve fitting algorithms, and assigned to maceral groups. This establishes absolute reflectance values, unique to the particular sample under investigation, which serve to distinguish one maceral group from another. Where maceral groups are identified by curve-fitting algorithms, integration of those curves then allows the relative proportions of the different maceral groups to be determined; however, in the simple example below (coal sample T15_13), a reflectance value (R) of 0.85% is deemed by eye to mark the transition from vitrinite to inertinite. Thus, a simple count of the number of macerals with R > 0.85% allows the amount of inertinite, relative to total phytoclasts (i.e. the proportion of phytoclasts which have been burned), to be calculated:

$$\text{Relative inertinite abundance (\%)} = (n(R > 0.85\%)/n)*100$$

$$= (195/500)*100 \qquad [3]$$

$$= 39.0\%$$

Equation 3: example calculation of relative inertinite abundance from phytoclast reflectogram for coal sample T15_13. n(R > 0.85%), number of phytoclasts with R > 0.85%; n, total number of phytoclasts.

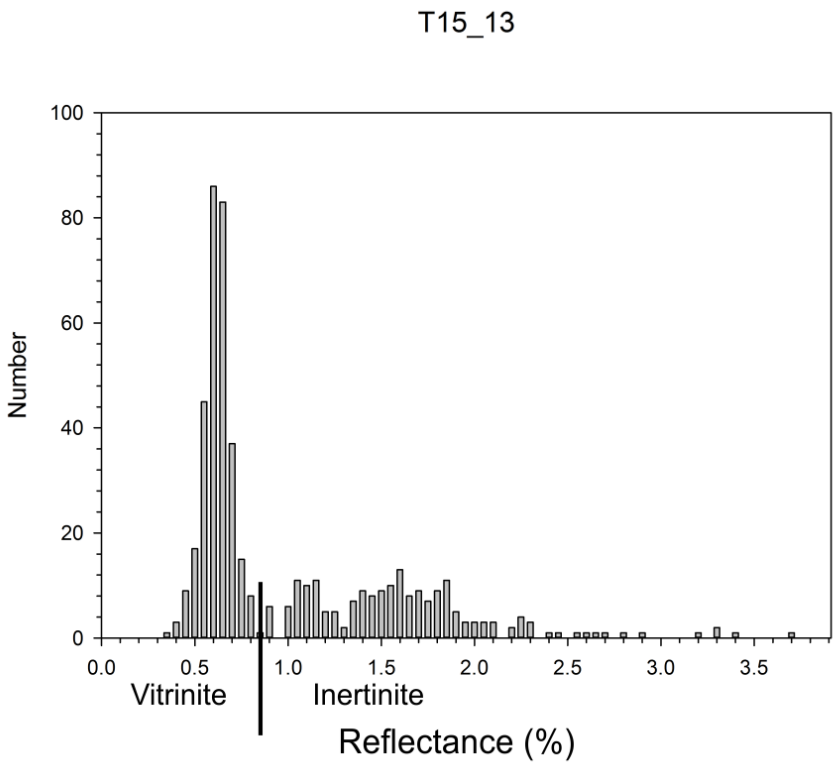

Figure 2.1: Reflectogram showing phytoclast reflectance profile for coal sample T15_13 (Bottom Hutton Coal, Tynemouth, Westphalian B). Black bar indicates separation, judged by eye, between vitrinite and inertinite. Based on Eq. 3, the sample comprises 39.0% inertinite.

Assertions of a clear and consistent separation in the reflectance of maceral groups (e.g. Hoover and Davis 1980; Taylor *et al*. 1998) may be suspect, because identification/selection for measurement in those studies was visual, and partly dependant on subjective judgements of reflectance (raising the possibility of circular reasoning). Nevertheless, there was reasonable agreement when this approach was compared against results obtained by standard point-counting (Hoover and Davis 1980).

This technique requires that there is a sufficient relative abundance of vitrinite and that median R_v is sufficiently distinct from median R_i in a sample to provide a clear peak on the reflectogram. Where these conditions are not met the reflectogram becomes much less tractable because, unlike vitrinite, the reflectance of inertinite does not follow a normal distribution (Taylor *et al*. 1998). This is because, whereas vitrinite reflectance is determined by thermal maturity (i.e. temperature at maximum burial depth, which affects the entire sample equally), inertinite reflectance is determined by the maximum

temperature experienced during pyrolysis. Natural wildfires exhibit significant small and medium-scale variations in temperature, often exhibiting a 'mosaic' burn pattern (Scott *et al*. 2014); hence, charcoal incorporated into sedimentary rocks will exhibit a variety of reflectance values. While reasonable for coals, in which vitrinite is often the most abundant component, it was soon found that these assumptions often do not hold for reflectograms produced from dispersed organic matter. In this situation, it becomes difficult to distinguish low-reflecting inertinite from vitrinite (Fig. 2.2), and reflectograms become ineffective.

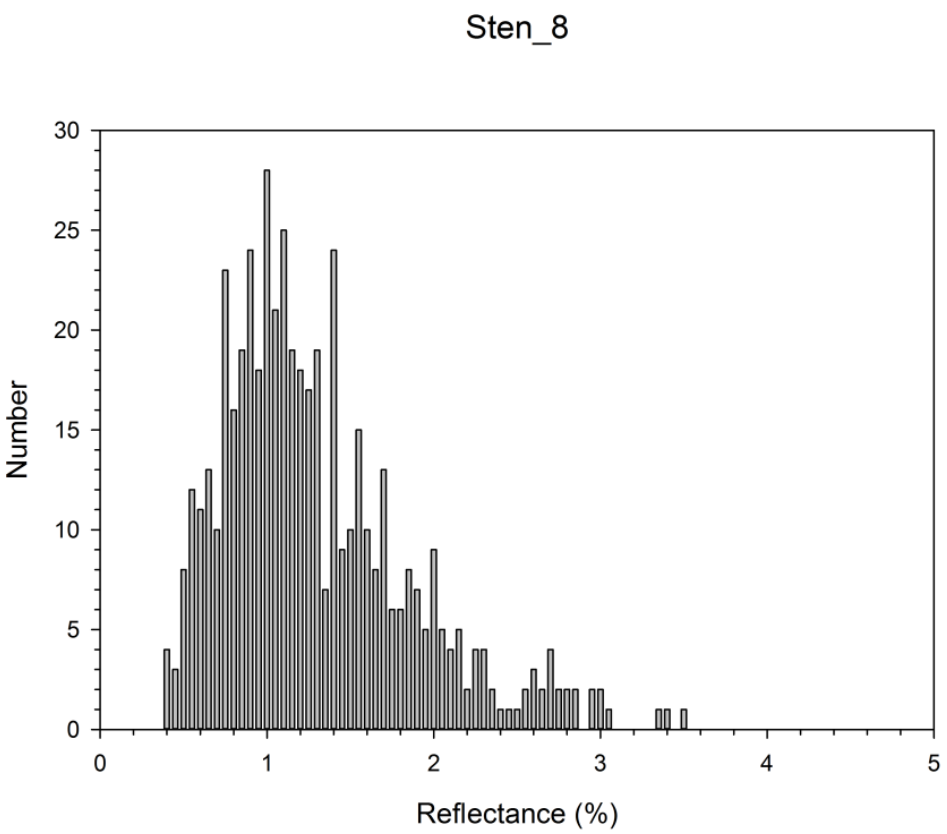

Figure 2.2: Reflectogram showing phytoclast reflectance profile for DOM extracted from shale sample Sten_8 (Stensiö Bjerg, Famennian). Strongly overlapping maceral reflectance profiles result in a mixture distribution.

Mixture distributions

Reflectograms such as that of STEN_8 (Fig. 2.2) occur when two populations with strongly overlapping reflectance distributions are superimposed, creating a 'mixture distribution'. To disentangle such mixtures in the absence of any other information that might allow the populations to be distinguished requires the application of a 'finite mixture model',

which is in essence a type of model-based cluster analysis (Everitt and Hane 1981; Benaglia *et al*. 2009). Finite mixture models commonly employ Maximum Likelihood Estimation (MLE), a probabilistic approach that seeks to identify the most likely true distribution which underlies the observed data; this method is widely used when the shape of the component distributions is unknown (Hunter *et al*. 2007).

The R package 'mixtools' provides an array of functions for analysing mixture distributions. The 'normalmixEM' function employs MLE, using an Expectation Maximisation (EM) algorithm; EM is a well-established approach, which has been applied to specific cases at least since Hartley (1958) and was explored in detail by Dempster *et al*. (1977). Though it operates in much the same way as the 'em' function of the model-based cluster analysis MCLUST (Fraley and Raftery 2006), normalmixEM allows the shapes (e.g. means, variance) and mixing proportions of the component distributions to be left undefined. To perform the analysis, a data matrix containing raw data (in this case 500 maceral reflectance measurements) is first imported into R. The function first produces a histogram of the data, then fits a two-component density plot representing the most likely reflectance distributions of the components. The mixing proportions (i.e. relative contribution of each component to the total) are then calculated automatically by integration of the curves; these are returned, along with basic statistical descriptions of each component (e.g. mean, σ, etc.).

MLE algorithms such as EM assume the mixture components are normally distributed. As previously noted, although this assumption is sound for vitrinite it is likely to be violated by inertinite (Taylor *et al*. 1998; see *Phytoclast reflectograms*, above). Nevertheless, when run using the minimum possible prior assumptions (i.e. lambda, mu, sigma, mean.constr, and sd.constr all left undefined; for annotated example code see SI 2.1) the 'normalmixEM' function was found to return results relatively similar to those determined 'by eye' using Eq. 3 for reflectance distributions in which a vitrinite peak was clearly visible; in the example below (Fig. 2.3A), the function returned a result of 74.4% inertinite, compared to a 'by eye' estimate of 63.8% (Fig. 2.3B).

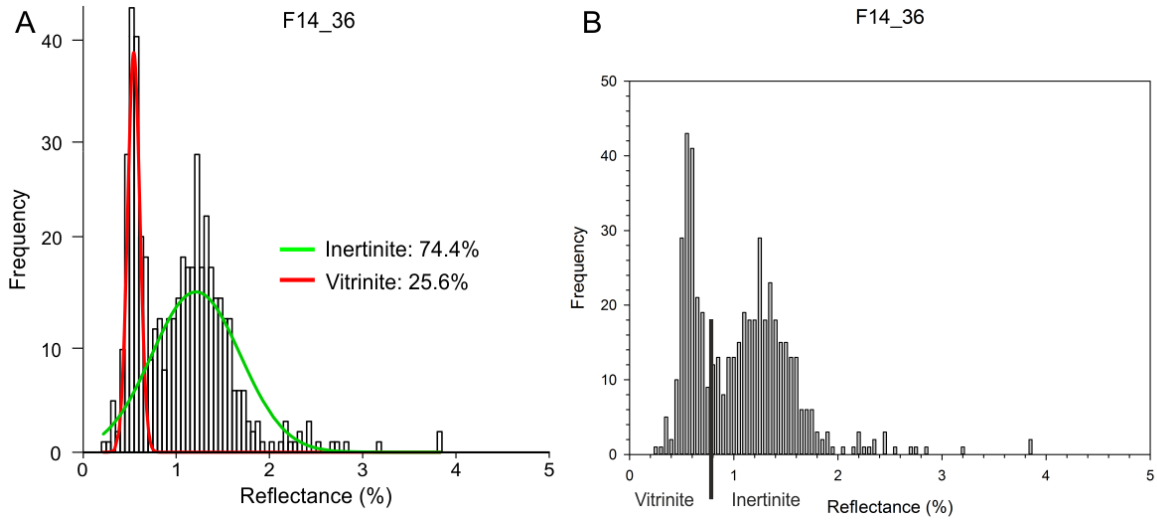

Figure 2.3: Comparison of inertinite abundance estimates provided by normalmixEM function (A) and reflectogram shape (B), for shale sample F14_36 (Fife, Viséan). Red/green curves (A) indicate density plot output of normalmixEM; position of black bar (B) is subjective, based on reflectogram shape.

Next, the function was applied to a more difficult sample, NYS14_71. Separate measurement runs of 500 random macerals and 50 vitrinite (insofar as it could be identified from maceral colour; see *Recognising inertinite under incident light*, above) indicated very similar means of 1.89% and 1.81%, respectively; quantifying each maceral group by eye from the reflectogram shape is impossible (Fig. 2.4).

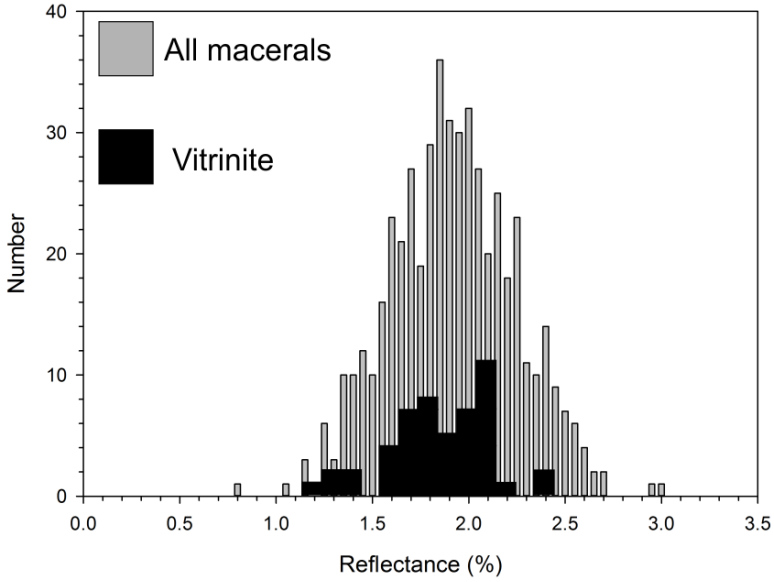

Figure 2.4: Phytoclast and vitrinite reflectograms for shale sample NYS14_71 (New York State, Givetian) superimposed, showing complete overlap of inertinite and vitrinite reflectance profiles.

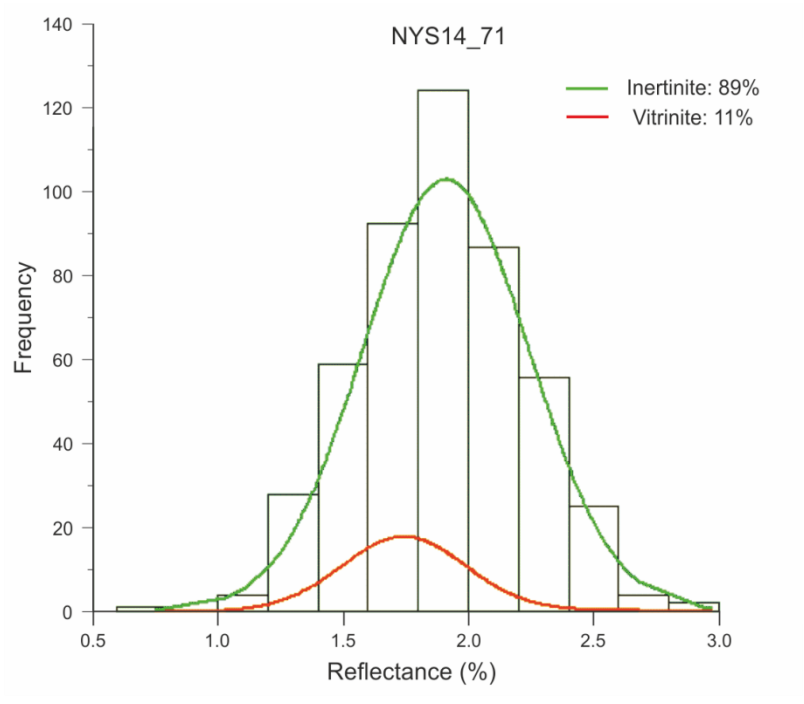

Figure 2.5: output of normalmixEM function for shale sample NYS14_71 (New York State, Givetian).

Applying the normalmixEM function results in the output shown in Fig. 2.5. In this solution, the mean reflectance of the 1st component (= vitrinite) was 1.74%, and of the 2nd (= inertinite) was 1.91%; these components comprised 11 and 89% of the total phytoclasts, respectively. Encouraged by these results, the comparison was extended to a selection of 26 samples, with various levels of thermal maturity. As before, approximate R_v was measured and the measured data compared against the output of the normalmixEM function; the results show a strong positive correlation (Pearson r = 0.893, p = <0.01), with a mean discrepancy of +0.25% R_v for the normalmixEM values (Fig. 2.6, SI 2.2). Interestingly, the largest discrepancies were associated with those samples for which the measured R_v did not produce a normal distribution as expected for vitrinite; this suggests the error may lie in the measured values, rather than the mixture model output.

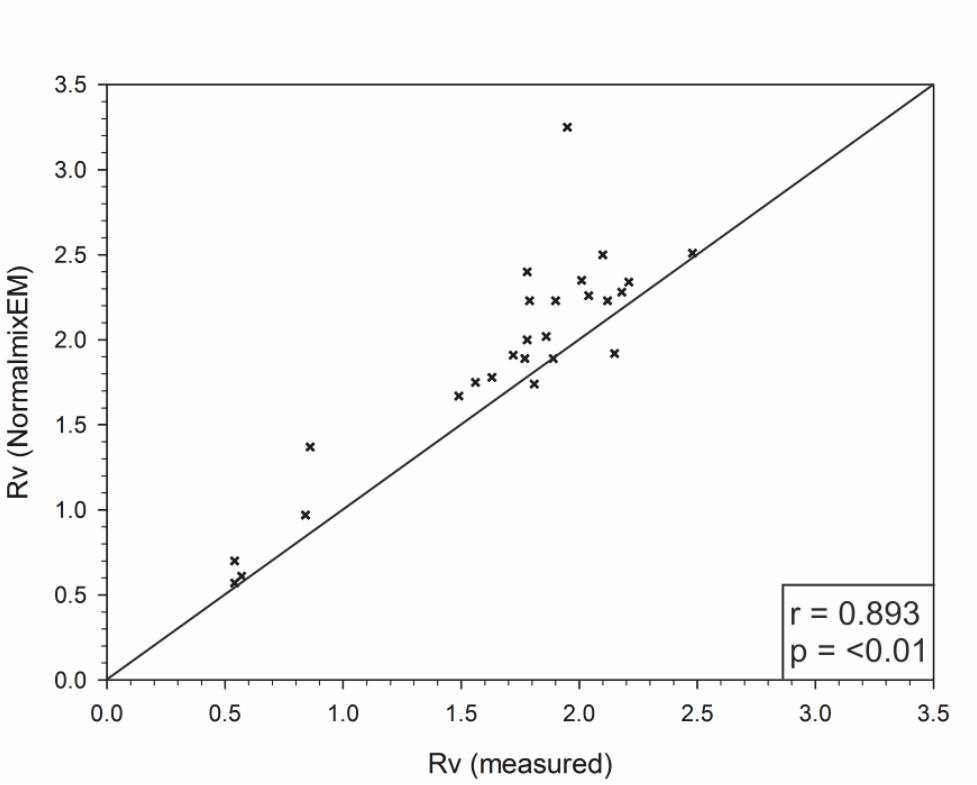

Figure 2.6: Comparison of normalmixEM estimate for R_v with measured values; 1:1 line added for reference. Pearson r = 0.893. For raw data and list of samples, see SI 2.2.

The consistently good fit between measured and estimated values for both simple and complex reflectograms suggests that this method is appropriate for use with DOM, where more traditional approaches are demonstrably ineffective.

Additional statistical analyses

Statistical analyses of results were performed using SigmaPlot 13.0. Comparisons of the means of normally distributed datasets were conducted using either an unpaired t-test (two groups), or a one-way ANOVA (multiple groups). One-way ANOVA was followed by pairwise comparison using the Holm-Sidak test. If the data were found to be non-normal (i.e. failed a Shapiro-Wilk normality test), non-parametric equivalents were used (Mann-Whitney Rank Sum test/Kruskal-Wallis one-way ANOVA on ranks with Dunn's pairwise comparison). Similarly, correlations were tested using either the Pearson Product Moment Correlation Coefficient or its non-parametric equivalent, the Spearman Rank Correlation Coefficient. When assessing the results of these tests, P values <0.01 were considered significant and ≤0.05 were considered marginally significant. Data files containing raw data, logs of the tests performed and their outcomes can be found in the attached supplementary information CD. Further details are provided in the results section of each chapter.

Measurement protocol 1: maceral selection

Given the impracticality of identifying each of the many thousands of individual macerals distributed on a standard cover slip, a search protocol is required whereby a subset are examined and conclusions extrapolated for the whole population. If the maceral types are evenly distributed, the location of the particles measured is irrelevant and the number of measurements is determined by the desired precision, e.g. 500 measurements would allow relative abundances ≥ 0.2% to be detected (because (1/500)*100 = 0.2). If the distribution is *not* even, the problem becomes less tractable; mathematically, random point-counting is the most statistically valid approach in this situation (Chayes 1956; Cochran, 1977) but this is only practical where macerals are contiguous (e.g. in polished coal blocks). For polished slides of DOM, where the organic concentrate is added in suspension by pipette and allowed to settle, many of the randomly selected points would fall on empty space (Fig. 2.7) and so achieving enough measurements would take a prohibitive amount of time. Thus, the transect method adopted here is the only practical option.

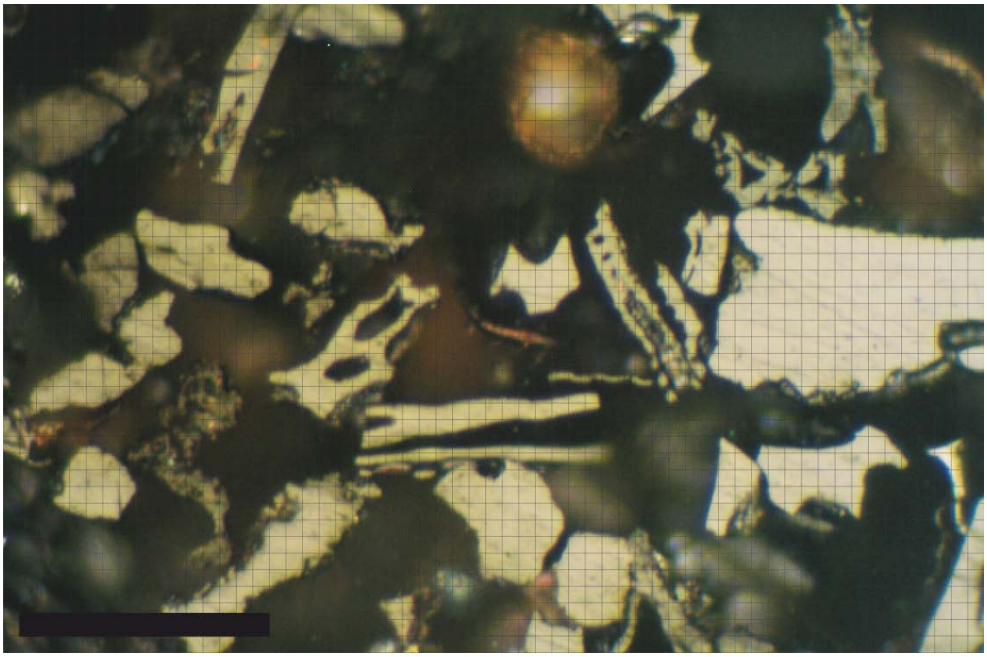

Figure 2.7: Incident light photomicrograph, showing densely clustered DOM on polished slide. 58% of grid squares cover empty space between macerals. Scale bar = 30 µm.

Organic particles in suspension do not necessarily settle evenly on a cover slip (J. Marshall, *pers. comm*., 2013) and it is possible that differences in density and structure between and within maceral types (e.g. due to different formation temperatures in charcoals) would cause different settling behaviours; if true, maceral distribution would be uneven. To address this issue, a closely spaced series of transects was conducted on a polished slide known to contain inertinite (shale sample MV_6), and the location and reflectance of each of the macerals encountered was noted. Overall the macerals formed a broadly circular shape with a lower concentration in the centre, but the distribution of higher reflecting particles within that shape appears to be random (Fig. 2.8; SI 2.3).

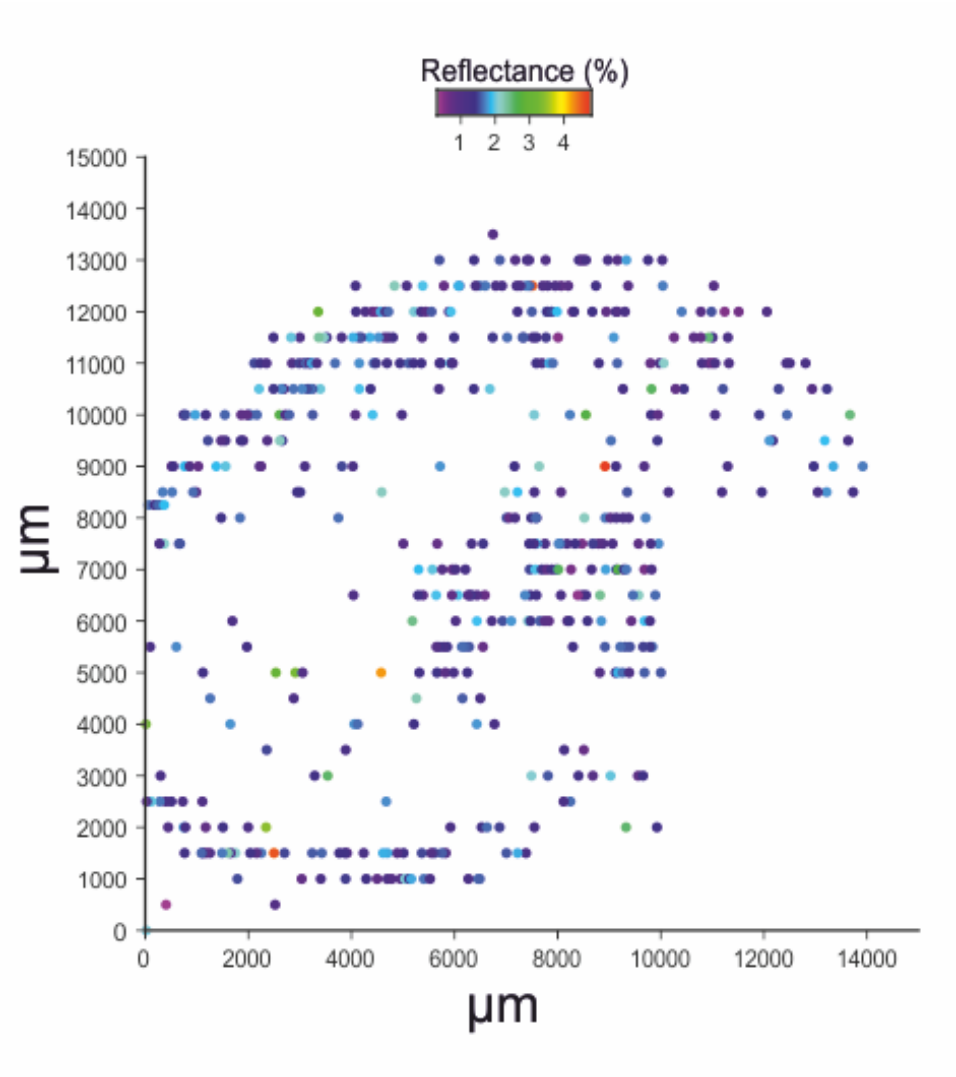

Figure 2.8: Maceral settling pattern and reflectance, mapped out on standard coverslip.

Measurement protocol 2: quantification

Microscope quantification techniques, whether using incident or transmitted light, involve either point counting (Clark 1982; Mooney and Tinner 2011), manual and computer-assisted area measurement (using an ocular grid and image analysis software, respectively; MacDonald *et al*. 1991), or estimation of volume (Weng 2005). Direct comparisons of these methods have been inconclusive: in some studies the differences in results were minimal (Tinner and Hu 2003; Ali *et al*. 2009), and in others significant (Leys *et al*. 2013). Logically, direct measurement of volume should be the most accurate method, but this is technically difficult and time-consuming; instead, volume is normally estimated based on area measurements (Weng 2005). The calculations which underpin

these estimates have been questioned on theoretical grounds, but appear to be fairly robust when tested empirically (Crawford and Belcher 2016).

2.3 Relationship between fusinite and total inertinite

During charring, organic carbon undergoes progressive aromatisation and graphitisation, causing reflectance to increase as a function of temperature and time (Franklin 1951; Jones *et al*. 1991; Scott and Glasspool 2005; Cohen-Ofri *et al*. 2006; Scott *et al*. 2014). As previously noted, wildfires typically involve the combustion of a variety of fuel types and pass through several stages that may not occur simultaneously in every area, thus temperature and burn duration may vary quite significantly between different parts of a fire, and 'mosaic' burn patterns are common (Scott *et al*. 2014). As a result, charcoal produced by a single fire exhibits a wide range of reflectance values which do not follow a normal distribution; for example, samples collected following a modern heathland fire (Scott *et al*. 2000) varied from 0.13 to 6.22% R_i. This is consistent with the reflectance range of inertinite-group macerals, and indicates that the distinction between fusinite and semifusinite is arbitrary; on this basis, Scott and Glasspool (2007) proposed a value of 1.5–2.0% R_i (representing a maximum charring temperature of c. 400°C) to distinguish the two macerals. Adopting this definition would provide a simple way for fusinite to be quantified, which could be applied regardless of vitrinite abundance, provided that the thermal maturity of the sample is low enough that Rv does not exceed c. 1.0%.

If fusinite abundance could be shown to be a good predictor of total inertinite, this approach would provide a simple way to quantify charcoal. Previous work comparing fusinite and semifusinite in Carboniferous–Recent coals (Robinson 1991, Fig. 2.9) indicated some correlation, but also substantial discrepancies between 300 and 150 Ma. Robinson was careful to note the variable quality of the data (which was drawn from industrial reports) and the potential for bias in that it was largely restricted to economically useful coals, which may not be representative; the criteria by which semifusinite is recognised has also changed significantly since publication of that study (see section 1.4). To investigate the matter further, the inertinite and fusinite contents of selected high-vitrinite coals, carbonaceous shales and sedimentary DOM samples from Carboniferous successions in east Fife, Northumbria, and the Scottish Borders were

compared (Fig. 2.10). Samples selected for analysis were those in which vitrinite and fusinite could be readily distinguished in reflectograms (see Appendix 1); detailed locality information is provided in sections 4.1 and 5.1. A value of 2.0% was chosen to represent the transition from semifusinite to fusinite.

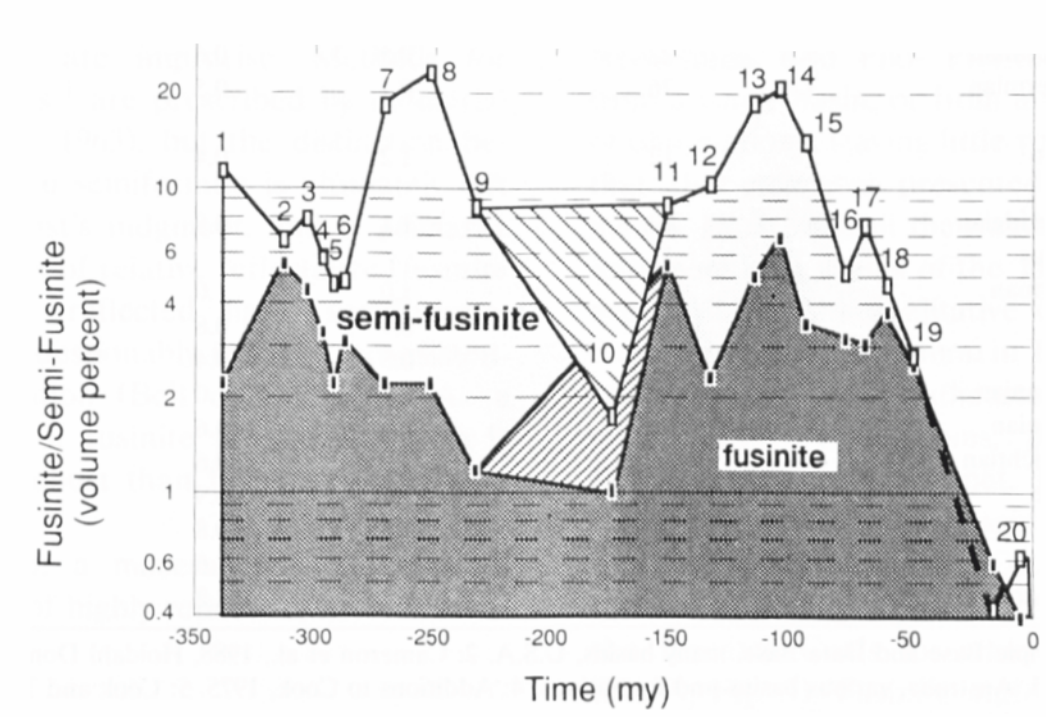

Figure 2.9. Trends in fusinite and semifusinite abundance through geological time, reproduced from Robinson (1991, fig.3) with permission from Elsevier.

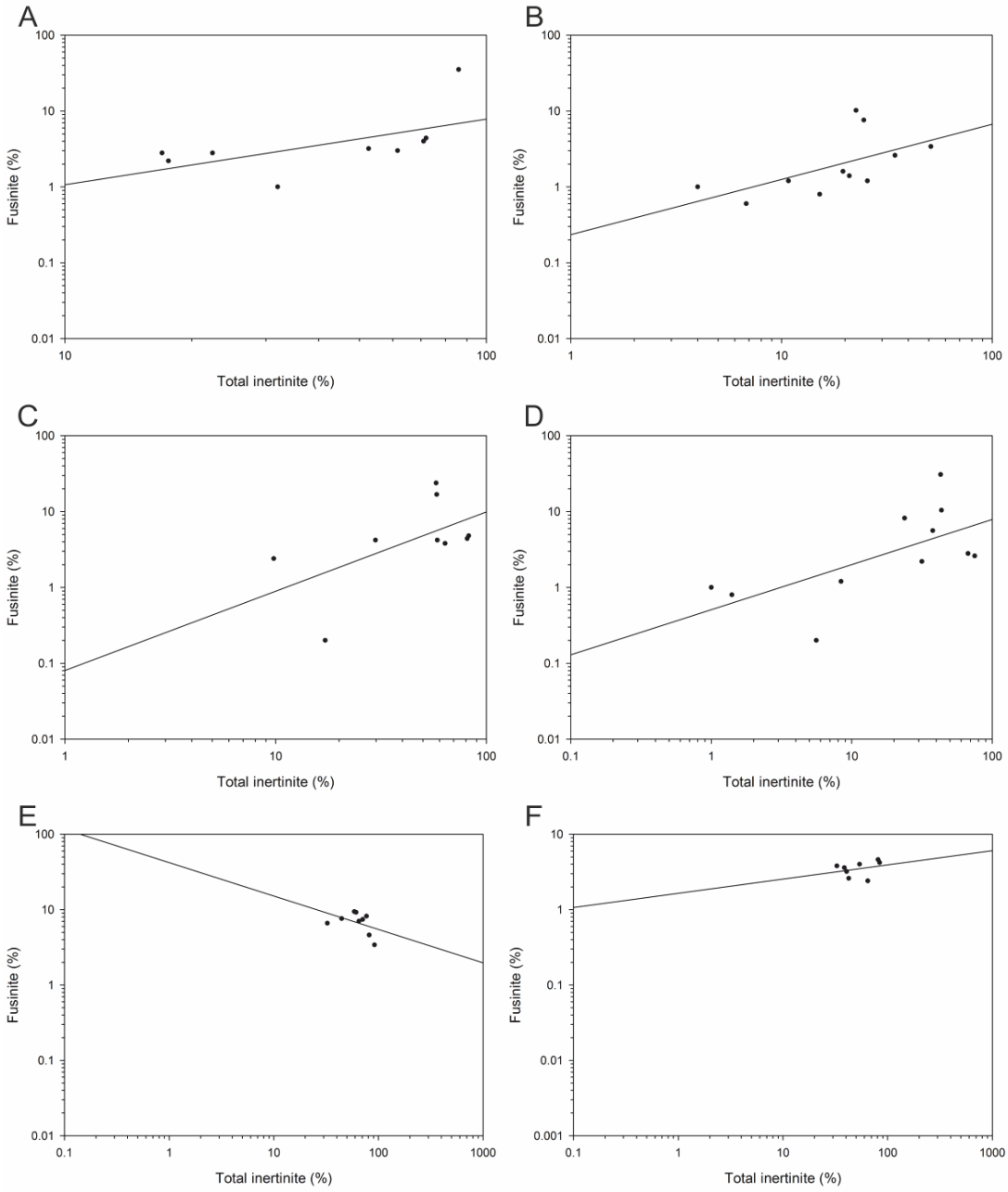

Figure 2.10: Scatter plots comparing Fusinite and total inertinite relative abundance and showing linear regression lines for high-vitrinite samples from Carboniferous successions in East Fife, Tynemouth, and Chirnside. For geological and biostratigraphical context for localities see sections 4.1 and 5.1. A, Fife carbonaceous shales; B, Fife DOM; C, Fife Coals; D, Tynemouth coals; E, Tynemouth DOM; F, Willie's Hole DOM.

Material	Mean inertinite (%)	Mean fusinite (%)	Correlation	P
Fife carb. shales	37.7	4.9	Rs = 0.93	$2x10^{-7}$
fife coals	19.9	2.8	Rs = 0.78	$2x10^{-3}$
Fife DOM	51.0	4.0	r = 0.28	0.47
Tynemouth coals	30.8	6.0	Rs = 0.68	0.02
Tynemouth DOM	64.9	6.7	r = -0.49	0.18
Willie's Hole DOM	54.8	5.0	r = 0.42	0.30

Table 2.1: Correlation coefficients for inertinite/fusinite abundance data. r, Pearson's Correlation; Rs, Spearman Correlation; P, P-value.

A strong and significant positive correlation was detected between fusinite and total inertinite for coals and carbonaceous shales, but not for DOM (Table 2.1; SI 2.4). Thus, while fusinite may be of value as a predictor of total inertinite in coals and carbonaceous shales, it does not appear to be effective for DOM.

2.4 Reflectance, fire intensity, and pO_2

For the purposes of the preceding discussion, the mean temperature of successive wildfires was assumed to be similar. In reality this is unlikely; modern fires vary quite widely in their intensity, and temperatures (as measured from above the flame tip) ranging from < 400–1200 °C have been recorded (Scott *et al*. 2014). Temperature variation in this case appears to be driven largely by vegetation type and fire type (i.e. ground, surface or crown fire; Scott *et al*. 2014). The relationship between temperature, heating duration and charcoal reflectance has been empirically determined (Jones *et al*. 1991; Scott & Glasspool 2005), allowing maximum temperature of charring to be calculated from reflectance, and the fact that fusinite abundance is a poor predictor of total inertinite abundance (see previous section) supports the view that fire temperature in successive fires is not normally distributed. Nonetheless, since fire correlates positively with oxygen supply (Belcher *et al*. 2010) it is worth considering the link between reflectance, fire intensity and pO_2.

Equating inertinite reflectance to the intensity of a natural wildfire is not trivial: intensity in this context refers to the time-averaged energy flux (Rothermal 1972) and, although it is reasonable to assume a correlation with flame temperature, the relationship is not

simple because, as mentioned above, wildfires are often highly heterogeneous. Despite this limitation, temperature estimates derived from mean charcoal reflectance following a modern heathland fire (Scott *et al*. 2000) were consistent with the expected temperature for a fire of that type (c. 400°C).

If it is accepted that charcoal reflectance provides at least a relative measure of fire intensity, there are further problems in linking this to atmospheric pO_2. Guo and Bustin (1998) demonstrated that fungal activity indirectly contributes to reflectance values, by making wood more susceptible to reflectance increase during charring; experimentally charred wood which had first been decayed by fungi was 10–50% more reflective than non-decayed wood. The cause was unclear; the authors speculated that dehydration, shrinkage and cracking provide an increased surface area. This also provides an additional argument against using fusinite as a proxy for total inertinite. More recently, Hudspith *et al*. (2014) recorded a strong link between charcoal reflectance and vegetative change during the Holocene, under presumed constant pO_2, suggesting that fire intensity over geological time is more likely to reflect evolutionary changes in plants than atmospheric O_2.

2.5 Maceral oxidation

Any process other than fire which affects maceral reflectance could potentially skew charcoal abundance estimates derived from phytoclast reflectance data. 'Oxidation' in this context may refer to oxidative decay prior to or during early-stage diagenesis (e.g. formation of 'degradofusinite'; Stach *et al*. 1982, Taylor *et al*. 1998), oxidative weathering of coals or sedimentary rocks containing dispersed organic matter (Chandra 1962, 1966; Lo and Cardott 1995), or treatment of organic material with an oxidising agent during palynological processing, (Stach and Teichmüller 1953; Copard *et al*. 2004). For clarity, these will be referred to here as primary, secondary, and artificial oxidation respectively. Effect on reflectance notwithstanding, the significance of secondary oxidation must ultimately depend on the contribution of reworked material to the accumulation of sedimentary organic matter, which appears to be quite variable (see section 2.6).

The ICCP considers some forms of inertinite to be the product of primary oxidation (ICCP 2001); these were discussed in section 1.4 and will not be considered further here. The

ICCP also notes that the inertinite-group maceral secretinite "may have an oxidised rim of higher or lower reflectance" (ICCP 2001, p. 465). Such rims occur in several vitrinite and inertinite-group macerals, and are routinely attributed to secondary oxidation regardless of whether they are more or less reflective than the maceral core (Stach *et al*. 1982; Bustin *et al*. 1985; Taylor *et al*. 1998).

Studies of secondary oxidation have yielded contradictory results. Comparison of the reflectances of naturally weathered with freshly exposed coal samples from the same outcrop revealed no significant difference (Chandra 1962), nor was any change observed in coals stored for 10 years in a normal atmosphere (Chandra 1966). This is in agreement with more recent work by Kruszewska and du Cann (1996), who detected no significant change over 134 weeks of 'natural' weathering (i.e. coal samples exposed to the elements on a rooftop). In contrast, similar work by Benedict and Berry (1964, 1966) and Goodarzi and Murchison (1973) indicated that Rv decreased during the first 10–20 days of natural oxidation, then began to increase steadily after approximately 3 months; this was accompanied by an increased spread of reflectance values. Stach *et al*. (1982) dismissed these findings, claiming (without explanation) that the authors had either misinterpreted or misrepresented their results. Marchioni (1983) and Lo and Cardott (1995) also observed a decrease in R_v in naturally weathered coals, but no subsequent increase. Naturally weathered fossil wood showed an increase in Rv in weathered sections, though the stage at which the weathering had occurred (i.e. whether this was an example of primary or secondary oxidation) could not be determined (Marynowski *et al*. 2011). The results of lab-based oxidation experiments are also inconsistent, but suggest that temperature may be an important factor. Chandra (1958) and Copard *et al*. (2004) found no significant change in the reflectance of vitrinite when oxidised under laboratory conditions by heating to 110–150 °C, even after several months; Bend and Kosloski (1993) and Calemma *et al*. (1995), however, observed after just a few days or hours an increase during oxidation at 70–210 and 200 °C of 0.5% and 0.2% R_v, respectively, with a positive correlation between reflectance and temperature. A notable outcome of Bend and Kosloski's study was that, although maceral reflectance increased overall when heated, the rate of increase was different between rim and core. Thus, the rim was relatively darker after low temperature oxidation, but became relatively brighter as temperature

increased Bend and Kosloski (1993, fig. 3). Artificially produced charcoal can also exhibit higher reflecting rims (Guo and Bustin 1998), demonstrating that the effects of temperature can be highly heterogeneous, even at a microscopic scale.

The changes in reflectance observed by Bend and Kosloski (1993) and Calemma *et al*. (1995) are trivial compared to the changes seen in vitrinite over the same range of temperatures during natural maturation (e.g. Taylor *et al*. 1998, fig. 3.1b). Although the lengths of time involved in artificial oxidation experiments are many orders of magnitude less, it has been shown that at temperatures > 250°C even very short heating intervals (c. 35 minutes) can produce significant increases in reflectance; at 400°C, an increase of 0.6% R_v was observed (Le Bayon *et al*. 2011, 2012). This was despite the high-pressure conditions (2–20Kbar) at which the tests were conducted, which were found to inhibit the rate of reflectance increase. Thus, it seems plausible that the increase in reflectance seen during artificial oxidation was entirely due to temperature.

Of particular relevance to this study is the effect of artificial oxidation. Although organic residues in the University of Southampton's palynological collection have not been subjected to this treatment, it is standard procedure in many other institutions (e.g. Sheffield). It is generally understood that charcoal is highly resistant to the actions of oxidising agents compared with other palynological material (Swain 1973; Corlett 1979; Batten 1981; Winkler 1985; Batten 2002), although some destruction does occur (Singh *et al*. 1981; Clark 1985). This was confirmed by Dobel *et al*. (1984), who found that treatment of coal samples with an oxidising agent (Schultze's solution) caused preferential loss of some vitrinite-group macerals; thus, the relative abundance of inertinite increased by as much as 35%. Studies of the effects of oxidation on sporomorph chemistry (Hemsley *et al*. 1996; Blokker *et al*. 2005) have demonstrated a loss of aromatic compounds when spores were treated with common oxidising agents such as nitric acid or Schultze's solution, which should theoretically reduce reflectance. However, more recent work by Jardine *et al*. (2015) indicates the effect is quite variable depending on the type of sporomorph and the oxidation method chosen. It could also be argued that the behaviour of sporopollenin, a highly resistant material, is unlikely to be representative of organic material in general. An extensive search of the literature revealed only one published study of the effects of an oxidising agent specifically on reflectance (Stach and

Teichmüller 1953), in which treatment of coal with sulphuric acid at 100°C caused reflectance to increase markedly from that of lignite to values more typical of medium-volatile bituminous coal, an increase of c. 1%. The chemical mechanism behind this increase is not understood (Stach *et al*. 1982; Taylor *et al*. 1998), but is too large to be directly attributed to heating effects.

To investigate the matter further, three subsamples of DOM previously extracted from shale sample F14_72 (following standard HCl/HF processing procedure; see section 2.1, and for geological and biostratigraphical context see section 4.1) were treated with 70% nitric acid solution (HNO_3) at room temperature for 300, 600 and 1200 seconds differing lengths of time. The chosen durations represent standard exposure times when using nitric acid during palynological processing (S. Patel, *Pers. Comm*. 2016). After neutralisation, samples were sieved at 15 µm and decanted, then mounted on polished slides for incident light microscopy following standard procedure (section 2.1).

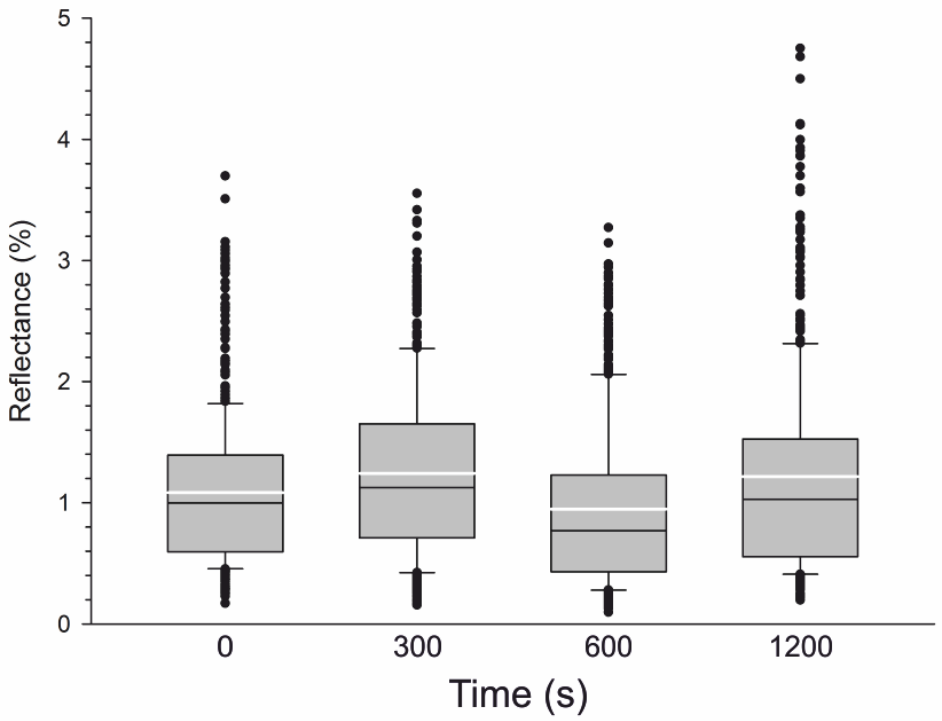

Figure 2.11: Response of phytoclast reflectance distribution to nitric acid exposure of varying duration, sample F14_72. White bars, mean; black bars, median; whiskers, $10^{th}/90^{th}$ percentile; dots, all outliers.

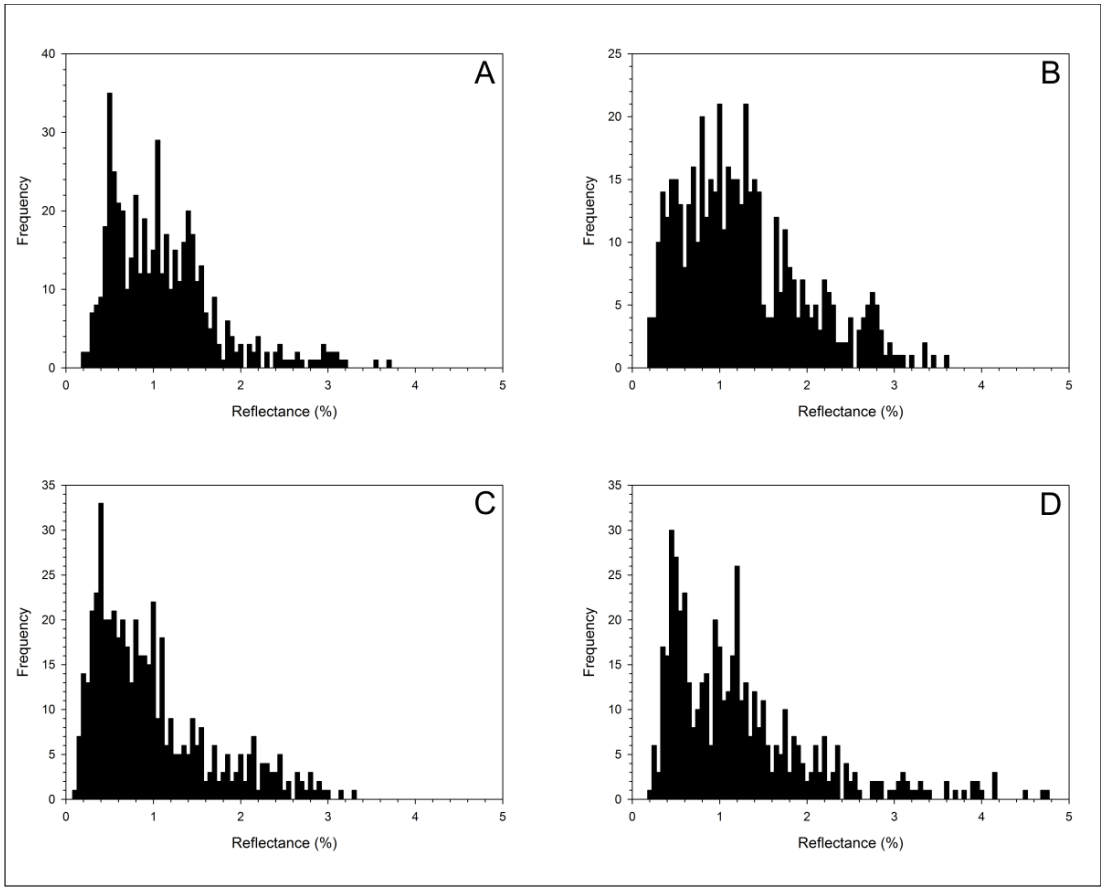

Figure 2.12: F14_72 reflectograms. A, 0 seconds (control); B, 300 seconds; C, 600 seconds; D, 1200 seconds.

Sample	Overall mean (%)	Mean Rv (%)	Mean Ri (%)	Abundance (%)
F14_72 (t = 0)	1.08	0.92	2.19	12.5
F14_72OX5 (t = 300)	1.24	0.87	1.92	35.5
F14_72OX10 (t = 600)	0.95	0.6	1.68	32.4
F14_72OX20 (t = 1200)	1.22	0.83	2.1	30.1

Table 2.2: Phytoclast reflectance data for shale sample F14_72; subsamples exposed to nitric acid for 300, 600, and 1200 seconds.

	Exposure time
Overall mean	Rs = 0.0, P = 1.00
Rv	Rs = -0.80, P = 0.333
Ri	Rs = -0.40, P = 0.750
Abundance	Rs = 0.20, P = 0.917

Table 2.3: Spearman rank correlation coefficients for exposure time with overall mean phytoclast reflectance, R_v, R_i, and relative abundance of inertinite as estimated by normalmixEM.

F14_72 showed no consistent change in phytoclast reflectance distribution with progressive oxidation; there was no significant correlation between exposure time and overall mean reflectance, R_v, R_i, or relative inertinite abundance (Figs. 2.11–2.12; Tables 2.2–2.3; SI 2.5). Given that the reaction in this case took place at room temperature, the discrepancy between this result and that of Stach and Teichmüller (1953) may reflect the increased reaction rate expected at 100°C. This is consistent with the findings of Jardine *et al*. (2015), who observed a greater rate and extent of chemical change and degradation at 90°C than at room temperature. Nevertheless, inertinite abundance was substantially lower in the control sample (12.5%) compared to the other three (30–35%); although conclusions drawn from such a limited number of tests must remain tentative, this may indicate preferential oxidation/destruction of non-inertinite macerals. As previously noted (section 1.3; Winkler (1985) observed a similar effect in recent (0 – c. 10,000 years bp) bog and lake sediments; treatment with nitric acid was found to be an effective way of isolating charcoal, which was much more resistant to oxidative destruction than other organic matter. Thus, these results suggest that even limited exposure to oxidising acid during processing has the potential to significantly distort the relative abundance of inertinite, and should be avoided.

2.6 Taphonomic considerations

Decay

Continued exposure of any organic material to oxygen results in its eventual destruction through oxidative decay (Tyson 1995). Charcoal is highly resistant to oxidation compared to other terrestrial plant material (Pessenda *et al*. 2001; Preston and Schmidt, 2006; Lehman *et al*. 2009), so the possibility of taphonomic bias due to differential preservation must be considered. Timing is critical; if significant decay occurs during transport, changes in relative charcoal abundance might reflect transport distance/duration rather than initial production. If most decay occurs before transport, during deposition or during early-stage diagenesis, the bias is systematic and can be accounted for.

Terrestrial organic matter in modern rivers is predominantly derived from vascular plants and is conventionally divided into dissolved (< 0.5 µm) and particulate (≥ 0.5 µm) organic carbon (DOC and POC; Hedges *et al*. 1997). Analysis of riverine and estuarine waters

(Ittekot 1988; Moran *et al*. 1999; Schlünz and Schneider 2000) has shown that, globally, 11–40% of POC and 1–30% of DOC is labile and hence vulnerable to rapid oxidation. It is generally assumed that most decay of labile material takes place at the site of deposition in estuarine and marine environments (Ittekot 1988; Tyson 1995; Schlünz and Schneider 2000) but the precise fate of this material is unimportant, because almost all will be destroyed during diagenesis (Tyson 1995); the vitrinite-group macerals are essentially humified refractory tissues (lignin and cellulose) from vascular plants (Dow 1977; Stach *et al*. 1982; Tyson 1995). Refractory DOC can also be disregarded, because the present study excludes particles < 15µm (see section 2.1). Thus, only refractory POC will be considered here.

Decay experiments indicate that fresh vascular plant material undergoes little oxidative decay during transport (Naiman 1982; Webster *et al*. 1999). Analyses of natural riverine POC, however, reveal that even lignin-rich tissues are often highly degraded (Hedges *et al*. 1986; 1997; Ittekot 1988; Schlünz and Schneider 2000). This apparent contradiction is explained by the fact that a significant proportion of the terrestrial organic matter (TOM) transported in rivers is eroded from soils and sedimentary rocks, and may be several thousand or even millions of years old (Hedges *et al*. 1986; Ittekot 1988; Goni *et al*. 1997, 1998; Onstad *et al*. 2000; Raymond and Bauer 2001; Goni *et al*. 2005; Guo and Macdonald, 2006; Blair *et al*. 2010; Blair and Aller 2012). Thus, although differential preservation does not present a problem, distortion by reworked material must also be considered.

Source

Modern plant debris, eroded soil, and weathered sedimentary rock all contribute to the TOM transported by modern rivers (Blair and Aller 2012). Therefore, at the point of deposition TOM comprises a mixture of modern biogenic, pedogenic (100–10000 years old) and lithogenic (≥ 1 million years old) organic carbon (Raymond and Bauer 2001; Goni *et al*. 2005; Blair *et al*. 2010). Carbon dating, and the presence of highly degraded lignin, both suggest that a significant proportion of POC is pedogenic or lithogenic (Hedges 1986; Goni *et al*. 1998; Raymond and Bauer 2001; Goni *et al*. 2005). The relative contribution of each source is chiefly governed by the geomorphology of the drainage basin in question;

small upland basins with fast-flowing, high-gradient rivers erode more rocks while larger lowland basins with slower, lower-gradient rivers erode more soil (Leithold *et al*. 2006; Blair *et al*. 2010; Blair and Aller 2012). Anthropogenic activity (e.g. mining, deforestation, road-building, agriculture) can also have a significant effect (Kao and Liu 1996; Hilton *et al*. 2008).

Reported values for the proportions of lithogenic and pedogenic riverine POC range from 7–75% (Kao and Liu 1996; Gomez *et al*. 2004; Blair *et al*. 2003; Leithold *et al*. 2006; Hilton *et al*. 2008; Blair *et al*. 2010) and 40–70% (Goni *et al*. 1998, 2005; Raymond and Bauer 2001) respectively. The effects of pedogenic TOM are unimportant at the temporal resolution of this study, though the slower rate of decay of charcoal compared to other plant material does introduce a systematic bias. Lithogenic TOM is potentially a concern, because it might overprint the contemporaneous charcoal influx. 'Recycled' macerals are anecdotally reported to be quite common amongst DOM (Dow 1977) but there is currently no consensus on what this might mean; quantification is difficult, because although anomalous reflectance values and increased rounding (Dow 1977; Meyers *et al*. 1984; Piasecki and Stemmerick 1991) can be indicative of reworking, neither characteristic is reliable (Tyson 1995). It is generally believed that lithogenic POC is concentrated in the clay size-fraction and in fact represents an organic coating on clay-minerals (Ransom *et al*. 1996; Leithold and Blair 2001; Blair *et al*. 2003, 2010; Blair and Aller 2012), but pending a detailed analysis of C_{org} provenance for each size-fraction this is unconfirmed. Therefore, the significance of reworked lithogenic TOM to studies of DOM remains unknown.

Fragmentation

As noted above, concerns have been raised that counts of charcoal abundance could be distorted by fragmentation during transport and processing (Weng 2005; Leys *et al*. 2013). It is known that phytoclasts decrease in size during river transport due to fragmentation (Naiman 1982; Wallace *et al*. 1983; Tyson 1995; Webster *et al*. 1999); because charcoal is chemically inert but mechanically weak, it is theoretically more vulnerable to breakage than other organic material (Scott and Glasspool 2007). This would initially result in a positive correlation between transport distance and relative

abundance; once reduced below 15 µm, charcoal would not be detected and the apparent abundance would fall. Counteracting this tendency to fragment is the fact that due to its low density, charcoal is quite buoyant and may remain in suspension over considerable distances, avoiding abrasion during transport, (Nichols *et al*. 2000; Scott 2010); to complicate matters still further, both the density and mechanical strength of charcoal are in part determined by fire temperature at the time of formation and the nature of the original plant material which was charcoalified (Vaughan and Nichols 1995; Nichols *et al*. 2000). Thus, the relationship between transport distance and extent of fragmentation is not simple.

Direct comparisons of particle counting and area measurement for fire history reconstruction have yielded mixed results; in some cases the impact was minimal (Tinner and Hu 2003; Ali *et al*. 2009) whereas Leys *et al*. (2013) found a significant difference. Unfortunately, those studies are not directly relevant here because charcoal was quantified per unit of unprocessed/minimally processed sediment (i.e. using only $NaPO_3$ and NaOCl; Ali *et al*. 2009; Leys *et al*. 2013) or, if samples were fully demineralised, with reference to added exotic *Lycopodium* spores (Tinner and Hu 2003). Charcoal in the present study is quantified relative to other DOM (Materials and Methods), so it is not the fragmentation of charcoal *per se* but the relative rate of fragmentation compared to other TOM that is of concern.

There is some evidence that palynological processing results in the loss of rare, very large charcoal fragments (somewhat unhelpfully described by Tinner *et al*. 1998, pp. 40 as “extraordinarily large”). A comprehensive investigation of the effects of a range of palynological processing techniques on modern charcoal by Clark (1985) revealed that while all stages reduced the total quantity of charcoal, the effects on fragmentation varied. Treatment with hydrofluoric acid reduced charcoal area but not particle number (implying fragmentation) while hydrochloric acid had the opposite effect, preferentially removing smaller particles but not affecting area. Overall, it was found that chemical treatments in combination tended to cancel out, and did not introduce a significant bias. Although encouraging, Clark (1985) cautioned that these results may not be applicable to charcoal in the fossil record; the effect of processing on fossil DOM cannot be tested in this way, because the initial quantity and size of the macerals is unknown.

Maceral size was examined in detail for sample EH_6, (Burnmouth Shore; see section 4.1) so that the size-distribution of different maceral groups and the outcome of particle counting and particle size could be compared (Fig. 2.13A; SI 2.6); EH_6 was chosen because its reflectogram allowed total inertinite to be distinguished easily (Fig. 2.13B). Slides were traversed horizontally at 500 µm vertical intervals; the reflectance and diameter of each phytoclast which passed directly under the target was recorded. Phytoclasts were treated as square for area calculation.

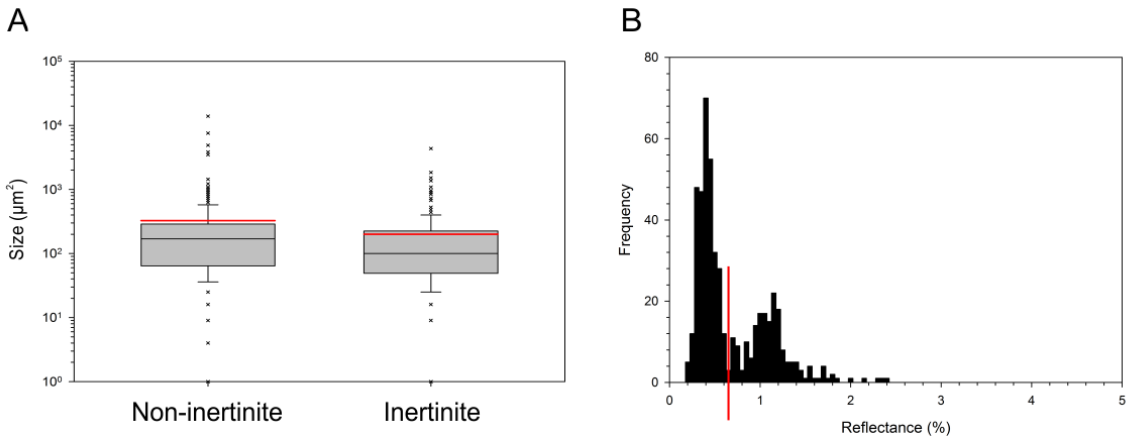

Figure 2.13: Maceral size distribution (A) and reflectogram (B) for shale sample EH_6, Burnmouth Shore (Tournaisian). A: Red bars, mean; black bars, median; whiskers, 10th/90th percentile; dots, all outliers. B: red bar separates inertinite (right of bar) from other macerals (left of bar).

Mean size was found to be 326.8 µm^2 for non-inertinite macerals, compared to only 200.4 µm^2 for inertinite. As a result, abundance values calculated by the two methods differed substantially: point counting yielded a result of 62.6%, whereas area estimation produced a much lower figure of 36.7%. While this demonstrates that particle counts can be distorted by fragmentation, it does not provide evidence of when the fragmentation took place; if fragmentation is rapid, this would constitute a systematic bias. It is also possible that the difference in particle size reflects a difference in the size of the source material, though this seems less likely.

Landscape evolution during the Palaeozoic

The progressive increase in rooting depth and complexity during the Palaeozoic is believed to have driven a corresponding evolution of fluvial landscapes, as soil production and slope stabilisation increased. In their review article, Gibling and Davies (2012)

identified three critical events which led to evolutionary feedback between plants and fluvial systems, whereby landscape changes promoted increased plant coverage and diversity:

1. Increased upland mud production from the Mid-Ordovician onwards, which was then eroded, transported, and deposited in alluvial settings, forming the first alluvial plains.
2. Increased bank stability from the Late Silurian, allowing the development of meandering rivers in place of braided channels. This promoted floodplain stability, and allowed a greater diversity of soil types.
3. Increased size of riparian corridors and channel margins, providing an important habitat for plant and animal species.

In the context of the present study, the increase in global plant coverage is not directly relevant because charcoal is quantified here relative to total organic matter. However, the development of widespread soils may be significant because of the long residence time of organic material (e.g. charcoal, wood etc.). As discussed in section 2.6, it is understood that because of differing decay rates, soils are relatively enriched in refractory forms of organic carbon, such as charcoal and wood, and that this constitutes an unquantified but systematic bias towards higher charcoal abundance in DOM. As soil-forming environments became more common over geological time, it is likely that the relative abundance of charcoal in DOM increased, and this should be borne in mind when interpreting results.

2.7 Summary

The quantification of DOM charcoal in the fossil record is problematic, regardless of the method chosen. This situation is in part due to the inadequacy of current definitions for inertinite-group macerals favoured by the ICCP, but also stems from the fact that approaches based on incident light microscopy were originally intended for use with coals rather than DOM. The use of reflectograms to identify inertinite is effective only if the vitrinite content of samples is sufficiently large and of low enough thermal maturity to form a distinct peak; furthermore, although an arbitrary 2% reflectance threshold can be used to identify fusinite in samples of low to moderate thermal maturity, there is poor

correlation between fusinite and total inertinite. Fire temperature, as recorded by inertinite reflectance, does not appear to be a viable proxy for atmospheric pO_2 because wildfire intensity is largely an effect of fuel type, and thus varies depending on the species of plant being burned. The use of mixture models for interpretation of maceral reflectance distributions appears to be sound, however, providing results which are consistent with empirically derived maceral abundance and reflectance data.

The effects of natural oxidation on maceral reflectance, and consequently the existence of non-pyrogenic inertinite, appear to have been overstated; past reports of reflectance increase due to oxidation can be more simply explained as the result of exposure to high temperatures. The effects of artificial oxidation during palynological processing (e.g. during pyrite removal) are less certain, and appear to be quite variable depending on the method used; treatment with nitric acid at room temperature caused no consistent change in the reflectance profile of a Viséan DOM sample, but nevertheless resulted in a significant increase in relative inertinite abundance after only 5 minutes of exposure. This is attributed to the preferential destruction of macerals other than inertinite, which are more vulnerable to oxidation. Another concern is the possibility of taphonomic bias, due to the different physical and chemical properties of charcoal compared to other plant material, and the unknown importance of re-worked organic material. Size distribution analysis indicates that differential fragmentation could significantly skew results; whether this occurs in practice is currently unknown, but where time permits it is advisable to adopt area estimation rather than particle counts. Finally, it is possible that, as soil-forming environments became more common over the course of the Palaeozoic, the relative abundance of inertinite as a component of DOM increased due to the different rates of decay experienced by organic materials in soils prior to erosion and transport. This possibility should be taken into account when interpreting long-term trends in charcoal abundance.

3. The Devonian Charcoal Gap

The major diversification of vascular plants which occurred during the Devonian led to a wholesale reorganisation of terrestrial floral ecosystems, and ultimately gave rise to the first forests. Late Silurian/Early Devonian forms were predominantly small (≤ 1m), restricted to moist environments, shallow-rooting, and lacked megaphyll leaves (Kenrick and Crane 1997; Beerling *et al*. 2001; Greb *et al*. 2006; Le Hir *et al*. 2011). By the Late Devonian, arborescent forms up to 25 m tall with large, complex rooting systems were commonplace, the evolution of gymnosperms had allowed dry habitats to be colonised (Davies and Gibling 2010; Pires and Dolan 2012; Edwards *et al*. 2014), and isotopic evidence suggests that global vegetation cover increased from 10–30% at the Middle/Upper Devonian boundary (Gibling and Davies 2012). It has been proposed that the global spread of large, deep-rooting trees resulted in major perturbations of the long term carbon cycle, primarily through enhanced silicate weathering (i.e. increased drawdown of atmospheric CO_2) but also via greater mobilisation and transport of nutrients such as phosphorous (increasing primary productivity and nutrient flux to the oceans) and burial of large quantities of refractory organic carbon (i.e. wood) (Robinson 1990; Berner 1997; Retallack 1997; Beerling and Berner 2005; Berner 2009; Pires and Dolan 2012; Morris *et al*. 2015). This 'Devonian plant hypothesis' is generally accepted as an explanation for the c. 90% fall in atmospheric CO_2 levels between the mid- and late Palaeozoic (Mora and Colarusso 1996; Gibling and Davies 2012; Morris *et al*. 2015) and, in the case of the latter two factors, is consistent with a predicted rise in O_2 from the Famennian onwards (Berner 1992, 2006, 2009; Pires and Dolan 2012). Less well explored are the implications for atmospheric O_2 during the Early and Mid-Devonian.

In their study of mid to late Palaeozoic fire activity, Scott and Glasspool (2006) were the first to note an apparent scarcity of charcoal in the late Early to early Late Devonian fossil record, which they referred to as the 'charcoal gap' (Fig. 3.1). Charcoalified plant mesofossils, though rare, have been identified in late Silurian and Early Devonian horizons (Glasspool *et al*. 2004; Edwards and Axe 2004; Pflug and Prössl 1989, 1991; Davies and Gibling 2010), but are seemingly absent from the late Emsian to the early Famennian (Rimmer *et al*. 2015). Coals are uncommon during this interval, but the relatively small

number that have been investigated (c. 34 samples from various localities worldwide) were found to be inertinite-poor compared to recent peats and lignites (Glasspool and Scott 2010; Glasspool *et al*. 2015); Pragian and Emsian carbonaceous shales from New Brunswick, Canada were similarly depleted (Kennedy *et al*. 2013). On this basis, the existence of the charcoal gap is now accepted by most workers (see e.g. Belcher *et al*. 2013; Scott *et al*. 2014; Rimmer *et al*. 2015; Lenton *et al*. 2016). Taken at face value, low charcoal production at a time when the supply of fuel was increasing would seem to support palaeoatmosphere models which predict a significant reduction in atmospheric pO_2 during the Early or Mid-Devonian (e.g. Berner 2006, 2009; Algeo and Ingall 2007). This is a counterintuitive result for a period which saw such a vast increase in terrestrial plant life, but this view has strongly influenced discussions of global biogeochemical change during the Devonian (e.g. Malkowski and Racki 2009; Gibling and Davies 2012; McGhee 2013).

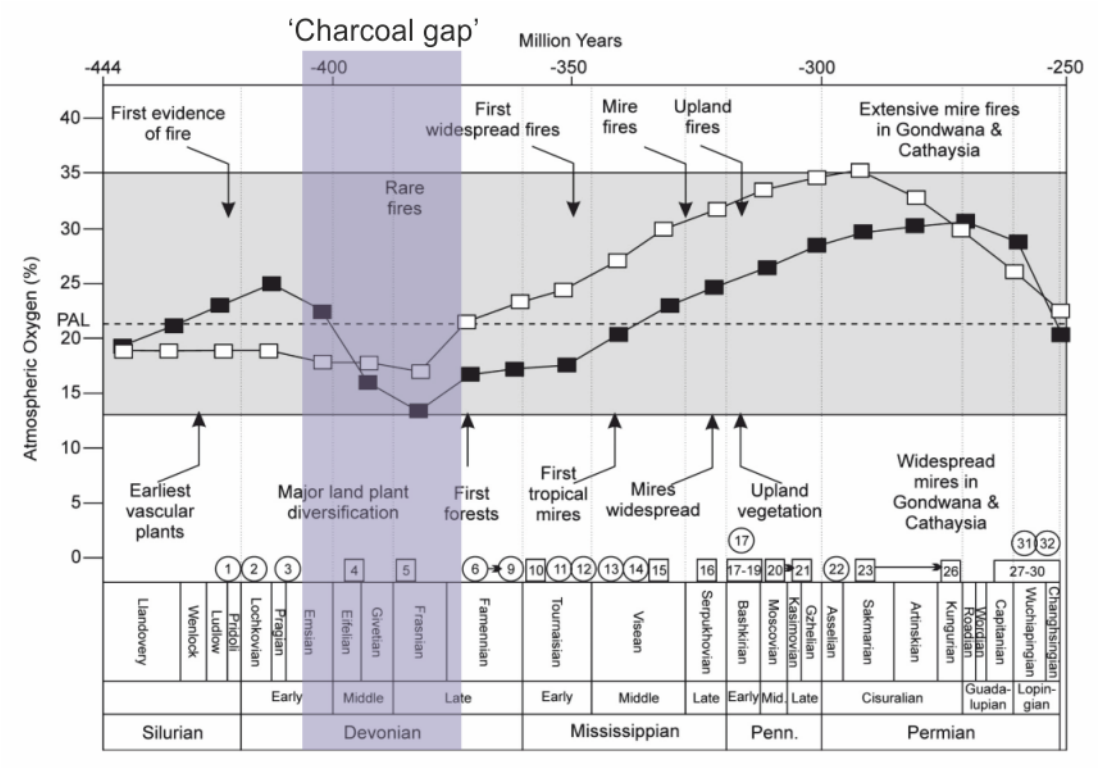

Figure 3.1: The 'charcoal gap', as originally defined by Scott and Glasspool (2006). Modified after Scott and Glasspool (2006, fig. 1).

In this chapter, the inertinite content of Silurian and Devonian shale samples collected during field expeditions to central Bolivia, eastern New York, and Pennsylvania is

examined with the intent of assembling a high-resolution record of its abundance through the 'charcoal gap'; this dataset was supplemented with additional material from the extensive palynological collections of the Universities of Southampton and Sheffield. The results are used to test the hypothesis:

that a charcoal gap exists from the late Emsian to the early Famennian, indicating that wildfire activity was significantly supressed by a reduction of atmospheric pO_2.

3.1 The Catskill Delta complex in New York and Pennsylvania

North America underwent a series of orogenic events over the course of the Palaeozoic, and experienced several cycles of uplift and erosion along what is now its eastern margin (Faill 1997). During the Devonian, the Acadian Orogeny created a substantial mountain range which extended from Nova Scotia to Alabama, and caused further subsidence of the pre-existing Appalachian foreland basin to the west (Ver Straeten 2007). Erosion of these mountains provided a massive influx of clastic sediments, which began to prograde into the epicontinental 'Catskill Sea'; marine facies were progressively displaced westwards by terrestrial ones during the Mid and Late Devonian, albeit with interruptions by marine transgressions (Woodrow *et al*. 1988). The resulting suite of intermixed marine, deltaic, and terrestrial facies is referred to informally as either the Catskill Delta (Barrell 1916; Woodrow and Sevon 1985; Daeschler and Cressler 2006; Ver Straeten 2013) or the Catskill Clastic Wedge (e.g. Bridge and Willis 1991, 1994; Ver Straeten 2009). Following Ver Straeten (2009), the Catskill Delta complex is defined here as beginning with the Middle Devonian Marcellus subgroup and lateral equivalents and ending with the Upper Devonian Catskill Fm. (Fig. 3.2), i.e., it is synonymous with the Mid- and Late Devonian in North America. Although present in seven eastern US states (Faill 1985), the least condensed successions are confined to New York and Pennsylvania, such as those of the Catskill Front in Greene and Delaware Counties, New York (Rickard 1989; Reed *et al*. 2005; Ver Straeten 2013). Middle and Upper Devonian shales were sampled at 20 localities in eastern New York and central Pennsylvania during a 2 week field excursion in the summer of 2014 (Fig. 3.3); further material from a New York State Power Authority (NYSPA) borehole in Schoharie County was provided by the New York State Museum, Albany.

Berg and Edmunds (1979) described the nomenclatural history of the Devonian strata of New York and Pennsylvania as “perhaps one of the most intricate and complicated in the annals of American stratigraphy”. After almost four decades of further research, the word ‘perhaps’ can safely be discarded. Intense interdigitation and extreme lateral variation in bed thickness and character has resulted in a proliferation of local names (see e.g. Ver Straeten 2007, fig. 2, 2011, fig. 1-3, Fig. 3.2), and basin-wide correlation is difficult. The progressive change from carbonate dominated successions in the west to clastic deposits in the east hinders biostratigraphic comparison, since different biozonation schemes (e.g. marine conodonts vs. terrestrial spores) must be used. In the following descriptions, biostratigraphical data are provided where available; for correlation of the different schemes, see Fig. 3.4.

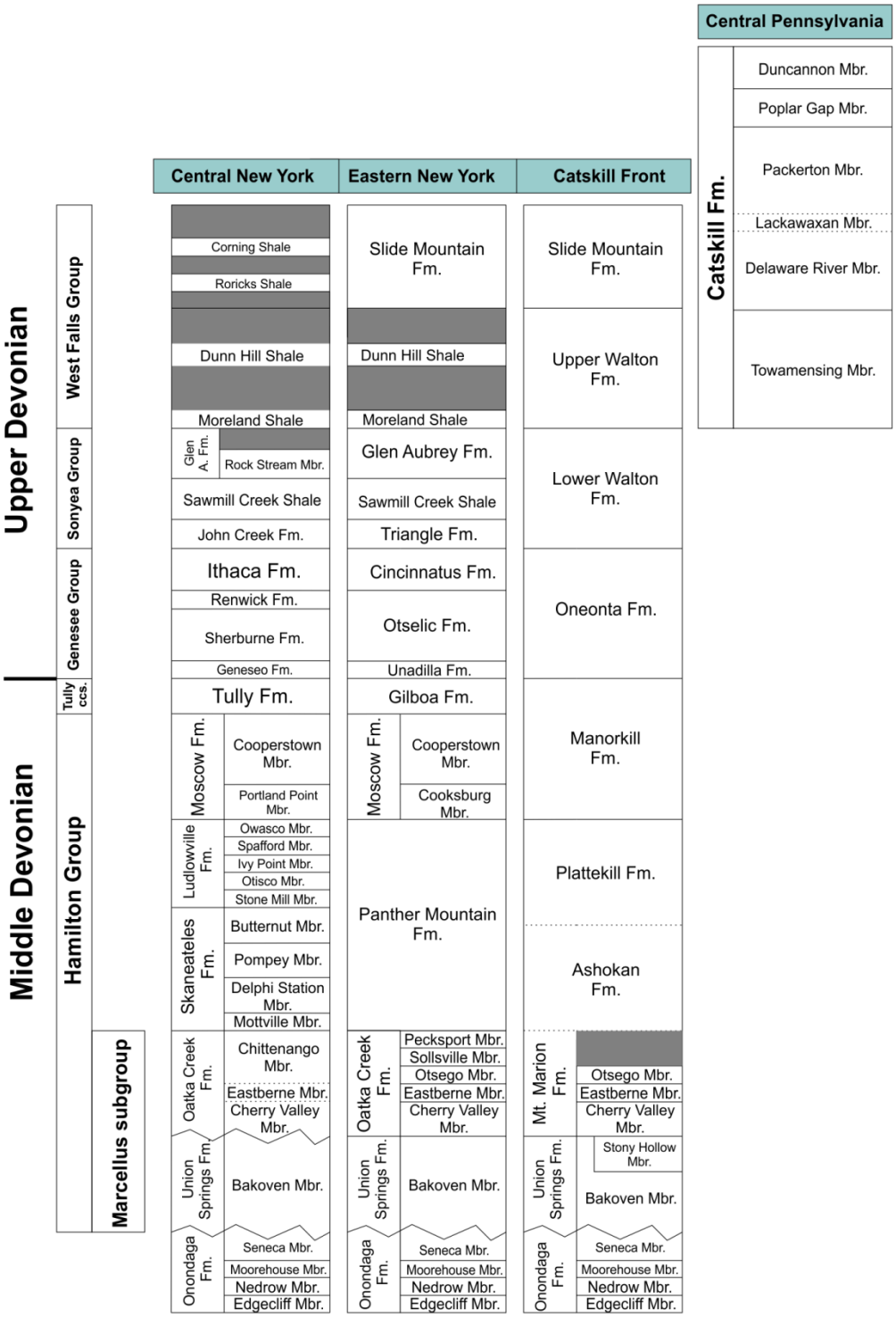

Figure 3.2: Stratigraphic overview of the Catskill Delta Complex in New York and Pennsylvania. Dotted lines indicate uncertain boundaries; grey shading indicates unnamed/undifferentiated units. Sources: Rickard 1975, 1989; Woodrow and Sevon 1985; Ver Straeten 2007; Ver Straeten *et al*. 2011.

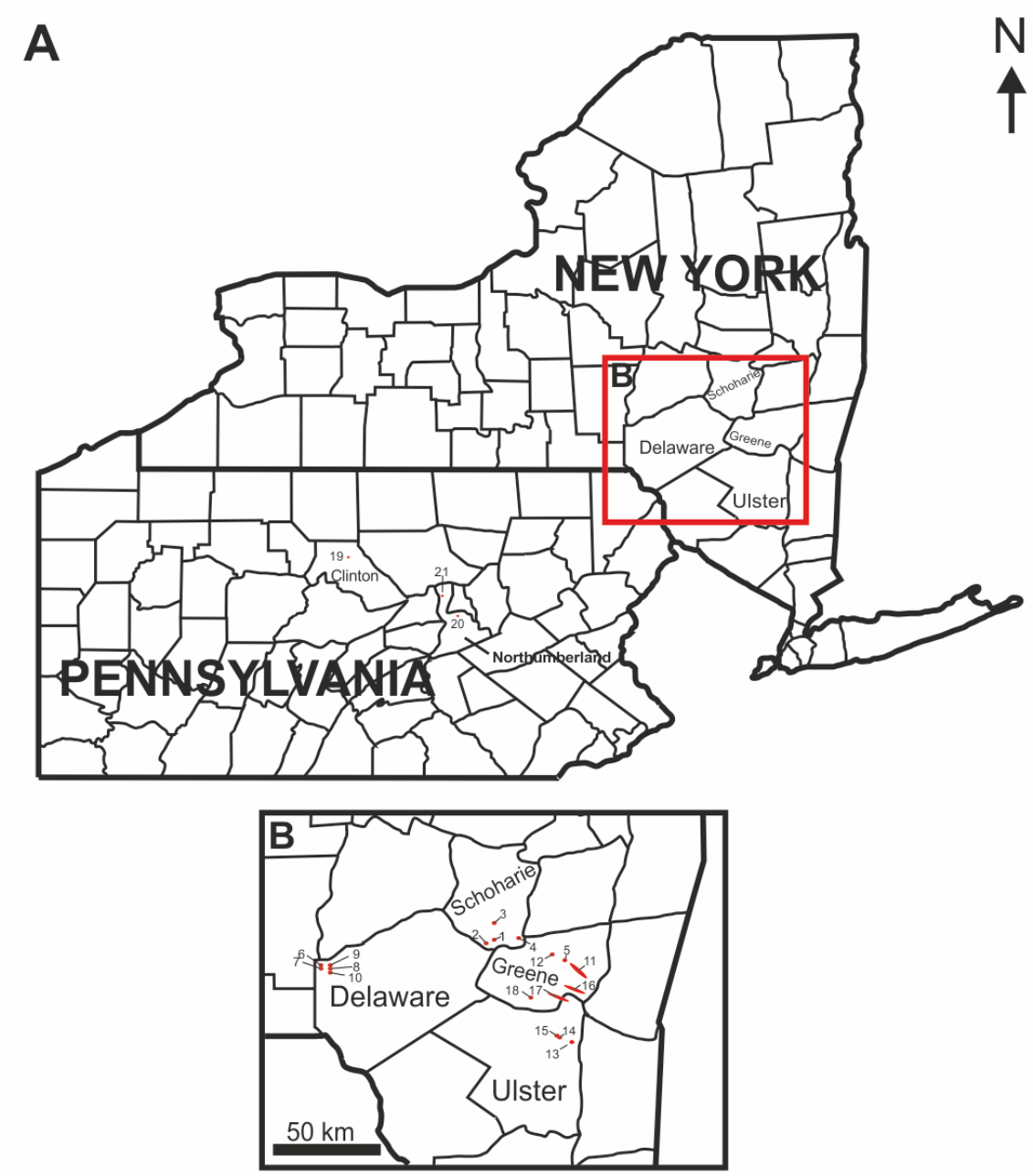

Figure 3.3: Sampled localities in New York and Pennsylvania. 1, Stevens Mountain Quarry; 2, Grand Gorge Road Section; 3, B-1 Borehole; 4, South Mountain Quarry; 5, Cairo Quarry; 6, NY 8 Road Section; 7, Sidney Mountain Quarry; 8, Skytop Lane Quarry; 9, Dunshee Hill Quarry #2 and #4/5; 10, CR 27 Road Section; 11, NY 23 Road Sections A–D; 12, NY 23 Road Sections E–I; 13, US 209 Road Section; 14, Bluestone Wild Forest Quarry; 15, NY 28 composite section; 16, Kaaterskill Clove (Kaaterskill Creek and NY 23A sections); 17, Platte Clove (Plattekill Creek and Plattekill Creek Road sections); 18, Blue Trail; 19, Red Hill, 20, US 11 roadcut; 21, Watsontown Brick Company Quarry.

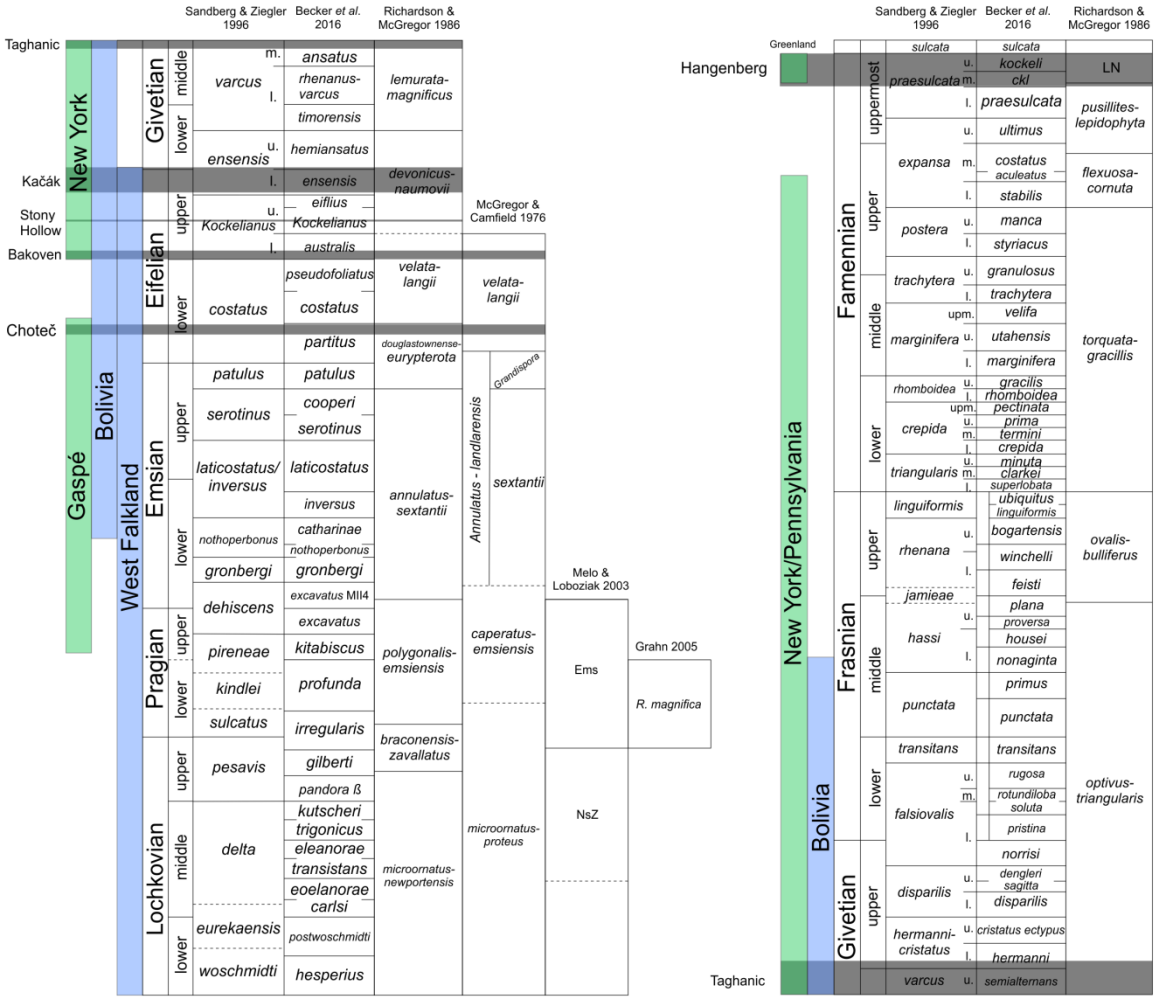

Figure 3.4: Correlation of Devonian biostratigraphic schemes, and sample coverage from Euramerica (green) and Gondwana (blue). Sources: Williams *et al*. 2000; Melo and Loboziak 2003; Grahn 2005; Kermandji *et al*. 2008; Becker *et al*. 2016.

3.2 Sampling localities – Devonian, USA

1. Stevens Mountain Quarry (42° 23' 18" N, 74° 25' 55" W)

Geological context and biostratigraphy

Approximately 34 m of the mid-Givetian Gilboa Formation (part of the Tully Formation Clastic Correlative Succession) is accessible in Stevens Mountain Quarry, 1.5 km SE of Gilboa, Schoharie County, New York State (Fig. 3.3). The sampled section corresponds to Stop 2, Stevens Mountain Quarry Log #2 of Bridge and Willis (1991) (Fig. 3.5).

The Gilboa Formation is the eastern New York State equivalent of the Tully Limestone (Johnson and Friedman 1969; Johnson 1972; Rickard 1989; Bridge and Willis 1994; Baird and Brett 2008), which is assigned by Baird and Brett (2008) to the middle Givetian *ansatus*–*semialternans*/*latifossatus* conodont biozones of Bultynck (1987, = *ansatus*–*semialternans* zones of Becker *et al*. 2016). This is consistent with the age assignment of Bridge and Willis (1994), who place the formation in the upper *l-m* spore biozone of Richardson and McGregor (1986). The Tully Limestone encompasses a major transgression, the Taghanic Onlap event (Johnson 1970; Baird and Brett 2008) and as such is an important correlative marker.

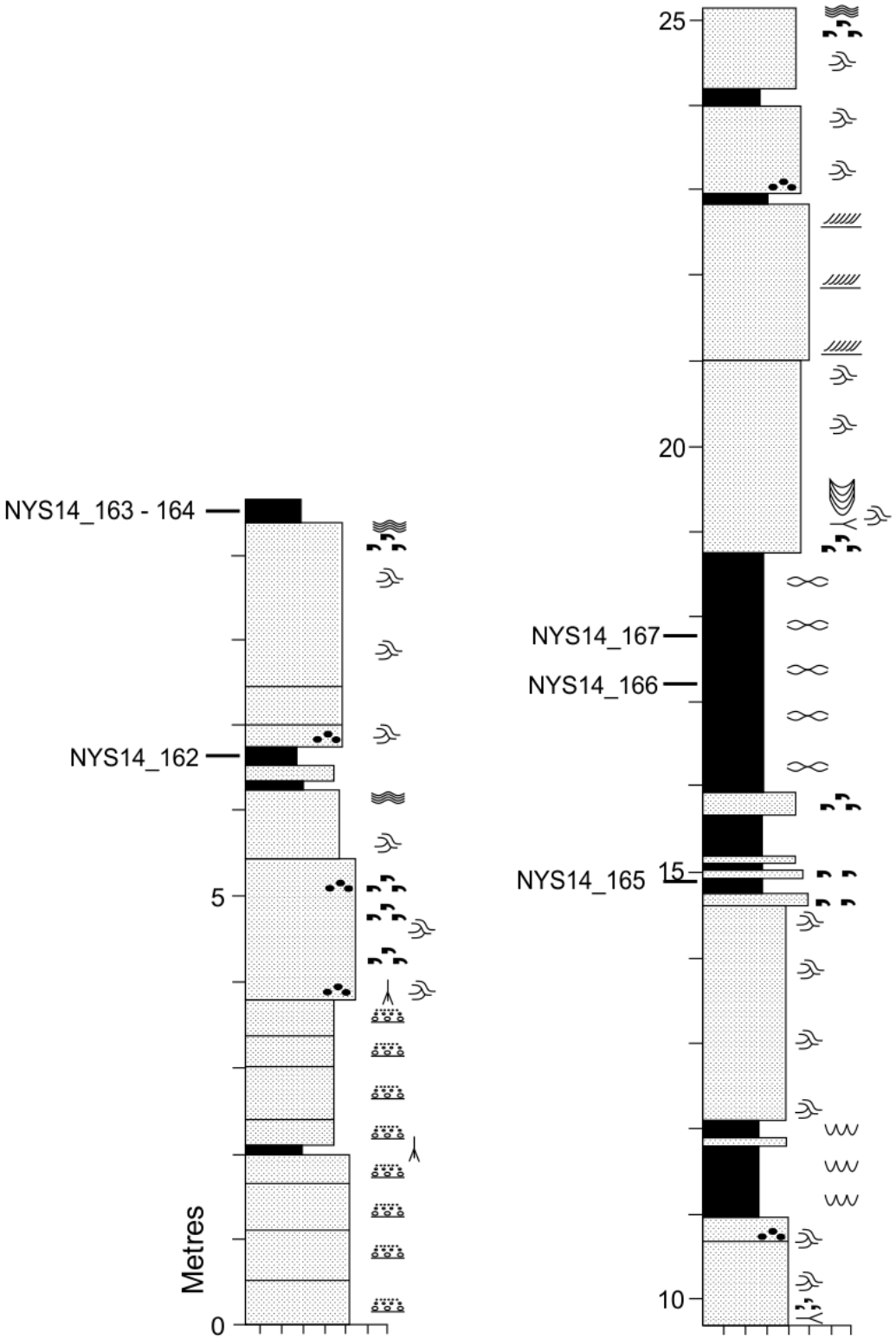

Figure 3.5: Sedimentary log of Steven's Mountain Quarry. Modified after Bridge and Willis 1991. For key see Appendix 3.

Palaeoenvironment

The succession at Stevens Mountain Quarry records deposition in an estuarine environment, comprising a mix of wave-dominated (channel mouth-bars) and tide-dominated (tidal inlet/channel) settings (Bridge and Willis 1994). Periodic disruption by storm events has introduced a wide assortment of marine invertebrates and terrestrial plant material to the standard nearshore marine trace fossils, and the sequence becomes progressively more proximal up-section (Bridge and Willis 1991).

2. Grand Gorge Road Section (42° 22′ 23″ N, 74° 28′ 11″ W–42° 22′ 49″ N, 74° 27′ 50″ W)

Geological context and biostratigraphy

The Gilboa and Oneonta Formations are exposed along a c. 1.25 km stretch of NY 30 (Mt. Davis Road), starting 3 km NE of Grand Gorge, Delaware County (Fig. 3.3). The sampled section corresponds to Stop 5, Grand Gorge Route 30 of Bridge and Willis (1991) and comprises a lower (Gilboa Fm.) and upper (Oneonta Fm.) part, each approximately 30 m thick, separated by a 25.5 m covered interval (Fig. 3.6); the nature of the contact between the two units is unknown. Large sandstone bodies in the lower part correlate with the Stevens Mountain Quarry section (Bridge and Willis 1994).

Spore assemblages recovered from various localities between Grand Gorge and Binghamton (Schuyler and Traverse 1990, fig. 2) place the Oneonta Formation in the *optivus-triangulatus* zone of Richardson and McGregor (1986), indicating a late Givetian to mid Frasnian age (Schuyler and Traverse 1990; Bridge and Willis 1994; Traverse and Schuyler 1994; Stein *et al*. 2007).

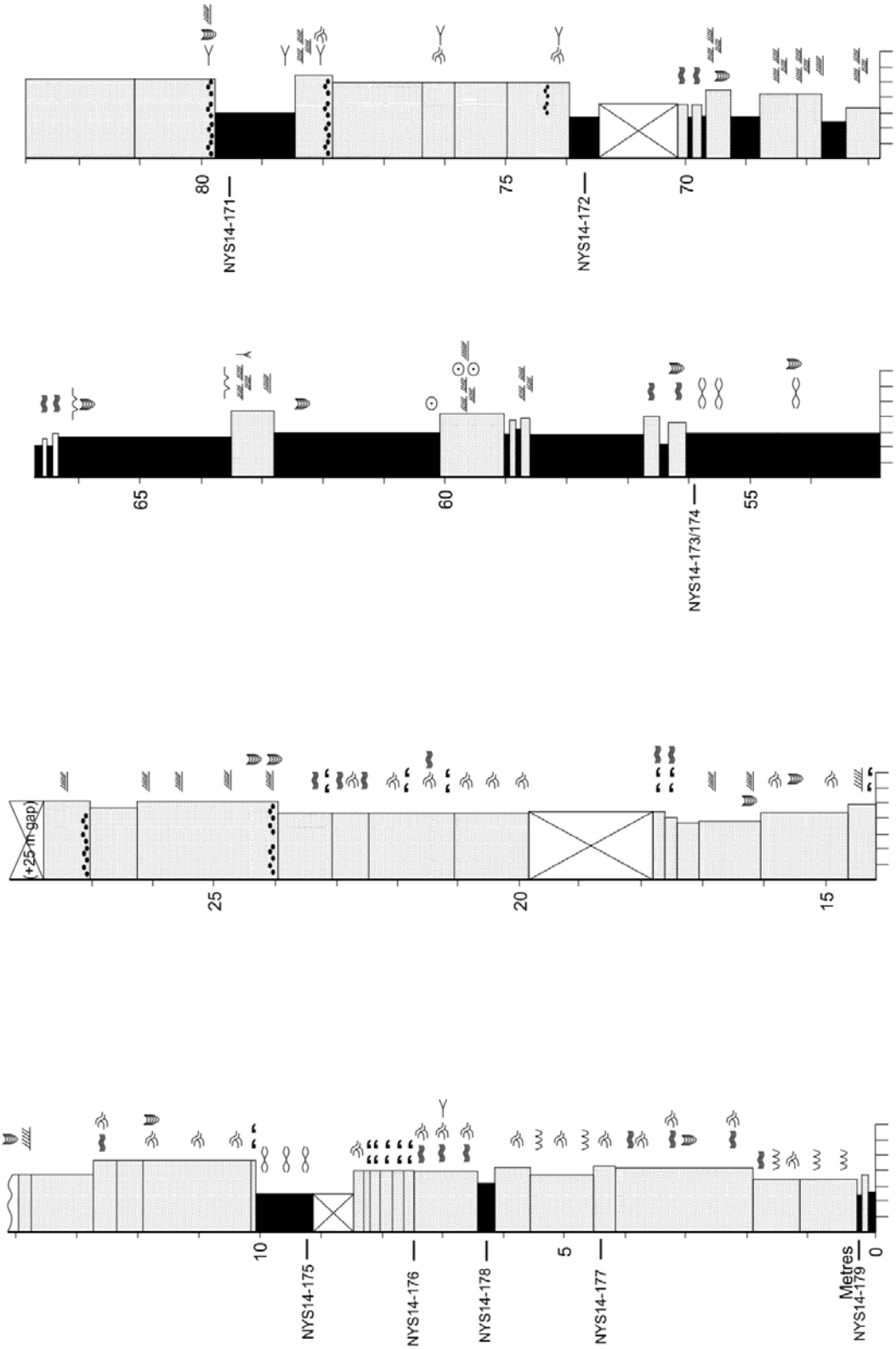

Figure 3.6: Sedimentary log of Grand Gorge road section; gaps indicate outcrop covered by vegetation. Modified after Bridge and Willis (1991). For key see Appendix 3.

Palaeoenvironment

In contrast to the nearshore-marine Gilboa Fm., the Oneonta Fm. is largely terrestrial. The lower half of the exposure is predominantly red in colour, rich in plant material, and likely represents overbank deposition on a coastal floodplain (Bridge and Willis 1991, 1994; Miller and Woodrow 1991); the upper part is more proximal, characterised by large, fluvial sandstones (Bridge and Willis 1994).

2i. Hardenburgh Falls (42° 20′ 17″ N, 74° 27′ 03″ W)

This river section corresponds to Stop 1, Hardenburgh Falls of Bridge and Willis (1991), and comprises 17 m of Gilboa Fm. strata. Unfortunately, access to the river is now prohibited (Fig. 3.7) and most of the section is inaccessible as a result.

Figure 3.7: Hardenburgh Falls access point.

3. B1 Borehole (42° 27′ N, 74° 26′ W)

The B1 borehole is one of several that were drilled by the New York State Power Authority (NYSPA) prior to the construction of the Blenheim-Gilboa Pumped Storage Power Station, a hydroelectric power plant on Brown Mountain, Schoharie County which began operation in 1973 (Fig. 3.3). Although alluded to by Shear *et al*. (1987) and Miller and Woodrow (1991), and mentioned explicitly by Bridge and Willis (1991, 1994) and

Richardson *et al*. (1993), it is not recorded by the USGS and any information held by the NYSPA is not in the public domain. Thus, the date of drilling, precise location, and formal designation are unknown; 'B1' is most likely an informal name assigned by Bridge and Willis (1991). Its approximate location was provided by Bridge and Willis (1991, fig. 2); Richardson *et al*. (1993) placed it "1143.8m N60E of the reservoir near the power plant" but the large size of the reservoir renders this unhelpful.

Geological context and biostratigraphy

The B1 borehole reaches a depth of 377.9 m (Richardson *et al*. 1993) and passes through the upper Panther Mountain, entire Moscow, and lowermost Gilboa Formations (Bridge and Willis 1994, fig. 2; Fig. 3.8). The Moscow Formation is the highest unit in the Hamilton Group, and in Schoharie is divided into the upper Cooperstown Member and lower Portland Point Member. The former, which constitutes the majority of the formation in Schoharie, can be placed in the mid Givetian *ansatus* conodont biozone based on the age of the Windom Shale, central New York State (Huddle and Repetski 1981; Baird and Brett 2008; Fig. 3.4); the age of the lower unit (only 20m thick in Schoharie; Bridge and Willis 1994) is less well constrained, but is generally assumed to also be within the *ansatus* zone (e.g. Rickard 1989, fig. 3). Thus, Bridge and Willis (1994) placed the entire Moscow Formation in the mid *lemurata magnificus* palynozone of Richardson and McGregor (1986).

The 'Panther Mountain Formation' is something of a wastebasket unit, encompassing the undifferentiated eastern New York State outcrops of the upper Marcellus subgroup (Formerly Marcellus Formation; Ver Straeten 2007) and Skaneateles and Ludlowville Formations (Shear *et al*. 1987; Rickard 1989). Although the borehole clearly intersects it (Bridge and Willis 1994, fig. 2, table 1), Bridge and Willis did not discuss the PMF in detail or provide any biostratigraphical context. Spores recovered from the core suggest that the upper PMF should be assigned to the *devonicus naumovae* palynozone (Richardson *et al*. 1993), which is of late Eifelian to early Givetian in age.

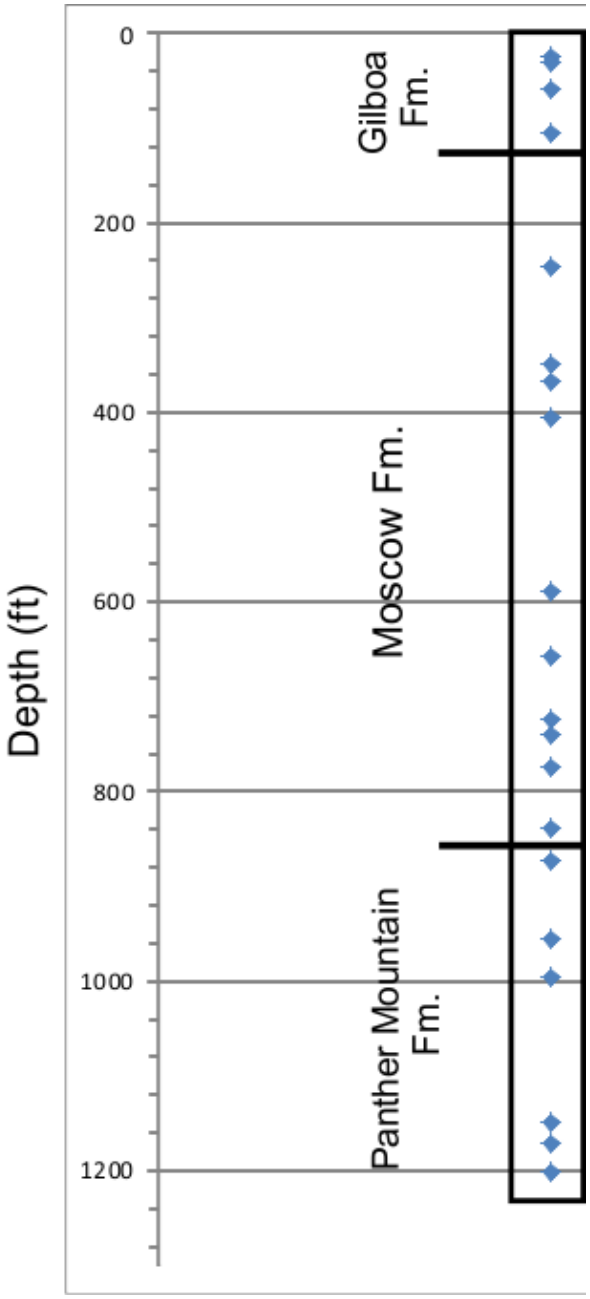

Figure 3.8: Formations intersected by the B1 borehole. Diamonds indicate sample points.

Palaeoenvironment

The Moscow Formation as a whole records a change from fully marine conditions (Portland Point Member) to a more proximal and ultimately subaerial setting (Cooperstown Member), albeit with smaller-scale cyclicity superimposed (Bridge and Willis 1994). The Cooperstown Mb. initially comprises tidal channel, flat and sandbar deposits of a type considered to be estuarine by Miller and Woodrow (1991); this gives way up-section to coastal-plain water-bodies, with periodic subaerial exposure leading to

plant growth (Bridge and Willis 1994). The upper part of the formation is mud-dominated, representing deposition on a vegetated coastal floodplain. A terrestrial facies comprising soil horizons, root casts and abundant plant macrofossils (including large tree trunks) is interrupted by lagoonal deposition, then re-established prior to the contact with the overlying Gilboa Formation (Miller and Woodrow 1991; Bridge and Willis 1991, 1994).

The sedimentary facies and depositional environment(s) represented by the Panther Mountain Formation have not been studied in detail; however, the upper part of the formation was temporarily exposed at Brown Mountain during construction of the power plant and found to be rich in carbonised and pyritised plant remains, including the previously unknown *Leclercqia complexa* Banks *et al*. (1972). Banks *et al*. (1985) reported that the style of preservation and lithology is very similar to that seen at South Mountain (see below), and suggested a densely vegetated, wholly terrestrial environment.

4. South Mountain Quarry (42° 23′ 27″ N, 74° 16′ 12″ W)

Geological context and biostratigraphy

The South Mountain Quarry is located on the west flank of South Mountain, in the Manorkill State Forest, approximately 2.8 km west of West Durham, Schoharie County, New York State (Fig. 3.3). A 7.5 m exposure of Oneonta Formation strata is accessible here (Stein *et al*. 2007), though much of this is covered by a layer of talus (Fig. 3.9). As noted above, this formation has been placed in the late Givetian–mid Frasnian *optivus triangulatus* zone of Richardson and McGregor (1986). Several spot samples were collected from loose material on the quarry floor.

Palaeoenvironment

The exposure at South Mountain quarry is divided into a lower part comprising palaeosols, rooted sandstones and terrestrial red beds, and an upper part consisting of proximal fluvio-deltaic sandstones, as seen in the Grand Gorge road section (Stein *et al*. 2007). The locality is well known as a source of large, well preserved plant macrofossils (e.g. Matten and Banks 1969; Hueber and Banks 1979; Banks *et al*. 1985; Stein *et al*. 2007) which have been recovered from both parts of the succession; plants from the sandstone unit show minimal evidence of transport (Stein *et al*. 2007).

Figure 3.9: Oneonta Formation exposed at South Mountain Quarry. Top right: Jenny Morris and John Marshall.

5. Cairo Quarry (42° 19′ 13″ N, 74° 02′ 42″ W)

Geological context and biostratigraphy

Part of the Plattekill Formation is exposed in the Cairo Highway Department Quarry, 3.2 km NW of Cairo, Greene County, New York State (Fig. 3.3). In addition to a 12 m thick composite section (Potvin-Leduc *et al*. 2015, fig. 2), eighteen 1.8–3 m cores drilled during 2012 and 2013 as part of this NERC-funded project are held by the New York State Museum, Albany (Morris *et al*. 2015). The high thermal maturity of the sediments at Cairo (Sarwar and Friedman 1995; Hernick *et al*. 2008; Potvin-Leduc *et al*. 2015) combined with the abundance of oxidising environments (i.e. palaeosols; Morris *et al*. 2015) has resulted in poor spore recovery; hence, in-situ palynostratigraphic data is not available. The Plattekill formation has been dated at other localities; Willis and Bridge (1988) placed the Plattekill and overlying Manorkill Formations in the mid *lemurata magnificus*–mid *optivus triangulatus* zones of Richardson and McGregor (1986), indicating a probable Givetian age.

19 samples were taken from a c. 1 m thick interval of interbedded mudstone and shale between the quarry floor palaeosol and a thick cross-bedded sandstone unit (Fig. 3.10); four further speculative spot-samples were collected from the quarry floor.

Figure 3.10: Sampled interval between quarry floor palaeosol and fluvial sandstone unit, Cairo Quarry. Top right: Bill Stein and Jenny Morris.

Palaeoenvironment

As with South Mountain Quarry, Cairo is a well-established source of plant macrofossils (e.g. Banks 1966; Matten 1973, 1974, 1975; Hernick *et al*. 2008; Feist and Hernick 2014; Labandeira *et al*. 2014; Morris *et al*. 2015). Of particular note is the quarry floor, which comprises a single, extensive, c. 1.6 m thick palaeosol horizon containing multiple moulds of complex tree rooting structures (Morris *et al*. 2015; Fig. 3.11). The size of the trees indicates this was a mature, long-lived forest; as with other similar 'forest floors' (e.g. Stein *et al*. 2012), mapping out the location of the moulds is revealing much about the growth and rooting behaviour of Givetian plant communities.

The exposed strata in Cairo Quarry comprise alternating palaeosols, fluvial sandstones, and dark shales, the latter containing abundant plant material and in-situ freshwater bivalves. It is unclear whether the shales represent coastal floodplain or lacustrine deposits, but in either case they are undoubtedly non-marine (Potvin-Leduc *et al*. 2015).

Figure 3.11: Cairo Quarry floor palaeosol, with *Archaeopteris* root impressions.

6. NY 8 Road section (42° 17′ 10″ N, 75° 23′ 50″ W)

Geological context and biostratigraphy

A 400 m stretch of the NY 8 beginning approximately 2.5 km south of Sidney, Delaware County (Fig. 3.3) provides exposure of undifferentiated Sonyea Group strata (Fig. 3.12), and is approximately equivalent to stop 4A of Bishuk *et al*. (1991)/outcrop 2 of Bishuk *et al*. (2003). The outcrop is likely referable to the uppermost Triangle and Glen Aubrey Formations as defined by Sutton *et al*. (1970) (Bishuk *et al*. 1991; D. Bishuk *pers. comm*. 2014). This assignment is tentative; the limited exposure and lithological similarity of some formations within the Sonyea Group makes them difficult to correlate between sections (Bishuk *et al*. 1991) and it is unclear whether the dark grey shales in the section represent the Sawmill Creek Shale (Bishuk *et al*. 2003; D. Bishuk *pers. comm*. 2014). Note also that the outcrop at stop 4B of Bishuk *et al*. (1991) on Thorpe Road is now inaccessible due to vegetation cover.

Although the Sonyea Group is widely considered to be of Frasnian age (e.g. Rickard 1975; Sevon and Woodrow 1985; Bishuk *et al*. 1991, 2003; Rode and Lieberman 2005),

biostratigraphic data are sparse. Rode and Lieberman (2005) anecdotally placed the Sonyea Group in the mid Frasnian *punctata* conodont zone of Sandberg and Ziegler (1996).

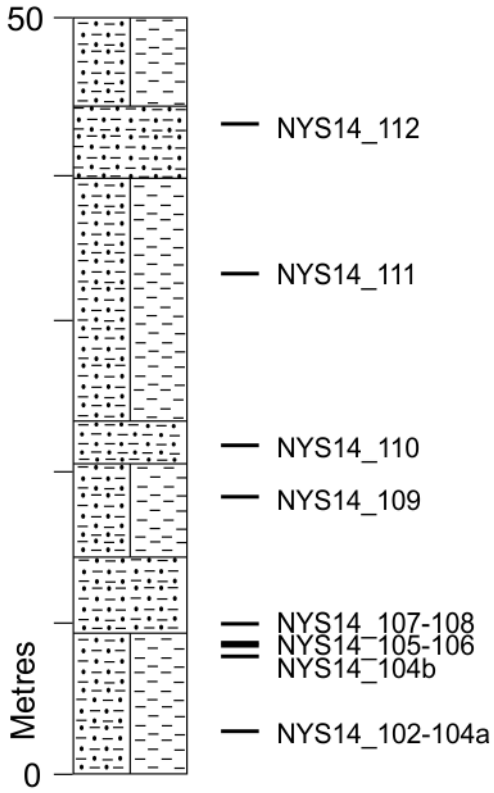

Figure 3.12: Sedimentary log of NY 8 road section. For key see Appendix 3.

Palaeoenvironment

The NY 8 section mostly consists of interbedded shales and siltstones belonging to the Hummocky and Swaley Cross-Stratified facies (HS_{CS}) of Bishuk *et al*. (2003), which represents deposition on a storm-dominated marine shelf. Three intervals of Dark Grey Shale facies (S_{dg}) indicate brief marine transgressions; the lack of bioturbation and benthic fossils in these units indicates anoxic to euxinic conditions. Both of these facies are included in the marine 'Chemung Magnafacies' (Bishuk *et al*. 2003).

7. Sidney Mountain Quarry (42° 16′ 35″ N 75° 23′ 20″ W)

Geological context and biostratigraphy

The Sidney Mountain Quarry (3.5 km south of Sidney; Stop 5 in Bishuk *et al*. 1991 and Stop 3/outcrop 6 in Bishuk *et al*. 2003; Fig. 3.3) provides c. 42 m of exposure of an unnamed unit, most likely equivalent to the Glen Aubrey Formation (D. Bishuk, *pers*. *comm*., 2014; Fig. 3.13). Note that due to ongoing quarrying, at the time of sampling the quarry floor was c. 15 m lower than in 2003 (D. Bishuk, *pers*. *comm*. 2014).

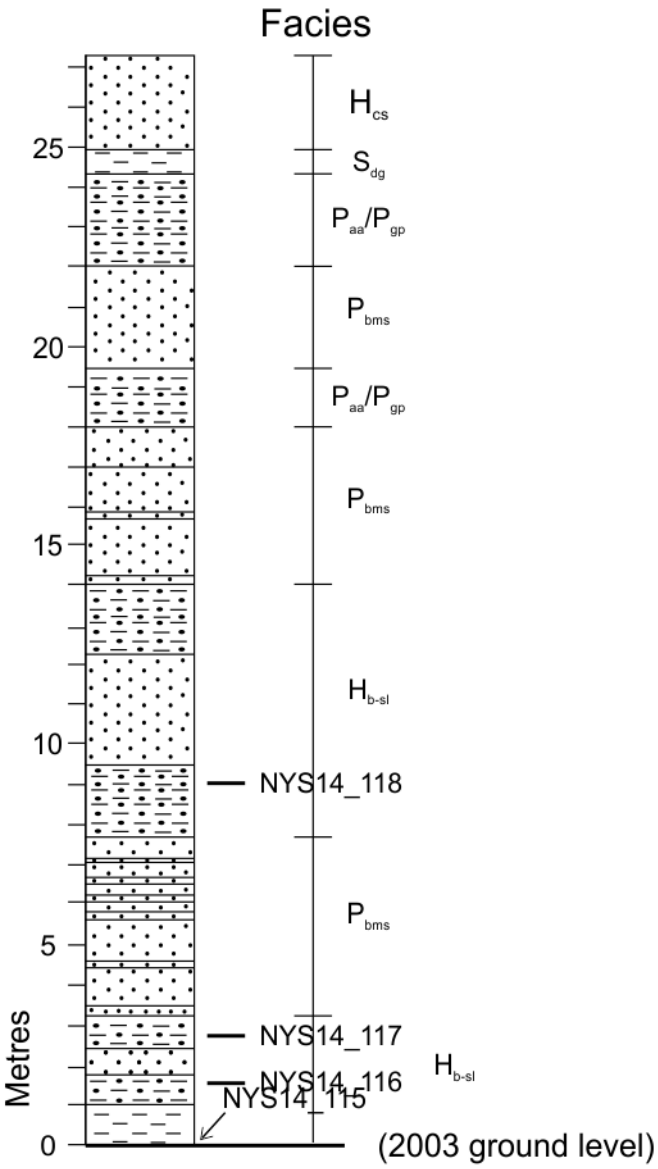

Figure 3.13: Sedimentary log of Sidney Mountain Quarry. Modified after Bishuk *et al*. (2003). For key see Appendix 3.

Palaeoenvironment

Samples NYS14_115–118 were collected from two units of the 'Heterolithic bedded streaky laminated subfacies' (H_b-SL), of Bishuk *et al*. (2003; Fig. 3.13), attributed to alternating storm- and tide-dominated marine conditions on the inner shelf and belonging to the Cattaraugus Magnafacies (Bishuk *et al*. 1991, 2003) which is transitional between terrestrial and fully marine environments (Woodrow and Sevon 1985; Bishuk *et al*. 1991, 2003). The lower part of the first unit is rich in plant macrofossils including tree bark (Bishuk *et al*. 2003; Fig. 3.14); this may indicate greater proximity to the palaeoshoreline, or an increased frequency of storm events washing plant debris out to sea.

Figure 3.14: Unidentified fossil plant material, Sidney Mountain Quarry.

8. Skytop Lane Quarry (42° 16′ 53″ N 75° 16′ 20″ W)

Geological context and biostratigraphy

Skytop Lane Quarry, 1.5 km South West of Sidney Center (Fig. 3.3) is Stop 1, outcrop 43 of Bishuk *et al*. (2003) and provides further exposure of the same unnamed formation present in Sidney Mountain Quarry (Fig. 3.15); as before, this is approximately equivalent to the Glen Aubrey Formation (D. Bishuk *pers*. *comm* 2014).

Palaeoenvironment

Samples from Skytop Lane Quarry were collected from the $P_{ao}/P_{bo}/P_b$ and H_b-I subfacies of Bishuk *et al*. (2003). The three palaeosol subfacies (P) represent soils which experienced occasional tidal flooding; they are interdigitated and highly variable laterally (Bishuk *et al*. 2003). Small in situ plant macrofossils and transported plant debris are common throughout this unit. The inclined heterolithic bedded facies (Hb-I) is interpreted by Bishuk *et al*. (2003) as indicative of tidal channels, flats, and point-bars. Fossil wood and other large plant debris is reportedly common in this unit; other fossils (brachiopods and fish) suggest brackish conditions (Bishuk *et al*. 2003).

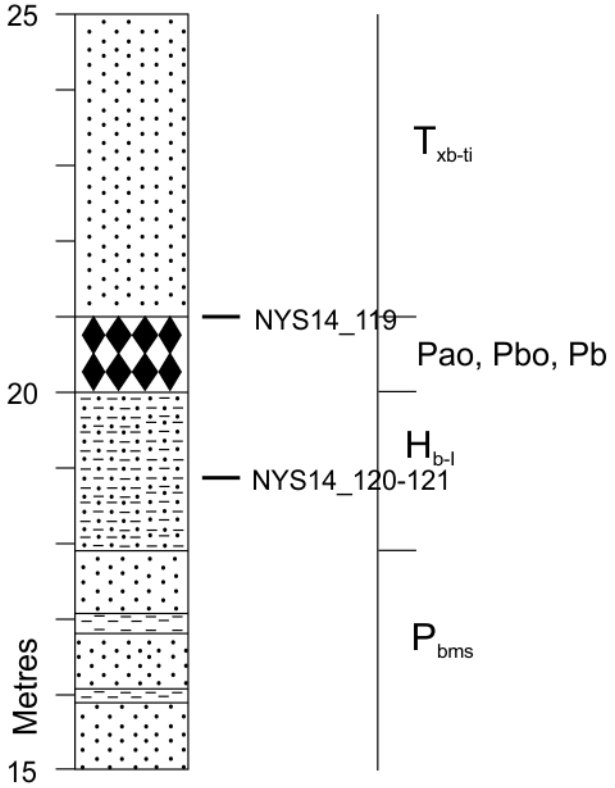

Figure 3.15: Sedimentary log of Skytop Lane Quarry. Modified after Bishuk *et al*. (2003). For key see Appendix 3.

9. Dunshee Hill Quarry #2 (42° 17′ 24″ N 75° 16′ 48″ W) and #4/5 (42° 17′ 24″ N 75° 16′ 45″ W)

Geological context and biostratigraphy

A series of quarries on Dunshee Hill, c. 2 km west of Sidney Center, also provide exposures of the same unnamed formation. Quarry #2 is outcrop 33 in Bishuk *et al*. (2003); quarries #4 and 5 (outcrops 35 and 36) have been merged since 2003 and are here treated as a single locality. A small number of spot-samples were taken from each quarry.

Palaeoenvironment

Only the planar-bedded multi-storey sand body facies (P_{bms}) is present at quarry #2; quarry 4 /5 (Fig. 3.16) contains elements of the P_{bms} and $H_{b\text{-}l}$ facies. Both facies represent deposition in tidal channels, point-bars and flats, but the former is more proximal in nature (Bishuk *et al*. 2003).

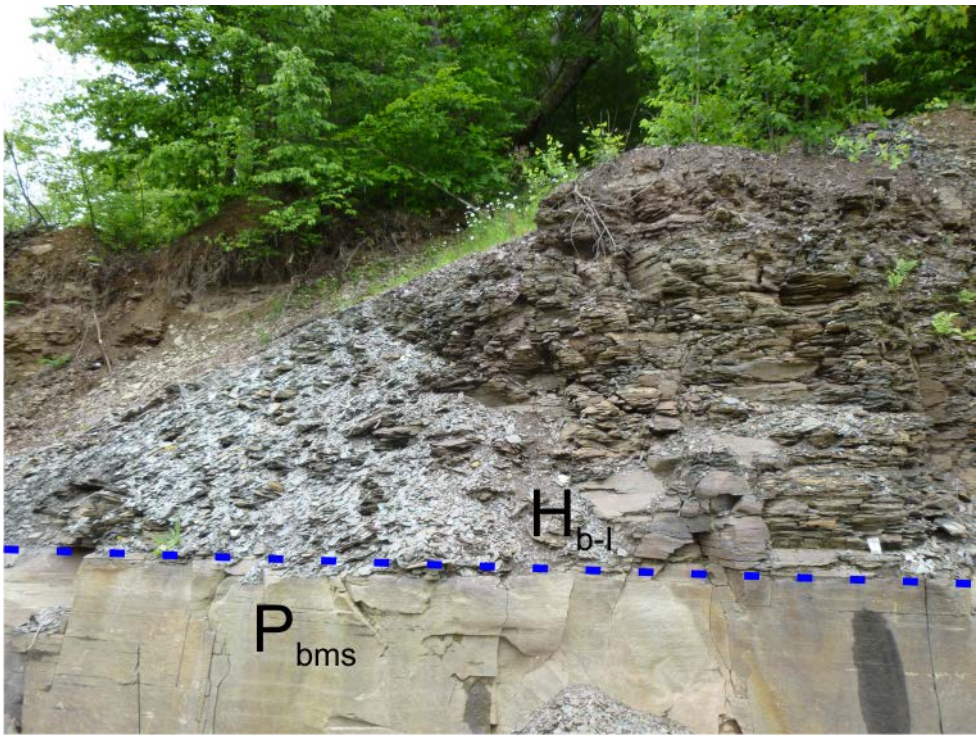

Figure 3.16: Exposure of undifferentiated Sonyea Group units in Dunshee Hill Quarry # 4/5, assigned to the ‘Pbms’ and ‘Hb-l’ facies of Bishuk *et al*. (2003). Dashed line indicates facies boundary.

10. CR 27 Road section

Geological context and biostratigraphy

Delaware County Route 27 (Pomeroy Corners Road), 3 km east of East Masonville, Delaware County is outcrop 53 in Bishuk *et al*. (2003). As with the Dunshee quarries, logs were not available; two further spot-samples were taken from the middle unit, approximately 4.5 m thick, of the three exposed at outcrop 53. All are assigned to the same unnamed formation (Bishuk *et al*. 2003).

Palaeoenvironment

The middle unit of the CR 27 road section was assigned by Bishuk *et al*. (2003) to the trough cross-bedded (tidally influenced) subfacies (= T_{xb}–Ti). Woody plant debris, the brachiopod *Cupularostrum* and rare crinoid ossicles are reported to be locally common in some beds, though none were observed on this occasion. The T_{xb}-Ti subfacies is attributed by Bishuk *et al*. (2003) to deposition in a tidal creek complex, near the mouth of a tidally-dominated delta.

11 – 12. NY 23 Road Sections

Geological context and biostratigraphy

Starting at the junction with Five Mile Woods Road, 1.5 km west of Leeds, Greene County and continuing northwest as far as Point Lookout, East Windham, the uppermost Mount Marion Formation, ?Ashokan, Plattekill, and Manorkill Formations are intermittently exposed in outcrop and road-cuts along New York State Route 23 (Fig. 3.3). This stretch of road encompasses stops 4–6 of Ver Straeten (2009), and location C of Mintz *et al*. (2010); most sampled localities are points of interest between formal stops, mentioned by Ver Straeten (2009).

The upper part of the Mount Marion Formation in eastern New York is undifferentiated, and the position of the contact with the overlying Ashokan Formation is unknown (Ver Straeten 2009, 2013; Ver Straeten *et al*. 2011). The former unit is placed in the *hemiansatus* conodont zone and the latter in either the *hemiansatus* or *timorensis* zone by Ver Straeten *et al*. (2011), making both early Givetian in age. For the Plattekill and

Manorkill Formations, see geological context and biostratigraphy for Cairo Quarry (above).

Palaeoenvironment

In the broadest terms, the succession between Leeds and East Windham represents a transition from nearshore marine (upper Mount Marion Fm.) to fully terrestrial (Ashokan–Manorkill Fm.) conditions (Ver Straeten 2013). This is complicated by the limited lateral extent of the terrestrial units, which grade into marine deposits to the east and west of the study area (Ver Straeten *et al*. 2011, fig. 1-3), and the interdigitated nature of the contacts between them (Ver Straeten 2007, 2009). In particular, the undifferentiated upper Mount Marion Fm. becomes increasingly terrestrial up-section, and the contact with the overlying Ashokan Fm. is not well defined (Ver Straeten 1994, 2009).

NY23-A (42° 15′ 24″ N 73° 55′ 12″ W)

This is stop 4 of Ver Straeten (2009), which represents the uppermost Mount Marion Formation (Ver Straeten 2009, 2013). The exposure is sand-dominated, with 1–3m sand bodies separated by smaller interbedded sandstone/mudstone units. HCS is evident in the lower sandstone units, indicating an inner-shelf marine setting; large ripples in the upper sandstones suggest a shore face setting (Ver Straeten 2009). The brachiopod *Camarotoechia*, indicative of a near-shore marine environment (Sutton and McGhee 1985), is common in the middle part of the outcrop (Fig. 3.17).

Figure 3.17: The brachiopod *Camarotoechia*, Mount Marion Fm., NY23-A outcrop.

NY23-B (42° 16′ 10″ N 73° 56′ 50″ W)

The lowest outcrop of Plattekill Formation 'red-beds', exposed on the north side of NY23, near a deer warning sign, noted at mile 56.2 of Ver Straeten 2009 road-log (Fig. 3.18). Interbedded red and green mudstones, dark grey shales, palaeosols, and fluvial sandstones indicate alluvial plain and river channel deposits. Due to uncertainty over the Mt. Marion/Ashokan contact, this may in fact be the upper part of the Ashokan Fm. (C. Ver Straeten, *pers*. *comm*., 2014).

Figure 3.18: Plattekill Fm. red-beds, NY23-B outcrop.

NY23-C (42° 16′ 59″ N 73° 58′ 14″ W)

Further exposure of the Plattekill Fm. is present along Silver Spur Road, just west of NY23, noted at mile 57.8 of the Ver Straeten (2009) road log. A single spot sample was taken from a dark shale unit (Fig. 3.19) resembling those observed at NY23-D, likely representing floodplain deposition (C. Ver Straeten, *pers. comm*; see below).

Figure 3.19: Plattekill Fm. exposure, NY23-C outcrop.

NY23-D (42° 18′ 21″ N 74° 00′ 02″ W)

The third Plattekill Fm. outcrop, Stop 5 of Ver Straeten (2009). The exposure comprises interbedded dark shales, green mudstones, palaeosols and thin sand bodies, interrupted by two major channel sandstones, and is interpreted by Ver Straeten (2009) as representing floodplain deposition, with periodic channel migration. While similar to NY23-B, this exposure lacks the former's characteristic red colour. Two spot-samples were taken from shales within the 'lower mudrock unit' of Ver Straeten (2009) (Fig. 3.20).

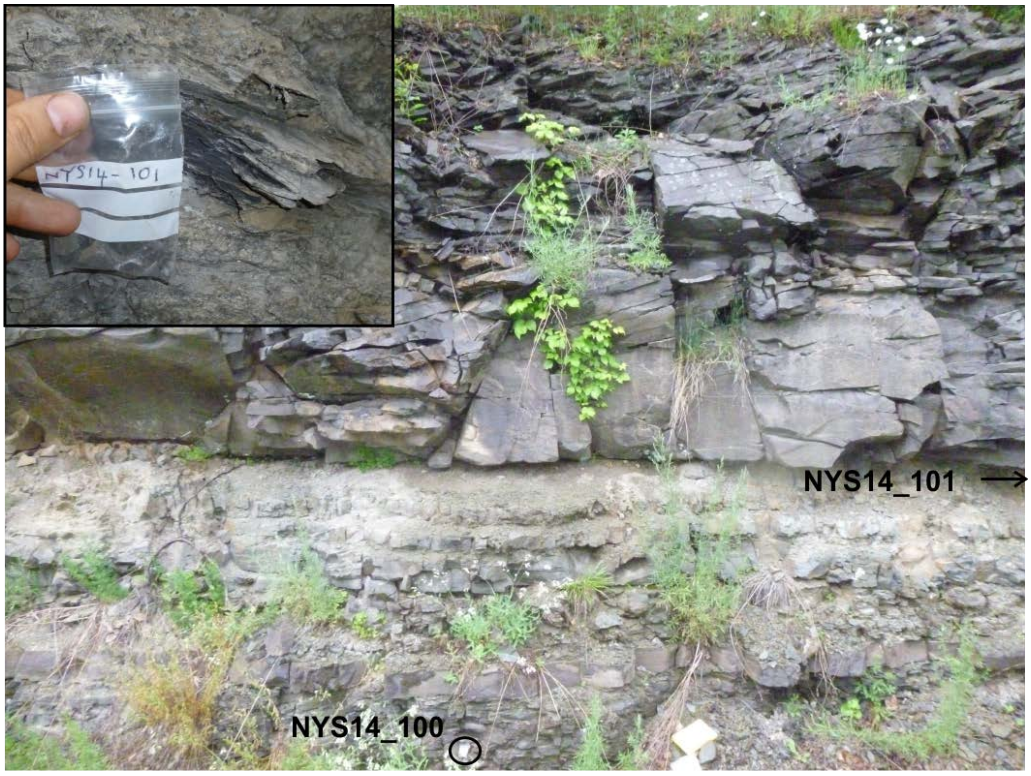

Figure 3.20: Plattekill Fm. outcrop at NY23-D; lower mudrock unit of Ver Straeten (2009).

NY23-E (42° 20′ 01″ N 74° 06′ 53″ W)

This is the first of five roadcuts on the NY23 north of Windham High Peak which provide exposures of the Manorkill Formation. The location is noted at mile 66.9 on the Ver Straeten 2009 road-log as being “near interesting and unusual buildings” (Ver Straeten 2009, p. 7-44), and is an example of Manorkill Fm. terrestrial red-beds, which are lithologically similar to those seen in the underlying Plattekill Fm. (Fig. 3.21).

Figure 3.21: Manorkill Fm. terrestrial red-beds at NY23-E. Left of photo: John Marshall.

NY23-F (42° 20′ 17″ N 74° 07′ 06″ W)

Second Manorkill Formation roadcut; Stop 6 in Ver Straeten (2009) and Location C in Mintz *et al*. (2010). This represents the stratigraphically highest point detailed by Ver Straeten (2009). Interbedded palaeosols, mudstones and thin sandstones similar to those seen at NY23-D are exposed in the lowest part of the section (Fig. 3.22); Mintz *et al*. (2010) recorded a 55 cm thick 'forest' palaeosol containing archaeopterid stump-casts in this unit. These are overlain by slumped mudstones, followed by a prominent thin limestone believed to be lacustrine (Ver Straeten *et al*. 2009) and indicative of a permanent water body on a low-lying coastal plain (Ver Straeten 2013). Three spot-samples were collected from the lower, interbedded unit.

Figure 3.22: Interbedded mudstones, sandstones, and palaeosols representing the Manorkill Fm. at NY23-F.

NY23-G (42° 20′ 07″ N 74° 08′ 04″ W)

Third Manorkill Formation roadcut, near a steep driveway on the south side of the road. A single thin limestone presumed to be the same as that observed at NY23-F allows tentative correlation. The mudstone-dominated strata above the limestone contain abundant fragmentary fish skeletal debris; this is in accord with NY23-F, where similar fish material has been reported (Ver Straeten 2009). Desiccation cracks and the presence of the trace fossil *Spirophyton* reported in the unit at NY23-F suggest ephemeral, possibly brackish water-bodies on a coastal plain, periodically filled by storm-driven floods (Miller 1991; Ver Straeten 2009, 2013). Samples from this part of the succession were collected from a prominent c. 80 cm thick shale bed (Fig. 3.23). The succession beneath the limestone is similar to that seen at NY23-F, but has a greater proportion of palaeosols and is predominantly red in colour. A dark shale band towards the bottom of the section (Fig. 3.24) was rich in carbonised plant debris and charcoal, suggesting well established vegetation growing in or around coastal wetlands with persistent water bodies.

Figure 3.23: Manorkill Fm. roadcut NY23-G. Samples collected from prominent shale bed (B). With John Marshall (left), Jenny Morris (centre) and Chuck Ver Straeten (right).

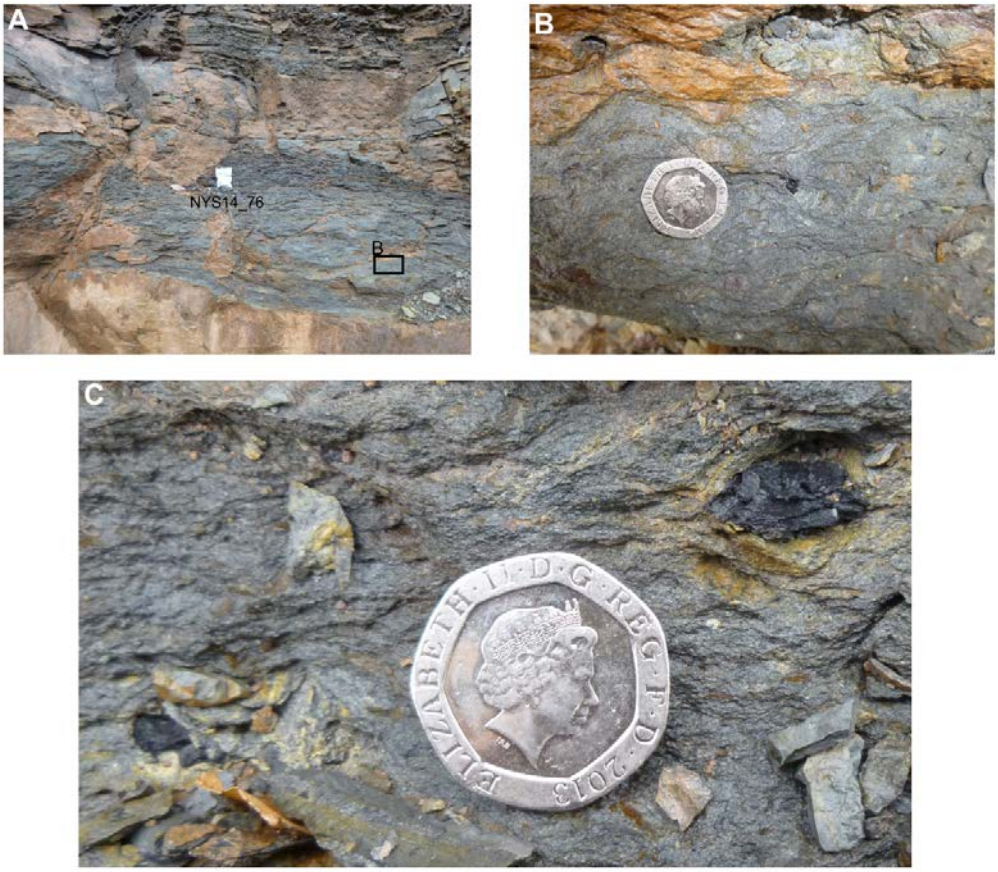

Figure 3.24: Charcoal-rich bed, Manorkill Fm., lower part of NY23-G road cut. 20p coin c. 2 cm.

NY23-H (42° 20′ 5″ N 74° 08′ 44″ W)

Fourth Manorkill Formation roadcut, south side of NY23, opposite a single, isolated house. Terrestrial red-beds comprising interbedded palaeosols, red, grey, and mottled mudstones (Fig. 3.25), and large sand-bodies similar to the lower part of NY23-G, representing floodplain deposition with periodic channel migration and occasional small standing water-bodies.

Figure 3.25: A, Manorkill Fm. outcrop NY 23-H; B, mottled mudstone (female *Plathemis Lydia*, c. 4cm, for scale).

NY23-I (42° 20′ 19″ N 74° 09′ 04″ W)

Final Manorkill Formation roadcut at Point Lookout, East Windham. A c. 25 m exposure of red-beds (Fig. 3.26), lithologically similar to those seen at the previous locality. Sample NYS14_88 was collected from a block which had fallen from the top of the section.

Figure 3.26: Manorkill Fm. roadcut NY 23-I.

13. US 209 Road cuts

Geological context and biostratigraphy

A road cut on the west side of US route 209, 4.5 km west of East Kingston, Ulster County, provides exposure of the uppermost Union Springs Formation (Bakoven, Stony Hollow and Hurley Members) and Mount Marion Formation (Cherry Valley and East Berne members; Fig. 3.27); this locality is stop 2 of Bartholemew *et al*. (2009). The majority of the exposure is of the East Berne Member, which is c. 60 m thick (Bartholemew *et al*. 2009).

As noted above, biostratigraphic control for the Marcellus subgroup is poor (Ver Straeten 2007; Ver Straeten *et al*. 1994, 2011; Becker *et al*. 2016) and the exact position of the Emsian/Eifelian stage boundary is unknown. Becker *et al*. (2016) place the Bakoven and Stony Hollow Members in the lower Eifelian *partitus* and upper Eifelian *australis* conodont zones, respectively; the Hurley and Cherry Valley Members are placed by Desantis *et al*. (*ibid*) in the *kockelianus* zone. The East Berne Member is placed tentatively in the uppermost Eifelian *ensensis* conodont zone by Desantis *et al*. (2007) but an earliest Givetian age for the upper part of the unit is also possible (C. Ver Straeten *pers*. *comm*. 2014).

In eastern New York the limestones which ordinarily characterise the Hurley and Cherry Valley Members are absent, replaced by calcareous shales, silts and sandstones which are quite similar to those of the Stony Hollow Member (Ver Straeten *et al*. 1994, Ver Straeten 2009). The US 209 exposure presents further difficulties, in that the Cherry Valley/East Berne contact is obscured by vegetation Bartholomew *et al*. (2009). As a result, the position of the contacts between these members is uncertain.

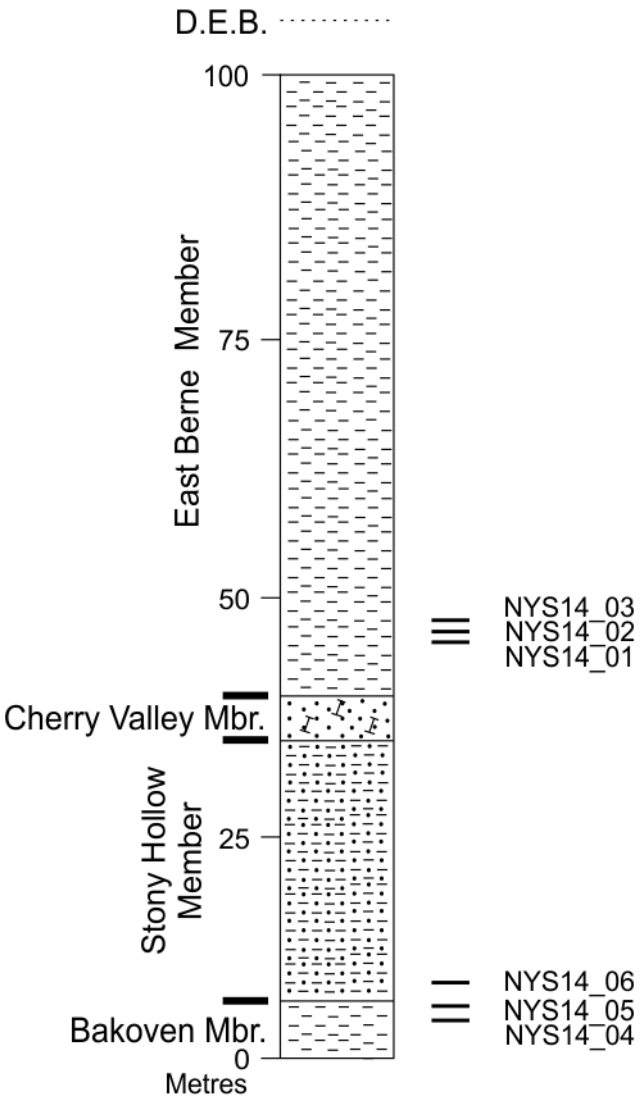

Figure 3.27: Sedimentary log of US 209 road cut. Modified after Bartholomew *et al*. (2009). For key see Appendix 3.

Palaeoenvironment

The Bakoven Member comprises black to dark grey, occasionally pyritic shales containing a dysaerobic marine fauna (the 'Stony Hollow Fauna') of brachiopods and trilobites (Griffing and Ver Straeten 1991; Koch and Day 1996; Bartholomew *et al*. 2009). The unit is interpreted as having been deposited in a marine basin c. 100–200 m deep (Ver Straeten 2009; Bartholomew *et al*. 2009).

The East Berne Member is characterised by grey to dark-grey shales, which become increasingly interbedded with thin (≤ 50 cm) silts and sandstones towards the top of the unit; these latter show evidence of storm activity, and are interpreted by Ver Straeten (1994) as tempestites. The succession as a whole is therefore a coarsening-upwards sequence, indicating a change in setting from basin to slope/coastal shelf. A thin fossil-rich band representing a marine transgression, the Dave Elliott Bed, contains abundant marine brachiopods and corals (Ver Straeten 1994; Bartholomew *et al*. 2009) but was not observed at the US 209 locality; the shales are otherwise generally lacking in fauna, though some indeterminate bivalves and the dysaerobic brachiopod *Leiorhynchus* have been reported (Ver Straeten 1994; Bartholomew *et al*. 2009).

14. Unnamed quarry, Bluestone Wild Forest (41° 58' 45" N, 74° 04' 42" W)

Geological context and biostratigraphy

An inactive flagstone quarry in Bluestone Wild Forest, c. 0.6 km east of Onteora Lake and 2.75 km SE of West Hurley, Ulster County (Fig. 3.3) provides exposure of the uppermost Mt. Marion Formation (Fig. 3.28). This is Stop 8 in Ver Straeten and Brett (1995). No biostratigraphic data is available for this locality, but as noted above (see geological context and biostratigraphy for NY 23 road sections) the formation has been assigned a lower Givetian age elsewhere in New York State (Ver Straeten *et al*. 2011; Ver Straeten 2013; Becker *et al*. 2016).

Palaeoenvironment

The succession is dominated by interbedded sands, silts and shales containing normal marine invertebrate faunas, and larger sandstone bodies; a 1 m thick unit of interbedded

thin sands and organic-rich shale beds containing abundant plant debris is also present in the upper level of the quarry, and it is from this unit that most of the samples were collected. The lithology is considered typical of a nearshore marine/non marine transitional environment, with periodic subaerial exposure (Ver Straeten and Brett 1995; C. Ver Straeten *pers. comm* 2014).

Figure 3.28: Uppermost Mt. Marion Fm., Bluestone Wild Forest quarry. With John Marshall (left) and Chuck Ver Straeten (right).

15. NY 28 composite section

Geological context and biostratigraphy

A small unnamed quarry (41° 58′ 56″ N, 74° 05′ 25″ W), 200 m rail-cut (41° 59′ 26″ N, 74° 05′ 12″ W), and 150 m road section along NY 28 (Onteora Trail: 41° 59′ 05″ N, 74° 05′ 07″ W) between Onteora Lake and Ashokan Reservoir together provide a composite section of the lower part of the Ashokan Formation and, possibly, the uppermost Mt. Marion Formation (Wolff 1968; Rickard 1989). The small quarry is within the grey channel-sandstones which are noted as a point of interest between stops 3b and 4 of Wolff

(1968); the rail-cut is stop 4, and the road section is stop 5 (*ibid*) and stop 6 in Pederson *et al*. (1976).

Palaeoenvironment

All three localities are characterised by thick channel sandstones alternating with interbedded sands, silts, and shales (Fig. 3.29); these were interpreted by Wolff (1968) and Pederson *et al*. (1976) as tidal channel, bar and flat deposits, supported by the presence of an invertebrate fauna suggestive of brackish conditions (Pederson *et al*. 1976). The road section (Fig. 3.30), which is stratigraphically lowest, reportedly contains a greater diversity of marine fossils (Wolff 1968) and hence may span the Mt. Marion/Ashokan Fm. boundary.

Figure 3.29: Outcrop at NY 28 section. A, channel sandstone; B, interbedded unit.

Figure 3.30: NY 28 road section.

16a. Kaaterskill Creek River Section (42° 10′ 19″ N, 74° 01′ 08″ W–42° 10′ 38″ N, 74° 03′ 10″ W)

Geological context and biostratigraphy

The Kaaterskill Creek River section (lower part of section F in Willis and Bridge 1988) comprises a c. 3 km stretch of the river NE (upstream) of Palenville, Greene County. It is placed by Willis and Bridge (1988) in the Givetian Plattekill/lowermost Manorkill Formations; for detailed biostratigraphic context see geological context and biostratigraphy for Cairo quarry. Spot-samples were collected from the bottom, middle, and top parts of the section.

16b. NY 23A Road section (42° 11′ 08″ N, 74° 04′ 15″ W–42° 11′ 37″ N, 74° 04′ 59″ W)

Geological context and biostratigraphy

A c. 1.35 km road section, starting 4.35 km NE of Palenville centre, incorporates section X of Willis and Bridge (1988) and is approximately equivalent to the upper part of their section F, which spans almost the entire Manorkill Fm. Spot-samples were collected from the top and bottom of the exposure.

Palaeoenvironment

The exposure along Kaaterskill Creek and equivalent roadside outcrops is characterised by trough cross-stratified channel sandstones and with interbedded sand/mudstone units, representing channel and overbank deposition on an alluvial plain (Willis and Bridge 1988). Mudstones commonly contain root traces, plant debris, and rare tree stump casts; the latter are also found in some sandstone units (Willis and Bridge 1988). Strata towards the top of the creek become increasingly red, and occasional mud cracks indicate subaerial exposure (Fig. 3.31).

Figure 3.31: red mudstones at Kaaterskill Creek, with mud cracks.

17a. Plattekill Creek River Section (42° 06′ 55″ N, 74° 03′ 21″ W–42° 07′ 14″ N, 74° 03′ 53″ W)

Geological context and biostratigraphy

The upper Plattekill, entire Manorkill, and lowermost Oneonta Formations are exposed in a continuous section along the banks of Plattekill Creek, which extends approximately 3.5 km NE from West Saugerties, Ulster County. This is Section C in Willis and Bridge (1988), and is located 3.5 km south of the Kaaterskill Creek river section; hence, the two sections are well correlated and lithologically very similar (Willis and Bridge 1988, fig. 3). The Oneonta Formation, which is not exposed at Plattekill Creek, is the most terrestrial unit, characterised by well-developed palaeosols (e.g. Fig. 3.32).

17b. Plattekill Creek Road Section (42° 07′ 10″ N, 74° 03′ 44″ W–42° 07′ 52″ N, 74° 04′ 47″ W)

Parts of the Manorkill Formation, and the lowermost Oneonta Formation, are exposed along the N side of Plattekill Creek Road, which runs parallel to Plattekill Creek; this is Section A in Willis and Bridge (1988), and can be correlated with the upper part of their Section C (*ibid*, fig. 3).

Figure 3.32: Palaeosol unit, Oneonta Fm., Plattekill Creek Road section. With Chuck Ver Straeten.

18. Blue Trail (42° 09′ 29″ N, 74° 12′ 32″ W)

Geological context and biostratigraphy

The Lower Walton Formation (Sonyea Group) is intermittently exposed along Blue Trail, which climbs the east flank of Southwest Hunter Mountain, Greene County; this is Outcrop 19 (‘Hunter Mountain’) of Gordon and Bridge (1987). The formation is undifferentiated, and as currently defined spans the entire Sonyea Group (Bishuk *et al*. 1991, fig. 5). As noted previously, although widely considered to be of Frasnian age (Retallack *et al*. 1985; Bridge *et al*. 1986; Gordon and Bridge 1987; Ver Straeten 2009, 2013) biostratigraphic control for the Sonyea Group is poor; Rickard (1975) placed the

Lower Walton Fm. in the upper *Polygnathus asymmetricus* conodont zone of Bischoff and Ziegler (1957), which is mid Frasnian in age. The exposure was found to be heavily sandstone dominated (Fig. 3.33), with few horizons suitable for sampling; only two spot samples were collected.

Figure 3.33: Sand-dominated Lower Walton Fm. exposure, Blue Trail.

Palaeoenvironment

The formation as a whole is typical of the Catskill Magnafacies, largely representing fluvial channel and floodplain deposition, albeit with some locally developed lacustrine components (Schieber 1999; Ver Straeten 2009, 2013). Palaeosols have been identified within mud units, and suggest a seasonal wet/dry cycle (Retallack *et al*. 1985; Schieber 1999).

19. Red Hill, Pennsylvania (41° 20′ 30″ N, 77° 40′ 30″ W)

Geological context and biostratigraphy

The Duncannon Member of the Famennian Catskill Formation is exposed at Red Hill, a c. 1km road cut on the N side of the PA 120 (Bucktail Trail) between North Bend and Hyner, Clinton County, Pennsylvania (Fig. 3.3). This is Stop 2 of Daeschler and Cressler (2006), and Stop 5 of Daeschler and Cressler (2011). Palynological investigation (Traverse 2003) has placed the exposure at Red Hill in the VCo spore biozone of Streel *et al*. (1987; = *flexuosa-cornuta* zone of Richardson and McGregor 1986), indicating a late Famennian age (Famennian 2c; Daeschler and Cressler 2006; Cressler 2006).

As implied by the name, material suitable for palynological processing is rare at Red Hill; as well as producing the iron oxide which gives the exposure its characteristic colour, oxidation has destroyed much of the organic content and palynological recovery is generally poor. Most samples were collected from fallen blocks/loose material amongst the talus at the bottom of the section, selected for visible plant fragments; an in-situ sample was collected from the Plant Layer of Cressler (2006; Figs. 3.34–3.35).

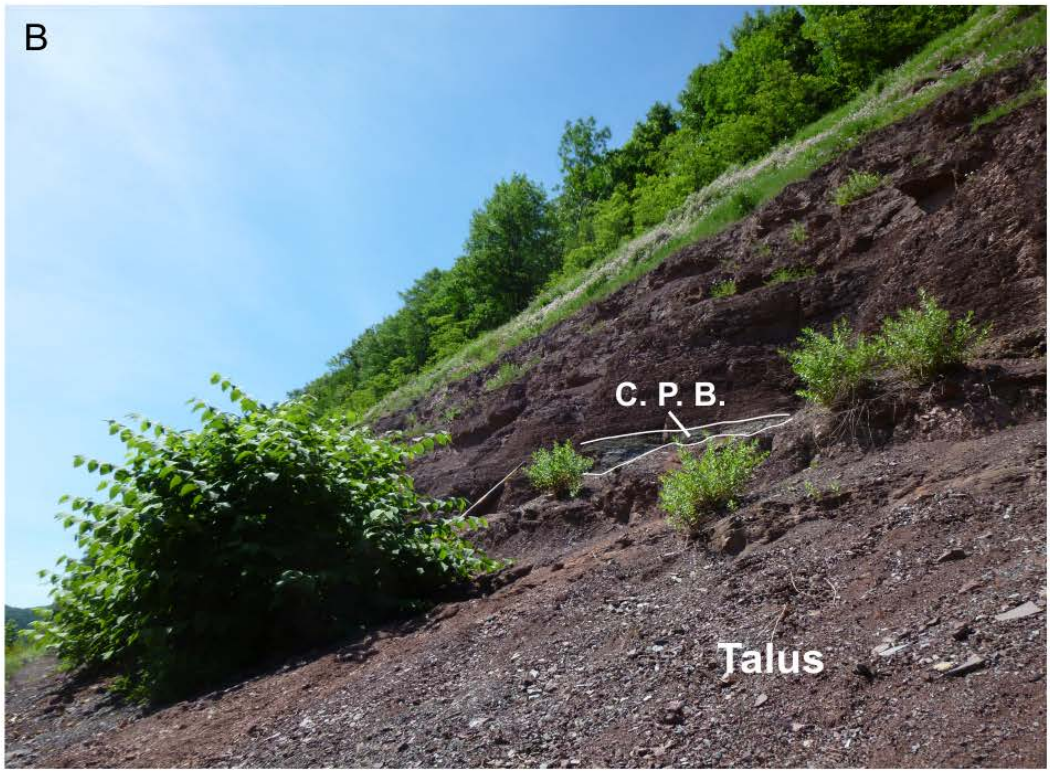

Figure 3.34: Outcrop at Red Hill, Pennsylvania. A, main section; B, sampling point, showing Cressler Plant Bed (C. P. B.). White lines indicate bed boundaries.

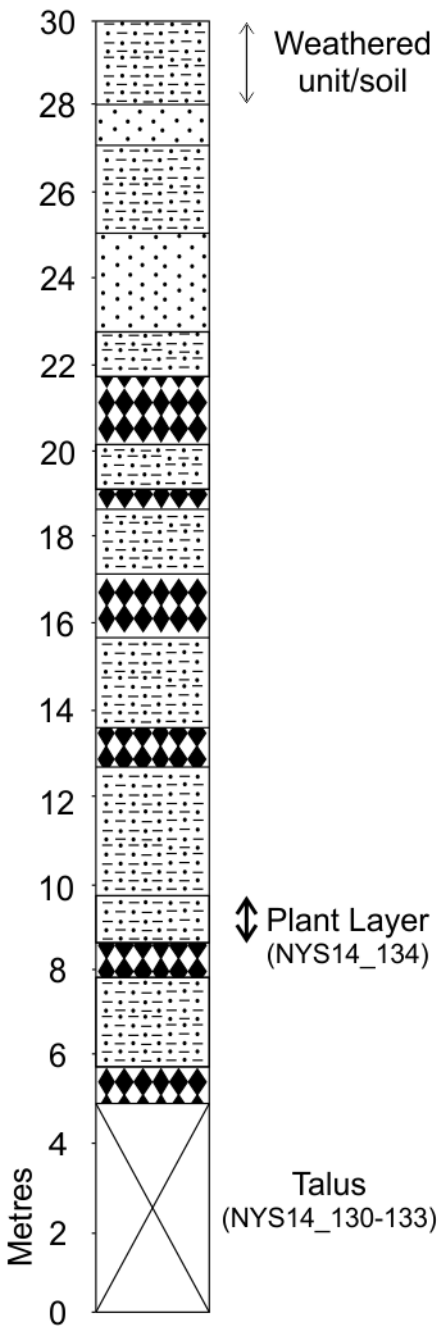

Figure 3.35: Sedimentary log of Red Hill. Modified after Cressler (2006). For key see Appendix 3.

Palaeoenvironment

The Duncannon Member is characterised by repeated 5–10 m thick fining-upward sequences, whereby cross-bedded channel sandstones are replaced by silts, muds and palaeosols (Daeschler and Cressler 2011). This is has been interpreted as a meandering stream facies, deposited on a large, forested, low-gradient flood-plain at a considerable distance from the palaeoshoreline, similar to the present-day Cumberland Marshes in

Saskatchewan, Canada (Sevon 1985; Woodrow *et al*. 1995; Cressler 2006; Daeschler and Cressler 2006, 2011; Cressler *et al*. 2010, fig. 3). Despite the predominance of red, oxidised units and palaeosols for which it is named, Red Hill has long been recognised as a source of abundant fossil remains (Thomson 1968; Reed 1986; Daeschler *et al*. 1994; Daeschler 2000; Downs and Daeschler 2001; Shubin *et al*. 2004; Wilson *et al*. 2005; Cressler 2006; Daeschler and Cressler 2011) including diverse fishes (actinopterygians, chondrichthyans, sarcopterygians, placoderms, and acanthodians) tetrapods (*Hynerpeton* and *Densignathus*), arthropods (arachnids and myriapods), and plants (*Rhacophyton*, *Archaeopteris*, and *Gillespiea*). Most fossil plant (and some fragmentary fish and arthropod) material is concentrated within lenses of green/grey siltstone, of which the Plant Layer of Cressler (2006) is an example; such units are believed to represent small floodplain ponds, or other similar low-energy standing water facies (Daeschler and Cressler 2011).

The Plant Layer is also noted for its abundance of large (i.e. macroscopic) fossil charcoal (Cressler 2001; Cressler *et al*. 2010; Fig. 3.36). Several samples were provided by Doug Rowe, (Red Hill Field Station) for analysis.

Figure 3.36: Macroscopic charcoal specimen from Cressler Plant Bed, Red Hill.

3.3 Sampling localities – Silurian, USA

20. US 11 Roadcut (40° 57′ 30″ N, 76° 39′ 36″ W)

Geological context and biostratigraphy

The opportunity was taken while in Pennsylvania to visit Stop 1 of Nickelsen and Cotter (1983), a c. 500 m road section running parallel to the Susquehanna River, southwest of Danville, Northumberland County, Pennsylvania (Fig. 3.37). The road-cut exposes Silurian strata from the Rose Hill Formation (Clinton Group) to the undifferentiated Mifflintown and lower Bloomsburg Formations (Nickelsen and Cotter 1983). The Rose Hill and Mifflintown Fms. were placed by Helfrich (1980) in the *Pterspathodus amorphognathoides* and *Kockellela patula* zones of Walliser (1964) respectively, which are late Llandovery and mid Wenlock in age (Märss and Männik 2013). The Bloomsburg Fm. near Danville has been placed between the *Ozarkodina snajdri* and *O. tillmani* conodont zones (Beck and Strother 2008; Retallack 2015), indicating a late Ludlow age (Märss and Männik 2013). The latter almost entirely consists of highly oxidised palaeosols and mudstones, and hence was not sampled (Fig. 3.37B).

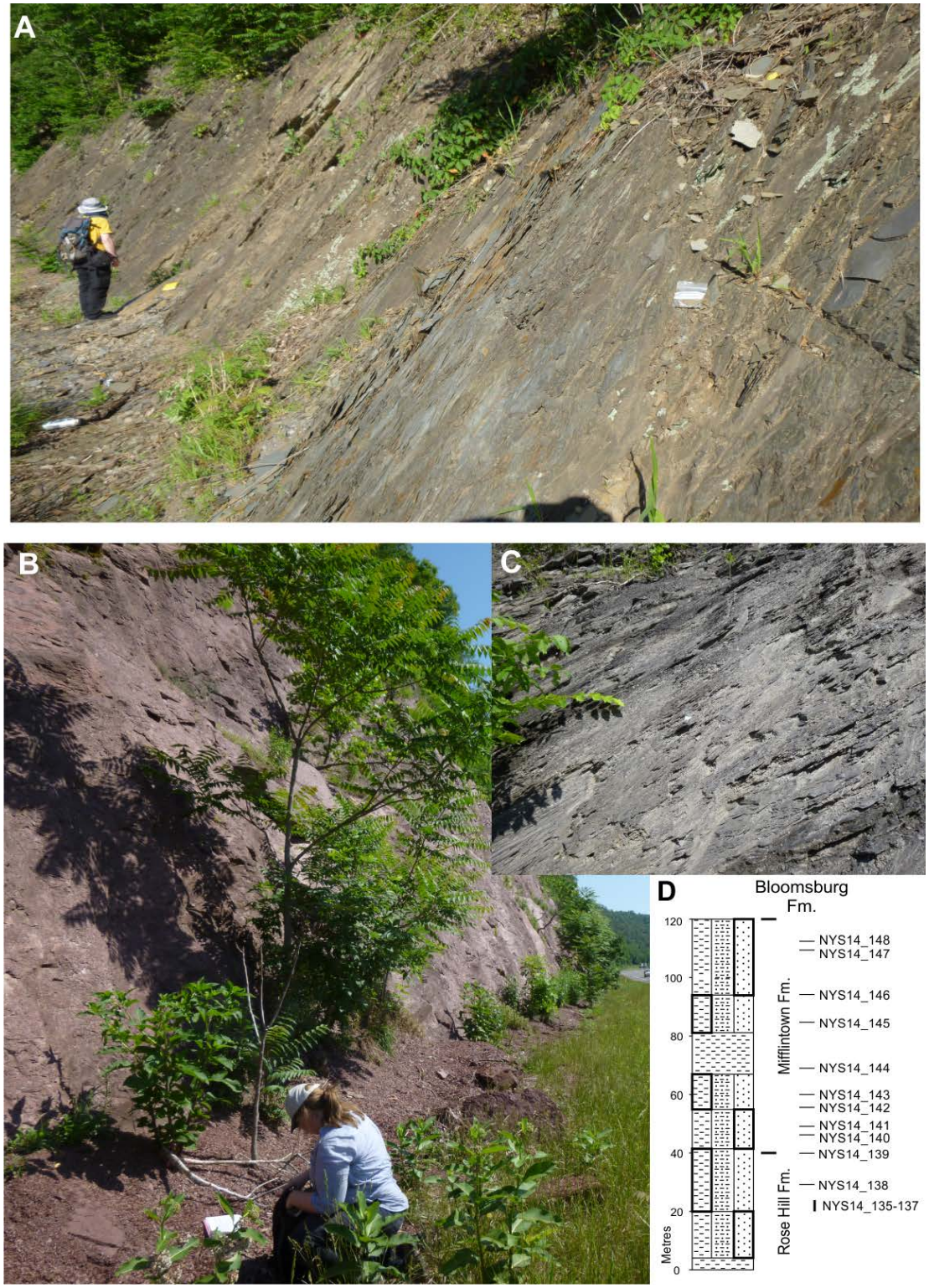

Figure 3.37: US 11 road cut. A, interbedded unit, Rose Hill Fm.; B, highly oxidised red-beds, Bloomsburg Fm.; C, dark shale representing marine transgression, Mifflintown Fm.; D, sedimentary log of US 11 road cut. For key see Appendix 3.

Palaeoenvironment

The Rose Hill and Mifflintown Fms. mainly consist of interbedded shales, silts, and sandstones which become increasingly calcareous up-section (Nickelsen and Cotter 1983; Fig. 3.37A). Shales vary between red, grey-green, and dark grey in colour; the level of oxidation in the succession is generally quite high. Invertebrate and trace fossil assemblages in the finer grained units indicate normal marine, generally dysaerobic conditions; the trace fossils are attributed to the Männik Ichnofacies (Nickelsen and Cotter 1983; Cotter and Link 1993). The coarser units exhibit a range of sedimentary structures, such as hummocky cross-stratification (HCS), which identify them as storm deposits (Cotter 1990). Overall, this kind of heterolithic bedded facies is typical of an outer shelf environment.

A large dark shale bed (c. 20m) in the middle of the Mifflintown Formation is rich in pyrite, and lacks bioturbation (Fig. 3.37C); this indicates deposition in low O_2 conditions below the storm-base, and has been interpreted as a marine transgression (Nickelsen and Cotter 1983; Cotter 1990; Cotter and Link 1993).

21. Watsontown Brick Company quarry (41° 04’ 04” N, 76° 51’ 05” W)

The Watsontown Brick Company quarry, Watsontown, Northumberland County (Stop 5 in Nickelsen and Cotter 1983), provides further exposure of the Bloomsburg Formation. Our request to enter the quarry itself was refused, but a small section of the outcrop was accessible on public land at the western edge of the exposure. As at the US 11 roadcut (see above), the succession in Watsontown comprises red palaeosols, mudstones and shales and hence was not sampled.

3.4 The Catskill Delta Complex in eastern Canada

The Lower and Middle Devonian coastal exposures around Gaspé Bay, eastern Quebec, are considered to be the best examples of the Devonian Clastic Wedge in the region (Lawrence and Rust 1988), and have long been recognised as a source of abundant and well preserved fossil plant material (Dawson 1859; Edwards 1924; Daber 1960; Banks and Davis 1969; Hotton *et al*. 2001). Shale samples collected from the logged sections of McGregor (1973) were provided by Prof. C. Wellman, University of Sheffield, for processing and analysis.

Geological context and biostratigraphy

The Lower–Middle Devonian Gaspé Sandstone Group and overlying Malbaie Formation are exposed on the north and south shores of Gaspé Bay, eastern Quebec, Canada (Fig. 3.38). Palynological sampling of the uppermost 90 m of the York River Fm., the entire Battery Point Fm., and the lower 350 m of the Malbaie Fm. by McGregor (1973) indicated a Pragian or early Emsian–early Eifelian age for the succession, with the Emsian/Eifelian stage boundary placed between his samples 5368 and 7122 (Fig. 3.39, SI 3.5). Both contacts are conformable, but correlation between the north and south shores is only approximate; hence, the Battery Point Fm. is divided into different members on opposite sides of the bay (McGregor 1977; Griffing *et al*. 2000). Samples examined here are from McGregor's sections TW (GA1–34), B (GA35) and D (GA36–48), though graphic logs of sections B and D are not available.

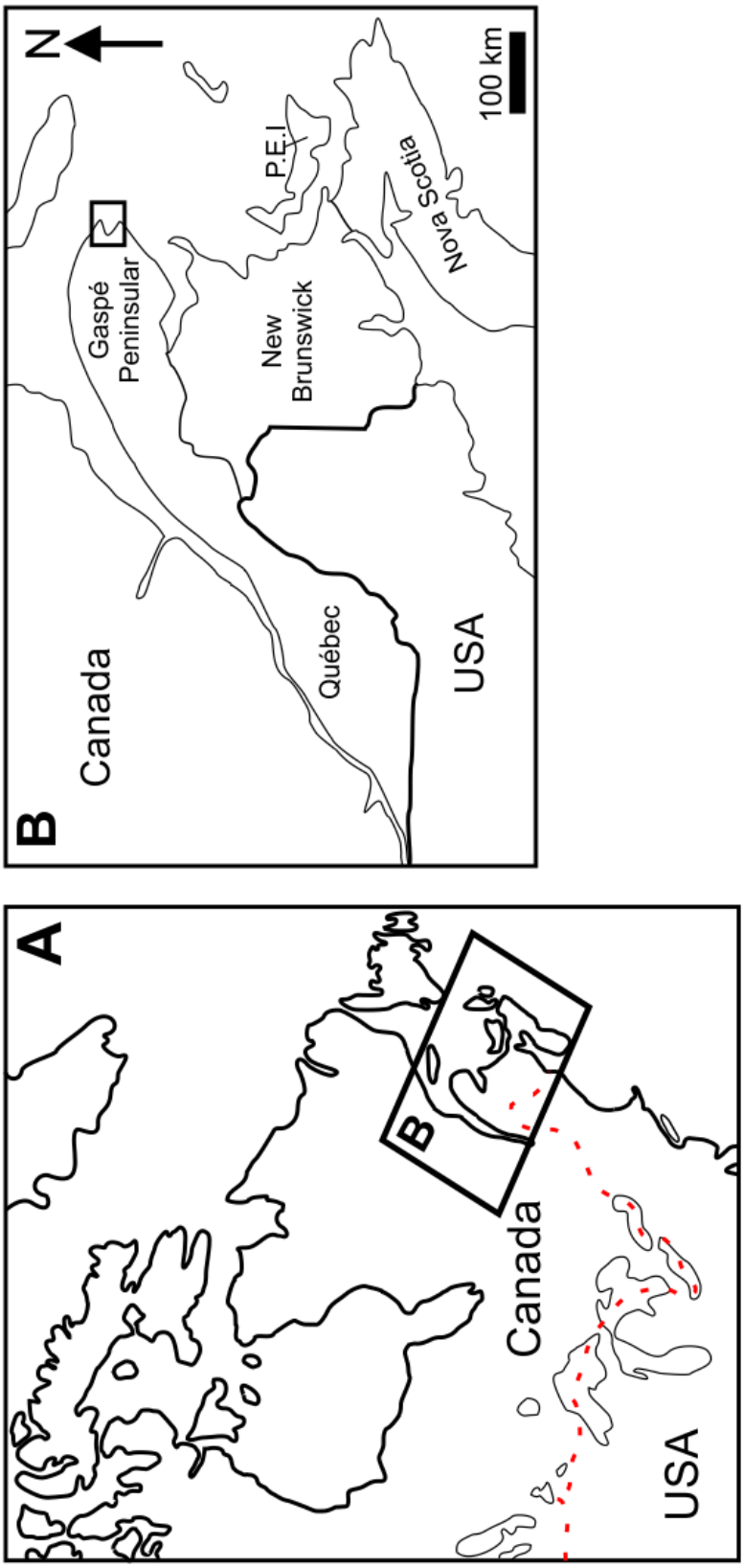

Figure 3.38: Location of coastal sections, Gaspé Peninsular, Québec.

McGregor (1977) assigned spores from the logged TW section to the c-e, *sextantii*, and *Grandispora* zone/subzones of McGregor and Camfield (1976), indicating a Pragian/early Emsian, Emsian, and late Emsian/early Eifelian age, respectively (Fig. 3.39). Spores from Little Gaspé Cove (e.g. GA36–37) were assigned to the c-e biozone, and those from the D'Aiguillon region (GA38–42) were found to span the c-e zone/sextantii subzone boundary (McGregor 1977). Finally, Wellman and Gensel (2004) reported that GA35 can be placed in the lowermost v-l zone of Richardson and McGregor (1986), indicating the sample is Eifelian.

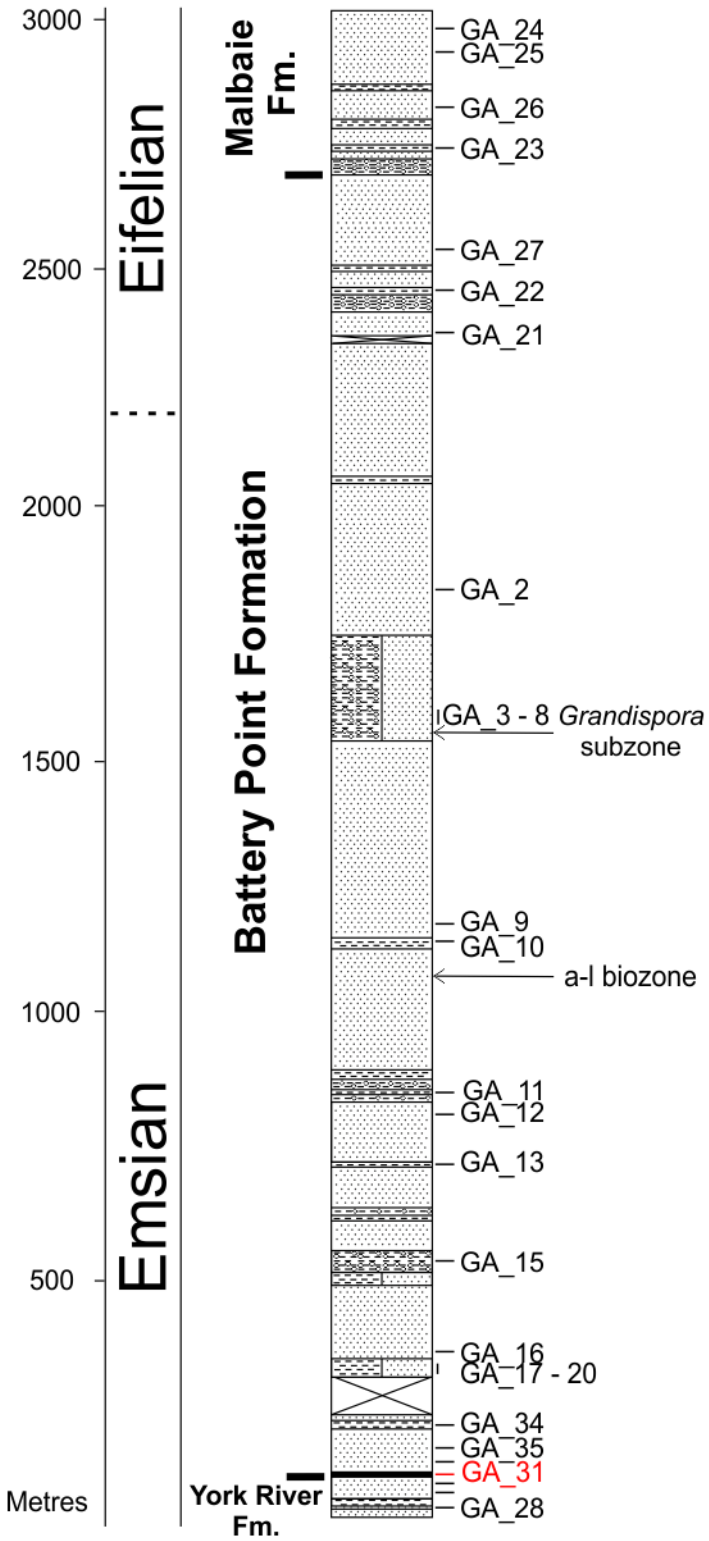

Figure 3.39: Sedimentary log of McGregor section TW, Gaspé Peninsular, with sampling points; GA_31: L'Anse-à-Brilliant Coal. Modified after McGregor (1973). For key see Appendix 3.

Palaeoenvironment

York River Formation

Although the majority of the York River Formation was deposited within the tidal zone (Elick *et al*. 1998), its upper part is sand-dominated and represents a prograding, fluvial-dominated delta (Rust *et al*. 1989). Plant fossils become increasingly common towards the top of the section as the setting becomes more proximal (McGregor 1973), a trend which continues into the Battery Point Formation and culminates with the occurrence of a thin (c. 8 cm) coal seam, the L'Anse-à-Brilliant Coal at Tar Point (McGregor 1973; Glasspool and Scott 2010). This 'coal' was most likely formed through coalification of a small log jam (J. Marshall, *pers*. *comm*., 2016).

Battery Point Formation

Deposition of the Battery Point Formation took place on a low-lying coastal plain (Hotton *et al*. 2001). Above the L'Anse-à-Brilliant Coal, a transition is seen from a braided fluvial facies (Petit Gaspe Member; Rust *et al*. 1989) to a more varied mix of tidal, fluvial and delta-plain facies (Cap-aux-Os Member; Griffing *et al*. 2000; Hotton *et al*. 2001), followed by a return to a more proximal braided facies (Fort Prével Member; Elick *et al*. 1998).

Malbaie Formation

The Malbaie Formation is the most proximal of the sampled units. Though still representing a braided channel facies on a coastal plain (Rust 1984; Rust *et al*. 1989), it is characterised by red sandstones and conglomerates, and progressively coarsens up-sequence (McGregor 1973; Rust 1984). The lower 350 m of the formation are the most productive, and contain plant macrofossils (McGregor 1973).

3.5 The Devonian in Gondwana: the Malvinokaffric Realm

Whereas Gaspé and the Catskill Front were situated 10–20° S during Devonian times, within the tropical and semiarid tropical climate zones (Gordon and Bridge 1987; Scotese and McKerrow 1990; Schuyler and Traverse 1990; Hotton *et al*. 2001), Bolivia and the Falkland islands occupied much higher palaeolatitudes (60° and c. 65° S, respectively; Scotese 2001; Hunter and Lomas 2003; Marshall 2016). These Gondwanan localities

occupied a region known as the Malvinokaffric Realm, an area characterised by highly endemic marine faunas which, until quite recently, made global correlation problematic (Boucot 1975; Troth *et al*. 2011). A total of 378 palynological concentrates from the University of Southampton collections, originating from the localities logged by Troth *et al*. (2011) and Marshall (2016), were analysed. The Bolivian material was supplemented by 24 fresh samples collected during the 2012 field season; unfortunately, when examined these latter were found to exhibit a high level of thermal maturity and were unsuitable for analysis (see section 4.6), so will not be discussed further here.

Port North coastal section, West Falkland (51° 30′ 20″ S, 60° 23′ 55″ W–51° 27′ 30″ S, 60° 25′ 08″ W)

Geological context and biostratigraphy

The Port North coastal section, West Falkland (Fig. 3.40) comprises c. 1.3 km of near-continuous Lochkovian–Givetian exposure, though the Lochkovian/Pragian and Emsian/Eifelian contacts are unconformable (Marshall, 2016). Age assignments have thus far been tentative because palynomorph abundance is low and preservation generally poor; assemblages are also dominated by smooth, simple spores which are quite distinct from their lower-latitude counterparts; Marshall (2016) placed the Fish Creek Member tentatively in the NsZ spore biozone of Melo and Loboziak (2003), and the Fox Bay Formation in the *R. magnifica* Zone of Grahn (2005). Marshall (2016) considered the appearance of *R. magnifica* in this instance to be facies-related rather than a true inception. Correlation with other Gondwanan successions is largely based on recognition of significant transgressions; the Fox Bay transgression is equivalent to sequence B of the Ponta Grossa Formation in Brazil, which is latest Pragian–earliest Emsian in age (Grahn *et al*. 2013), and the globally significant Choteč and Kačák events can also be identified (Marshall 2016; Fig. 3.42).

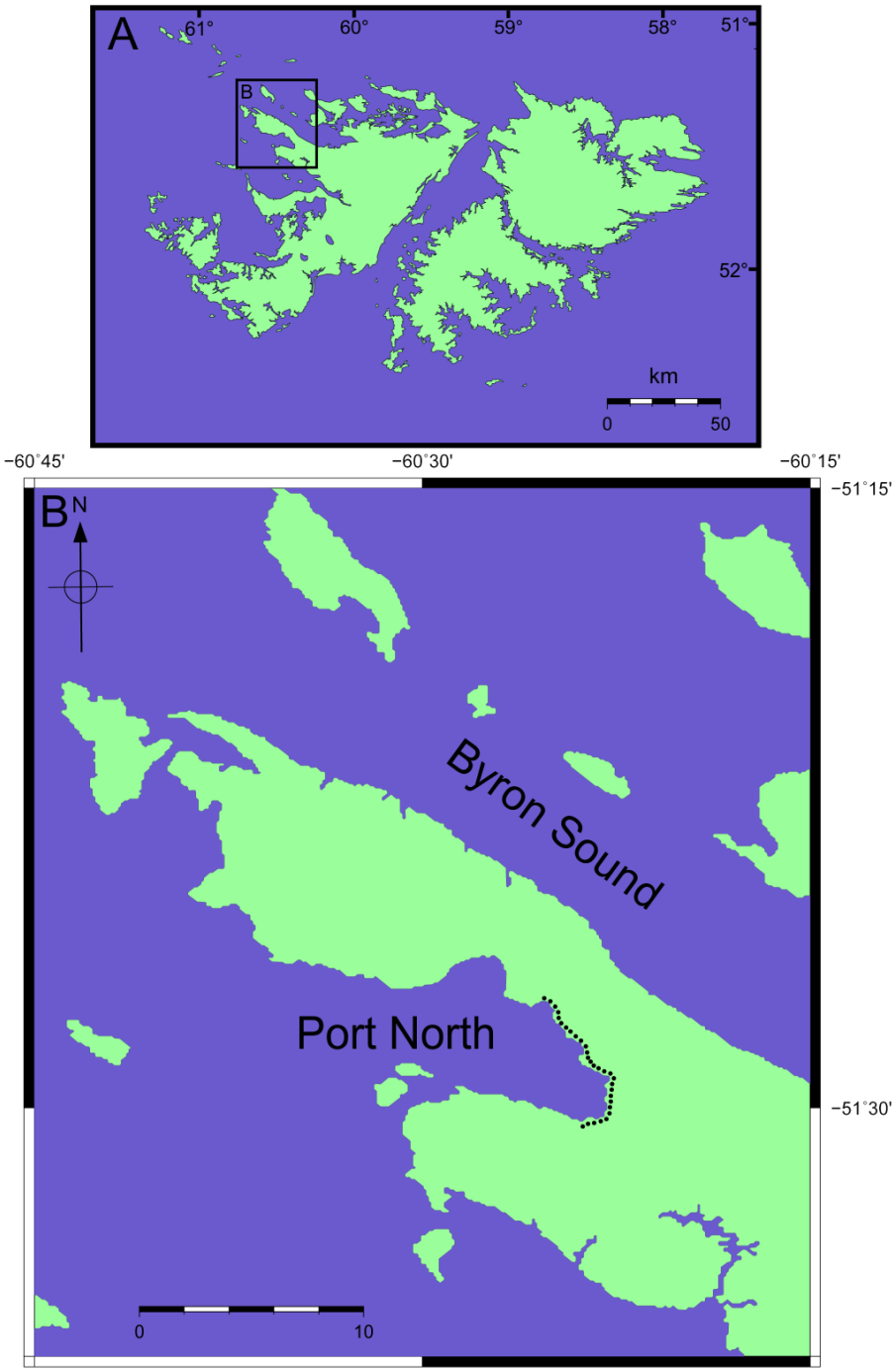

Figure 3.40: Port North coastal section, West Falkland.

Palaeoenvironment

The sequence as a whole represents deposition on a low-gradient coastal plain, subject to the effects of sea-level fluctuation (Hunter and Lomas 2003). The South Harbour and Fish

Creek Members of the Port Stephens Formation are the most terrestrial units; the former represents a braided river system and the latter a poorly drained floodplain, with channels stabilised by permanent vegetation (Aldiss and Edwards 1999; Hunter and Lomas 2003). The Fox Bay Fm. is largely proximal-marine, but also includes two major transgressive episodes featuring a diverse marine invertebrate and ichnofauna (Aldiss and Edwards 1999; Marshall 2016); "at least four" large-scale fining-upward sequences have also been identified (Aldiss and Edwards 1999, pp. 25). Plant macrofossils occur towards the top of the unit, indicating an increasingly proximal setting. The Port Philomel Fm. is intermediate between the preceding two units; it is lithologically similar to the Fox Bay Fm. (albeit with a higher proportion of sandstone) but lacks marine invertebrates; instead, plant macrofossils are common throughout (Aldiss and Edwards 1999). Interestingly, the organic residues were predominantly terrestrial, even when sampled from intervals that were unambiguously marine (Marshall 2016).

Bolivia

Two localities in south-central Bolivia (Santa Cruz and Chiquisaca Departments), provide exposure of Emsian–Frasnian successions which can be correlated with West Falkland and, more tentatively, Euramerican localities.

Bermejo (18° 08' 08" S, 63° 39' 46" W)

Geological context and biostratigraphy

1.2km of Eifelian–Frasnian strata are exposed along the banks of the Rio Lajas at Bermejo; the section runs parallel to the Samaipata Road, 80 km SW of Santa Cruz (Fig. 3.42). Well preserved palynomorphs including the cosmopolitan spores *Geminospora lemurata*, *Cristatisporites triangulatus* and *Verrucosisporites bulliferus*, which have been used to correlate Devonian sections in Brazil with those of western Europe (Melo and Loboziak 2003), allowed Troth *et al*. (2011) to assign ages to parts of the section, though the exact positions of the stage boundaries are uncertain. On this basis, three significant marine transgressions were identified as the Kačák event, Taghanic onlap and TRCIIc transgression respectively. The Huamampampa/Los Monos and Iquiri/Ituaca Fm. boundaries are unconformable; latest Famennian spores (*Retispora lepidophyta*) higher in

the Ituaca Fm. indicate that a significant hiatus occurred, whereas the Huamampampa/Los Monos unconformity appears to have been of shorter duration (Troth *et al*. 2011). The Phytoclast Dominated Interval (on the assumption that it represents a marine regression) was tentatively correlated with the Ludlowville/Moscow Fm. boundary in the Hamilton Group of New York State by Troth *et al*. (2011).

Figure 3.41: Sampling localities in central Bolivia.

Campo Redondo (19° 18' 38" S, 64° 20' 00" W)

Geological context and biostratigraphy

Approximately 550 m of Pragian–Eifelian strata are exposed along the Campo Redondo river section, which is located in the Rio Sillani, 3 Km west of Padilla (Fig. 3.41). Palynomorphs recovered from Campo Redondo are generally more poorly preserved, and exhibit higher thermal maturity, than those from Bermejo (Troth *et al*. 2011). Spot samples from below the logged interval contain abundant examples of the Pragian chitinozoan *Ramochitina magnifica*, allowing approximate correlation with West Falkland (Troth *et al*. 2011; Marshall 2016); recognition of the Choteč event provides another correlative unit. The presence of the goniatite *Tornoceras bolivianum*, for which Campo Redondo is the type locality, indicates an Eifelian age for the lower part of the Huamampampa Fm.; note that a previous interpretation of the species as Givetian/Frasnian (Hünicken *et al*. 1980) was shown by Becker in Troth *et al*. (2011) to be incorrect. Correlation with the Bermejo section was based on a significant *Evittia sommeri* influx marking the basal Los Monos Fm. (Troth *et al*. 2011).

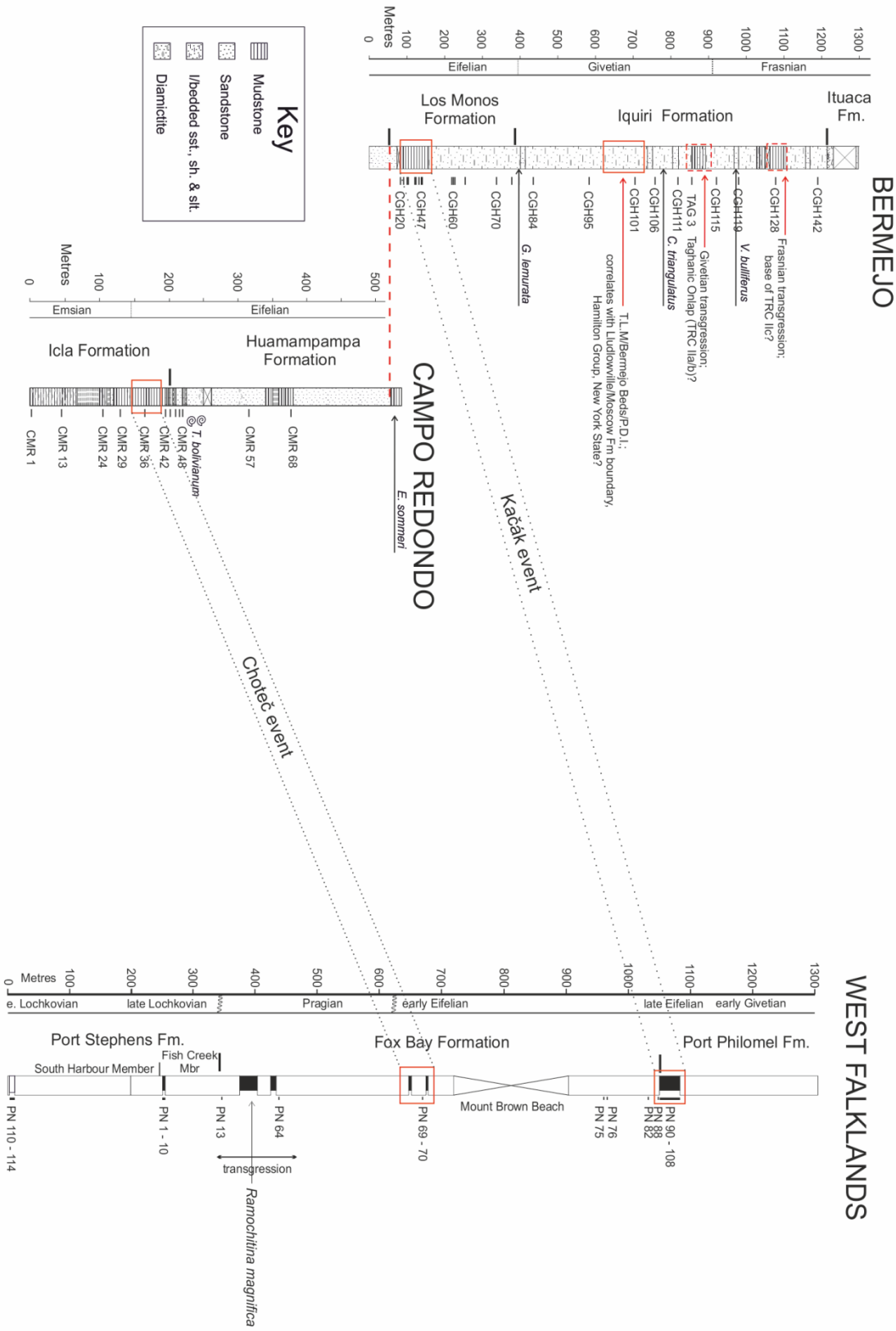

Figure 3.42: Correlated sedimentary logs for Bolivia and West Falkland. Modified after Troth (2006), Troth *et al*. (2011) and Marshall (2016).

Palaeoenvironment

The successions at Bermejo and Campo Redondo are generally indicative of shallow-water marine deposition, albeit interrupted by major transgressions. Infrequent marine palynomorphs and invertebrates (echinoderms) within the PDI indicate the unit was created by an increase in the supply of terrestrial spores and phytodebris rather than a local switch to non-marine conditions; this increase may be due to a marine regression in the region (Troth *et al*. 2011) and consequent increased runoff.

The Devonian Charcoal Gap - Scope of data

A total of 783 samples were assembled, comprising shales collected during field expeditions (USA and Bolivia) and shales or organic concentrates selected from existing palynological collections (Canada and West Falkland). This material represents low (Euramerica) and high latitude (Gondwana) locales subject to a variety of depositional environments, from nearshore marine through coastal wetland/alluvial, to fully terrestrial lacustrine and fluvial settings. Samples are Late Silurian to Late Devonian in age, representing a span of approximately 80 million years, and were used to produce a high-resolution record of inertinite levels (and hence wildfire activity), thus testing the hypothesis that *a charcoal gap exists from the late Emsian to the early Famennian, indicating that wildfire activity was significantly supressed by a reduction of atmospheric* pO_2.

3.6 Results

177 of the 317 available Euramerican samples were either deemed to be unsuitable for analysis due to high thermal maturity or found to have insufficient phytoclast content when analysis was attempted (see section 2.1). This total includes 43 Famennian samples from Stensiö Bjerg, central East Greenland; the geological and palaeoenvironmental context for this locality is discussed in section 4.2. Significantly, all material collected from the only sampled Silurian locality, the US 11 Roadcut, was found to have a spore colour index of 9–10, which is consistent with values reported by Taylor (2003) for the Keefer and Bloomsburg Formations. In total, ten of the 29 Catskill Delta localities provided no data, and several others provided only a handful of useful samples (SI 3.1–3.2).

Analysis of the Gondwanan material was even more challenging. As with the Euramerican samples, high thermal maturity and low phytoclast counts were recurrent issues, and only 47 of 378 Devonian samples provided usable data (SI 3.1–3.2); once again, all 88 Silurian samples collected from a second locality during the 2012 field season in Bolivia were of no use due to high thermal maturity.

The mean relative abundance of inertinite varied widely between localities, from 7.5–94.7% in Euramerica and 8.0–46.2% in Gondwana, with overall means of 24.6 and 34.8%, respectively; very high locality means were typically the result of a small dataset containing a single high value (SI 3.2). Comparison of the two palaeocontinents revealed no statistically significant difference in results (Mann-Whitney U = 3009.5, P = 0.348; Fig. 3.43A; SI 3.3A); Gondwanan and Euramerican inertinite time-series (Fig. 3.43B) also show no statistically significant correlation (Pearson r = -0.144, P = 0.908; SI 3.3B). Kruskal-Wallis ANOVA identified significant differences when comparing the Emsian with the Eifelian, Givetian and Famennian for Euramerican data, though with marginal significance for the Emsian/Eifelian and Emsian/Famennian (Table 3.1); in contrast, there was no significant difference between any pair of Gondwanan Stages (SI 3.3C).

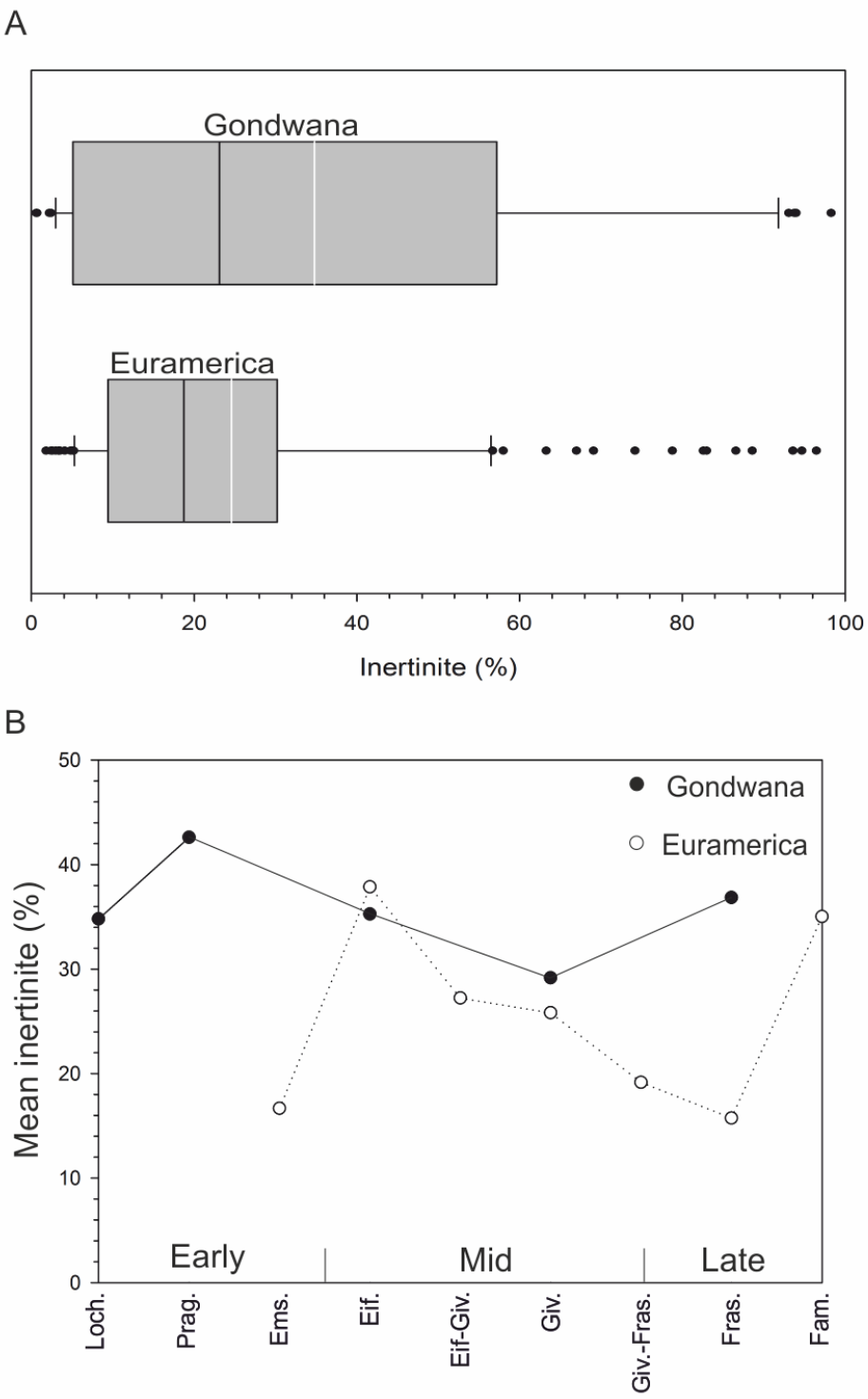

Figure 3.43: Devonian inertinite abundance in Euramerica and Gondwana. A: box-plot comparing all data for each palaeocontinent. Black bars, median; white bars, mean; whiskers, 10th/90th percentile. B, time series comparison through Early, Mid- and Late Devonian.

Comparison	Q	P
Emsian Vs Eifelian	3.141	0.035
Emsian Vs Givetian	4.174	0.001
Emsian Vs Famennian	3.812	0.003

Table 3.1: Significant differences identified by pairwise comparison of Kruskal-Wallis ANOVA results (Dunn's method) for Euramerican time-series data.

When grouped by palaeoenvironment, Kruskal-Wallis ANOVA identifies a marginally significant difference between terrestrial and transitional environments (Q = 2.68, P = 0.02), but not between any other pairing (Table 3.2, Fig. 3.44A, SI 3.3D); when Gondwanan and Euramerican data are analysed separately (Fig. 3.44B–C, SI 3.3E), this difference persists only for Euramerica (no transitional environments were sampled in Gondwana). However, when environment is coded numerically (i.e. 1 = marine, 2 = transitional and 3 = terrestrial), correlation between terrestriality and inertinite content is negligible and statistically insignificant (Spearman R = 0.0816, P = 0.243; SI 3.3D).

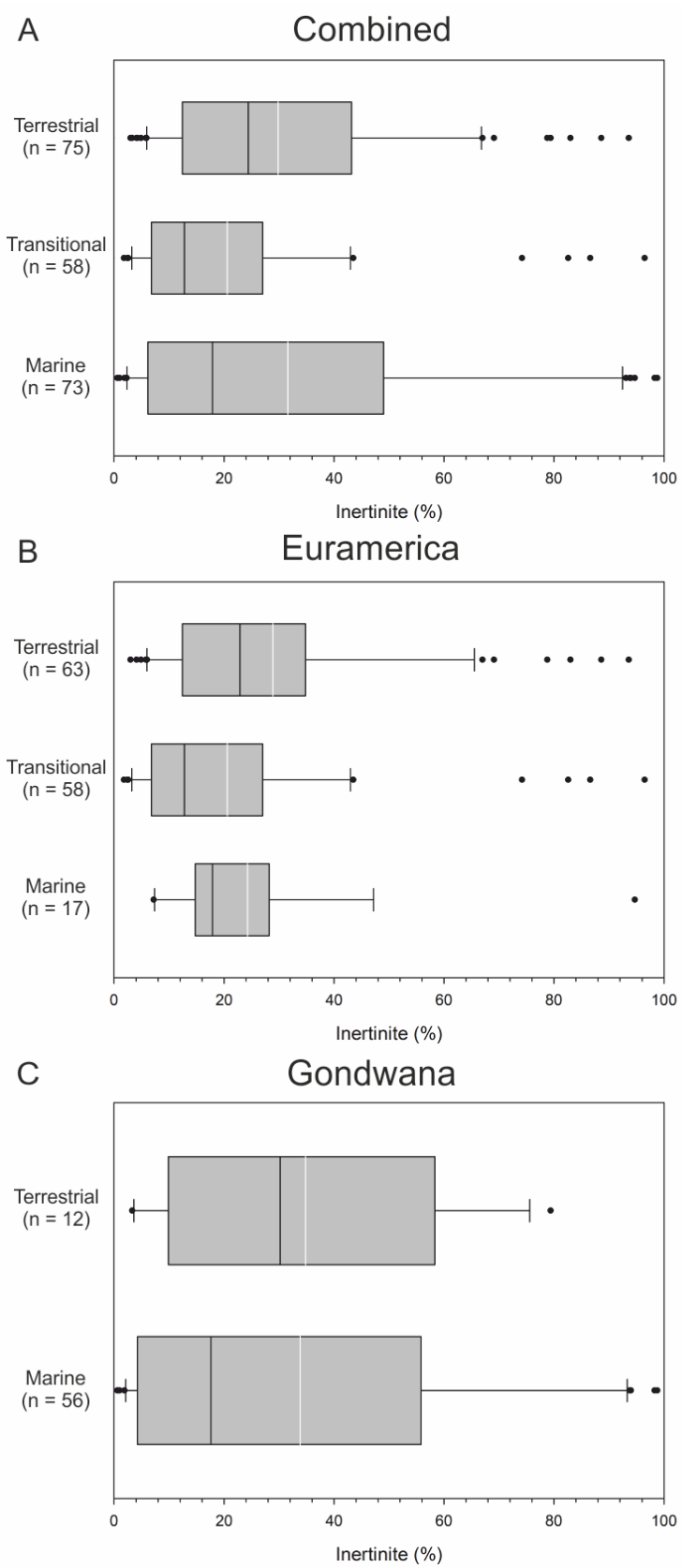

Figure 3.44: Inertinite abundance compared by palaeoenvironment. Black bars, median; white bars, mean; whiskers, $10^{th}/95^{th}$ percentile.

Comparison	Q	P
Terr/Trans	2.68	0.02
Terr/Marine	1.14	0.76
Marine/Trans	1.6	0.33

Table 3.2: Pairwise comparison of Kruskal-Wallis ANOVA results (Dunn's method) for inertinite abundance in marine, transitional, and terrestrial environments (all data).

When examined through the Bermejo Section, no relationship between sedimentary facies and relative inertinite abundance is apparent; neither of the global environmental perturbations (Kačák and Taghanic events) nor the regional Phytoclast Dominated Interval (PDI) identified by Troth *et al*. (2011) are accompanied by any obvious change in fire activity (Fig. 3.45). The Taghanic and PDI are each represented by only a single sample, precluding any meaningful statistical comparison; inertinite levels in the nine samples representing the Kačák were not statistically distinct from the rest of the succession (excluding Taghanic and PDI; Mann-Whitney Rank Sum U = 51.5, P = 0.355; SI 3.3F).

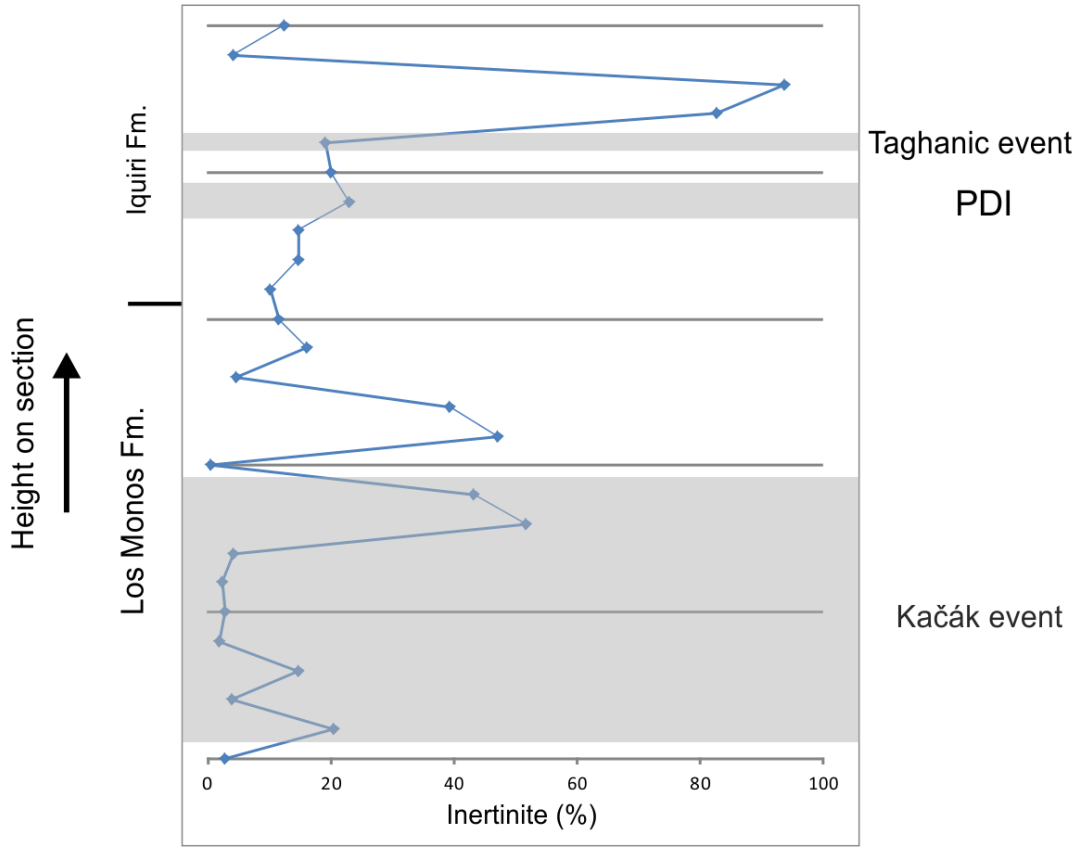

Figure 3.45: Inertinite abundance through Bermejo section, Bolivia. Known large-scale environmental perturbances (Kačák and Taghanic events) and regional 'Phytoclast Dominated Interval' (PDI) of Troth *et al*. (2011) indicated by grey shading.

Euramerican and Gondwanan inertinite data were combined for comparison with the equivalent coal-inertinite data of Glasspool *et al*. (2015), who did not control for palaeolatitude in their study (Fig. 3.46). Kruskal-Wallace ANOVA indicates that the Eifelian, Givetian, and Famennian are each significantly different from the Emsian but not from each other (Table 3.3; SI 3.3G), though the significance is marginal for the Eifelian/Emsian. The single Devonian coal sample, from the L'Anse-à-Brilliant seam, Gaspé, was found to comprise 6.9% inertinite. All raw reflectance data and normalmixEM outputs are provided in SI 3.4.

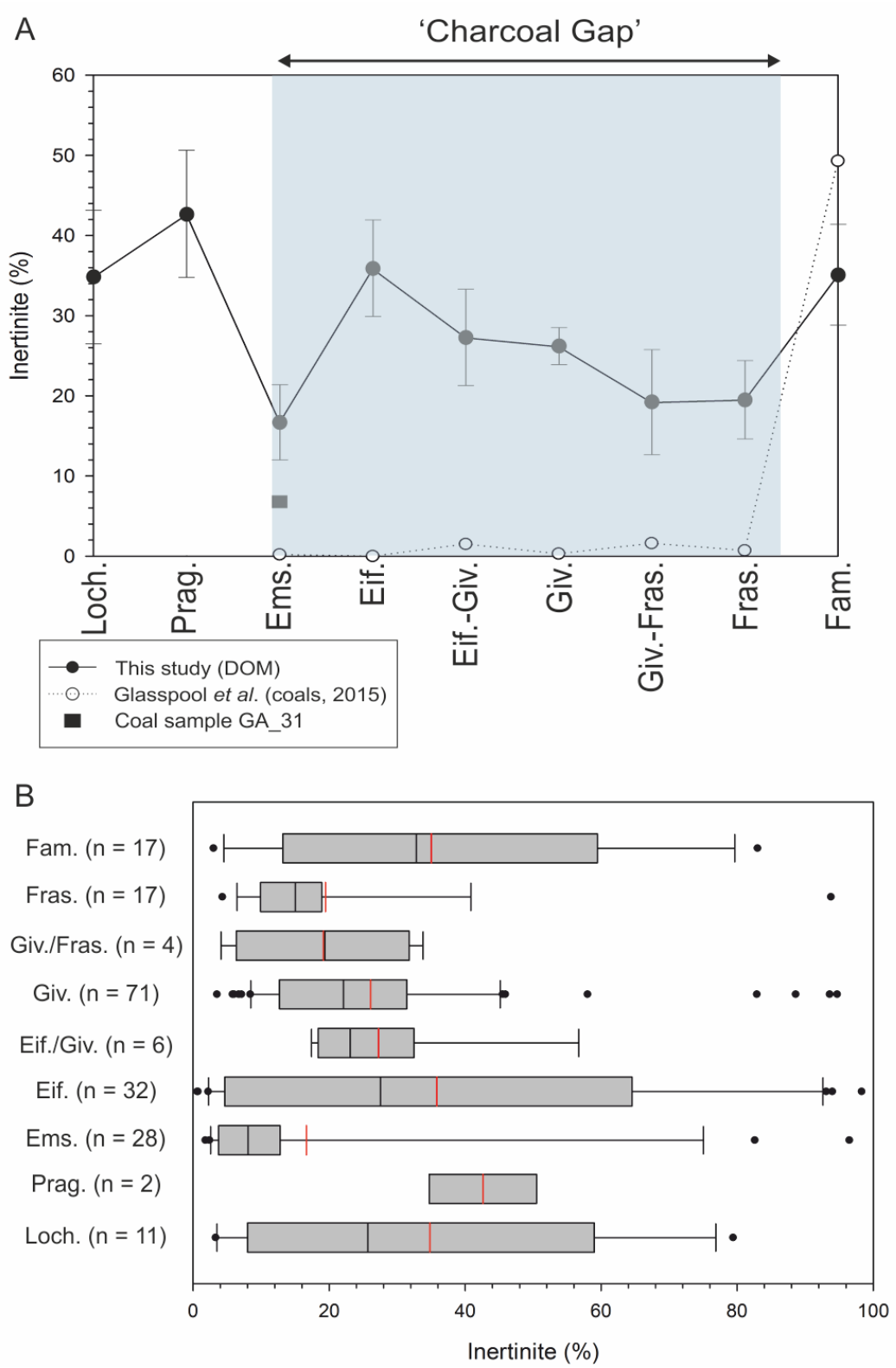

Figure 3.46: A, comparison of DOM inertinite data and coal sample GA_31 (this study) with coal-inertinite data of Glasspool *et al*. (2015) for the Devonian, spanning the 'charcoal gap' (grey shading). Error bars indicate standard error. B, spread of DOM inertinite data: black bars, median; red bars, mean; whiskers, 10th/90th percentiles.

Comparison	Q	P
Eifelian Vs Emsian	3.204	0.049
Givetian Vs Emsian	3.794	0.005
Famennian Vs Emsian	3.462	0.019

Table 3.3: Pairwise comparison of kruskal-Wallis ANOVA results (Dunn's method), combined Euramerica/Gondwana time series.

3.7 Discussion

That the results of the present study show few statistically significant correlations or differences is unsurprising given the small sample size and wide spread of data for some intervals. The apparent reduction in Emsian–Frasnian inertinite levels shown by the combined time-series data does not constitute a statistically significant trend (see results, above) and is likely an artefact, created by the lack of pre-Emsian Euramerican data and the higher overall mean of the Gondwanan results; examined separately, this pattern is not seen in Euramerica or Gondwana. Ignoring all but the statistically significant differences between mean values, the former shows a modest increase between the Early and Mid-Devonian followed by a modest reduction going into the Late Devonian, and the latter is largely stable through the entire interval. While at first glance this seems to contradict the coal-inertinite data reported by Glasspool *et al*. (2015), it is important to note they too were hampered by the paucity of available data (Table 3.4); no pre-Emsian coals were available to them, and their only Emsian data point was obtained from a single sample of the L'Anse-à-Brilliant coal in Gaspé, for which a value of 0.2% inertinite was reported. In contrast, analysis of a sample of the same seam in the present study returned a result of 6.9%, which is not only substantially higher than Glasspool *et al*.'s figure but also exceeds their estimate for expected inertinite under PAL O_2 (4.3%). This is significant because it means that no quantitative data exist which demonstrate a fall in charcoal production during the Early Devonian; although the inertinite abundance values reported by Glasspool *et al*. (2015) are consistent with this model, they equally support sustained low charcoal production during the Silurian and Early–Mid Devonian followed by a rapid increase in the Famennian. The existence of the 'charcoal gap' rests entirely on the absence of Emsian–Frasnian reports of charcoalified plant remains, compared to the very small number from the Late Silurian and early Devonian. The discovery of macroscopic charcoal of Givetian age (Figs. 3.24, 3.47) considerably weakens this

argument. Thus, models predicting a profound drop in pO_2 during the early Devonian are not supported by the charcoal record.

Age	Glasspool *et al*. (2015)	This study
Lochkovian	-	11
Pragian	-	2
Emsian	1	28
Eifelian	3	32
Eifelian/Givetian	4	6
Givetian	6	71
Givetian/Frasnian	21	4
Frasnian	6	17
Famennian	18	17

Table 3.4: sample density for this study, compared to that of Glasspool *et al*. (2015) for the Devonian.

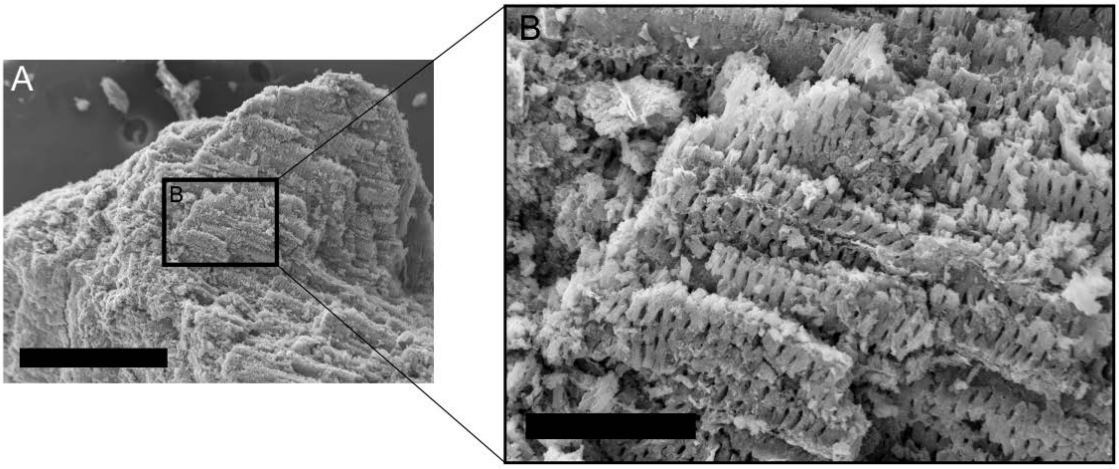

Figure 3.47: SEM image of Givetian charcoal sample collected from locality NY 23-G. Scale bars = 500 µm (A) and 100 µm (B).

Whereas there is little evidence for a drop in charcoal production during the Early Devonian, studies have reported a substantial increase in the inertinite content of coals (Glasspool *et al*. 2015) and marine shales (Rimmer *et al*. 2015) during the Famennian;. In addition, Red Hill is one of a number of late Famennian sites at which macroscopic charcoal is common, such as Oese, central Germany (Rowe and Jones 2000), the Refrath 1

borehole near Cologne, western Germany (Fairon-Demaret and Hartkopf-Fröder 2004) and the Arbre and Trooz quarries, southern Belgium (Prestianni *et al*. 2010). The fact that no significant increase was seen in the inertinite content of Famennian DOM is surprising, but it should be noted that the coal data reported by Glasspool *et al*. (2015) for the Famennian were all derived from a single stratigraphic level and locality (Tunheim Mbr., Roedvika Fm., Bear Island, Norway) and hence may record a local increase in fire activity; it should also be noted that, in their study of Frasnian–Tournaisian marine shales, Rimmer *et al*. (2015) only considered inertodetrinite, fusinite, and semifusinite to be pyrogenic; other inertinite-group macerals were not counted as fossil charcoal. Until further coal data are collected from this interval, the cause of the discrepancy remains open.

Conflicting records of fire history in different geographical regions through most of the Devonian, as indicated by DOM-inertinite abundance, suggest either that no significant changes in atmospheric pO_2 occurred or that oxygen supply was not the main control on long-term fire activity (note that these are not mutually exclusive). Given that there is good evidence for a constant supply of lightning strikes (the main ignition source for wildfires) through geological time (Cope and Chaloner 1980; Scott and Jones 1991; Christian *et al*. 2003), it is reasonable to consider the possible effects of fuel supply. An increase in biomass should not, as of itself, lead directly to an increase in charcoal as a proportion of total plant matter, and in fact the rise of *Archaeopteris* and *Rhacophyton*-dominated biomes during the Mid Givetian (Scheckler 2001; Rimmer *et al*. 2015; Morris *et al*. 2015) is here associated with a decrease in DOM inertinite. It is undoubtedly the case that some plant types combust or carbonise more readily than others, and that evolutionary adaptations to fire can include increased flammability (linked to fire-stimulated germination) or a greater propensity for producing charcoal (Belcher *et al*. 2010b; Keeley *et al*. 2011; Midgely and Bond 2013). However, there is currently no evidence that *Archaeopteris* or *Rhacophyton* developed such features. Thus, while it clearly does not support the existence of a ‘charcoal gap’ the main drivers of fire activity during the Devonian remain unclear.

3.8 Summary

The existence of a Mid–Late Devonian 'charcoal gap' has been widely accepted since it was first identified by Scott and Glasspool (2006); as recently as 2015, Rimmer *et al*. were able to confidently state that no terrestrial charcoal records from the Late Emsian to Givetian of Euramerica were known, and that occurrences of macroscopic charcoal were restricted to the latest Famennian. The DOM inertinite record does not support this view, with analysis of 187 Lochkovian–Famennian shale samples revealing no statistically significant trend through the Devonian; fire activity appears to have been relatively stable, and the apparent scarcity of Emsian–Frasnian charcoal reported in previous studies (Scott and Glasspool 2006; Glasspool and Scott 2010; Glasspool *et al*. 2015) is here considered to be an artefact of limited data. This assessment is supported by the discovery of macroscopic charcoal of Givetian age in the Mid-Devonian successions of the Catskill Front, New York State. Thus, fire activity is judged to have been relatively stable through the supposed 'charcoal gap'. When examined separately, no significant correlation is seen between Gondwanan and Euramerican inertinite levels through time, suggesting that variations in fire activity were not driven by changes in atmospheric pO_2. This record of fire activity is inconsistent with models predicting a profound fall in pO_2 during the Early or Mid-Devonian followed by a rapid rise during the late Famennian, and as such do not support the existence of a 'charcoal gap'. It is surprising that inertinite does not increase significantly during the Famennian, despite the increase in macroscopic charcoal and coal inertinite that is known to have occurred during this stage (e.g. Rowe and Jones 2000; Prestianni *et al*. 2010; Glasspool *et al*. 2015; Rimmer *et al*. 2015); the reasons for this discrepancy are unclear, and further sampling and analysis of Famennian coals and shales are needed if the issue is to be resolved.

4. Atmospheric O_2 during Romer's Gap

Vertebrate terrestrialisation, or the 'fin-to-limb' transition, was a key evolutionary event which has been intensively studied over the last century (Säve-Söderbergh 1932; Jarvik 1952; Romer 1956; Wood *et al*. 1985; Coates and Clack 1995; Jarvik 1996; Clack 2002, 2007, 2011; Smithson *et al*. 2012; Anderson *et al*. 2015). This has been hampered by the scarcity of relevant fossils; Romer (1956) noted that almost no informative fossil material had been recovered from between the End-Devonian and late Viséan, representing a gap of approximately 30 million years. The timing of 'Romer's Gap' is unfortunate, because it is during this hiatus that the tetrapod crown-group is believed to have originated and true terrestriality to have been achieved (Smithson *et al*. 2012). Prior to the End-Devonian Mass Extinction (EDME, or Hangenberg Crisis), during which many vertebrate lineages were lost, tetrapods were aquatic and equipped with a variable number of digits, front and back; after the gap, they were fully terrestrialised and pentadactylous (Coates and Clack 1991; Clack 2011). New discoveries over the last three decades (e.g. Wellstead 1982; Wood 1985; Paton 1999; Clack 2002; Smithson *et al*. 2012; Anderson *et al*. 2015; Clack *et al*. 2016) have progressively narrowed the gap, but tetrapods are still scarce during the Tournaisian and early Viséan.

The nature of Romer's Gap is disputed; some consider it to be an artefact of taphonomic bias and/or collection failure (e.g. Clack 2007; Clack 2011; Smithson *et al*. 2012; Clack *et al*. 2016) while others interpret it as a true reflection of diversity, indicating either an extended post-extinction recovery interval (Sallan & Coates 2010; McGhee 2013; Kaiser *et al*. 2015) or persistent hostile conditions on land (Ward *et al*. 2006; Koch and Britton 2008).

The hypoxia hypothesis

Based on a review of Silurian–Permian arthropod diversity, Ward *et al*. (2006) concluded that the origination rate for major terrestrial arthropod clades fell to zero during the late Devonian and did not increase again until the late Viséan, an interval encompassing Romer's Gap. This co-occurrence of a vertebrate and invertebrate diversity crisis was interpreted as evidence that the Gap was real, and not simply due to collection failure.

Ward *et al*. (2006) compared this against the GEOCARBSULF Phanerozoic atmosphere model (Berner 2006), which predicted a sharp drop in atmospheric O_2 to < 15% vol. during the early Late-Devonian, followed by a gradual rise across the D/C boundary and into the Mississippian, surpassing 20% at about the same time as Romer's Gap was then understood to end. It was proposed that 20% vol. represents an oxygen threshold below which terrestrialisation is not possible and survival of existing terrestrial clades becomes difficult, therefore attributing Romer's Gap to the biological effects of hypoxia.

Studies of modern animals (Graham 1988, Graham *et al*. 1995) indicate that for obligate or facultative skin-breathers (that is, animals which obtain oxygen primarily or secondarily by direct cutaneous diffusion, as the earliest tetrapods are assumed to have been) a reduction in atmospheric pO_2 could present a serious problem, requiring either a reduction in body size to cope with the reduced diffusive distance or the development/improvement of alternative strategies (e.g. lung breathing). Exactly how much of a problem this would be for early tetrapods depends on the relative contribution of direct diffusion to their overall gas exchange, which for extinct Palaeozoic groups is unclear; it appears that most early tetrapods relied on a combination of air-gulping ('bucal pumping') and skin-breathing (Clack 2011). Speculation that tetrapod body size decreased in response to reduced pO_2 is supported by the fossil record to some extent, in that small forms such as *Casineria* first appeared during the Mid-Mississippian, apparently having evolved during Romer's Gap (Clack 2007).

There are several possible objections to the hypoxia hypothesis. First, because of its lower O_2 content and greater viscosity, water is a less effective medium for gas transfer than air (Graham 1990), and aquatic animals are more likely to experience hypoxic stress; if facultative air-gulping developed as a strategy for coping with variable levels of dissolved oxygen in shallow coastal or ephemeral inland water bodies (as suggested by Little 1983) this might actually encourage terrestrialisation rather than inhibit it (Clack 2007). Second, the stark differences between pre- and post-EDME tetrapods indicate that many terrestrial features evolved during Romer's Gap; this is difficult to reconcile with a return to an aquatic lifestyle. Third, the GEOCARBSULF model has been updated since 2006, and now predicts less extreme (though still lower) O_2 values for the Tournaisian (Berner 2009). Finally, inertinite-based reconstructions (Glasspool and Scott 2010; Glasspool *et al*.

2015) suggest there was substantially more wildfire activity (and hence atmospheric O_2) during the Tournaisian than today, and macroscopic charcoal has been anecdotally reported in the Tournaisian Blue Beach Formation in Nova Scotia (Mansky and Lucas 2013) and the Ballagan Formation at Burnmouth Shore (see section 4.4). As with the mid-Devonian charcoal gap, however, the number of Tournaisian coals is limited.

To examine charcoal production across Romer's Gap, organic concentrates from central East Greenland (Famennian–Viséan), Spitsbergen (Famennian–Tournaisian), and the Tweed Basin (three Tournaisian localities in the Scottish Borders and Northumbria) were supplemented with new material collected from the Viséan successions of the Fife coast, Scotland. Samples of purported macroscopic charcoal from the Ballagan Formation were obtained for analysis, and a number of Tournaisian and Viséan coals were also opportunistically collected and examined, for comparison against the coal data of Glasspool *et al*. (2015). This chapter tests the hypothesis of Ward *et al*. (2006), that:

'Romer's Gap' represents a genuine bottleneck in tetrapod diversity caused by global hypoxia following the End Devonian Mass Extinction (EDME), resulting in a significant reduction in wildfire activity during the Tournaisian.

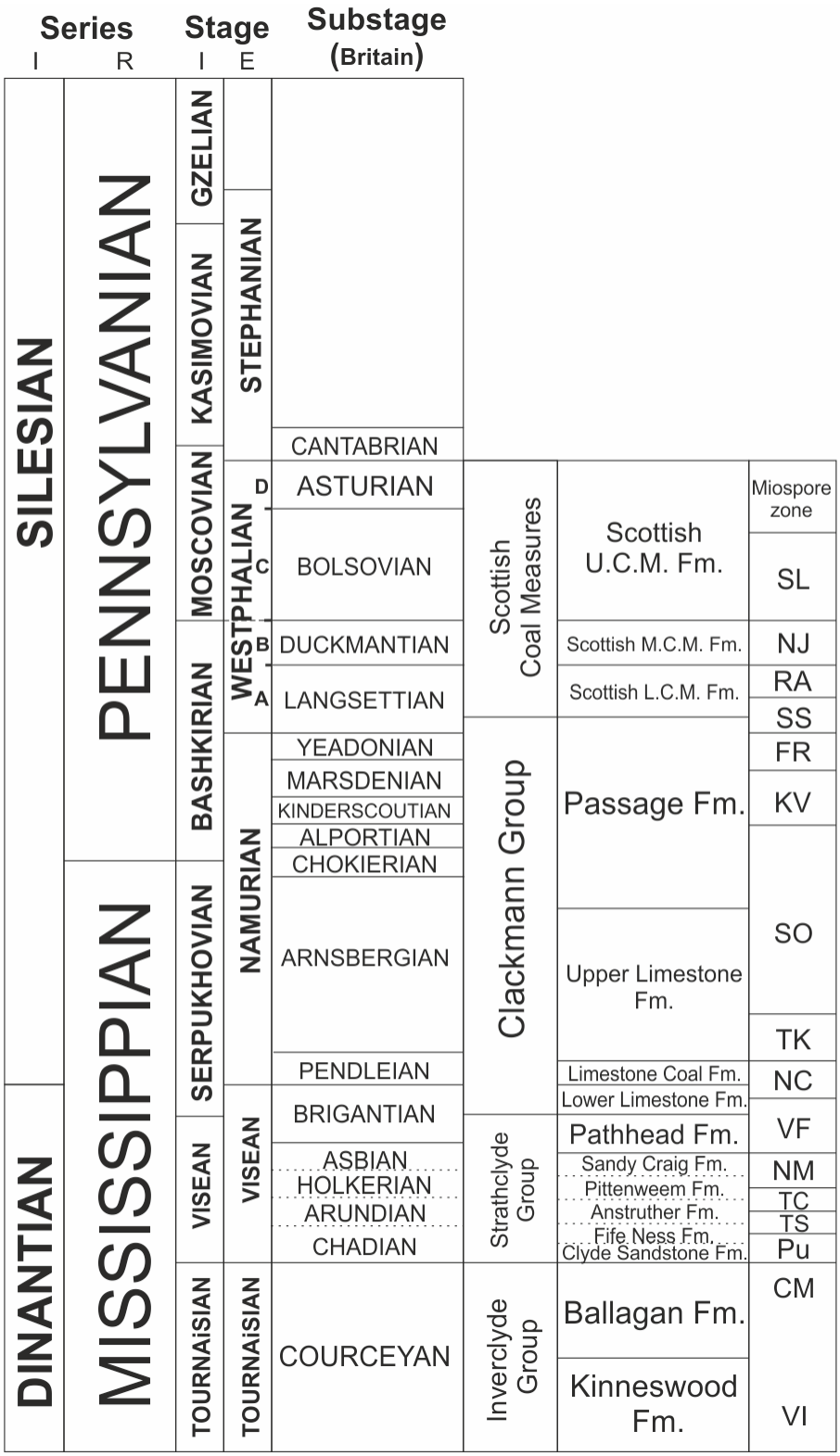

Figure 4.1: International and regional stage names, with UK lithostratigraphic units discussed in sections 5.1 and 6.1. Spore biozones of Neves *et al*. (1973), Clayton *et al*. (1977), Owens *et al*. (1977), Higgs *et al*. (1988). Additional sources: Browne *et al*. (1999), Waters *et al*. (2007), Gradstein *et al*. (2012).

4.1 Sampling localities – Northumberland, Fife, and the Scottish Borders

Burnmouth Shore (BNG NT 95797 60944)

The Tournaisian Ballagan Formation is exposed in its entirety in a 520 m coastal section at Burnmouth Shore, approximately 10 km NW of Berwick-upon-Tweed, Berwickshire, Scotland (Figs. 4.2–4.3). Clear contacts with the underlying Kinnesswood Fm. and overlying Fell Sandstone Fm. confirm that the entire Ballagan is present (Bennet *et al*. 2016). It is currently placed within the Inverclyde Group (Browne *et al*. 1999; Waters *et al*. 2007), and spans the VI–CM palynomorph biozones of Higgs *et al*. (1988) (Smithson *et al*. 2012; Bennet *et al*. 2016).

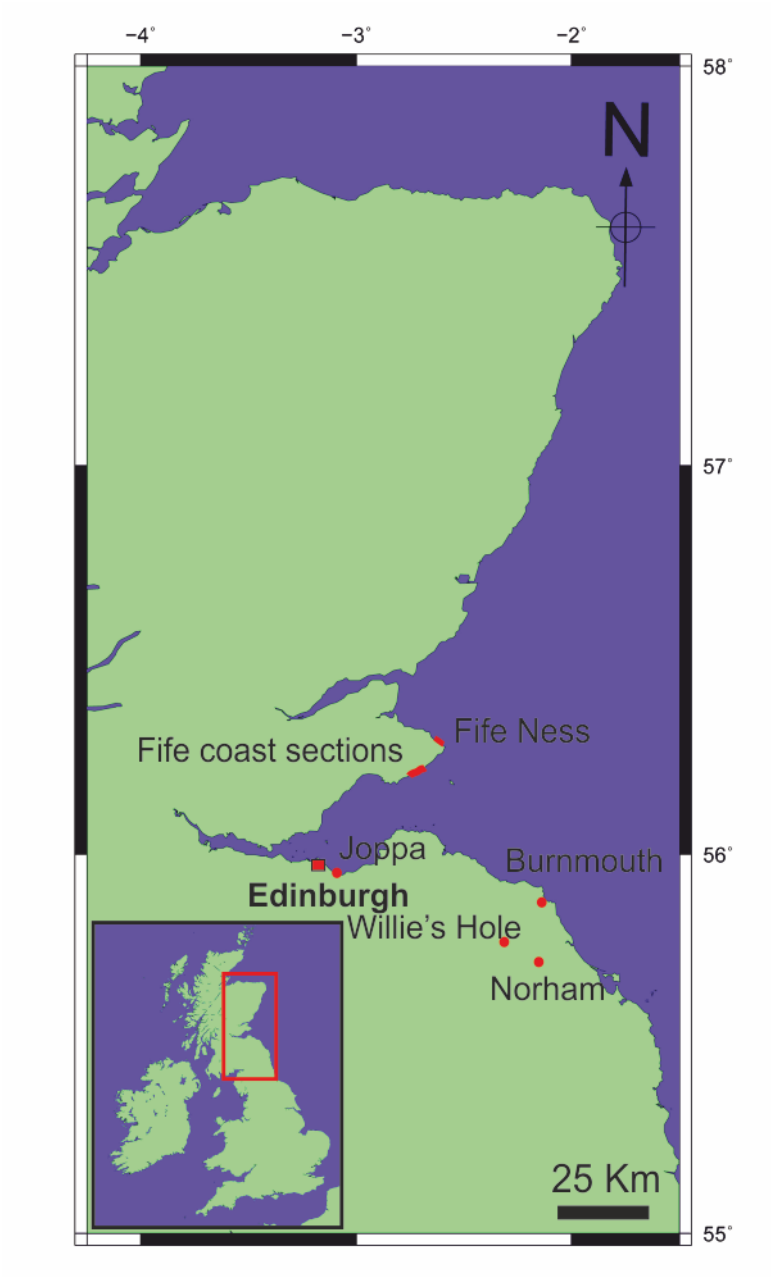

Figure 4.2: Sampling localities, Northern UK.

BGS borehole NT94NW20 (BNG NT 91589 48135)

A 500 m BGS borehole at Norham West Mains Farm, Northumbria, England (Figs. 4.2–4.3) passes through most (c. 485m) of the Ballagan Formation, (Kearsey *et al*. 2016, fig. 3). It does not reach the top Kinnesswood, and there is only one point of correlation between the Norham borehole and the Burnmouth Shore section (Kearsey *et al*. 2016).

Willie's Hole (BNG NT 878 547)

Part of the lower Ballagan Fm. is exposed in a 9m river section along Whiteadder Water near Chirnside, Berwickshire, approximately 14 km west of Berwick-upon-Tweed (Cater *et al*. 1989; Smithson *et al*. 2012; Figs. 4.2–4.3). Its stratigraphic position within the Ballagan is uncertain, as it does not correlate directly with Burnmouth Shore or the Norham Borehole; based on the nearby Hutton Hall Barns borehole (BGS NT85SE1), it is approximately 150 m from the base (Clack *et al*. 2016). The section is placed within the CM palynomorph biozone (Smithson *et al*. 2012).

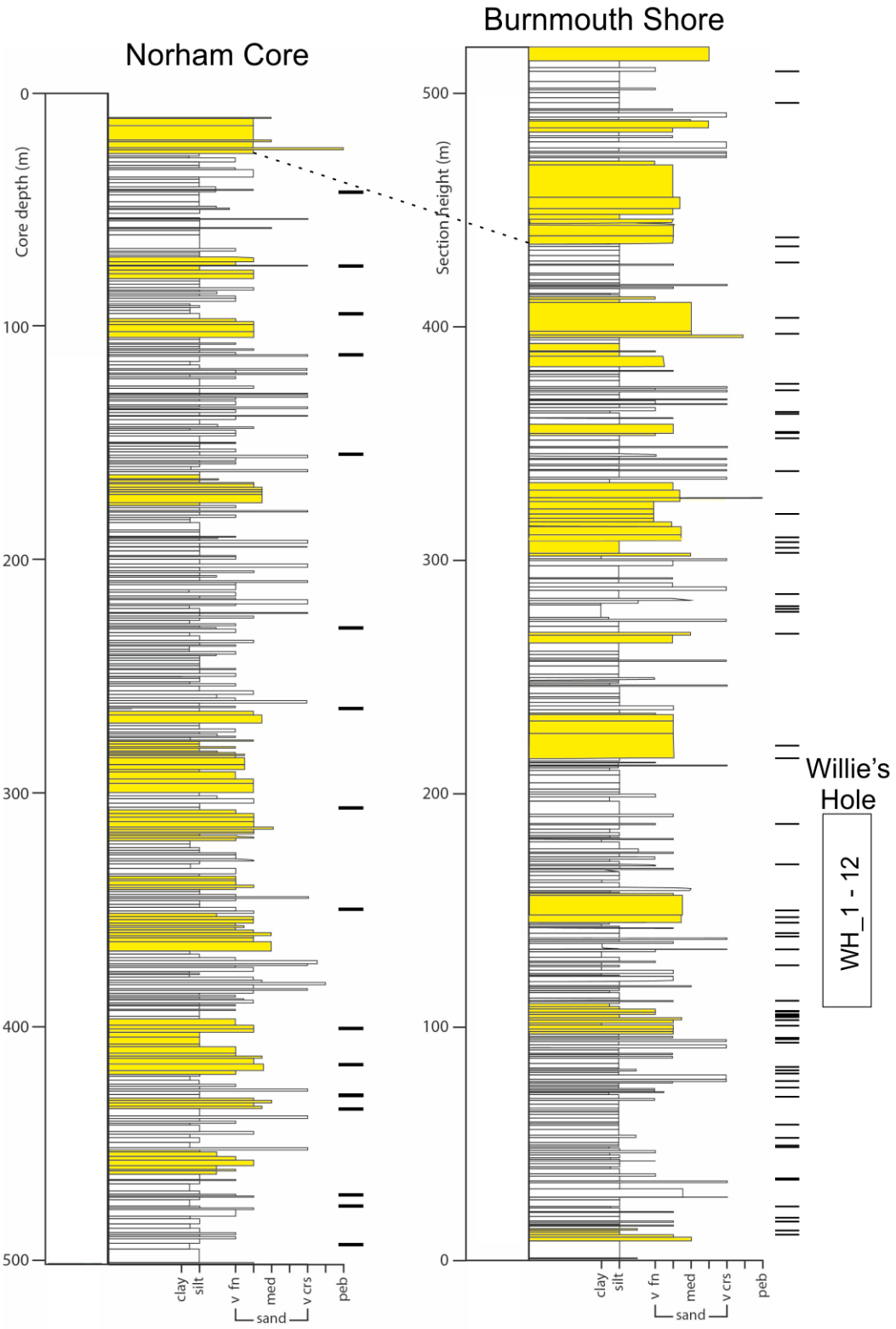

Figure 4.3: Sedimentary logs and correlation for Burnmouth Shore, the Norham Borehole, and Willie's Hole. Logs courtesy of Carys Bennett and Tim Kearsey.

Ballagan Formation palaeoenvironment

The Ballagan Formation consists of alternating fluvial, overbank, and saline/hypersaline-lake facies associations deposited on a low-lying coastal floodplain (Anderton 1985; Andrews *et al*. 1991; Stephenson *et al*. 2004; Bennett *et al*. 2016; Kearsey *et al*. 2016). The climate appears to have been monsoonal (Falcon-Lang 1999; Bennett *et al*. 2016), with distinct wet and dry seasons leading to seasonal flooding and desiccation, respectively (Kearsey *et al*. 2016). Macroscopic charcoal fragments have been recovered from the Burnmouth Shore section, providing evidence of wildfires (T. Smithson, *pers. comm* 2015; section 4.4). The fossil content and geochemistry of dolomite beds (known locally as 'cementstones') within the lake facies indicates a complex system with varying levels of marine connection; their limited lateral extent suggests there was no large-scale marine transgression (Bennett *et al*. *2017*).

East Fife coast

The Viséan Strathclyde Group (formerly Calciferous Sandstone Measures; Forsythe and Chisholm 1977) is exposed in multiple coastal sections along a three mile stretch of the SE Fife coast, Scotland, between St Monans and Anstruther, and at Fife Ness (Figs. 4.2, 4.4). Although these are the type sections for the formations of the Strathclyde Group, and are described in detail by Forsythe and Chisholm (1977), they are often incomplete and fault-bounded, making stratigraphic age determinations difficult; furthermore, spores in the Fife Ness Formation are typically rare and rather degraded, leading to disagreement over its age (Browne *et al*. 1999; Owens *et al*. 2005). Unless otherwise stated, spore biozones quoted here are those of Neves *et al*. (1973). The sampled sections are those described by Forsythe and Chisholm (1977).

Geological context and palaeoenvironment

Fife Ness Section (BNG NO 63281013–63581017)

Approximately 250 m of the Fife Ness Formation, which is conventionally placed in the Pu–TS spore biozones (Browne *et al*. 1999; Stephenson *et al*. 2005), is exposed on the foreshore at Fife Ness (Forsythe and Chisholm 1977). Contact with the overlying Anstruther Formation is faulted, so its true thickness and youngest age is unknown;

Owens *et al*. (2005) reported spores indicating a much younger age (TC–NM biozones), arguing that the Fife Ness beds are actually a downthrown section of the Pittenweem Formation.

Anstruther Wester Section (BNG NO 56700330–56350300), *Billow Ness Section* (BNG NO 56300288–55900269), *Chain Road Section* (BNG NO 55900269–55980265), *Lower Cuniger Rock Section* (BNG NO 55980265–55660271).

These sections together comprise the type for the Anstruther Formation, though only around two thirds (c. 500m) of the total known thickness is present (Forsythe and Chisholm 1977). The formation is early to mid-Viséan in age, and is placed in the TS–TC biozones (Browne *et al*. 1999; Stephenson *et al*. 2004; Owens *et al*. 2005). As noted above, the contact with the underlying Fife Ness Formation is faulted, and an unknown thickness of strata are missing; the Anstruther Borehole (BGS NO 50 SE/5) proved an additional 300 m, but did not reach the base of the formation (Forsythe and Chisholm 1977).

Upper Cuniger Rock Section (BNG NO 55660271– 55100249).

Somewhat counterintuitively, Upper Cuniger is the type section for the Pittenweem Formation rather than the Pittenweem Harbour sections. The 260m of exposure are placed in the TC–NM biozones (Browne *et al*. 1999; Stephenson *et al*. 2004; Owens *et al*. 2005), indicating a mid-Viséan age. Although the lower boundary is conformable, the contact with the overlying Sandy Craig Formation is faulted, and hence the upper part of the formation, is not present (Forsythe and Chisholm 1977).

Lower Pittenweem Harbour Section (BNG NO 55180236–54930234), *Middle Pittenweem Harbour Section* (BNG NO 54900232–54600218), *Upper Pittenweem Harbour Section* (BNG NO 54700236–54520238), *Sandy Craig Section* (BNG NO 54560236–54340222).

The Sandy Craig Formation is placed in the NM biozone by Owens *et al*. (2005). As noted above, the contact between the Pittenweem and Sandy Craig formations is faulted; only the uppermost 140 m of the Sandy Craig is present, from a total known thickness of approximately 670 m (Forsythe and Chisholm 1977; Browne *et al*. 1999). The upper contact with the overlying Pathhead Formation is conformable.

Pathhead Section (BNG NO 54350224–53810212)

The highest unit in the Strathclyde Group, the Pathhead Formation is late Viséan in age and placed in the VF biozone (Browne *et al*. 1999; Stephenson *et al*. 2004; Owens *et al*. 2005). The 220 m thick formation is exposed in its entirety along the Pathhead Section, with conformable boundaries above and below (Bowne *et al*. 1999).

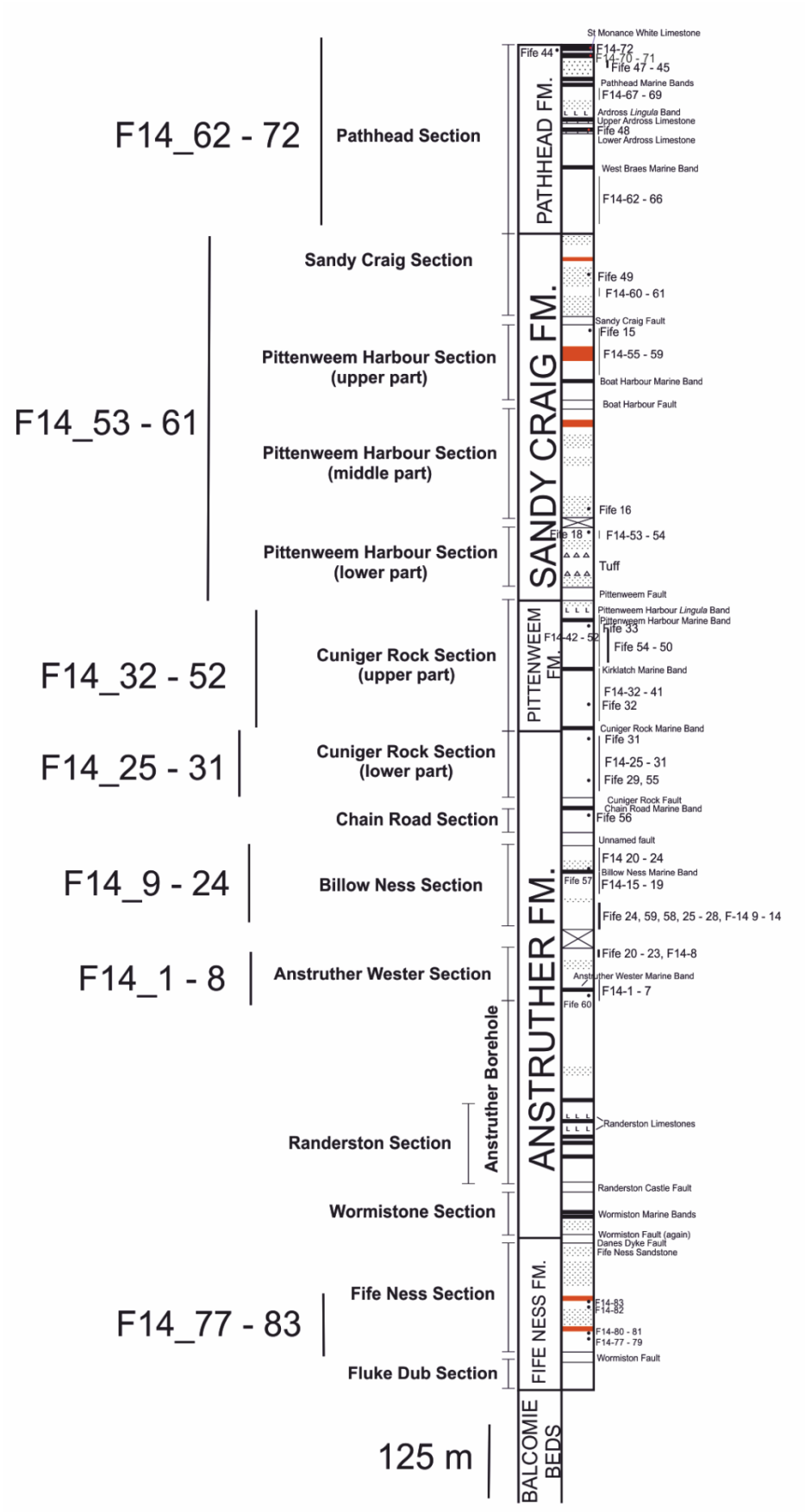

Figure 4.4: Composite log of east Fife succession; modified after Forsythe and Chisholm (1977).

Strathclyde Group palaeoenvironment

The Strathclyde Group as a whole represents fluviodeltaic deposition against a backdrop of cyclically changing sea levels (Forsythe and Chisholm 1977; MacGregor 1996; Browne *et al*. 1999; Owens *et al*. 2005). The Fife Ness Formation is somewhat different in that it is predominantly fluvial, with some short-lived lacustrine deposition. Massive sandstones are common; marine bands and coals are absent, and the formation shows no evidence of marine influence (Forsyth and Chisholm 1977; MacGregor 1996; Browne *et al*. 1999). It is worth noting that if, as suggested by Owens *et al*. (2005), the Fife Ness Formation is actually a tectonically displaced part of the Pittenweem Formation, it would represent a significant lithological change within the marine-influenced Pittenweem.

The Anstruther Formation is more varied, comprising a classic 'cyclothemic' sequence; marine bands and coals are frequent, but rarely develop to any great thickness or lateral extent. The former become less common towards the top of the sequence, and throughout the unit exhibit a restricted fauna more characteristic of marginal environments than fully marine conditions. Bedded dolomites and non-marine limestones, likely deposited in lagoonal conditions, are also common. In contrast, the Pittenweem Formation shows a stronger marine influence; bedded dolomites are rare, and marine bands contain a fully developed marine fauna of corals, echinoderms, and diverse brachiopods. This trend is reversed in the overlying Sandy Craig Formation, which is more similar to the Anstruther. Finally, the Pathhead Formation becomes increasingly marine over time, and overall has the greatest number and thickness of marine bands; these contain a diverse, fully marine fauna.

4.2 Sampling localities - Central East Greenland

The East Greenland Devonian Basin is well known as the source of two extremely significant Devonian tetrapods, *Acanthostega* (Jarvik 1952) from Wiman Bjerg, Gauss Halvø and *Ichthyostega* (Säve-Söderbergh 1932) from Celsius Bjerg, Ymer Ø, which at the time of discovery were the oldest known. The basin contains a near-complete Famennian–Viséan succession through the Celsius Bjerg and Traill Ø Groups, albeit in the form of a composite section split between several islands over a 750 km^2 area (Astin *et al*. 2010; Figs. 4.5–4.6). Stensiö Bjerg, Gauss Halvø, provides a continuous section from the

Britta Dal to the Obrutschew Formation, before being truncated by Permian strata (Marshall *et al*. 1999; Marshall 2015). Spore assemblages described by Marshall *et al*. (1999, fig. 2) place the upper Britta Dal, entire Stensiö Bjerg and lower Obrutschew Formations within the LN biozone of Higgs *et al*. (1988), indicating a latest Famennian age, and the upper part of the Obrutschew Fm. within the VI biozone, indicating an earliest Mississippian age. The Tournaisian–Viséan Harderbjerg Formation is exposed on Rebild Bakker, Traill Ø, and Backlund Ridge, Geographical Society Ø, but the former is structurally complex due to frequent faulting and gaps, and the latter is highly condensed and covered early Tournaisian (Marshall 2015). The Harderbjerg Formation at these localities is placed in the VI–Pu biozones, indicating a Tournaisian–Viséan age (Vigran *et al*. 1999; Marshall 2015).

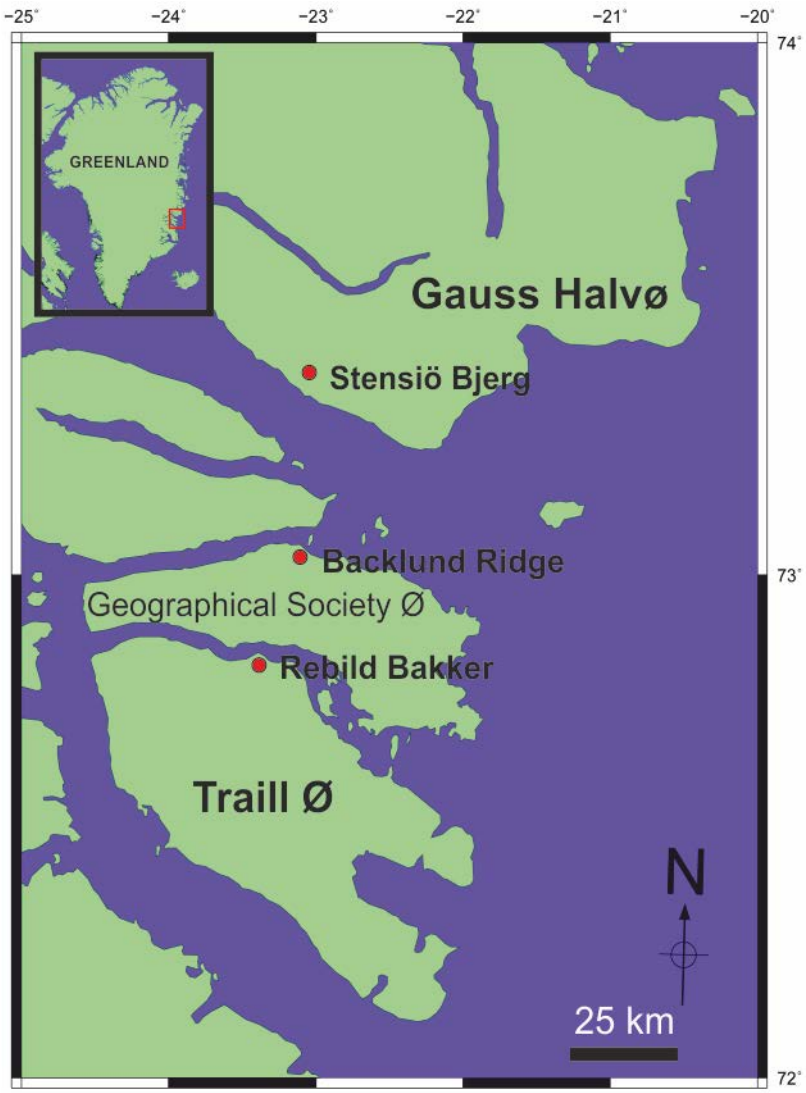

Figure 4.5: Sampling localities in East Greenland.

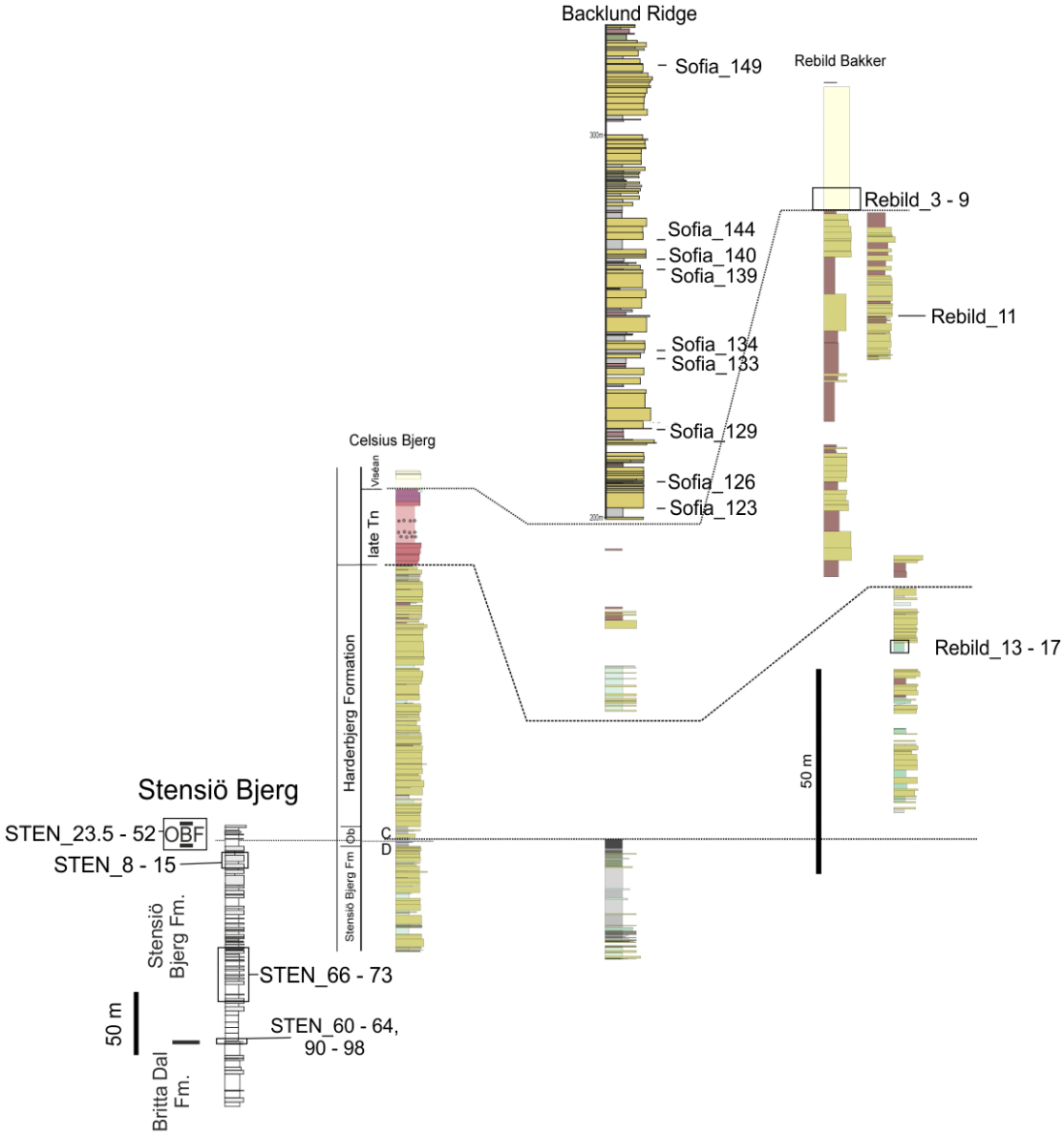

Figure 4.6: Correlative logs for east Greenland Celsius Bjerg Group; courtesy of J. Marshall.

Celsius Bjerg Group palaeoenvironment

The Britta Dal Formation on Gauss Halvø consists of a cyclical sequence of vertisols, indicating a seasonally arid alluvial plain, with occasional fine-grained sandstones representing large flooding events (Astin *et al*. 2010). Outcrops of the same formation further south on Ymer, Geographical Society and Traill Ø are increasingly proximal and sand-dominated; it has been suggested that the Britta Dal Fm. as a whole represents a large, ephemeral river system comparable to the modern-day Cooper Creek in Australia (Astin *et al*. 2010). The overlying Stensiö Bjerg Formation records a shift to a less arid environment, indicated by a variety of fluvial, lacustrine and alluvial horizons (Astin *et al.*

2010); this trend is continued with the onset of fully lacustrine conditions in the Obrutschew Formation, comprising a thin sequence of limestones and organic-rich laminated mudstones deposited in an extensive, deep, and long-lived lake (Marshall 2015).

Traill Ø Group palaeoenvironment

The Harderbjerg Formation on Traill Ø is initially dominated by shallow lacustrine deposits, whereas the formation on Ymer Ø is predominantly fluvial; seasonal aridity is apparent in both cases, but was evidently not so extreme as to preclude the formation of permanent lakes (Marshall 2015). The late Tournaisian on both islands is characterised by pervasive vertisols, indicating a switch to sustained arid conditions (Marshall 2015). Finally, the Viséan saw the onset of a far wetter climate in which the formation of thin coals seams was possible.

4.3 Sampling localities - Spitsbergen

Devonian exposures in Svalbard occupy an 11200 km^2 fault-bounded basin in Dicksonland, NW Spitsbergen (Piepjohn *et al*. 2000). At Triungen, early Devonian strata are unconformably overlain by the Famennian–Viséan Hørbyebreen Formation (Billefjorden Group; Figs. 4.7–4.8) which is divided into the Triungen and Hoelbreen Members (Lindemann *et al*. 2013). The former was traditionally considered to be early Carboniferous (Cutbill and Challinor 1965; Abdullah *et al*. 1987); a Famennian age was subsequently adopted (Vigran 1994; Dallmann 1999) before being abandoned following the identification of Viséan spores in its upper part (Piepjohn *et al*. 2000). More recently, a mid- to late Famennian spore assemblage has been recovered from the hitherto undated basal part of the member (Lindemann *et al*. 2013) though this has been dismissed by Piepjohn and Dallmann (2014) as a reworked assemblage. The Triungen Member is present only at Triungen; in other sections it is truncated by the Hoelbreen Member. The Hoelbreen is generally considered to be Tournaisian or Viséan (Playford 1962; Vigran 1994; Harland and Geddes 1997; Vigran *et al*. 1999; Stemmerik 2000), though a Tournaisian age conflicts with the presence of Viséan spores in the Triungen Member (Piepjohn *et al*. 2000). Samples were collected from c. 120 m of logged section

by J. Marshall; a further 130 metres above this point were measured and sampled but not logged (Fig. 4.8).

Figure 4.7: Locality map for Triungen, Spitsbergen.

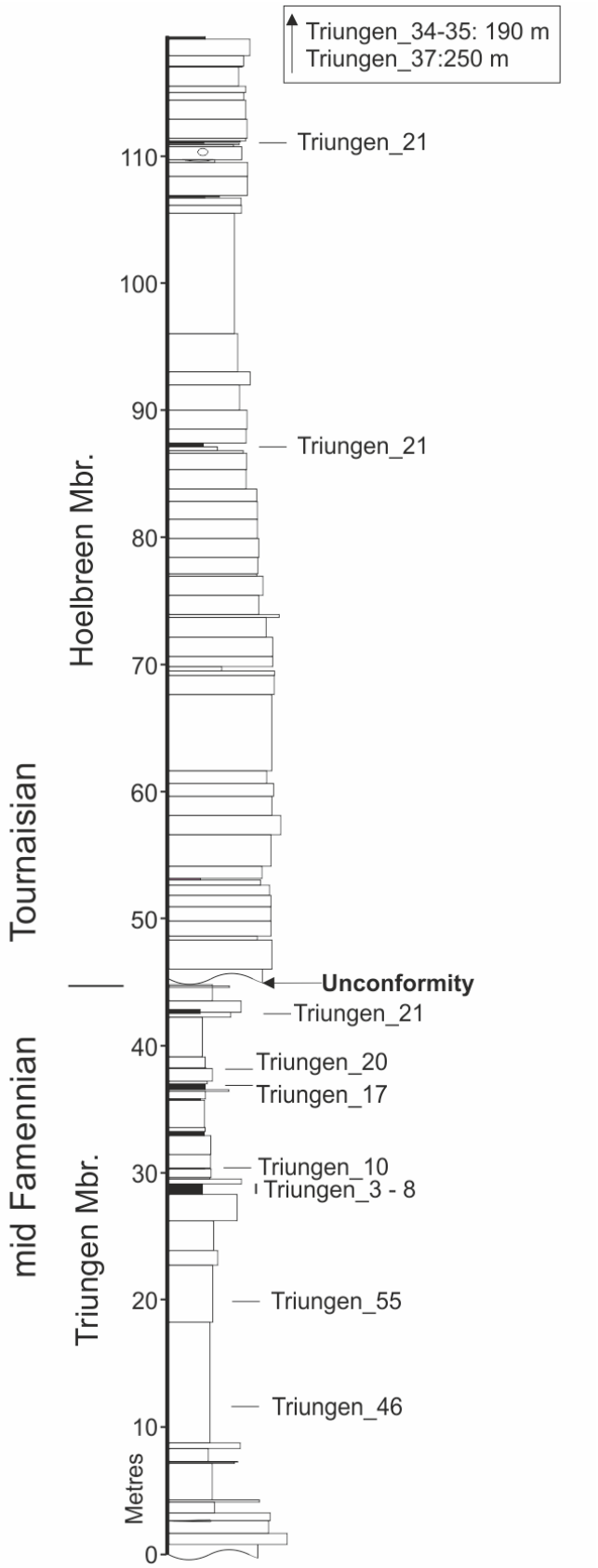

Figure 4.8: Sedimentary log, showing Hørbyebreen Fm. succession at Triungen. Courtesy J. Marshall.

Hørbyebreen Formation palaeoenvironment

The Hørbyebreen Formation as a whole is terrestrial, and in general is coarser grained and richer in plant material (hence presumably more proximal) towards the east (Harland and Geddes 1997). The Triungen Member is predominantly fluvial in nature, characterised by thick sandstones and conglomerates (Abdullah *et al*. 1987; van Koeverden *et al*. 2011) but also local developments of lacustrine mudstones (Harland and Geddes 1997). It is believed to represent a braided river system and associated overbank deposits. The Hoelbreen Member is more varied in its lithology, but in general is dominated by finer-grained muds and silts deposited by a meandering river on a large and poorly-drained floodplain. Thin coals are commonplace, indicating swampy conditions (Harland and Geddes 1997; Koeverden *et al*. 2011).

Romer's Gap – scope of data

A total of 301 shale samples and 36 coals spanning the latest Devonian (Famennian) to the Mid-Mississippian (Viséan) were examined, in an effort to chart wildfire activity as recorded by DOM inertinite immediately before, during, and after Romer's Gap, examining the hypoxia hypothesis of Ward *et al*. (2006) *that Romer's Gap represents a genuine bottleneck in tetrapod diversity caused by global hypoxia following the End Devonian Mass Extinction (EDME)*. Examination of coals allows a direct comparison with the coal inertinite data of Glasspool *et al*. (2015) for the Tournaisian and Viséan. Samples collected during fieldwork in east Fife was supplemented with organic residues from the University of Southampton's palynological collections (Greenland, Triungen, and Ballagan Formation localities); samples of macroscopic charcoal were provided for analysis by T. Smithson under the remit of the TW:eed project (section 4.7). Although all material examined was from Euramerica, it represents a range of palaeolatitudes from c. 15° S to 10° N, allowing the relationship between fire activity and climate zone to be investigated.

4.4 Results

A total of 301 shale samples and 36 coals were examined, of which 251 were deemed suitable for analysis (SI 4.1–4.2). Locality means for inertinite abundance ranged from 16.8%–65.7%; mean inertinite level was largely stable over time at 28–32%, but was markedly higher around the D/C boundary at 46.5% (Fig. 4.9A). Kruskal-Wallis ANOVA indicates this to be a marginally significant difference ($H = 7.975$, $P = 0.047$; SI 4.3A). In contrast to results from the Middle Devonian, a clear positive correlation was seen between inertinite and palaeolatitude (Pearson $r = 0.253$, $P = <0.01$; Fig. 4.9B; SI 4.3B). The three Ballagan Fm. localities (Norham, Burnmouth, and Willie's Hole) yielded similar results, with mean inertinite ranging from 24.7–30.2%; Kruskal-Wallis ANOVA indicates there is no statistically significant differences between them ($H = 0.46$, $P = 0.79$; Fig. 4.9C; SI 4.3C), and neither Norham nor Burnmouth show any obvious trend through time, or link between inertinite and sedimentary facies (Fig. 4.10).

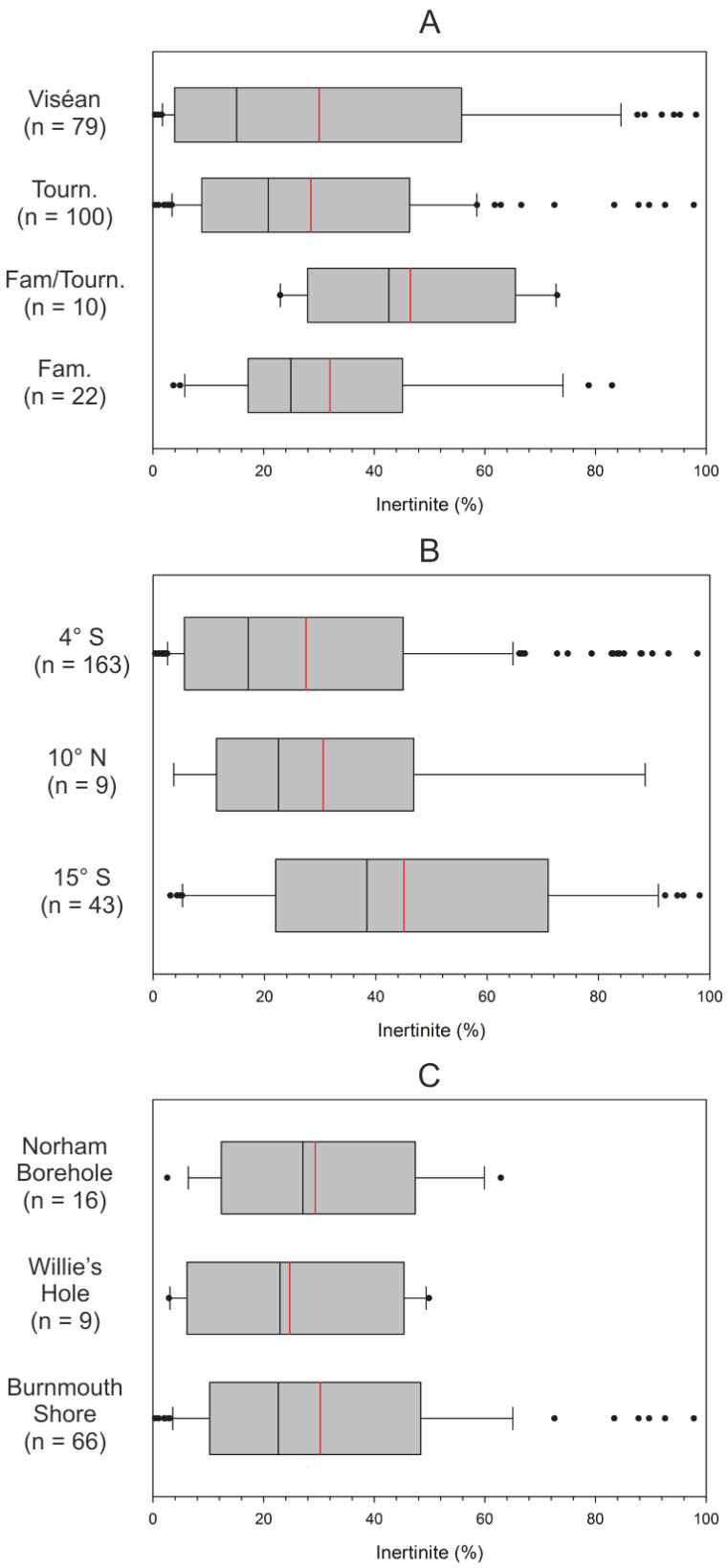

Figure 4.9: Results. A, inertinite abundance compared by age; B, palaeolatitude; C, Ballagan Fm. locality. Black bars, median; red bars, mean; whiskers, 10th/90th percentiles.

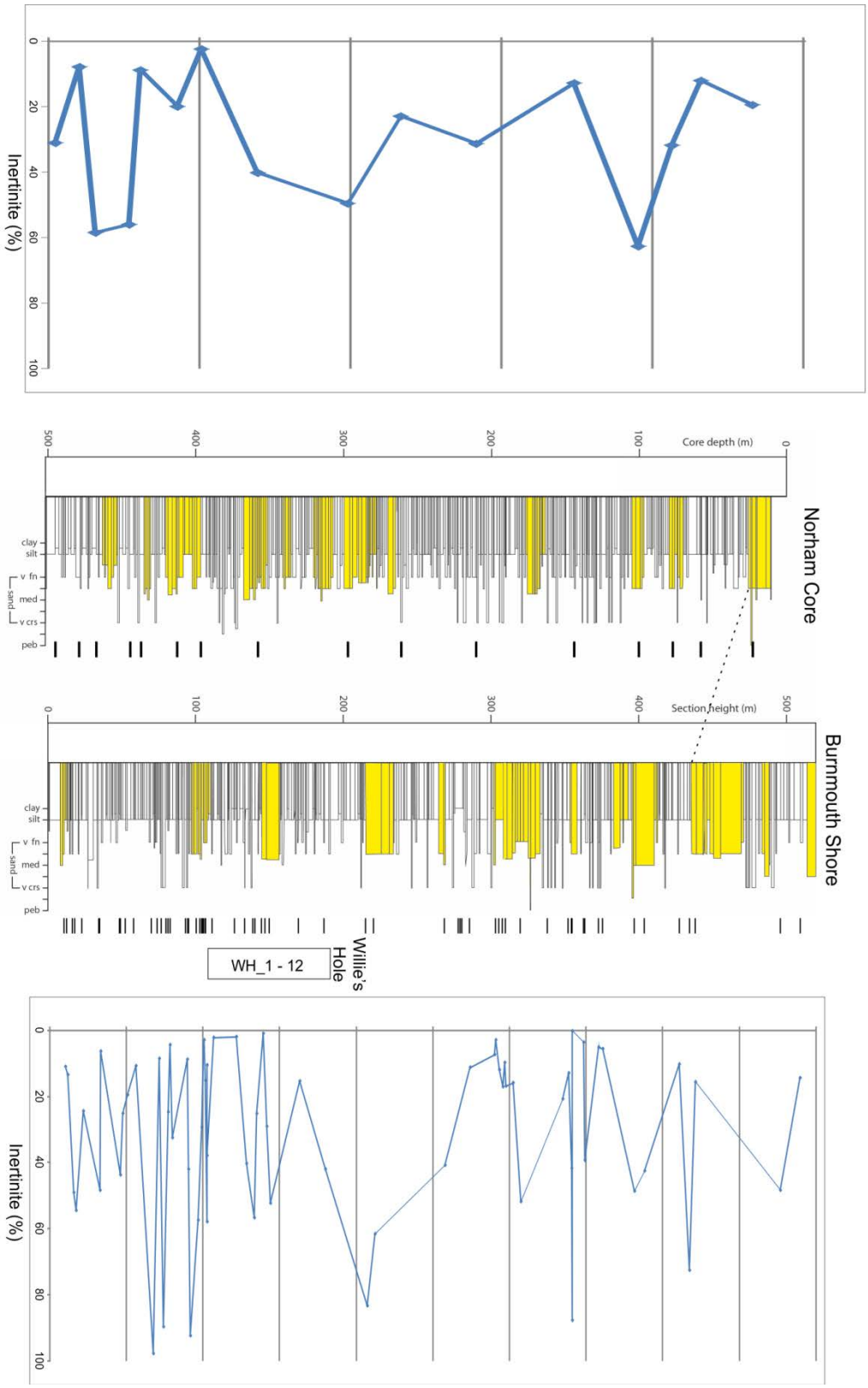

Figure 4.10: Relative inertinite abundance data for the Ballagan Fm., Burnmouth Shore section (left) and Norham core (right).

When examined under incident light, samples of macroscopic charcoal (i.e. ≥ 1cm) from the Ballagan Formation (provided courtesy of T. Smithson) were found to consist of xylem tissue (Fig. 4.11), with reflectance values ranging from 1.65–4.53% (mean 2.57%; SI 4.4).

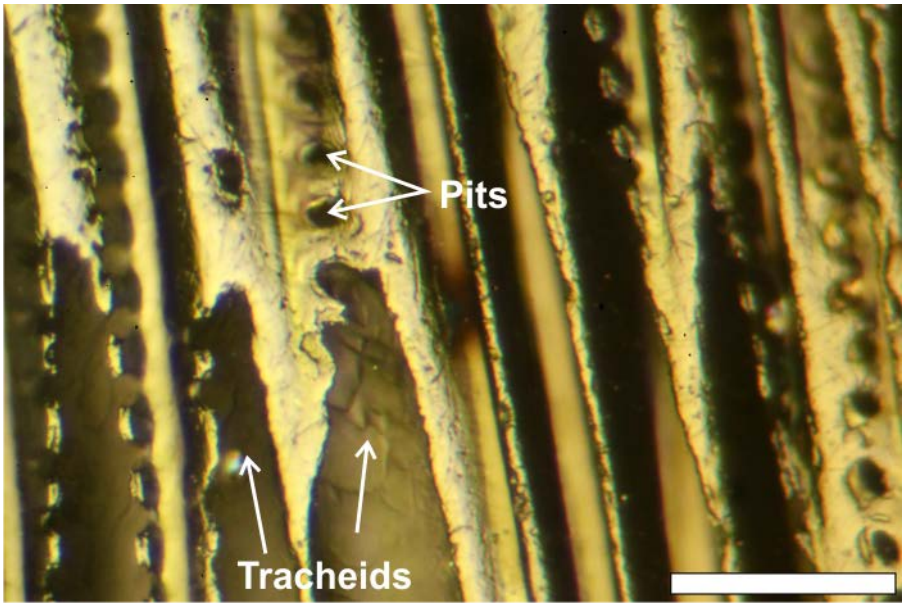

Figure 4.11: Incident-light photomicrograph of fusinized wood from the Ballagan Formation at Burnmouth Shore. Scale bar = 32.5 µm.

Five Tournaisian and 31 Viséan coals were also analysed, providing mean relative inertinite abundances of 52.6 and 33.8% respectively. This falls between coal-inertinite values reported by Diessel (2010) and Glasspool *et al*. (2015) for the Viséan (27.8% and 38.4%), but is substantially higher than Glasspool *et al*.'s Tournaisian result (31.4%; Fig. 4.12). Despite this large difference, Kruskal-Wallis ANOVA indicated no significant differences between any pair of datasets ($H = 3.494$, $P = 0.479$; SI 4.5); this is most likely due to the small sample size and wide spread of data for the Tournaisian ($\sigma = 30.1$).

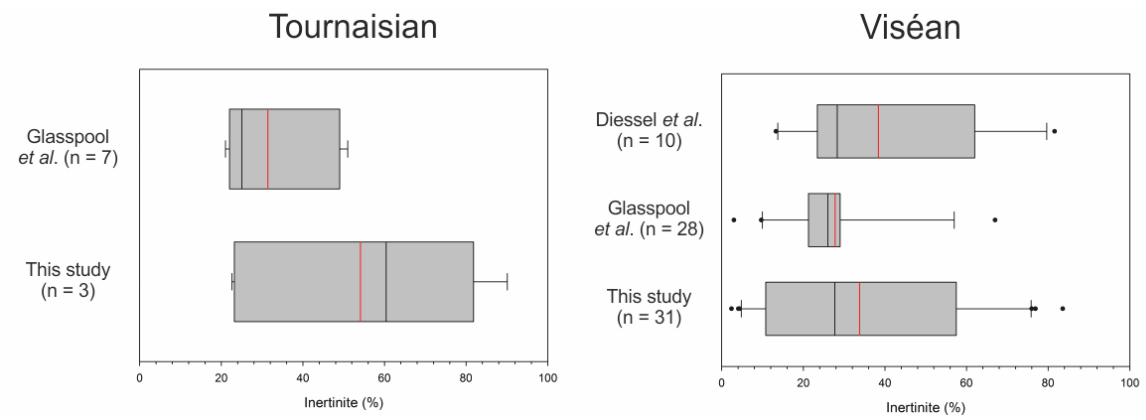

Figure 4.12: Comparison of inertinite abundance results for Tournaisian and Viséan coals, as determined by Glasspool et al. (2015), Diessel (2010) and this study. Black bars, median; red bars mean; whiskers, $10^{th}/90^{th}$ percentile.

4.5 Discussion

The inertinite values obtained are not consistent with a substantial fall in atmospheric pO_2 during Romer's Gap and consequent reduction in charcoal production. DOM inertinite content appears to have been reasonably stable with the exception of an increase in the latest Famennian/earliest Tournaisian, and the three localities at which the Ballagan Fm. was sampled were similar in age, palaeogeography, and palaeoenvironment yet showed a greater range in mean inertinite abundance than is seen between different stages through Romer's Gap, again with the exception of the latest Famennian/earliest Tournaisian data. The discovery of macroscopic charcoal in the Ballagan Fm. at Burnmouth Shore also argues against fire suppression; reflectance values between 1.5 and 4.5% indicate minimum temperatures at the time of formation between 400 and 600°C, which likely represent flaming rather than smouldering combustion (Scott *et al*. 2014). Finally, though statistically weak due to the small number of Tournaisian coals examined, coal inertinite levels also fail to support reduced charcoal production during the Tournaisian relative to the Viséan.

The results of the coal analysis are consistent with previously published Viséan data, but conflict with those reported by Glasspool *et al*. (2015) for the Tournaisian (Fig. 4.12, Table 4.1). This is assumed to be an effect of small sample size, exacerbated by the fact that both Tournaisian datasets include coals from the Hoelbreen Member in Spitsbergen, which appears to be particularly variable in its inertinite content (SI 4.2). Note that this

follows Glasspool *et al*. (2015) in assuming the sampled part of the Hoelbreen Mbr. to be Tournaisian and not Viséan in age. The much larger spread of results reported by Diessel (2010) and in this study compared to that of Glasspool *et al*. (2015) may reflect the fact that some of Glasspool *et al*.'s data are seam or locality means. Nevertheless, in both cases mean coal-inertinite was lower in the Viséan than in the Tournaisian.

Age/unit	This study		Glasspool *et al*. (2015)		Diessel (2010)	
	Mean inertinite	σ	Mean inertinite	σ	Mean inertinite	σ
Tournaisian	52.6%	30.1	31.4%	12.9	-	-
Viséan	33.8%	24.5	27.8%	14.0	38.9%	22.5

Table 4.1: Comparison of mean relative inertinite abundance in coals reported in this study and by previous workers.

The Obrutschew Formation

The sharp increase in inertinite around the D/C boundary is the result of a higher mean content in samples from the Obrutschew Formation, which as previously discussed represents an extended period of lacustrine conditions (section 4.2). Although climatic and environmental changes associated with lake formation cannot be ruled out as a cause, this is the only occasion on which a link between lacustrine conditions and charcoal accumulation is apparent in the dataset. It has also been noted that lakes and lagoons can act as traps for wind-borne charcoal, and lacustrine successions may contain a greater abundance of inertinite than coeval nearshore marine deposits (Bojesen-Koefoed *et al*. 1997; Scott 2000); however, charcoal particles transported in this way are typically ≤ 10 µm, which is below the minimum size (15 µm) that can be detected in this study. Given that a major unconformity truncates these deposits (Marshall *et al*. 1999; Marshall 2015), an alternative possibility is that increased oxidation has led to destruction of organic material,with preferential preservation of the more refractory components (i.e. charcoal), as observed during lab-based oxidation experiments (Winkler 1985; section 2.6).

Latitudinal controls on charcoal production

During the late Devonian and early Carboniferous, northern Britain and Triungen (which provided most of the Mississippian material) were located 4° S and 10° N, respectively, experiencing a tropical, probably monsoonal climate. In contrast, Greenland (which provided most of the Famennian material) was situated within the interior of the Old Red Sandstone continent, at approximately 15° S, within the southern arid zone (Peel *et al*. 2007; Astin *et al*. 2010; Marshall 2015; Bennett *et al*. 2016); although conditions appear to have been quite variable through time in both regions there is a clear tendency towards aridity in the Greenland successions that is not seen in northern Britain. As previously noted, it is reasonable to assume a greater propensity for fire in more arid regions, and some studies have reported a strong latitudinal control on Holocene charcoal production (Herring 1985; Power *et al*. 2008). The positive correlation between palaeolatitude and inertinite seen here remains even if material from the Obrutschew Fm. (which, as discussed above, may have been subjected to preservational bias) is discounted (Pearson $r = 0.225$, $P = 0.001$; SI 4.3B); thus, the data in this case support climate as a major control on fire activity.

4.6 Summary

The first c. 30 Ma of the Carboniferous are characterised by a striking scarcity of tetrapods in the fossil record, in contrast to the uppermost Devonian and subsequent Carboniferous stages. 'Romer's Gap' has been attributed to a variety of causes, which can broadly be divided into taphonomic and environmental explanations. The most popular amongst the latter category is the hypoxia hypothesis of Ward *et al*. (2006), which suggests that a drop in pO_2 (supported by some palaeoatmosphere models) made life on land untenable for early limbed vertebrates.

DOM and coal inertinite levels do not support this proposal; based on analysis of 251 shale and coal samples and in agreement with previously published coal data for this interval, fire activity appears to have been relatively stable through Romer's Gap, with the exception of DOM samples from the uppermost Famennian/lowermost Carboniferous in Greenland. The significantly higher inertinite values recorded from that locality are tentatively attributed to the major unconformity which truncates the Obrutschew Fm.,

causing relative enrichment of inertinite through preferential oxidation/destruction of less resistant organic material. A clear positive correlation is seen between inertinite abundance and palaeolatitude, suggesting climate (i.e. aridity) was a significant control on fire frequency at this time, but no change is seen that could reasonably be attributed to vegetative changes. These results suggest that palaeoatmosphere models predicting a sudden decrease in pO_2 immediately after the D/C boundary are incorrect, and that the disappearance of *Archaeopteris*-dominated forests at this time (representing a reduction in fuel-laden, possibly fire-prone ecosystems) did not significantly affect fire activity.

4.7 Tetrapod World: early evolution and diversification

The TW:eed project is a multidisciplinary research effort undertaken jointly by the Universities of Southampton, Cambridge, and Leicester, the British Geological Survey, and the National Museum of Scotland to investigate the environments and ecologies of Romer's Gap. Work in Southampton was funded by NERC consortium grant NE/J021091/1, '*The mid-Palaeozoic biotic crisis: setting the trajectory of tetrapod evolution*'. Palynological processing of shale samples from the Ballagan Formation in Northumbria and the Scottish Borders, UK provided organic residues for charcoal analysis in order to address the hypothesis of Ward *et al*. (2006): that Romer's Gap represents a genuine diversity crisis triggered by global hypoxia. Preliminary results and discussion were included in a joint paper, published in Nature Ecology and Evolution, *Phylogenetic and environmental context of a Tournaisian tetrapod fauna*, included below. These results are based on fusinite abundance only, rather than total inertinite; although this method was subsequently shown to be unreliable due to the poor correlation between these two components (see section 2.3), the conclusion that atmospheric pO_2 remained stable through Romer's Gap is in accord with the results of this chapter, and thus remains valid.

nature ecology & evolution

ARTICLES

PUBLISHED: 5 DECEMBER 2016 | VOLUME: 1 | ARTICLE NUMBER: 0002

Phylogenetic and environmental context of a Tournaisian tetrapod fauna

Jennifer A. Clack[1]*, Carys E. Bennett[2], David K. Carpenter[3], Sarah J. Davies[2], Nicholas C. Fraser[4], Timothy I. Kearsey[5], John E. A. Marshall[3], David Millward[5], Benjamin K. A. Otoo[1†], Emma J. Reeves[3], Andrew J. Ross[4], Marcello Ruta[6], Keturah Z. Smithson[1], Timothy R. Smithson[1] and Stig A. Walsh[4]

The end-Devonian to mid-Mississippian time interval has long been known for its depauperate palaeontological record, especially for tetrapods. This interval encapsulates the time of increasing terrestriality among tetrapods, but only two Tournaisian localities previously produced tetrapod fossils. Here we describe five new Tournaisian tetrapods (*Perittodus apsconditus*, *Koilops herma*, *Ossirarus kierani*, *Diploradus austiumensis* and *Aytonerpeton microps*) from two localities in their environmental context. A phylogenetic analysis retrieved three taxa as stem tetrapods, interspersed among Devonian and Carboniferous forms, and two as stem amphibians, suggesting a deep split among crown tetrapods. We also illustrate new tetrapod specimens from these and additional localities in the Scottish Borders region. The new taxa and specimens suggest that tetrapod diversification was well established by the Tournaisian. Sedimentary evidence indicates that the tetrapod fossils are usually associated with sandy siltstones overlying wetland palaeosols. Tetrapods were probably living on vegetated surfaces that were subsequently flooded. We show that atmospheric oxygen levels were stable across the Devonian/Carboniferous boundary, and did not inhibit the evolution of terrestriality. This wealth of tetrapods from Tournaisian localities highlights the potential for discoveries elsewhere.

The term 'Romer's Gap' was coined[1,2] for a hiatus of approximately 25 million years (Myr) in the fossil record of tetrapods[3], from the end-Devonian to the mid-Mississippian (Viséan). Following the end-Devonian, the earliest terrestrial tetrapod fauna was known from the early Brigantian (late Viséan) locality of East Kirkton near Bathgate, Scotland[4,5]. By that time, tetrapods were ecologically diverse, and were terrestrially capable. With five or fewer digits, some had gracile limbs[6,7]—unlike the polydactylous, predominantly aquatic, fish-like tetrapods of the Late Devonian[8]. Fossils representing transitional morphologies between these disparate forms were almost entirely lacking, limiting both understanding of the acquisition of terrestrial characteristics and the relationships between the diverse mid-Carboniferous taxa. Alternative hypotheses to explain the hiatus have included a low oxygen regime[9] or lack of successful collecting in Tournaisian strata[2].

Although isolated tetrapod limb bones, girdle elements and trackways are known from the Tournaisian of the Horton Bluff Formation at Blue Beach, Nova Scotia[10,11], only a small fraction has been fully described[12]. The only other Tournaisian tetrapod material was the articulated skeleton of *Pederpes finneyae*, from the Tournaisian Ballagan Formation near Dumbarton, western Scotland[13,14]. More recently, new taxa from this formation in the Scottish Borders region were reported[3]. Further collecting from five localities (Supplementary Fig. 1) has since produced more data about the fauna, its environment and climatic conditions.

Our analysis shows that the Tournaisian included a rich and diverse assemblage of taxa, which included close relatives of some Devonian forms on the tetrapod stem and basal members of the amphibian stem. We diagnose, name and analyse five taxa (Figs 1–5), and summarize at least seven others that are distinct but undiagnosable at present (Fig. 6 and Supplementary Figs 2–6).

Tetrapods occupied a mosaic of juxtaposed microhabitats including ponds, swamps, streams and floodplains, the last of these with highly variable salinity and water levels in a sharply contrasting seasonal climate. Their fossils are most closely associated with palaeosols and the overlying sandy siltstones. These indicate exposed and vegetated land surfaces that were then flooded[15,16] (Supplementary Fig. 7). This varied environment persisted over the 12 Myr of the Tournaisian[3]. In contrast to a previous study[9], we show that atmospheric oxygen levels were stable across the Devonian/Carboniferous boundary and did not therefore compromise terrestrial faunal life.

Differential diagnoses below give the characters in which each taxa differs from all other tetrapods in its combination of autapomorphic and derived (relative to Devonian taxa) characters.

Results

Systematic palaeontology.

Tetrapoda Goodrich, 1930 indet.

Perittodus apsconditus gen. et sp. nov. Clack and Smithson T.R. (Fig. 1c–g).

Smithson *et al.*, 2012, 'new taxon A'

Etymology. Genus from *perittos* (Greek) 'odd' and *odus* (Greek) 'tooth' referring to the unusual dentition of the mandible. Species from *apsconditus* (Latin) 'covert, disguised, hidden, secret or concealed', referring to the fact that key parts were only discovered by micro-computed tomography (micro-CT) scanning.

[1]University Museum of Zoology Cambridge, Downing Street, Cambridge CB2 3EJ, UK. [2]Department of Geology, University of Leicester, Leicester LE1 7RH, UK. [3]National Oceanography Centre University of Southampton, Waterfront Campus European Way, Southampton SO14 3ZH, UK. [4]National Museums Scotland, Chambers Street, Edinburgh EH1 1JF, UK. [5]British Geological Survey, The Lyell Centre, Research Avenue South, Edinburgh EH14 4AP, UK. [6]School of Life Sciences, University of Lincoln, Joseph Banks Laboratories, Green Lane, Lincoln LN6 7DL, UK. †Present address: Department of Organismal Biology & Anatomy, University of Chicago, 1027 E. 57th St., Chicago, IL 60637, USA. *e-mail: j.a.clack@zoo.cam.ac.uk

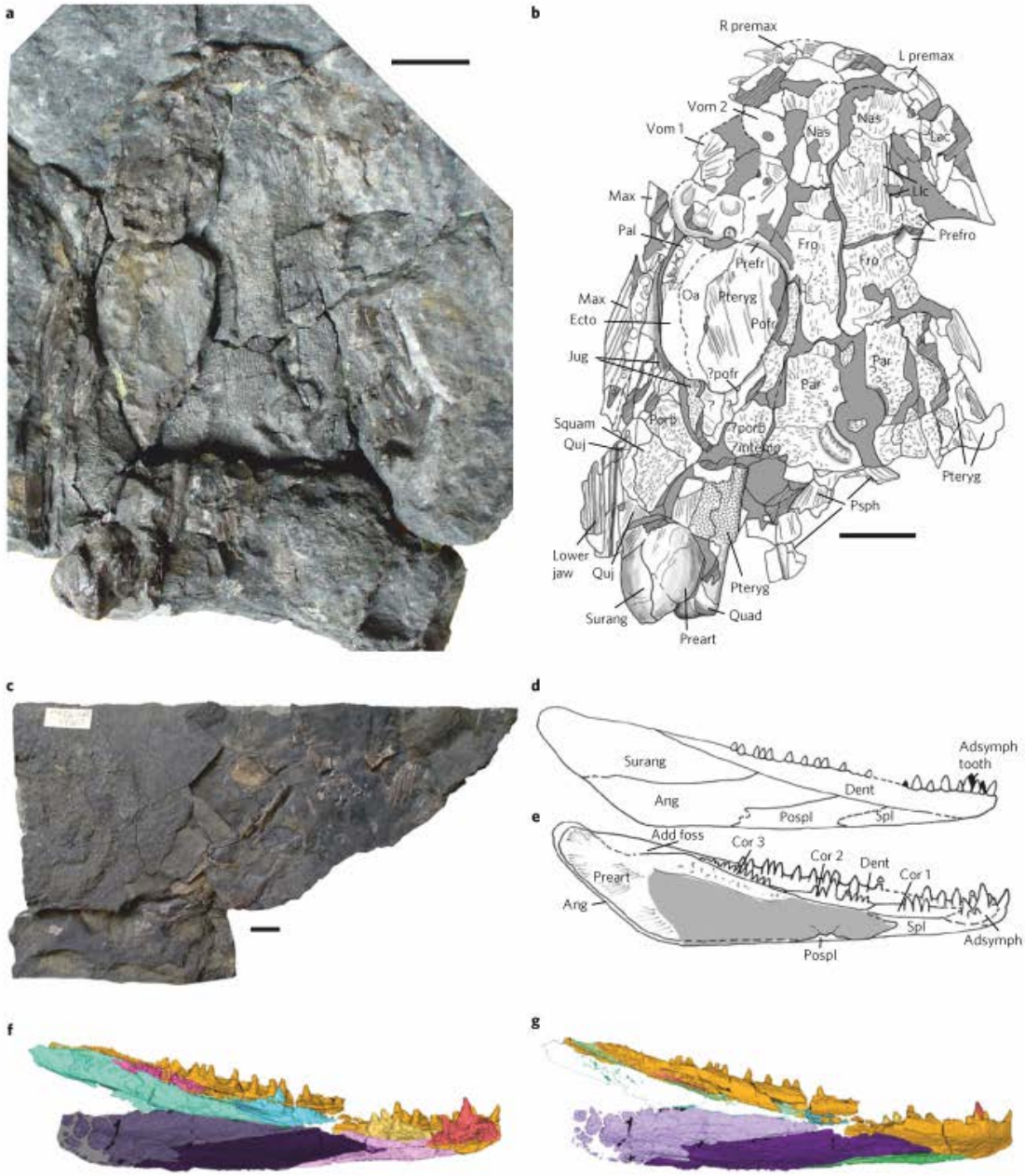

Figure 1 | New tetrapod taxa from Willie's Hole. a,b, *Koilops herma* gen. et sp. nov. (National Museum of Scotland NMS G. 2013.39/14). **a**, Photograph of the specimen, mainly preserved as natural mould. **b**, Interpretive drawing of the specimen. **c–g**, *Perittodus apsconditus* gen. et sp. nov. (University Museum of Zoology, Cambridge UMZC 2011.7.2a). **c**, Photograph of the main specimen block. **d**, Reconstruction of the lower jaw in external view made from scan data, and part and counterpart specimens. **e**, Reconstruction of the lower jaw in internal view made from scan data, and part and counter part specimens. **f**, Segmented model made from scans of lower jaw in internal view; external bones (seen in internal view) greyed out. **g**, Segmented model made from scans of lower jaw in internal view. Colour coding in **f**: yellow, dentary; red, adsymphysial plate; turquoise, part of prearticular; pale yellow, first coronoid; blue, second coronoid; cerise, third coronoid; pink, splenial; violet, angular; purple, prearticular. The colour coding used in **g** is the same except for the splenial (green in **g**). Scale bar in **a–c**, 10 mm. Add foss, adductor fossa; Adsymph, adsymphysial; Ang, angular; Cor, coronoid; Dent, dentary; Ecto, ectopterygoid; Fro, frontal; Intemp, intertemporal; Jug, jugal; L, left; Lac, lacrimal; Llc, lateral line canal; Max, maxilla; Oa, overlap area for pterygoid; Pal, palatine; Par, parietal; Pofr, postfrontal; Porb, postorbital; Pospl, postsplenial; Preart, prearticular; Prefro, prefrontal; Premax, premaxilla; Psph, parasphenoid; Pteryg, pterygoid; Quad, quadrate; Quj, quadratojugal; R, right; Surang, surangular; Vom, vomer.

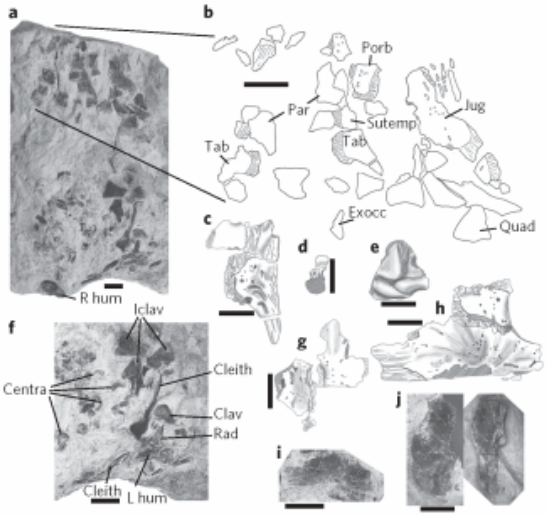

Figure 2 | *Ossirarus kierani* gen. et sp. nov. (UMZC 2016.3) from Burnmouth Ross end cliffs. a, Photograph of the complete specimen. **b**, Map of the skull bones in the area indicated by the black lines in **a**. **c**, Drawing of the right tabular, supratemporal and a partial unidentified bone. **d**, Drawing of the exoccipital. **e**, Drawing of the quadrate. **f**, Photograph enlargement of part of the postcranial portion of the specimen. **g**, Drawings of the left and right parietal bones placed in articulation. **h**, Drawing of the jugal and postorbital placed in articulation. **i**, Photograph of the jugal. **j**, Photograph enlargement of the right humerus. Scale bar in **b**, 10 mm; scale bars in **c–j**, 5 mm. Clav, clavicle; Cleith, cleithrum; Exocc, exoccipital; Iclav, interclavicle; Jug, jugal; L/R hum, left/right humerus; Par, parietal; Porb, postorbital; Quad, quadrate; Rad, radius; Sutemp, supratemporal; Tab, tabular.

Holotype. UMZC 2011.7.2a and b. Cheek region of skull, lower jaw, and postcranial elements in part and counterpart.
Locality. Willie's Hole, Whiteadder Water near Chirnside.
Horizon. Ballagan Formation. Early mid-Tournaisian.
Diagnosis. Autapomorphies: unique adsymphysial and coronoid dentition—adsymphysial with two tusks and at least two smaller teeth, anterior coronoid with two or three larger tusks, middle coronoid with two larger and two or three smaller teeth, posterior coronoid row of small teeth; lozenge-shaped dorsal scales bearing concentric ridges centred close to one edge nearer to one end. Derived characters: deeply excavated jugal with narrow suborbital bar; lateral line an open groove on jugal.
Plesiomorphies and characters of uncertain polarity. No mesial lamina of postspenial (state of angular not known); 35 dentary teeth including spaces; 29 maxillary teeth including spaces; room for possibly six teeth on premaxilla; marginal teeth similar in size; short broad phalanges, rounded unguals longer than wide with ventral ridge.
Attributed specimen. UMZC 2016.1. Isolated dentary and adsymphysial (in micro-CT scan) from Burnmouth Ross end cliffs, 373.95 m above the base of the Ballagan Formation. Mid-Tournaisian.
Remarks. Lower jaw length 68 mm. Maxilla of holotype visible in micro-CT scan. UMZC 2016.1 is almost identical in size and dentition to the holotype. The pattern is most similar, but not identical, to that of the Devonian taxon *Ymeria*[17]. A distinct denticulated ridge on the prearticular is set off from the remainder of the bone by a ventral groove. Radius and ulna are of approximately equal length. A partial ischium reveals similarities to *Baphetes*[18].

Koilops herma gen. et sp. nov. Clack and Smithson T.R. (Fig. 1a,b). Smithson *et al.*, 2012, 'probable new taxon'.

Etymology. Genus from *koilos* (Greek) 'hollow or empty', and *ops* (Greek) 'face', referring to the skull mainly preserved as natural mould. Species from *herma* (Greek) 'boundary marker, cairn, pile of stones'. The specimen, from the Scottish Borders region, has transitional morphology between Devonian and Carboniferous tetrapods.
Holotype. NMS G. 2013.39/14. Isolated skull mainly as a natural mould.
Locality. Willie's Hole, Whiteadder Water near Chirnside.
Horizon. Ballagan Formation. Early mid-Tournaisian.
Diagnosis. Autapomorphies: fine irregular dermal ornament with conspicuous curved ridges around the parietal foramen and larger pustular ornament anterior to parietal foramen. Derived characters: deeply excavated jugal with narrow suborbital bar; large parietal foramen.
Plesiomorphies and characters of uncertain polarity. Orbit oval with slight anterior embayment; prefrontal–postfrontal contact narrow, anterior to orbit mid-length; about eight premaxillary teeth recurved, sharply pointed, ridged towards base; closed palate, denticulated pterygoid; vomers bearing tusks and smaller teeth, at least four moderately large teeth on palatine; short rounded snout, only slightly longer than maximum orbit length.
Remarks. Skull length 80 mm. The dermal bones are robust and well integrated so the individual was almost certainly not a juvenile.

Ossirarus kierani gen. et sp. nov. Clack and Smithson T.R. (Fig. 2).

Etymology. Genus from *ossi* (Latin) 'bones' and *rarus* (Latin) 'scattered or rare'. Species to honour O. Kieran and B. Kieran, representing the Burnmouth community, who have supported us and encouraged local interest and cooperation.
Holotype. UMZC 2016.3. A single block containing scattered skull and postcranial remains.
Locality. Burnmouth Ross end cliffs.
Horizon. 340.5 m above the base of the Ballagan Formation. Mid-Tournaisian.
Diagnosis. Autapomorphies: tabular elongate triangle forming a conspicuous tabular horn with a convex lateral margin. Derived character: tabular-parietal contact; exoccipital separate from basioccipital.
Plesiomorphies and characters of uncertain polarity. Jugal with extensive posterior component, with anteriorly placed shallow contribution to orbit; lozenge-shaped interclavicle; humerus with elongate and oblique pectoralis process comparable with the ventral humeral ridge of elpistostegalians and *Acanthostega*; multipartite vertebrae with diplospondylous widely notochordal centra and neural arches as unfused bilateral halves.
Remarks. Estimated skull length 50 mm on the basis of comparisons with *Acanthostega*, *Ichthyostega* and *Greererpeton*[19–21]. The primitive jugal morphology, with an elongated postorbital region and an anteriorly placed orbital margin contributing less than 25% of the orbit margin, is similar to that in *Acanthostega*[19] and *Ichthyostega*[20]. The tabular has an elongated posterior process, but its lateral margin does not show an embayment for a spiracular notch. The bones are robust, with well defined overlap areas for interdigitating sutures. Though disarticulated, these suggest that the individual was not a juvenile. The specimen shows the earliest known occurrence of a separate exoccipital.

Diploradus austiumensis gen. et sp. nov. Clack and Smithson T.R. (Fig. 3).

Etymology. Genus from *diplo* (Greek) 'double' and *radus* (Greek) 'row' referring to the double coronoid tooth row. Species from *austium* (Latin) 'mouth of a river or stream' referring to Burnmouth.
Holotype. UMZC 2015.30. Small disrupted skull with lower jaw, palate and skull roofing bones.
Locality. Burnmouth Ross end cliffs.
Horizon. 373.95 m above the base of the Ballagan Formation. Mid-Tournaisian.

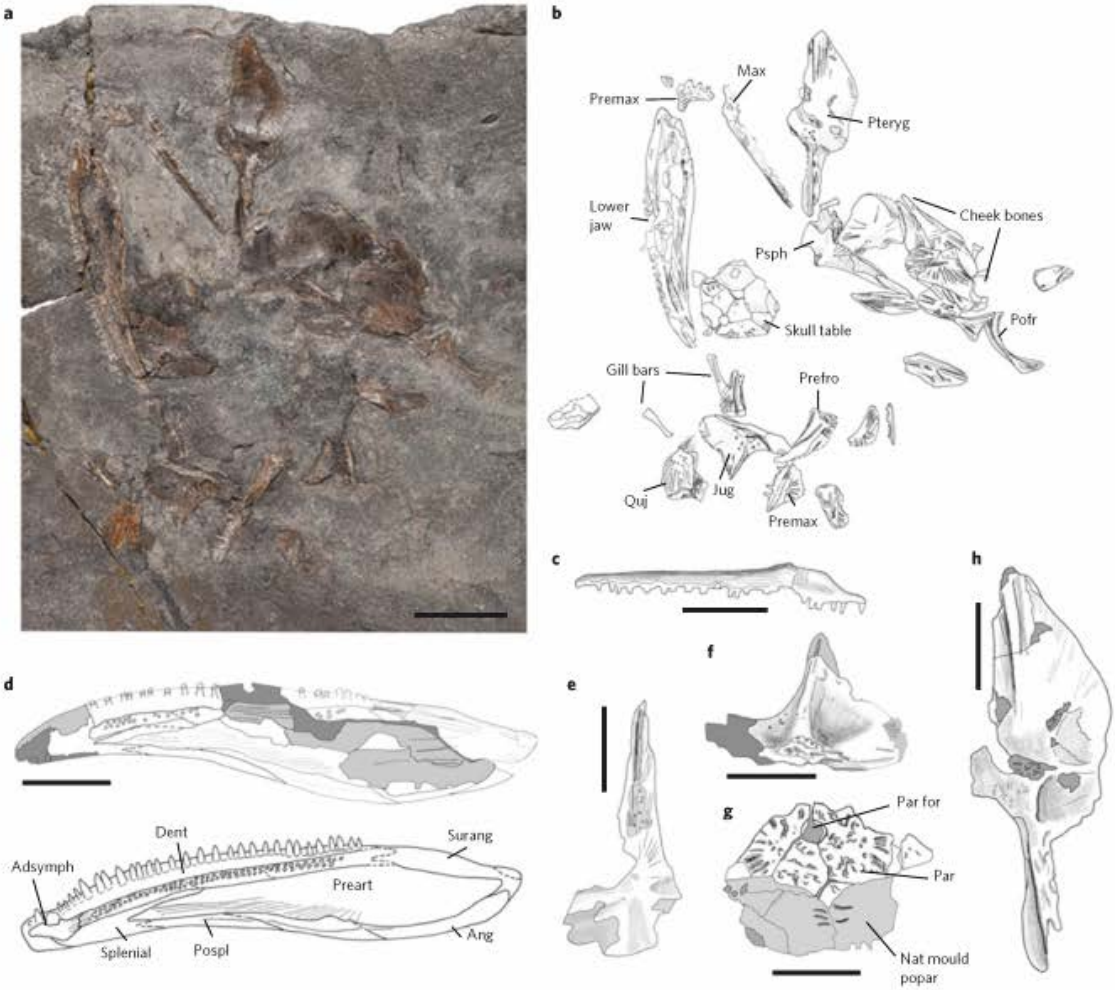

Figure 3 | *Diploradus austiumensis* gen. et sp. nov. (UMZC 2015.30) from Burnmouth Ross end cliffs. a, Photograph of the complete specimen. **b**, Map of the specimen showing the distribution of elements. **c**, Drawing of the right maxilla. **d**, Upper, interpretive drawing of the specimen; lower, reconstruction of the jaw in internal view. **e**, Drawing of the parasphenoid. **f**, Drawing of the right jugal in internal view. **g**, Drawing of the skull table. **h**, Drawing of the pterygoid in dorsal view. Scale bar in **a**, 10 mm; scale bars in **b–h**, 5 mm. Nat mould popar, natural mould of postparietal. All other abbreivations are as for Figs 1 and 2.

Diagnosis. Autapomorphies: lower jaw with irregular double row of denticles along the coronoids; around 51 dentary teeth and spaces, with enlarged tusk at position 3 and the largest teeth in positions 8–13; parietals short, pineal foramen anteriorly placed; ?narrow curved pre- and postfrontals. Derived characters: deeply excavated jugal with narrow suborbital bar; parasphenoid with broad, flattened posterior portion with lateral wings, earliest known occurrence of a parasphenoid crossing the ventral cranial fissure, cultriform process flat, narrow.

Attributed specimen. UMZC 2016.4 a and b. The anterior end of a mandible from 341 m above the base of the Ballagan Formation at Burnmouth.

Plesiomorphies and characters of uncertain polarity. Unsutured junction between prearticular and splenial series; adductor fossa dorsally placed; adsymphysial plate possibly lacking dentition; closed, denticulated palate; broad pterygoid, quadrate ramus narrow with vertically orientated medial ascending lamina; ossified hyobranchial elements; maxilla and premaxilla with spaces for 35 and 10–12 teeth respectively; maxilla–premaxilla contact narrow, lacking interdigitations; dermal ornament with low profile, irregular on skull table, ridged on squamosal and quadratojugal.

Remarks. Lower jaw length 30 mm, superficially resembling that of *Sigournea*[22], although a relationship is not supported by cladistic analysis. The thinness of the bones and their distribution suggest a juvenile.

Aytonerpeton microps gen. et sp. nov. Otoo, Clack and Smithson T.R. (Fig. 4).

Etymology. Genus name from Ayton, the parish in the Scottish Borders from which the specimen came, and *erpeton* (Greek) 'crawler' or 'creeping one'. Species from *micro* (Greek) 'small' and *ops* (Greek) 'face'.

Holotype. UMZC 2015.46b. Partial skull and scattered post-crania visible only in micro-CT scan (Supplementary Videos 1 and 2).

Locality. Burnmouth Ross end shore exposure.

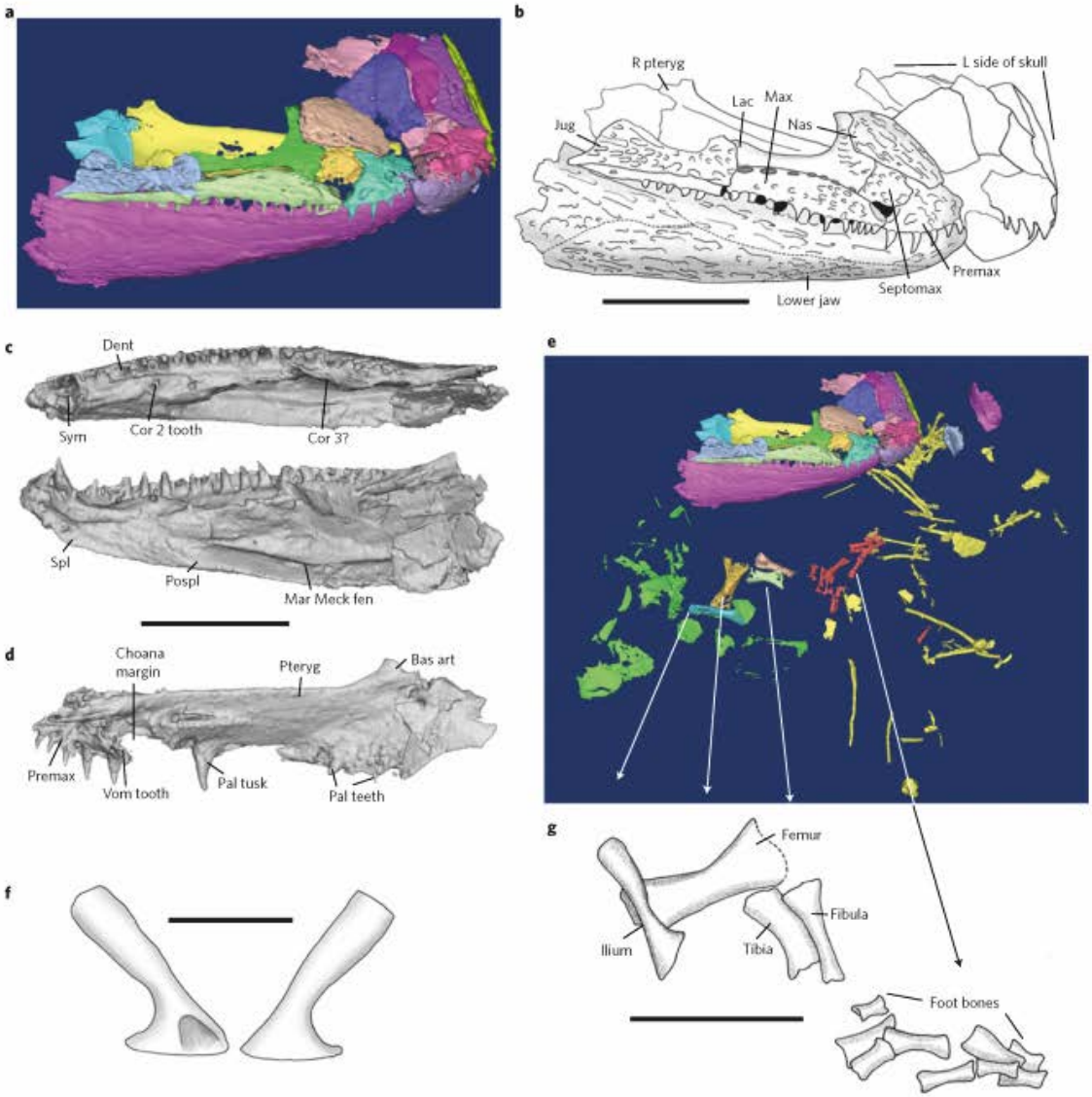

Figure 4 | *Aytonerpeton microps* gen. et sp. nov. (UMZC 2015.46b) from Burnmouth Ross end shore exposure. a, Still from a micro-CT scan of the block containing most of the specimen. **b**, Interpretive drawing of the right side of the skull and palate. **c**, Stills from a micro-CT scan of the right lower jaw in dorsal view (upper image) and mesial view (lower image). **d**, Still from a micro-CT scan of the right palate in approximately ventrolateral view. In **c** and **d** note the sutures between pterygoid and marginal palatal bones, and the lower jaw bones, are tightly sutured and difficult to see in the scan. **e**, Still from a micro-CT scan of the entire specimen in the main block. Arrows point to elements in **g**. **f**, Enlargement of the ilium in lateral (left image) and medial (right image) views. **g**, Elements of the hind limb. Scale bars in **a**–**e**,**g**, 10 mm; scale bar in **f**, 5 mm. Mar Meck fen, margin of Meckelian fenestra; Sym, symphysis; Septomax, septomaxilla. All other abbreivations are as for Figs 1 and 2.

Horizon. 340.6 m above the base of the Ballagan Formation. Mid-Tournaisian.

Diagnosis. Autapomorphies: two enlarged premaxillary teeth plus one large tooth space at posterior end of premaxilla; five teeth on premaxilla; adsymphysial with a single tooth; coronoids apparently lacking shagreen; L-shaped lacrimal; vomer with at least one tooth, palatine with one large fang but lacking smaller teeth; ectopterygoid with at least two teeth and possible smaller teeth. Derived characters shared with colosteids: course of lateral line on maxilla and nasal; dentary teeth larger and fewer than upper marginal teeth; single large Meckelian fenestra; interpterygoid vacuities longer than wide; single large parasymphysial fang on dentary; ilium with a single strap-shaped iliac process.

Remarks. Reconstructed skull length about 50 mm. Other distinguishing features: short snout, approximately similar in length to orbit diameter; naris and choana both very large relative to skull size—larger than in *Greererpeton*. The enlarged premaxillary teeth prefigure those of more derived colosteids[21], but the dentary lacks

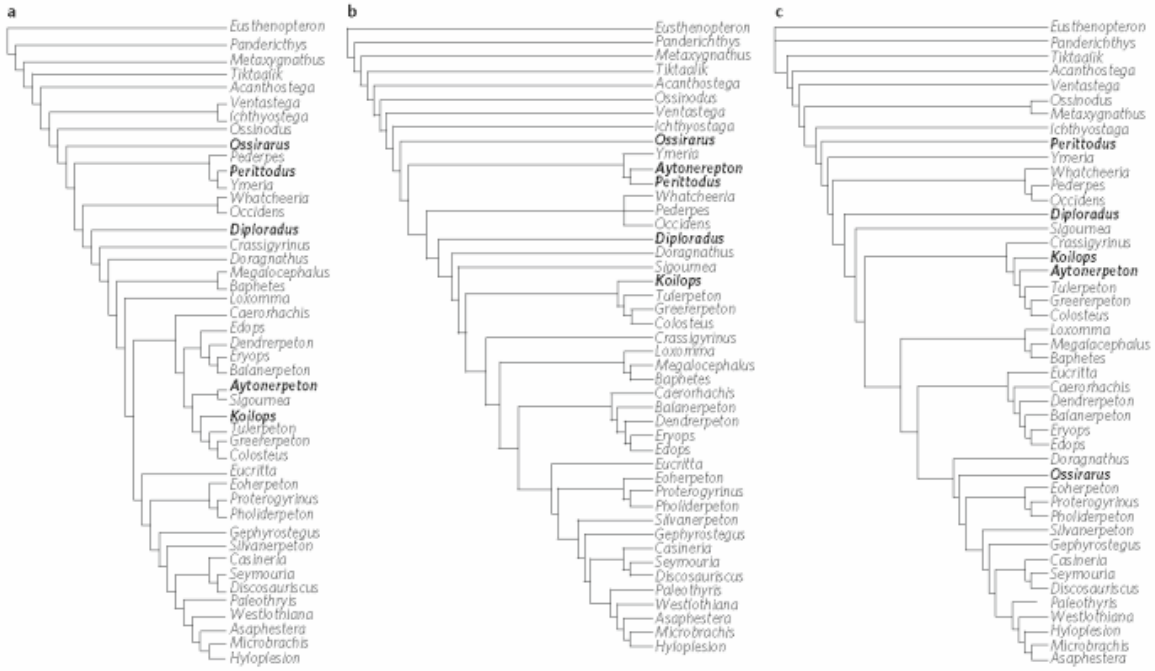

Figure 5 | Phylogenetic analysis of early tetrapods. a–c, Cladograms created using either TNT (**a**,**b**) or Bayesian (**c**) analysis. **a**, Single most parsimonious tree obtained from implied weights search with $K=3$ (see text and Supplementary Information for details). **b**, Strict consensus of four equally parsimonious trees obtained from implied weights search with $K=4$. **c**, Bayesian analysis tree; see text, Methods and Supplementary Information for details. The new taxa described here are highlighted in bold.

the corresponding reciprocal notch. This appears to be an early expression of a feature that becomes more elaborate in later taxa. All coronoids bear at least one tooth. Some colosteids lack coronoid teeth, and instead bear shagreen, a variable condition among individuals[23]. The small size of the skull but the strong integration of the lower jaw bones suggest a subadult or adult in which case the large orbit is unlikely to be a juvenile feature (see juvenile *Greererpeton* CMNH 11095)[24]. Its gracile limbs, metapodial bones and phalanges resemble *Colosteus* rather than *Greererpeton*. Clavicular ornament is similar to that of other colosteids[25,26]. The single iliac process is shared with other colosteids and with temnospondyls. This is the earliest known occurrence of this feature.

Cladistic analysis. We performed parsimony and Bayesian analyses of a new data matrix (character list and data matrix in Supplementary Data) incorporating the new tetrapods. No taxon could be safely deleted[27]. Parsimony with all characters unordered and equally weighted produced 4,718 shortest trees, a poorly resolved strict consensus (Fig. 5 and Supplementary Fig. 8) and moderate branch support.

Four parsimony analyses with implied weighting, each using a different value (3, 4, 5, 10) of the concavity constant[28] (K) produced many fewer trees (Fig. 5a,b), with novel topologies and increased stability for most of the new taxa. In these analyses, the relative positions of *Ossirarus*, *Perittodus* and *Diploradus* remain unaltered (Methods and Supplementary Fig. 8). Except in the analysis with $K=10$, *Koilops* and *Aytonerpeton* emerge as stem amphibians[29–31], but see refs [32,33] for an alternative view of stem amphibians, with *Aytonerpeton* close to *Tulerpeton* + colosteids. With characters reweighted by their rescaled consistency index, all new taxa emerge as stem tetrapods.

We also performed a Bayesian analysis (Fig. 5c). The results were largely similar to the parsimony analysis, except for the position of *Ossirarus*. In the Bayesian analysis, *Ossirarus* appears as a stem amniote, whilst *Perittodus*, *Diploradus*, *Koilops* and *Aytonerpeton* are stem tetrapods.

Despite inconsistencies, these results imply a substantial reshuffling of the branching sequence of Carboniferous stem tetrapods relative to previous studies[29–33], with interspersed Carboniferous and Devonian taxa pointing to a more ramified stem of tetrapod diversification. If corroborated by further evidence, a firmer placement of *Aytonerpeton* and *Koilops* within crown tetrapods would suggest a deep split between stem amphibians and stem amniotes within the Tournaisian.

Geology and environment. The Ballagan Formation (Inverclyde Group) underlies much of the Midland Valley of Scotland and the northern margin of the Northumberland Basin. At Burnmouth, the vertically dipping strata probably span the entire Tournaisian[2,34]. Environmental interpretation was based on a 490 m core from a borehole through the formation, a complete logged succession at centimetre-scale intervals through 520 m at Burnmouth and an 8 m section at Willie's Hole (Fig. 6, Methods and Supplementary Fig. 7).

Perittodus apsconditus occurs within a 6 cm thick laminated grey siltstone[16] that contains a network of cracks filled with sandy siltstone identical to that of the overlying bed. Occurring within laminated siltstones, this may record an autochthonous lake dweller. Associated fossils comprise plants, actinopterygians, myriapods and ostracods. *Koilops* occurs within a unit comprising four beds of alternating black and green siltstone in which abundant palaeosol clasts indicate erosion and transport of land-surface sediment during flooding events.

Diploradus occurs in a 40 cm thick, bedded, black sandy siltstone that lies between pedogenically modified grey siltstones. Associated

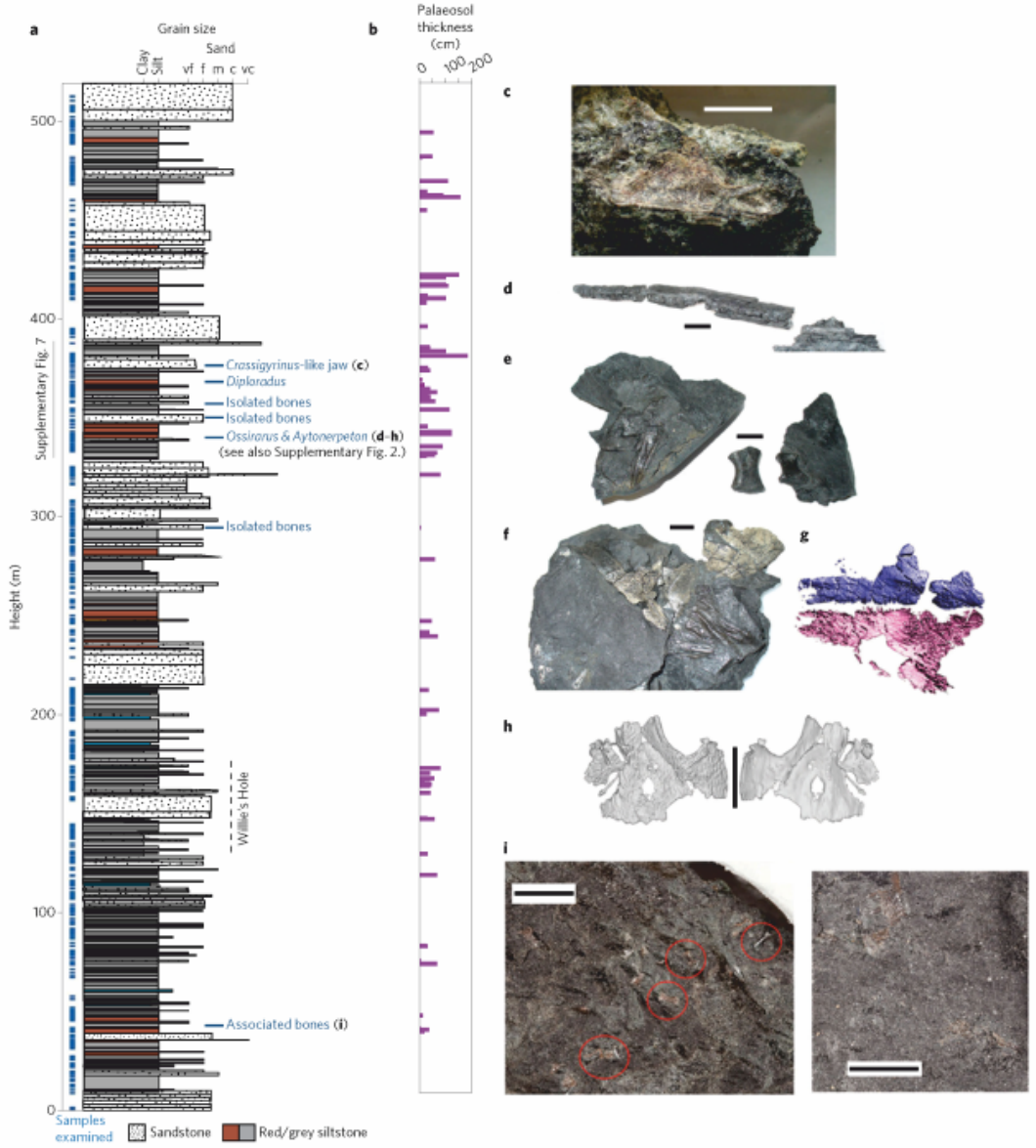

Figure 6 | Burnmouth sedimentary log showing palaeosol and tetrapod fossil distribution. a, The sedimentary log for Burnmouth with the tetrapod horizons indicated. **b**, The distribution of palaeosols and their thicknesses. **c–i**, Photographs of some of the tetrapod specimens found in addition to those in Figs 1–4. **c**, an isolated jugal (UMZC 2016.13) from the same bed that yielded the partial *Crassigyrinus*-like jaw in ref. [2]; horizon approximately 383 m above the base of the Ballagan Formation. This is a thick localized conglomerate lag containing many isolated vertebrate bones, plant remains and charcoal. The shape of the jugal is unique among the tetrapods so far collected from the Ballagan Formation, in its relative contribution to the orbit margin. Probable new taxon 1. **d–h**, Tetrapod specimens from a closely juxtaposed set of horizons beyond the resolution of the log to differentiate, between 340–341 m above the base of the Ballagan Formation: **d**, an isolated tetrapod maxilla (UMZC 2016.9); **e**, tetrapod belly scales (UMZC 2016.12) and metapodials/phalanges (UMZC 2016.10,11); **f**, skull bones and belly scales (UMZC 2016.8); **g**, micro-CT scan of the two overlapping bones in **f** (probable frontal bones of a *Pederpes*-like tetrapod); and **h**, partial skull table and postorbitals from slightly above the Burnmouth horizon yielding *Aytonerpeton microps* (UMZC 2016.7). Probable new taxon 2? May be associated with those in Supplementary Fig. 2, but not with *Aytonerpeton* (micro-CT by K. Z. Smithson). **i**, Phalanges or metapodials and skull elements of a small tetrapod from Burnmouth (UMZC 2016.5 **a**,**b**). Probable new taxon 3. Left hand image, largest elements circled. Right hand image, dentigerous bone near top left corner. Other elements include a probable jugal and rib fragments (not figured). These remains are the earliest post-Devonian tetrapod specimens found in the UK. They come from a horizon approximately 33 m above the base of the Ballagan Formation that was probably deposited about 1 Myr after the start of the Carboniferous. Scale bars in **c–h**, 10 mm; scale bar in **i**, 5 mm.

fossils comprise fish scales, abundant plant fragments, megaspores and shrimp and scorpion cuticle.

Ossirarus and *Aytonerpeton* occur within a complex 15 cm thick grey-black sandy siltstone that overlies a gleyed palaeosol and grades upwards into a laminated grey siltstone with brecciation cracks (Fig. 6, Methods and Supplementary Fig. 7). *Ossirarus* occurred just above the palaeosol in a light grey clay-rich sandy siltstone, whereas *Aytonerpeton* occurred within an overlying black sandy siltstone with abundant plant material. Associated fauna comprise abundant plants, megaspores, unusually abundant rhizodont bones and scales, actinopterygians, chondrichthyans (*Ageleodus*, gyracanthids), dipnoans, eurypterids and ostracods.

An association between wetland palaeosols and tetrapod-bearing facies has emerged from our studies, which is important because those horizons indicate a vegetated land surface (Fig. 6)[15,16]. The floodplain environments of semi-permanent water bodies, marsh, river banks and areas of dry land with trees were laid down at a time of change in the land plant flora of the Mississippian, following the end-Devonian extinctions. The new flora initiated a change in fluvial and floodplain architecture[35–37]. Progymnosperms had been almost eliminated in the extinctions, but thickets and forests were re-established in the early mid-Tournaisian with lycopods as the dominant flora. At Burnmouth many beds with abundant spores of the creeping lycopod *Oxroadia* include tetrapods. Terrestrial ground-dwelling arthropods, such as myriapods and scorpions, the fossils of which have been found at Burnmouth and at Willie's Hole, form a possible food supply for the tetrapods.

Atmospheric oxygen levels in the Tournaisian. To address the low oxygen hypothesis[9], we examined fossil charcoal (fusinite) in the Ballagan Formation to compare atmospheric oxygen levels in the Tournaisian with the Late Devonian and later Mississippian.

Charcoal, either as microscopic dispersed organic matter (DOM) or visible in hand specimens, is relatively common at Burnmouth and Willie's Hole. Although charcoal is reported from the Tournaisian Horton Bluff Formation, Nova Scotia[38], as indicating O_2 concentrations above 16%, no quantitative study to validate this result has been undertaken.

We analysed DOM from 73 rock samples from Burnmouth shore and Willie's Hole. For comparison with wildfire activity before and after Romer's Gap, we also analysed 42 samples from the Viséan of East Fife, Scotland (Strathclyde Group) and nine samples from the Famennian of Greenland (Stensiö Bjerg Formation) (Supplementary Fig. 9 and Supplementary Table 1). All were found to contain fusinite, with a mean abundance relative to total phytoclasts of 2.2%, 2.3% and 2.6% for the Famennian, Tournaisian and Viséan, respectively. We also analysed 12 samples from Willie's Hole, which had a mean value of 2.0% (Supplementary Table 1). These results mean that fire activity persisted through Romer's Gap and indicate that atmospheric O_2 did not fall below 16%; they also show that there was no substantial change in charcoal production compared with the Famennian and Viséan (Supplementary Fig. 9). This strongly suggests that atmospheric O_2 was stable across this time interval, directly refuting hypoxia[9] as an explanation for Romer's Gap.

Discussion

Although an extinction event at the end of the Devonian saw the demise of many archaic fish groups[39], our studies provide new perspectives on the recovery and diversification of surviving groups that went on to found the basis of modern vertebrate diversity[40,41].

The new tetrapods show no close relationship to each other, exhibiting different combinations of plesiomorphic and derived characters. Some taxa cluster with Devonian forms, suggesting a possible relict fauna, whereas others appear more crownward, even clustering near the base of the crown group. They imply an early radiation of tetrapods during the Tournaisian and, at the same time, suggest a blurring of the Devonian/Carboniferous boundary, in respect of tetrapod evolution—a feature also noted in tetrapod remains from Nova Scotia[12].

If confirmed, our results imply a deep split between stem amphibians and stem amniotes in the earliest Carboniferous. This accords with most molecular dates[42,43] for the split, which place it at an average of 355 Myr ago, a date only 4 Myr after the end-Devonian. It suggests that the origin of the tetrapod crown group occurred soon after the extinction event as tetrapods began to recover. Their radiation into a range of new taxa parallels that of lungfish[40] and chondrichthyans[41] as they adapted to a post-extinction world.

The occurrence of probable plesiomorphic members of the Crassigyrinidae[1] and Colosteidae indicates an inception 20–24 Myr earlier than the Late Mississippian, as previously considered[44]. Other tetrapod material of uncertain attribution are distinct and increase known tetrapod diversity in the Tournaisian (Fig. 6 and Supplementary Figs 2–6).

The preponderance of small animals throughout the sequence is unusual, particularly the very small tetrapod found in a horizon 33 m above the Devonian/Carboniferous boundary, around 1 Myr after the extinction event (Fig. 6). None of the five taxa described above has a skull length of more than 80 mm. This could indicate preservational or collector bias, but they occur throughout different lithologies, horizons and localities (Fig. 6 and Supplementary Figs 2–6). Larger tetrapod taxa are found at Willie's Hole, about one quarter of the way up the sequence, probably representing about 3 or 4 Myr after the Devonian/Carboniferous boundary. Larger sizes seem to have appeared relatively rapidly in the Tournaisian, as also documented by trackways[38]; this challenges suggestions of a prolonged period of reduced body size in vertebrates following the DC extinction event[45].

The tetrapods of the Ballagan Formation lived in a mosaic of floodplain environments. Some were under water for long periods, others alternated between land surface and standing water. A recent study of the development of *Polypterus* shows how, early in life, their skeletons can be differentially modified in response to exposure to water-based or land-based conditions[46]. Such skeletal flexibility might have contributed to the origin of tetrapod terrestrial morphology in the varied environments of the Ballagan Formation.

The wealth and diversity of tetrapod taxa from the Tournaisian refutes the proposal of a depauperate Tournaisian stage, and our charcoal studies show that atmospheric oxygen levels, stable from the Famennian to the Viséan, were not a causal factor of the apparent gap. We emphasize the importance of exploring or re-exploring non-marine Tournaisian sites elsewhere in the world, and examining previously overlooked lithologies.

Methods

Micro-CT data. Specimens UMZC 2016.3 *Ossirarus*, NMS G. 2013.39/14 *Kollops* and UMZC 2011.7.2a *Perittodus* were prepared mechanically with mounted needles; some matrix was removed from *Ossirarus* with a brush and water, and consolidated where necessary with Paraloid B72. Specimens UMZC 2011.7.2a *Perittodus* and UMZC 2015.46b *Aytonerpeton* were scanned at the Cambridge Tomography Centre with a Nikon XTH225 ST scanner. For *Perittodus* the settings used were: isotropic voxel size 0.0444 mm, 1,080 projections, 0.25 mm Cu filter, X-ray 160 kV 70 μA, 1,647 slices, 1,000 milliseconds per slice exposure, 24 dB gain. For *Aytonerpeton* the following were used: isotropic voxel size 0.0609 mm, 1,080 projections, no filter, X-ray 120 kV, 125 μA, 1,789 slices, 1,000 milliseconds per slice exposure, 24 dB gain.

Cladistic analysis. A new database of 46 taxa coded for 214 osteological characters (170 cranial, 43 postcranial) was subjected to maximum parsimony analyses. It was designed to include representative early tetrapods. Characters were drawn up to capture the features of the new taxa as far as possible in the context of the range of early tetrapods that are available for comparison. Most were drawn from recent analyses[24,28–31,46,47,48]. Some characters were reworded or reformulated and all were independently scored by J.A.C. from personal observation or from the literature. These were checked for accuracy by M.R. Characters are arranged in

alphabetical order and grouped into regions of the anatomy (see the character list and data matrix in Supplementary Data).

The data matrix was subjected to maximum parsimony analyses in TNT v. 1.1 (ref. [49]). Several experiments of taxon and character manipulation were carried out, as detailed below, with identical search protocols throughout. Given the size of the matrix, tree searches relied on heuristic algorithms, following a simple series of steps under the 'Traditional search' option in the 'Analyze' menu in TNT. Before each search, we modified memory requirements under the 'Memory' option in the 'Settings' menu. One hundred megabytes of general RAM were allocated and a total of 50,000 trees were selected as the maximum size of tree space for the exploration of alternative tree topologies. In the initial part of the 'Traditional search' ('Wagner trees' box ticked), we chose 10,000 replicates (random stepwise addition sequences of taxa), keeping a maximum of five trees at the end of each replicate, using the bisection–reconnection algorithm for tree branch swapping and retaining all trees found at the end of all replicates. A new round of branch swapping was then applied to all trees retained from the initial search ('trees from RAM' box ticked). For each set of experiments, where applicable, we summarized the results in the form of a strict consensus (a 50% majority-rule consensus).

Using the search settings explained above, we carried out three types of parsimony analysis. The first parsimony analysis, employing all taxa and characters from the original matrix, treated all characters as having equal unit weight (default TNT option). The second analysis, again using all taxa and characters, was based on implied character reweighting[28], briefly described as follows. Given a character, its implied weight (W) is given by $K/(K+M-O)$, where M and O represent, respectively, the greatest number of character-state changes and the observed number of character-state changes for that character. The constant of concavity (K) is an integer, the value of which determines the most parsimonious trees as those trees for which W is maximized across all characters. As the selection of K is arbitrary, we experimented with increasing values ($K=3$, 4, 5 and 10) (Fig. 5 and Supplementary Fig. 8). We did not report details of searches with other K values, as our goal was to establish whether the Tournaisian taxa showed stable positions within a minimal range of implied weighting increments. However, we ran analyses with values varying between 6 and 10, with mixed outcomes. In some cases, the Tournaisian taxa were heavily reshuffled, in others the branching sequence of other groups revealed implausible arrangements that, we feel, were dictated by varying amounts of homoplasy in the data. However, a proper characterization of this phenomenon requires further testing. Topologies with $K=10$ are reported as an example.

In the third analysis, characters were reweighted by the maximum value (best fit) of their rescaled consistency indexes, obtained from the first analysis.

Statistical branch support was evaluated through character resampling via bootstrap (resampling with replacement[50]) and jackknife (resampling without replacement, with 33% of characters removed[51]), using 1,000 replicates in each case and collapsing nodes with less than 50% support.

Of the new Tournaisian taxa, only *Diploradus* appeared in a maximum agreement subtree (a taxonomically pruned tree showing only taxa for which all most parsimonious trees agree on relationships).

As for the implied weighting analysis, we found stable mutual arrangements for most Tournaisian taxa with $K=3$, 4 and 5. With $K=10$, the branching sequence of Tournaisian taxa differed from those found with smaller K values. In addition, slightly different branching patterns emerged for various early tetrapod taxa/groups following different implied weighting searches. Below, we highlight key differences among various tree topologies.

In trees generated with $K=3$, 4 and 5, *Ossirarus*, *Perittodus* and *Diploradus* emerged as increasingly crownward taxa, in that sequence, along the tetrapod stem group, whereas *Aytonerpeton* and *Koilops* were placed among stem amphibians and were thus part of the tetrapod crown group. *Ossirarus* was crownward of a (*Ventastega* + *Ichthyostega*) clade, with *Ossinodus* placed either immediately anti-crownward of ($K=3$), in a polytomy with ($K=4$), or immediately crownward of *Ossirarus* ($K=5$). *Perittodus* was the sister taxon to the Devonian *Ichthyostega*-like taxon *Ymeria*, and the (*Perittodus* + *Ymeria*) clade formed the sister group to *Pederpes*. *Diploradus* was immediately crownward of a (*Whatcheeria* + *Occidens*) clade, which in turn occurred crownward of (*Pederpes* + (*Perittodus* + *Ymeria*)). However, the branching sequence of Carboniferous stem tetrapods more crownward than *Diploradus* varied. Thus, in trees with $K=3$, the branching sequence included *Crassigyrinus*, *Doragnathus*, (*Megalocephalus* + *Baphetes*) and *Loxomma*. In trees with $K=4$, the sequence included only *Crassigyrinus* and *Doragnathus*, whereas all baphetids formed a clade on the amphibian stem (*Megalocephalus* + (*Loxomma* + *Baphetes*)). In trees with $K=5$, the baphetid clade was, once again, on the amphibian stem, but the sequence of stem tetrapods crownward of *Diploradus* differed substantially and included (*Eucritta* + *Doragnathus*), *Sigournea* and *Crassigyrinus*. In trees from $K=3$ and 4, the (*Aytonerpeton* + *Sigournea*) clade formed the sister group to a (*Koilops* + (*Tulerpeton* + (*Greererpeton* + *Colosteus*))) clade. In turn, this wider group joined temnospondyls on the amphibian stem, with *Caerorhachis* as a more immediate sister taxon. In trees from K = 5, *Aytonerpeton* was collapsed in a trichotomy with temnospondyls and the (*Koilops* + (*Tulerpeton* + (*Greererpeton* + *Colosteus*))) clade. With $K=10$, the results matched those from the second set of parsimony analyses (reweighting).

As for other tetrapod groups, the amniote stem underwent little reshuffling in trees derived from different K values. The most noticeable difference among such trees was the placement of *Silvanerpeton* and *Gephyrostegus*, both of which were immediately crownward of the 'anthracosauroids' (*Eoherpeton* + (*Pholiderpeton* + *Proterogyrinus*)) but swapped their positions as the first and second most crownward plesion after anthracosauroids.

With characters reweighted by the maximum value of the rescaled consistency index, we found three trees differing only in the relative positions of *Whatcheeria*, *Pederpes* and *Occidens*, all of which formed a clade. In those trees, all new Tournaisian taxa appeared on the tetrapod stem. In particular, *Aytonerpeton* and *Perittodus* were sister taxa, and together they joined *Ymeria*. In crownward order, the sequence of stem tetrapods included: *Acanthostega*, *Ossinodus*, *Ventastega*, *Ichthyostega*, *Ossirarus*, the (*Ymeria* (*Aytonerpeton* + *Perittodus*)) clade, the (*Whatcheeria*, *Pederpes*, *Occidens*) clade, *Diploradus*, *Doragnathus*, *Sigournea*, a (*Koilops* + (*Tulerpeton* + (*Greererpeton* + *Colosteus*))) clade, *Crassigyrinus* and a baphetid clade. *Caerorhachis* and *Eucritta* appeared as the earliest diverging plesions on the amphibian and amniote stem groups, respectively.

Sedimentological and environmental interpretation. The borehole was located at Norham near Berwick-Upon-Tweed, British National Grid Reference (BNGR) 391589, 648135, and the Burnmouth section was at BNGR 396000, 661000.

The stratigraphical position of the succession at Willie's Hole was inferred from a nearby borehole (Hutton Hall Barns, BGS Registered number NT85SE1). The exact stratigraphical position of the Willie's Hole section was uncertain within the overall succession. No direct correlation with the succession recorded in the Hutton Hall Barns borehole was possible because the borehole was old and the level of detail insufficient; in addition, distinctive markers are not present in the Ballagan Formation. However, that borehole proved 142.5 m of Ballagan Formation strata; the log is good enough to define precisely where the base is, resting on Kinnesswood Formation. The proximity of Willie's Hole to the borehole allowed us to infer that the Willie's Hole section lies approximately 150 m above the base of the Ballagan Formation. The palynological samples from Willie's Hole contained *Umbonatisporites distinctus*, a spore that was only found in the lower part of our borehole core. We argue that the Willie's Hole section belongs to the lower part of the Ballagan Formation. We indicated some uncertainty in the figure and gave an approximate range.

The dominance of actinopterygians and rhizodonts within these lakes indicated brackish–freshwater salinity levels[52,53]. Diverse palaeosols[15] and palynology suggest habitats including forest, low-growing and creeping flora, wetland and desiccating pools traversed by rivers (predominantly meandering channels) and saline–hypersaline lakes depositing cementstones and evaporites (Fig. 6 and Supplementary Fig. 7)[27–31,54]. The saline–hypersaline lake deposits in the Ballagan Formation have been interpreted to represent brackish marginal marine or hypersaline[54–58] conditions. Other dolomitic units from the Mississippian are interpreted as saline coastal marshes[58–63]. Erosive-based, cross-bedded sandstone units (one to tens of metres thick) with basal conglomerate lags cut into all other facies[34]. The lags contain disarticulated vertebrate material including acanthodian, rhizodont and tetrapod bones[16].

Charcoal analysis. DOM was extracted by standard palynological demineralization techniques[64]. Measurement of maceral reflectance in oil was by means of a Zeiss UMSP 50 Microspectrophotometer, housed in the School of Ocean and Earth Science, National Oceanography Centre Southampton, University of Southampton Waterfront Campus. Measurements were made under standard conditions, as defined by the International Committee for Coal Petrology[65].

Model-based estimates of atmospheric oxygen concentrations during the early Tournaisian vary from 10–20%, with more recent models favouring the higher figure[66–70]. As an alternative, fossil charcoal (fusinite) has been used by several authors as a proxy for atmospheric oxygen[71–76], because wildfire activity, and hence charcoal production, is proportional to oxygen supply[75]. Controlled burning experiments[75] have demonstrated that when O_2 exceeds the present atmospheric level (PAL) of 20.9%, fire activity rapidly increases and reaches a plateau at around 24%; therefore, we infer that fusinite abundance is probably insensitive to any further increase. Conversely, fire activity is strongly supressed below 20% O_2 and switched off completely below 16%, even in very dry conditions[75]. The most comprehensive attempt thus far to reconstruct Phanerozoic O_2 in this way[71] indicated 25.6% O_2 during Romer's Gap—substantially higher than PAL and exceeding the presumed upper limit of fusain sensitivity (24%). However, this study was based on the inertinite (microscopic fusinite) content of coals, which are infrequent during the Tournaisian, so sampling density was relatively low. Furthermore, we assume that large-scale forest fires would have had a far greater influence on coal deposits formed *in situ* in forest mires, than on the more distal deposits of the kind examined here.

By focusing on DOM extracted from sedimentary rocks other than coal, fusinite content can be measured through stratigraphic successions in which coals are rare or absent. The values reported here represent the proportion of fusinite within the organic matter isolated from each 5 g shale sample, on the basis of

examination of 500 organic (that is, plant derived) macerals. This indicates the proportion of plant-derived material in the sample which has been burned at high temperatures, and is therefore independent of sediment supply.

The specific Famennian and Viséan sampling localities chosen were selected because, apart from being of the required age:

- The stratigraphic context of the sampled formations is well understood, with well-established biozonation (Supplementary Table 1).
- Thermal maturity in these successions is low. This is essential, because with increasing thermal maturity the reflectance of non-pyrolitic macerals (most notably vitrinite) increases, eventually rendering them indistinguishable from fusinite.
- Both localities represent largely terrestrial environments, containing a succession of fluviodeltaic, lacustrine or nearshore marine deposits (Supplementary Table 1). Sediments deposited in such environments represent an accumulation point for river-transported organic material derived from the wider region; this mitigates the distorting effect of local fire activity.

The organic maceral fusinite is considered synonymous with charcoal and can be distinguished from other maceral types by its reflectance under incident light[76]; we focused solely on fusinite for this study because, although most other members (semi-fusinite) of the inertinite group are also accepted as pyrolitic in origin[77], their reflectance forms a continuum between that of vitrinite and fusinite, and forms the bulk of the organic matter. This makes the per cent sum of semi-fusinite and fusinite very large (>90%) and less reliable.

Supplementary Table 1b gives the samples taken from Famennian sites, Burnmouth, Willie's Hole and Viséan sites. These were analysed for charcoal content. Mean abundance was 2.0%, which is within the margin of error of the data obtained from Burnmouth Shore; this suggests that the contribution from local fire activity (if any) was similar at both sites (Supplementary Table 1 and Supplementary Fig. 9).

Data availabiltity. Specimen information is available from the respective housing institutions. Micro-CT scan data will be placed in the NERC National Geoscience Data Centre. This published work and the nomenclature act it contains have been registered in Zoobank: http://www.zoobank.org:pub:4BFFB544-7B0B-4F2F-80EC-11226C0FDAAB. The names *Peritiodus apsconditus*, *Koilops herma*, *Ossirarus kierani*, *Diploradus austiumensis and Aytonerpeton microps* have been deposited in the Zoobank database under LSIDs urn:lsid:zoobank.org:pub:69DB72E5-F9BD-49C6-B471-CD8E03767732, urn:lsid:zoobank.org:pub:8C43E66A-3822-49B4-B3B5-E43C79FA9C70, urn:lsid:zoobank.org:pub:FC9FAB5C-CC3E-4D0D-B7D7-8030FBAA4F0C, urn:lsid:zoobank.org:pub:268DDD4F-289D-4F83-8172-1A18A1007B7C and urn:lsid:zoobank.org:pub:E1E094A8-FAC0-4A2A-A13D-487D7775FBE1.

Received 16 May 2016; accepted 11 October 2016; published 5 December 2016

References

1. Coates, M. I & Clack, J. A. Romer's Gap – tetrapod origins and terrestriality. *Bull. Mus. Nat. Hist. Nat.* **17,** 373–388 (1995).
2. Smithson, T. R., Wood, S. P., Marshall, J. E. A. & Clack, J. A. Earliest Carboniferous tetrapod and arthropod faunas from Scotland populate Romer's Gap. *Proc. Natl Acad. Sci. USA* **109,** 4532–4537 (2012).
3. Cohen, K. M., Finney, S. C., Gibbard, P. L. & Fan, J.-X. *The ICS International Chronostratigraphical Chart v. 2016/04* (ICS, 2013); http://stratigraphy.org/ICSchart/ChronostratChart2016-04.pdf
4. Wood, S. P., Panchen, A. L. & Smithson, T. R. A terrestrial fauna from the Scottish Lower Carboniferous. *Nature* **314,** 355–356 (1985).
5. Rolfe, W. D. I., Clarkson, E. N. K. & Panchen, A. L. (eds) Volcanism and early terrestrial biotas. *Trans. R. Soc. Edinb.* **84,** 175–464 (1994).
6. Milner, A. R. & Sequeira, S. E. K. The temnospondyl amphibians from the Viséan of East Kirkton, West Lothian, Scotland. *Trans. R. Soc. Edinb.* **84,** 331–362 (1994).
7. Smithson, T. R., Carroll, R. L., Panchen, A. L. & Andrews, S. M. *Westlothiana lizziae* from the Viséan of East Kirkton, West Lothian, Scotland. *Trans. R. Soc. Edinb.* **84,** 417–431 (1994).
8. Clack, J. A. *Gaining Ground: The Origin and Evolution of Tetrapods* 2nd edn (Indiana Univ. Press, 2012).
9. Ward, P. D., Labandeira, C., Laurin, M. & Berner, R. A. Confirmation of Romer's Gap as a low oxygen interval constraining the timing of initial arthropod and vertebrate terrestrialisation. *Proc. Natl Acad. Sci. USA* **103,** 16818–16822 (2006).
10. Carroll, R. L., Belt, E. S., Dineley, D. L., Baird, D. & McGregor, D. C. Excursion A59, Vertebrate palaeontology of Eastern Canada. In *24th Int. Geol. Congr.* 1–113 (1972).
11. Clack, J. A. & Carroll, R. L. in *Amphibian Biology* Vol. 4 (eds Heatwole, H. & Carroll, R. L.) 1030–1043 (Surrey Beatty, 2000).
12. Anderson, J. S., Smithson, T. R., Mansky, C. F., Meyer, T. & Clack, J. A. A diverse tetrapod fauna at the base of Romer's Gap. *PLoS ONE* **10,** e0125446 (2015).
13. Clack, J. A. An early tetrapod from 'Romer's Gap'. *Nature* **418,** 72–76 (2002).
14. Clack, J. A. & Finney, S. M. *Pederpes finneyae*, an articulated tetrapod from the Tournaisian of western Scotland. *J. Syst. Palaeontol.* **2,** 311–346 (2005).
15. Kearsey, T. I. *et al.* The terrestrial landscapes of tetrapod evolution in earliest Carboniferous seasonal wetlands of SE Scotland. *Palaeogeogr. Palaeoclimatol. Palaeoecol.* **457,** 52–69 (2016).
16. Bennett, C. E. *et al.* Early Mississippian sandy siltstones preserve rare vertebrate fossils in seasonal flooding episodes. *Sedimentology* **63,** 1677–1700 (2016).
17. Clack, J. A., Ahlberg P. E., Blom H. & Finney S. M. A new genus of Devonian tetrapod from East Greenland, with new information on the lower jaw of *Ichthyostega*. *Palaeontology* **55,** 73–86 (2012).
18. Milner, A. C. & Lindsay, W. Postcranial remains of *Baphetes* and their bearing on the relationships of the Baphetidae (= Loxommatidae). *Zool. J. Linn. Soc.* **122,** 211–235 (1998).
19. Clack, J. A. The dermal skull roof of *Acanthostega*, an early tetrapod from the Late Devonian. *Trans. R. Soc. Edinb.* **93,** 17–33 (2002).
20. Jarvik, E. The Devonian tetrapod *Ichthyostega*. *Fossils Strata* **40,** 1–206 (1996).
21. Smithson, T. R. The cranial morphology of *Greererpeton burkemorani* (Amphibia: Temnospondyli). *Zool. J. Linn. Soc.* **76,** 29–90 (1982).
22. Lombard, R. E. & Bolt, J. R. *Sigournea multidentata*, a new stem tetrapod from the Upper Mississippian of Iowa, USA. *J. Palaeontol.* **80,** 717–725 (2006).
23. Bolt J. R. & Lombard, R. E. The mandible of the primitive tetrapod *Greererpeton*, and the early evolution of the tetrapod lower jaw. *J. Palaeontol.* **75,** 1016–1042 (2001).
24. Godfrey, S. J. Ontogenetic changes in the skull of the Carboniferous tetrapod *Greererpeton burkemorani* Romer 1969. *Phil. Trans. R. Soc. Lond. B* **323,** 135–153 (1989a).
25. Hook, R. W. *Colosteus scutellatus* (Newberry) a primitive temnospondyl amphibian from the Middle Pennsylvanian of Linton, Ohio. *Am. Mus. Novit.* **2770,** 1–41 (1983).
26. Godfrey, S. J. The postcranial skeletal anatomy of the Carboniferous tetrapod *Greererpeton burkemorani* Romer 1969. *Phil. Trans. Roy. Soc. Lond. B* **323,** 75–133 (1989b).
27. Wilkinson, M. Coping with abundant missing entries in phylogenetic inference using parsimony. *Syst. Biol.* **44,** 501–514 (1995).
28. Goloboff, P. A. Estimating character weights during tree search. *Cladistics* **9,** 83–89 (1993).
29. Ruta, M., Coates, M. I. & Quicke, D. L. J. Early tetrapod relationships revisited. *Biol. Rev.* **78,** 251–345 (2003).
30. Ruta, M. & Clack, J. A. A review of *Silvanerpeton miripedes*, a stem amniote from the Lower Carboniferous of East Kirkton, West Lothian, Scotland. *Trans. R. Soc. Edinb.* **97,** 31–63 (2006).
31. Klembara J., Clack, J. A. & Milner A. R. Cranial anatomy, ontogeny, and relationships of the Late Carboniferous tetrapod *Gephyrostegus bohemicus* Jaekel, 1902. *J. Vertebr. Paleontol.* **34,** 774–792. (2014).
32. Laurin, M. The evolution of body size, Cope's rule and the origin of amniotes. *Syst. Biol.* **53,** 594–622 (2004).
33. Marjanović, D. & Laurin, M. The origin(s) of extant amphibians: a review with emphasis on the "lepospondyl hypothesis". *Geodiversitas* **35,** 207–272. (2013).
34. Greig, D. C. *Geology of the Eyemouth District: Memoir for 1:50000 Geological Sheet 34* Mem. Geol. Surv. GB (Scotland, sheet 34) (1988).
35. Garcia, W. J., Storrs, G. W. & Greb, S. F. The Hancock County tetrapod locality: a new Mississippian (Chesterian) wetlands fauna from western Kentucky (USA). *Geol. Soc. Am. S.* **399,** 155–167 (2006).
36. Davies, N. S. & Gibling, M. R. The sedimentary record of Carboniferous rivers: Continuing influence of land plant evolution on alluvial processes and Palaeozoic ecosystems. *Earth-Sci. Rev.* **120,** 40–79 (2013).
37. Corenblit, D., Davies, N. S., Steiger, J., Gibling, M. R. & Bornette, G. Considering river structure and stability in the light of evolution: feedbacks between riparian vegetation and hydrogeomorphology. *Earth Surf. Proc. Land.* **40,** 189–207 (2015).
38. Mansky, C. F. & Lucas, S. G. Romer's Gap revisited: continental assemblages and ichno-assemblages from the basal Carboniferous of Blue Beach, Nova Scotia, Canada. *Bull. New Mex. Mus. Nat. Hist.* **60,** 244–273 (2013).
39. Sallan, L. C. & Coates, M. I. End-Devonian extinction and a bottleneck in the early evolution of modern jawed vertebrates. *Proc. Natl Acad. Sci. USA* **107,** 10131–10135 (2010).
40. Smithson, T. R., Richards, K. R. & Clack, J. A. Lungfish diversity in Romer's Gap: reaction to the end-Devonian extinction. *Palaeontology* **59,** 29–44 (2016).
41. Richards, K. R. et al. A new fauna of early Carboniferous chondrichthyans from the Scottish Borders. In *59th Ann. Meeting Palaeontological Assoc.* (2015); http://www.palass.org/meetings-events/annual-meeting/2015/annual-meeting-2015-cardiff-poster-abstracts

42. Hedges, S. B., Marin, J., Suleski, M., Paymer, M. & Kumar, S. Tree of Life reveals clock-like speciation and diversification. *Mol. Biol. Evol.* **32,** 835–845 (2015).
43. Kumar S. & Hedges S. B. TimeTree2: species divergence times on the iPhone. *Bioinformatics* **27,** 2023–2024 (2011).
44. Clack, J. A., Witzmann, F., Snyder D. & Müller, J. A colosteid-like early tetrapod from the St. Louis Limestone (Early Carboniferous, Meramecian), St. Louis, Missouri, USA. *Fieldiana Life Earth Sci.* **5,** 17–39 (2012).
45. Sallan L. C. & Gallimberti, A. K. Body-size reduction in vertebrates following the end-Devonian mass extinction. *Science* **350,** 812–815 (2015).
46. Standen, E. M., Du, T. Y. & Larsson, C. E. Developmental plasticity and the origin of tetrapods. *Nature* **513,** 54–58 (2014).
47. Ahlberg, P. E. & Clack, J. A. Lower jaws, lower tetrapods: a review based on the Devonian tetrapod *Acanthostega*. *Trans. R. Soc. Edinb.* **89,** 11–46 (1998).
48. Clack, J. A. The Scottish Carboniferous tetrapod *Crassigyrinus scoticus* (Lydekker)—cranial anatomy and relationships. *Trans. R. Soc. Edinb.* **88,** 127–142 (1998).
49. Goloboff, P. A., Farris, J. S. & Nixon, K. C. TNT, a free program for phylogenetic analysis. *Cladistics* **24,** 1–13 (2008).
50. Efron, B. & Tibshirani, R. J. *An Introduction to the Bootstrap* (Chapman and Hall, 1979).
51. Efron, B. in *Breakthroughs in Statistics* (eds Kotz, S & Johnson, N.L.) 569–593 (Springer, 1997).
52. Carpenter, D. K., Falcon-Lang, H. J., Benton, M. J. & Henderson, E. Carboniferous (Tournaisian) fish assemblages from the Isle of Bute, Scotland: systematics and palaeoecology. *Palaeontology* **57,** 1215–1240 (2014).
53. Friedman, M. & Sallan, L. C. Five hundred million years of extinction and recovery: a Phanerozoic survey of large-scale diversity patterns in fishes. *Palaeontology* **55,** 707–742 (2012).
54. Andrews, J. E., Turner, M. S., Nabi, G. & Spiro, B. The anatomy of an early Dinantian terraced floodplain: palaeo-environment and early diagenesis. *Sedimentology* **38,** 271–287 (1991).
55. Turner, M.S. *Geochemistry and Diagenesis of Basal Carboniferous Dolostones from Southern Scotland* PhD thesis, Univ. East Anglia (1991).
56. Belt, E. S., Freshney, E. C. & Read, W. A. Sedimentology of Carboniferous cementstone facies, British Isles and Eastern Canada. *J. Geol.* **75,** 711–721. (1967).
57. Scott, W. B. *The Sedimentology of the Cementstone Group in the Tweed Basin: Burnmouth and the Merse of Berwick* PhD thesis, Sunderland Polytechnic (1971).
58. Scott, W. B. Nodular carbonates in the Lower Carboniferous, Cementstone Group of the Tweed Embayment, Berwickshire: evidence for a former sulphate evaporite facies. *Scot. J. Geol.* **22,** 325–345 (1986).
59. Barnet, A. J., Wright, V. P. & Crowley, S. F. Recognition and significance of paludal dolomites: Late Mississippian, Kentucky, USA. In *Linking Diagenesis to Sequence Stratigraphy* (eds Morad, S., Ketzer, J. M. & De Ros, L. F.) 477–500 (Special Publication 45 of the IAS, John Wiley & Sons, 2012).
60. Muchez, P. & Viaene, W. Dolocretes from the Lower Carboniferous of the Campine-Brabant Basin, Belgium. *Pedologie* **37,** 187–202 (1987).
61. Searl, A. Pedogenic dolomites from the Oolite Group (Lower Carboniferous) South Wales. *Geol. J.* **23,**157–169 (1988).
62. Vanstone, S. D. Early Carboniferous (Mississippian) palaeosols from southwest Britain: influence of climatic change on soil development. *J. Sediment. Res.* **61,** 445–457 (1991).
63. Wright, V. P., Vanstone, S. D. & Marshall, J. D. Contrasting flooding histories of Mississippian carbonate platforms revealed by marine alteration effects in palaeosols. *Sedimentology* **44,** 825–842 (1997).
64. Wood, G., Gabriel, A.M. & Lawson, J.C. Palynological techniques – processing and microscopy. In *Palynology: Principles and Applications* Vol. 1 (eds Jansonius, J. & McGregor, D. C.) 29–50 (American Association of Stratigraphic Palynologists Foundation, 1996).
65. American Society for Testing and Materials (ASTM) in *Annual Book of ASTM Standards Section 5: Petroleum Products, Lubricants, and Their Fossil Fuels* Vol. 05.06, D2799-13 (ASTM International, 2013); http://www.astm.org/Standards/D2799.htm
66. Hansen, K. W. & Wallmann, K. Cretaceous and Cenozoic evolution of seawater composition, atmospheric O_2 and CO_2: A model perspective. *Am. J. Sci.* **303,** 94–148 (2003).
67. Bergman, N. M., Lenton, T. M. & Watson, A. J. COPSE: a new model of biogeochemical cycling over Phanerozoic time. *Am. J. Sci.* **304,** 397–437 (2004).
68. Arvidson, R.S., Mackenzie, F.T. & Guidry, M. Magic: A Phanerozoic model for the geochemical cycling of major rock-forming components. *Am. J. Sci.* **306,** 135–190 (2006).
69. Berner, R. A. GEOCARBSULF: A combined model for Phanerozoic atmospheric O_2 and CO_2. *Geochim. Cosmochim. Ac.* **70,** 5653–5664 (2006).
70. Berner, R. A. Phanerozoic atmospheric oxygen: new results using the GEOCARBSULF model. *Am. J. Sci.* **309,** 603–606 (2009).
71. Robinson, J. M. Phanerozoic atmospheric reconstructions: a terrestrial perspective. *Palaeogeogr. Palaeoclimatol. Palaeoecol.* **97,** 51–62 (1991).
72. Scott, A. C. & Glasspool, I. J. The diversification of Paleozoic fire systems and fluctuations in atmospheric oxygen concentration. *Proc. Natl Acad. Sci. USA* **103,** 10861–10865 (2006).
73. Glasspool, I. J. & Scott, A. C. Phanerozoic concentrations of atmospheric oxygen reconstructed from sedimentary charcoal. *Nat. Geosci.* **3,** 627–630 (2010).
74. Glasspool, I. J., Scott, A. C., Waltham, D., Pronina, N. & Shao, L. The impact of fire on the Late Paleozoic Earth system. *Front. Plant Sci.* **6,** 1–13 (2015).
75. Belcher, C. M., Yearsley, J. M., Hadden, R. M., McElwain, J. C. & Guillermo, R. Baseline intrinsic flammability of Earth's ecosystems estimated from paleoatmospheric oxygen over the past 350 million years. *Proc. Natl Acad. Sci. USA* **107,** 22448–22453 (2010).
76. Tyson, R. V. *Sedimentary Organic Matter* (Chapman & Hall, 1995).
77. Scott, A. J. & Glasspool, I. J. Observations and experiments on the origin and formation of the inertinite group macerals. *Int. J. Coal Geol.*, **70,** 53–66. (2007).

Acknowledgements

We acknowledge funding from NERC consortium grants NE/J022713/1 (Cambridge), NE/J020729/1 (Leicester), NE/J021067/1 (BGS), NE/J020621/1 (NMS) and NE/J021091/1 (Southampton). We thank the following for their support and contributions: the late S. Wood and M. Wood for discovery of and access to collections; O. Kieran and B. Kieran and the Burnmouth community for support for the project; M. Browne for field assistance and information on stratigraphy; M. Lowe for access to UMZC collections; S. Finney for field assistance, conservation advice and preparation of *Koilops*; V. Carrió for conservation and preparation of NMS specimens; J. Sherwin for stratigraphy and field assistance; and S. Akbari (Southampton) for contribution to palynological processing. T.I.K. and D.M. publish with the permission of the Executive Director, British Geological Survey (NERC). A. Brown and C. MacFadyen of Scottish Natural Heritage gave permission to collect at sites in their care and P. Bancks, from The Crown Estates Office in Edinburgh, gave permission to collect on Crown land. PRISM, the Isaac Newton Trust Fund (Trinity College, Cambridge), the Crotch Fund (UMZC) and an anonymous donor provided funding for the purchase of specimens. This is a contribution to IGCP project 596.

Author contributions

J.A.C. was lead principal investigator. T.R.S., J.A.C., B.K.A.O. and K.Z.S. collected, described and analysed the tetrapod specimens. C.E.B., T.I.K., S.J.D. and D.M. contributed to the stratigraphical, sedimentological and environmental studies. J.E.A.M., D.K.C., and E.J.R. contributed to the charcoal, palynological and stratigraphical studies. M.R. and J.A.C. contributed to the phylogenetic analysis. A.J.R. contributed information on the arthropods. S.A.W. provided additional work on micro-CT scan data. A.J.R., S.A.W. and N.C.F. organized the Willie's Hole excavation that provided the sedimentological information. All authors contributed to discussion, preparation and writing of the paper.

Additional information

Supplementary information is available for this paper.

Reprints and permissions information is available at www.nature.com/reprints.

Correspondence and requests for materials should be addressed to J.A.C.

How to cite this article: Clack, J. A. *et al.* Phylogenetic and environmental context of a Tournaisian tetrapod fauna. *Nat. Ecol. Evol.* **1,** 0002 (2016).

Competing interests

The authors declare no competing interests.

Supplementary Figure 9. Visean fusinite abundance in Euramerica, based on analysis of material from the Stensiö Bjerg Formation (Greenland), Burnmouth Shore/Willie's Hole, and the Strathclyde Group (Fife, Scotland). White bars indicate mean values.

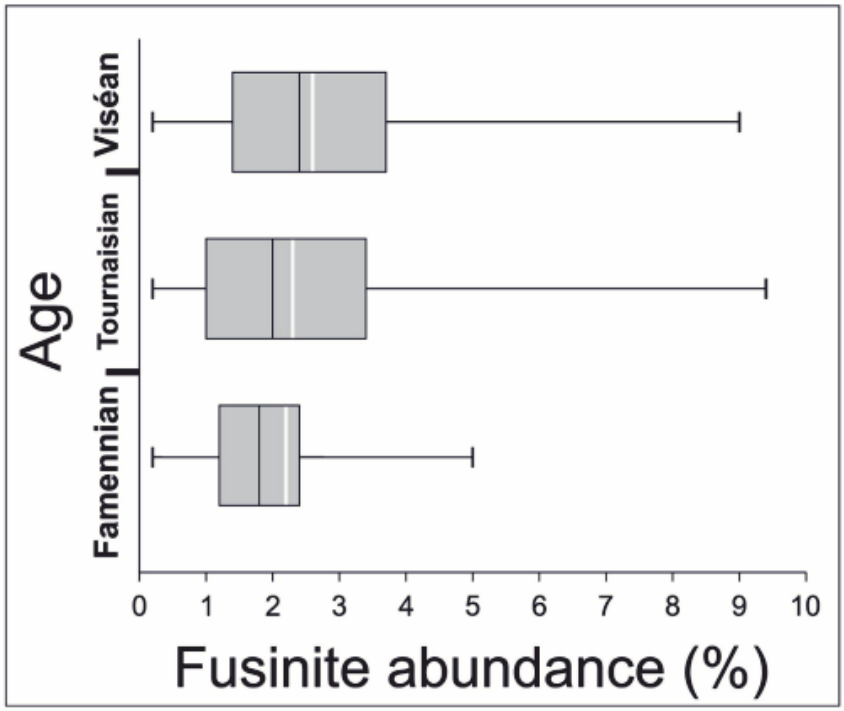

© 2016 Macmillan Publishers Limited, part of Springer Nature. All rights reserved.

SUPPLEMENTARY INFORMATION

Supplementary Table 1. Table 1a shows the localities, stratigraphy, age, spore zone, environment and number of samples from each site. Table 1b shows the fusinite abundances as a percentage of total phytoclasts taken for each stage sampled.

Extended data table 1a

Locality/references	Stratigraphy	Age	Spore Biozone(s)	Environment	Number of samples
1[78,79]	Pathead Fm	Late Viséan	VF	Deltaic – nearshore marine	8
1[78,79]	Sandy Craig Fm	Mid-Viséan	NM – VF	Fluvio-deltaic	3
1[78,79]	Pittenweem Fm	Mid-Viséan	NM	Deltaic – nearshore marine	14
1[78,79]	Anstruther Fm	Early – mid-Viséan	TC	Deltaic – nearshore marine[2]	13
2[79,80]	Fife Ness Fm	Earliest Viséan	Pu – TS	Fluvio-deltaic	4
3[15,80]	Ballagan Fm	Tournaisian	CM	Fluvio-lacustrine	12
4[15780]	Ballagan Fm	Tournaisian	VI – CM	Fluvio-lacustrine	61
5[81,82]	Stensiö Bjerg Fm	Latest Famennian	LL – LN[5]	Fluvio-lacustrine	9

Localities: 1, Anstruther to St Monans coastal sections, East Fife, Scotland; 2, Fife Ness, Scotland; 3, 'Willie's Hole', Chirnside; 4, Burnmouth Shore; 5, Celsius Bjerg, East Greenland.

Extended data table 1b

Famennian	Tournaisian		Viséan
2.4	**Burnmouth**	**Willie's Hole**	4.8
1.8	5.2	2.8	0.8
1.2	4.0	2.4	1.2
0.2	0.6	3.0	6.0
4.2	4.8	3.0	1.8
2.4	1.4	0.6	1.2
1.6	1.6	1.6	2.8
0.8	5.2	2.4	1.0
5.0	4.6	0.6	1.4
	3.0	2.3	2.0
	2.8	3.6	0.4
	0.2	1.2	2.4
	3.4	0.2	2.4
	0.2		1.6
	0.2		2.2
	1.0		2.4
	3.4		4.2
	1.2		0.4
	2.2		2.6
	1.0		2.6

© 2016 Macmillan Publishers Limited, part of Springer Nature. All rights reserved.

	2.8		3.8
	0.6		9.0
	2.0		2.6
	2.0		0.6
	2.0		1.6
	2.2		1.4
	4.2		2.6
	5.2		0.2
	1.2		0.8
	2.2		3.0
	1.2		4.2
	1.8		2.4
	2.2		2.6
	1.8		0.4
	0.4		3.8
	0.8		3.4
	0.4		3.2
	4.2		5.4
	5.8		4.2
	4.6		2.2
	1.0		4.8
	0.4		4.2
	0.4		
	1.0		
	1.2		
	0.6		
	1.8		
	9.4		
	3.8		
	0.4		
	2.0		
	2.0		
	1.6		
	3.4		
	2.2		
	3.4		
	5.6		
	1.8		
	0.6		
	0.6		
	2.2		
	1.4		

Famennian – Viséan Fusinite abundance (% total phytoclasts)

78. Owens, B., McLean, D. and Simpson, K. R. M. Reappraisals of the Mississippian palynostratigraphy of the East Fife coast, Scotland, United Kingdom. *Palynology*, **29**, 23–47 (2005)

© 2016 Macmillan Publishers Limited, part of Springer Nature. All rights reserved.

5. Late Palaeozoic hyperoxia

The behaviour of the various palaeoatmosphere models during the late Palaeozoic is unusual, in that they agree more closely than at any other point in the Phanerozoic (Figs. 1.3, 5.1). Almost all predict a near-continuous increase in pO_2 from the Famennian onwards, reaching highs of 25–35% vol. during the late Permian – perhaps the highest at any time in Earth's history, and approaching the theoretical upper limit of the 'fire window' (see section 1.3). This consistency may reflect the fact that the Carboniferous and Permian are unique in providing what many regard as independent biological evidence of unusually high atmospheric pO_2.

Arthropod gigantism and atmospheric O_2

Arthropod gigantism was widespread during the late Palaeozoic; iconic genera such as the dragonfly *Meganeura* (Brongniart 1884) and the myriapod *Arthropleura* (Jordan and Meyer 1854) have been recognised since the 19th century, and a variety of winged and flightless hexapods, myriapods, and arachnids are known to have attained very large sizes during the Carboniferous and Permian (Briggs 1985; Kukalová-Peck 1987; Carpenter 1992). Harlé and Harlé (1911) were the first to propose a link between atmospheric composition and insect wingspan, though this was in the context of atmospheric density rather than O_2 concentration *per se*. Assuming a constant partial pressure of nitrogen, an atmosphere containing 35% vol. O_2 would be 21% denser than that of the present day (Graham *et al*. 1995), providing greater lift and more favourable conditions for large flying insects. Weis-Fogh (1964) established an upper size limit at which tracheal diffusion (the mechanism by which arthropods breathe) becomes untenable in flying insects under PAL O_2; Rutten (1966) noted that this limit would be relaxed under hyperoxic conditions, and that the presence of giant arthropods during the Carboniferous therefore implied global hyperoxia during the late Palaeozoic. Subsequent work by Graham (1988) and Graham *et al*. (1995) established that 35% O_2 would allow a 27% size increase. The hyperoxia hypothesis is supported by model predictions (e.g. Berner and Canfield 1989), as is the extinction of giant forms at the end-Permian when O_2 levels are believed to have crashed (Graham *et al*. 1995; Dudley 1998). More recently, Clapham and Carr (2012) identified a strong correlation between pO_2 as predicted by the GEOCARBSULF model of Berner

(2009) and insect wing size from the Serpukhovian to the earliest Cretaceous (Berriasian), but found that this relationship largely disappeared thereafter (Barremian–Mid-Miocene). This was attributed to the radiation of birds during the Cretaceous, which is assumed to have increased insect predation and favoured smaller, more manoeuvrable forms. Dorrington (2012) questioned this "mixed hypothesis", noting the presence of several outliers (giant insects during purported hypoxic intervals) and the evolution of at least two large insect species during the last 10 Myr despite continued bird predation.

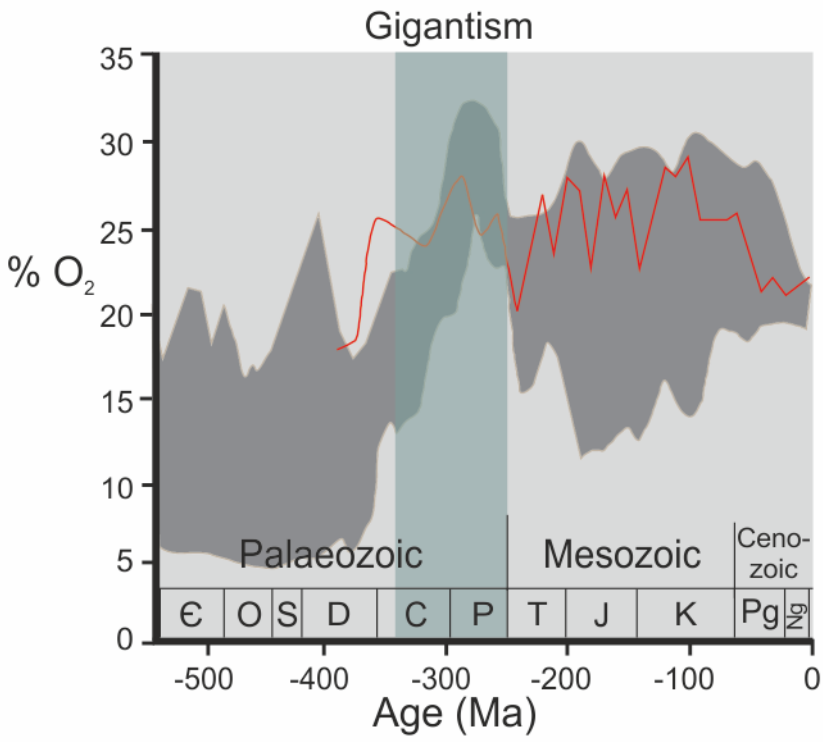

Figure 5.1: Range of model predictions for atmospheric pO_2 (grey shading), and O_2 curve of Glasspool and Scott (2010)/Glasspool *et al*. (2015) (red line). Vertical shaded area indicates approximate span of arthropod gigantism during the Palaeozoic.

Wildfire evidence for late Palaeozoic hyperoxia

The existence of a late Palaeozoic oxygen pulse is in part supported by the data of Glasspool *et al*. (2015), in which mean coal inertinite exceeds 50% during the early Permian. However, their inertinite-based O_2 curve departs markedly in shape from all models for Carboniferous pO_2 except GEOCARBSULF, showing a steady Tournaisian–Bashkirian decline before rising sharply again through the final 15 million years of the

Pennsylvanian (Fig. 5.1). In this chapter, shale samples collected from Serpukhovian–Bashkirian successions in the Northumberland Basin and Scottish Midland Valley provide a new DOM-inertinite dataset for the Late Mississippian and Early Pennsylvanian, and opportunistically collected coal samples allow comparison of coal and DOM inertinite abundance through individual successions. The results are then combined with those reported in chapters 4 and 5 to produce a complete Early Devonian–Early Pennsylvanian history of DOM inertinite, which is compared with the corresponding coal-inertinite data of Glasspool *et al*. (2015). Thus, this chapter addresses two main hypotheses: first,

that there was a progressive increase in pO_2 during the Carboniferous which is reflected by a corresponding increase in wildfire activity and is associated with arthropod gigantism,

and second, the core research hypothesis,

that the spread of forests significantly increased the production and retention of atmospheric oxygen by fuelling increasing organic carbon burial to fundamentally alter biotic regulation of Earth's O_2 concentration and that this is recorded in the abundance of fossil charcoal.

5.1 Sampling Localities

Joppa Shore (55° 56′ 57″ N, 3° 05′ 38″ W–55° 56′ 55″ N, 3° 05′ 09″ W)

Geological context and biostratigraphy

A 525m coastal section exposed on the foreshore at Joppa, 5.8 km east of Edinburgh centre (Fig. 5.2) extends from the Pendleian/Arnsbergian Upper Limestone Formation (Clackmannan Group) to the Westphalian A Lower Coal Measures (Tulloch and Walters 1958; Mitchell *et al*. 1962; Browne *et al*. 1999; Fig. 5.3). The section is designated as a Local Geodiversity Site by the Lothian and Borders RIGS Group.

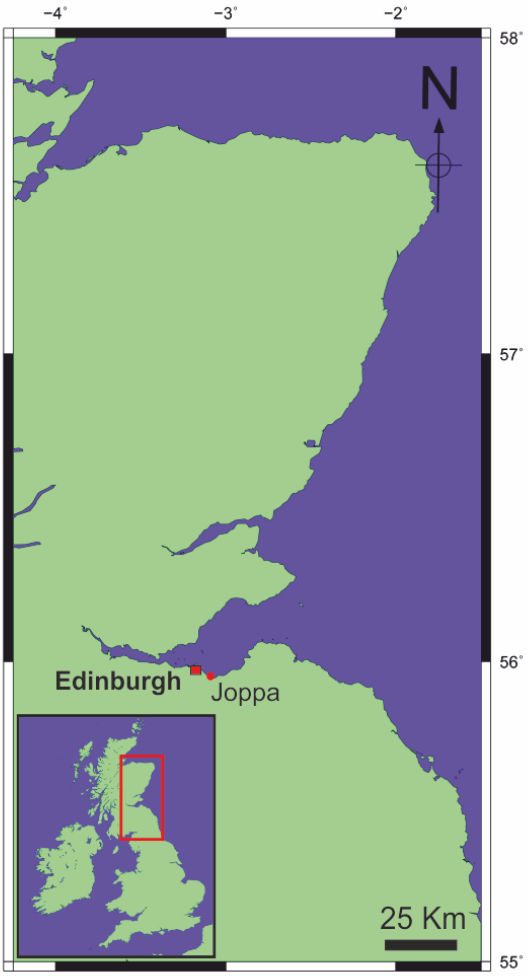

Figure 5.2: Location of Joppa Shore, Scotland.

Upper Limestone Formation

The upper 62 m of the Upper Limestone Formation is present at Joppa (Peach 1910; Cleal and Thomas 1996) and has been placed in the E_2 ammonoid zone of Bisat (1924; Currie 1954; Waters *et al*. 2007), equivalent to the TK–lower SO spore zones of Clayton *et al*. (1977) (McLean *et al*. 2013).

Passage Formation

The entire Passage Formation (formerly Roslin Sandstone Fm.; Cleal and Thomas 1996) is exposed at Joppa; the upper contact is defined regionally by the Lowstone Marine Band (Browne *et al*. 1999) but locally by the Seven Foot Coal (Cleal and Thomas 1996). McLean *et al*. (2013) place it in the upper SO–FR spore zones of Clayton *et al*. (1977).

Lower Scottish Coal Measures Formation

Bivalves discovered c. 9m above the Fifteen Foot Coal by Peach *et al*. (1910) are from the *Carbonicola communis* zone, equivalent to the VI spore zone of Smith and Butterworth (1967; Cleal and Thomas 1996; Waters *et al*. 2007) or lower RA spore zone of Clayton *et al*. (1977) (McLean *et al*. 2013).

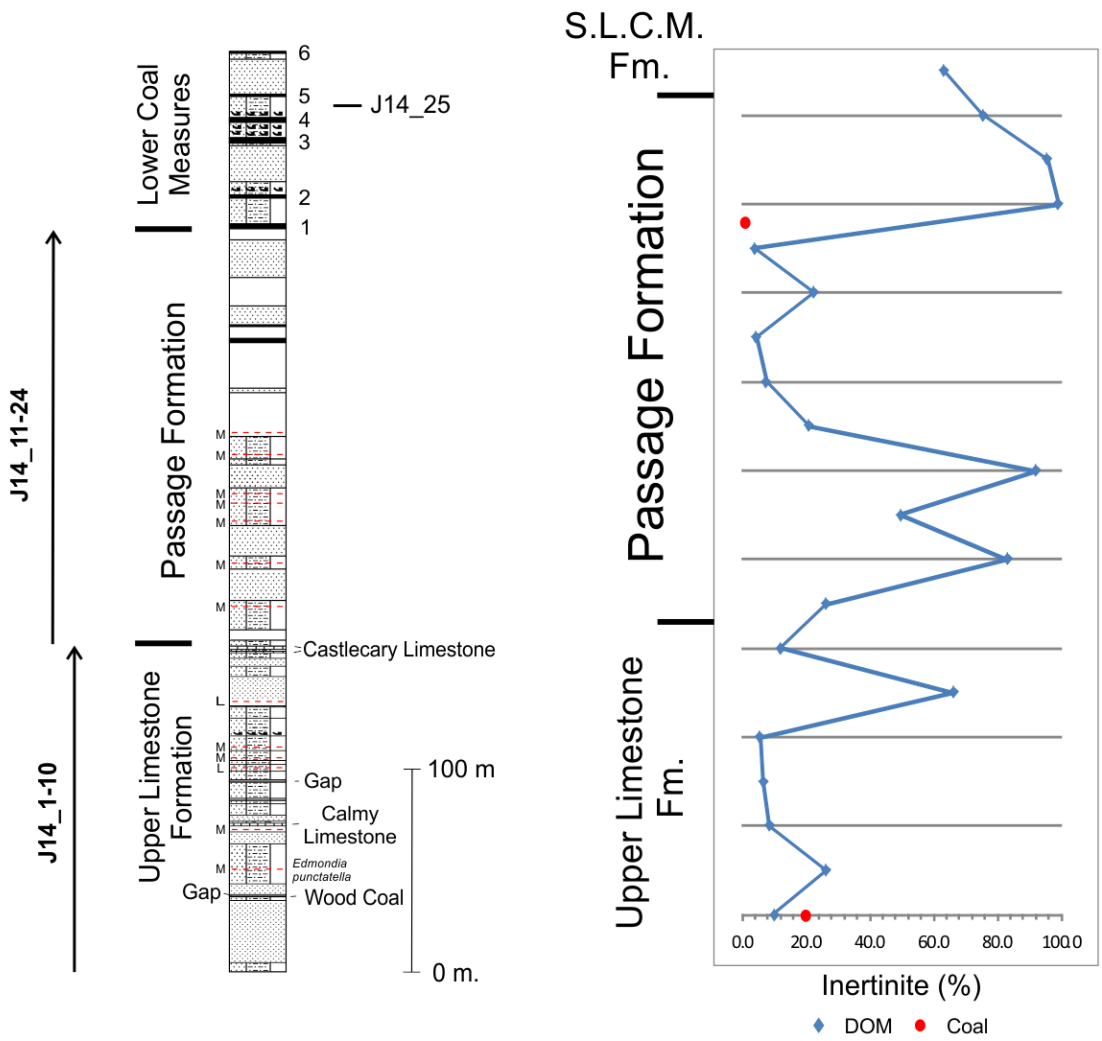

Figure 5.3: Joppa Shore stratigraphy and coal/DOM inertinite abundance results. 1, Seven Foot Coal; 2, Pinkie Four Foot Coal; 3, Fifteen Foot Coal; 4, Nine Foot Coal; 5, Salters Coal; 6, Glass Coal. Modified after Tulloch and Walton (1958) and Mitchell *et al*. (1962). For key see Appendix 3.

Palaeoenvironment

The Upper Limestone Formation is characterised by repeated coarsening upwards sequences, each beginning with marine limestones and ending with palaeosols and thin coals (Browne *et al*. 1999). At Joppa these cycles are less obvious, much of the recessive finer-grained units being obscured by sand; exposed parts of the section mostly consist of finely interbedded calcareous muds, silts, and shales, interspersed with thicker sand units (Fig. 5.4). A prominent marine unit, the Castlecary Limestone, defines the top of the formation.

Figure 5.4: Outcrop of the Upper Limestone Fm. at Joppa Shore.

The Passage Formation is predominantly marine in its lower part, characterised by a rich marine fauna and frequent limestones; these become increasingly depauperate and widely spaced up-section (Browne *et al*. 1999). At Joppa the exposure consists of interbedded mudstones, siltstones, and fluvial sandstones, interrupted by a number of prominent marine bands but also two plant beds in its lower part (Peach *et al*. 1910; Tulloch and Walton 1958; Cleal and Thomas 1996). Thick 'fireclays and seatearths' (= palaeosols) were reported by Tulloch and Walton (1958) towards the top of the formation, though these appear to have been subsequently mined and were not mentioned by Cleal and Thomas (1996). This part of the succession at Joppa is interpreted by Cleal and Thomas (1996) to represent a prograding delta complex, progressively infilling a shallow basin.

As suggested by the name, the Scottish Lower Coal Measures Fm. was once host to several thick coal seams at Joppa, though most of these have reportedly been mined out (Tulloch and Walton 1958; Cleal and Thomas 1996). The rest of the formation consists of interbedded fluvial sands and alluvial or lacustrine silts and mudstones, hence this is the most terrestrial of the three sampled formations; the 'mussel bands' identified by Tulloch and Walton (1958) are dominated by *Carbonicola*, a non-marine bivalve (Cleal and Thomas 1996). Unfortunately, very little of the formation was exposed at the time of visiting (Fig. 5.5), the rest having been buried under beach sand during winter storms.

Figure 5.5: Exposure of the Scottish Lower Coal Measures at Joppa Shore.

Tynemouth–Seaton Sluice coast, Northumbria, UK (50° 01' 01" N, 1° 24' 54" W – 55° 05' 04" N, 1° 28' 12" W)

Geological context and biostratigraphy

The Westphalian B succession between Tynemouth and Seaton Sluice, Northumbria (Fig. 5.6) was once among the best exposed in Britain (Absalom & Hopkins 1926), comprising a c. 6.5 km composite coastal section (Fig. 5.7); much of the classic exposures are now obscured by coastal defences (Jones 1967; Turner & Smith, 1995), but can still be

accessed on the foreshore at low tide. Placed in the Pennine Middle Coal Measures Formation of the Pennine Coal Measures Group (O'Mara and Turner 1999; Waters *et al*. 2007), the region is structurally complex and extensively faulted due to the nearby Whitely Dome and a south-plunging anticline west of Tynemouth (Jones 1967). O'Mara and Turner (1999, fig. 3) placed the lower part of the formation (up to the Low Main coal) in the *Anthraconaia modiolaris* non-marine bivalve zone, which is equivalent to the lower part of the *Dictyotriletes bireticulatus* miospore zone of Owens *et al*. (1977), or lower NJ zone of Clayton *et al*. (1977) (Waters *et al*. 2007). Unless otherwise stated, biozones discussed below are those of Clayton *et al*. (1977).

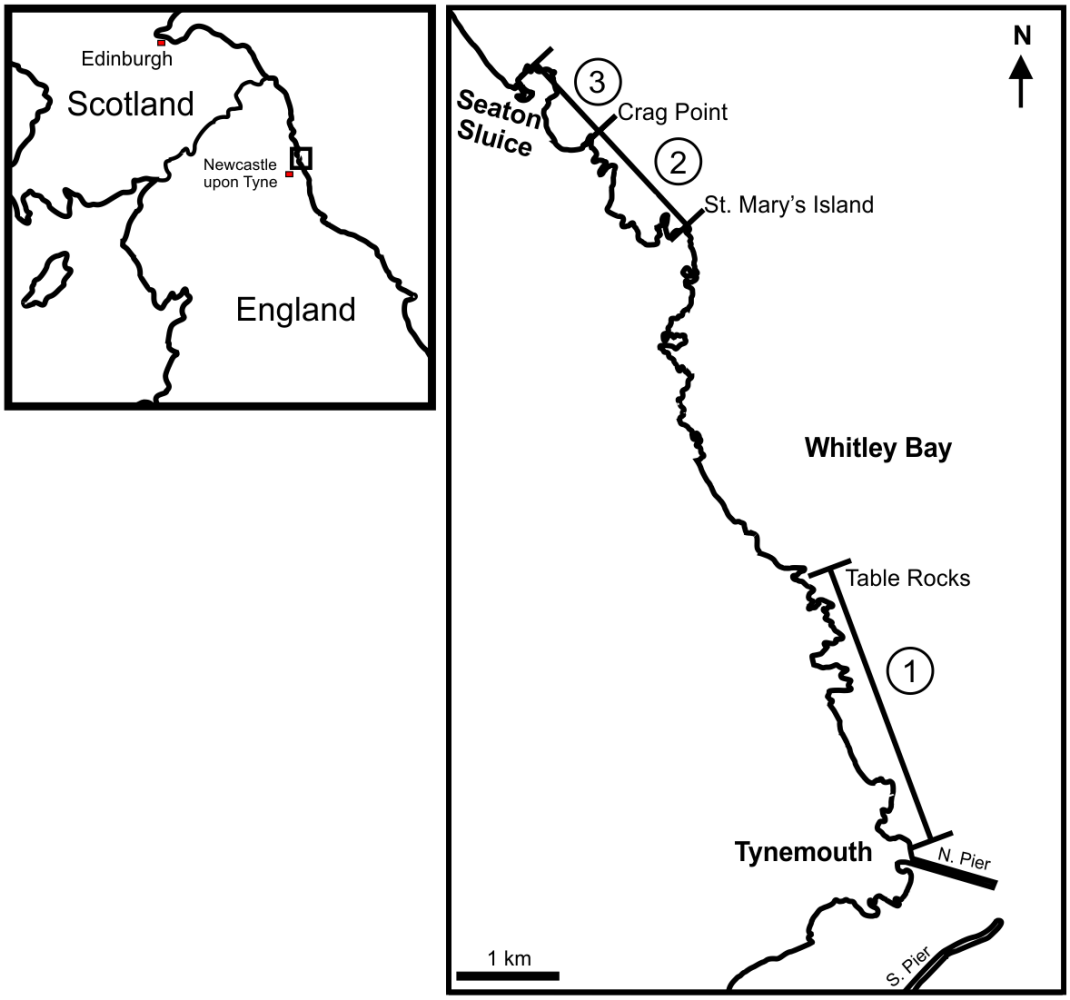

Figure 5.6: Coastal sections between Tynemouth and Seaton Sluice, Northumberland. 1, Tynemouth to Table Rocks; 2, St. Mary's Island to Crag Point; 3, Crag Point to Seaton Sluice. For key see Appendix 3.

Palaeoenvironment

The exposure comprises c. 115 m of repeating coarsening upwards sequences, each capped with a palaeosol and coal seam, many of which are substantial enough to be individually named. Prominent channel sand-bodies are common, and are also often significant enough to be named separately. The succession is largely fluviodeltaic in nature and represents deposition on a low-lying, humid coastal plain by a complex system of channels, interdistributary bays, and well-established peat swamps (O'Mara and Turner 1999). The sequence is 'cyclothemic', with recurrent coals and thin marine bands indicating changes in relative sea level. Black shales overlying coals in the sequence were mainly deposited in shallow fresh or brackish interdistributary bay or lake environments (O'Mara 1995; O'Mara and Turner 1999); where they do occur, marine bands indicate shallow and relatively brief flooding events. Thus, deposition throughout the sequence was predominantly terrestrial.

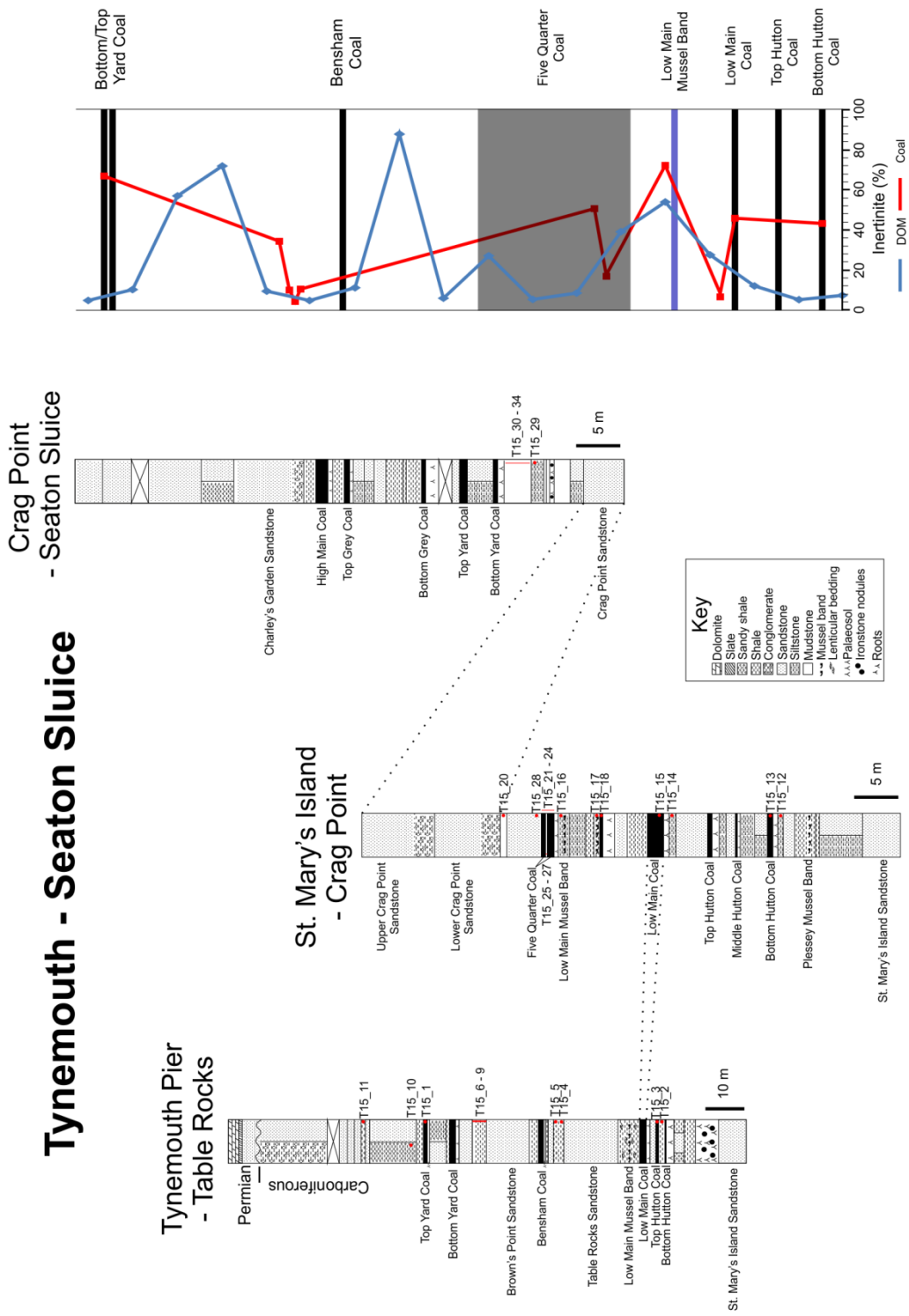

Figure 5.7: Westphalian B coastal section between Tynemouth and Seaton Sluice, with inertinite results.

Late Palaeozoic hyperoxia – scope of data

A total of 48 shale samples and 13 coals of Serpukhovian and Bashkirian age were examined, providing a record of Late Mississippian to Early Pennsylvanian inertinite. Samples were collected during fieldwork in Edinburgh (Joppa Shore) and Northumbria (Tynemouth–Seaton Sluice coastal section), and thus represent similar palaeolatitudes on a single palaeocontinent, Euramerica. As in previous chapters, examination of coals allows a direct comparison with the coal inertinite data of Glasspool *et al*. (2015), albeit with far lower sampling density. This data provides a means to test the hypothesis *that there was a progressive increase in pO_2 during the Carboniferous which is reflected by a corresponding increase in wildfire activity and is associated with arthropod gigantism.* Furthermore, by compiling results from this and each of the previous two chapters, a complete Lochkovian–Bashkirian dataset is obtained. This is applied to the core research hypothesis, as initially stated in the introduction (p. XX), that *the spread of forests significantly increased the production and retention of atmospheric oxygen by fuelling increasing organic carbon burial to fundamentally alter biotic regulation of Earth's O_2 concentration and that this is recorded in the abundance of fossil charcoal*.

5.2 Results

A total of 48 shale samples and 13 coals were processed and examined, of which 38 shales and all coals were found to be suitable for analysis; locality means for DOM inertinite were 39.0% for Joppa Shore and 25.1% for Tynemouth (SI 5.1–5.2). When compared by palaeoenvironment, no statistically significant difference was detected (Mann Whitney U = 142, P = 0.386; Fig. 5.8B, SI 5.3A). Mean inertinite was found to be substantially higher in the Passage Formation at Joppa (48.5%) than in the underlying Upper Limestone Fm. (19.4%), and the succession at Tynemouth (25.1%; Fig. 5.8A; SI 5.3B), with several individual Passage Fm. samples yielding > 90% inertinite; the single sample collected from the Scottish Lower Coal Measures Fm. at Joppa comprised 63.4% inertinite. Once again, however, Kruskal-Wallis ANOVA indicates these differences are not statistically significant (H = 3.616, P = 0.306).

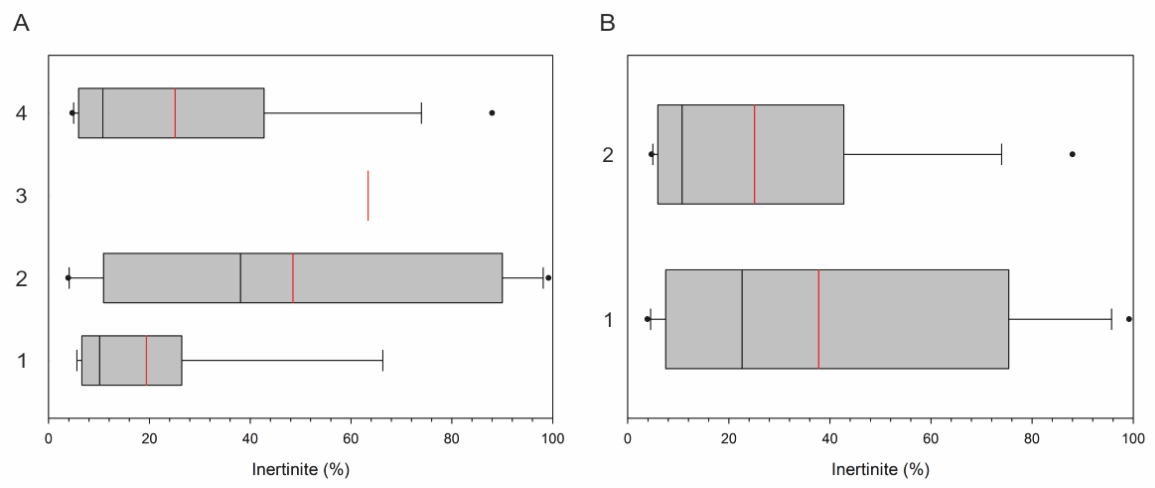

Figure 5.8: Inertinite levels compared by age (A) and palaeoenvironment (B). A: 1, Upper Limestone Fm. (n = 7); 2, Passage Fm. (n = 12); 3, Scottish Lower Coal Measures Fm. (n = 1); 4, Pennine Middle Coal Measures Fm. (n = 18). B: 1, transitional (n = 19); 2, terrestrial (n = 18). Black bars, median; red bars, mean; whiskers, $10^{th}/90^{th}$ percentile.

Mean coal inertinite for the Serpukhovian (Joppa Shore sample J14_3) was 20.0%, and for the Bashkirian (all other samples) was 30.3%; the former only consists of one sample, so inertinite abundance cannot be meaningfully compared between the two periods except to say that the former falls comfortably within the range of the latter. In comparison, Glasspool *et al*. (2015 SI) reported mean coal inertinite values of 22.5% for both the Serpukhovian and Bashkirian (Fig. 5.9). These values were not deemed to be statistically distinct from the results of this study (Mann-Whitney U = 648, P = 0.333 for Bashkirian data), though this is unsurprising given the very large difference in sample sizes (Glasspool *et al*. 2015 = 41/144, this study = 1/11; SI 5.4). As with coal data from Romer's Gap (see previous chapter), σ was substantially higher than that calculated for Glasspool *et al*.'s data; as previously stated, this likely reflects the fact that some of the data provided by Glasspool *et al*. (2015) are actually seam or locality means.

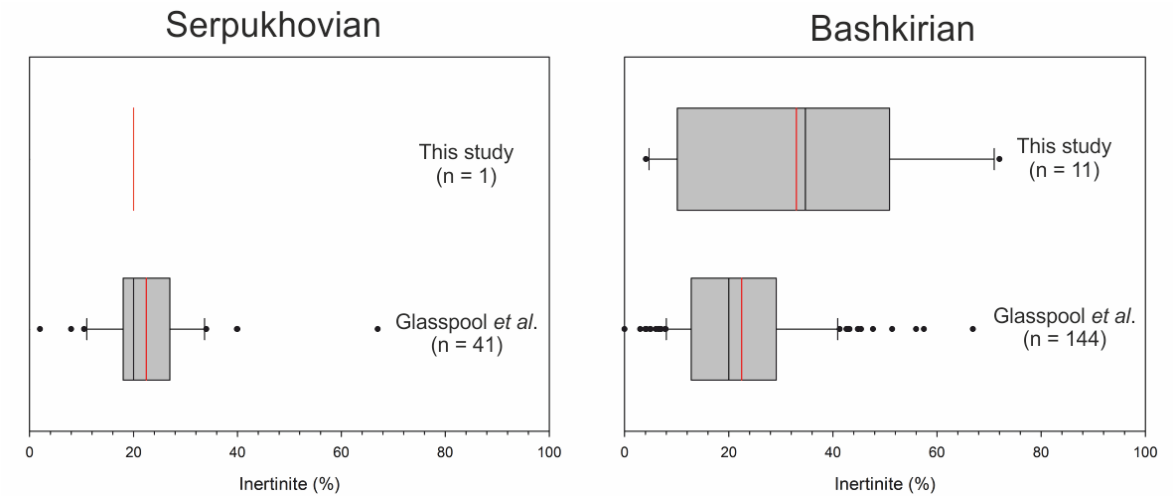

Figure 5.9: Comparison of Serpukhovian and Bashkirian coal data (this study) with that of Glasspool *et al*. (2015). Black bars, median; red bars, mean; whiskers, 10th/90th percentile.

Results from Tynemouth and Joppa were added to the Lochkovian–Viséan data discussed in preceding chapters to produce a combined dataset spanning the Devonian, Mississippian, and Early Pennsylvanian. The data was binned to 10 Ma intervals, so that it could be compared directly against the coal data of Glasspool *et al*. (2015; Fig. 5.10; SI 5.5). DOM and coal inertinite differ substantially for the Devonian, with no significant correlation between them (Pearson r = 0.712, P = 0.288; SI 5.6); for DOM inertinite, few significant differences were detected between time bins (Table 5.1) and the conclusion that there is no statistically significant reduction during the charcoal gap remains valid (Mann-Whitney U = 2082, P = 0.056 for charcoal gap compared with rest of Devonian; SI 5.5).

Comparison	Q	P
400/370 Ma	3.362	0.008
400/390 Ma	3.592	0.003

Table 5.1: Significant differences in DOM-inertinite identified by pairwise Kruskal-Wallis ANOVA.

In contrast, results are in close agreement through much of the Mississippian, showing a steady decline over a 30 million year period; the two curves then diverge, with DOM charcoal showing a marked increase during the Bashkirian to levels not reached in coals until the latest Pennsylvanian. Despite this apparent similarity, which is particularly evident at 330 Ma, correlation between the two datasets was deemed non-significant

(Pearson r = 0.843, P = 0.157). Though based on far fewer data points, coal inertinite values follow the same basic pattern, converging with those of Glasspool *et al*. (2015) over the course of the Mississippian; perhaps unsurprisingly these showed a strong correlation, though the significance was still only marginal (Pearson r = 0.880, P = 0.049; SI 5.7). Kruskal-Wallis ANOVA indicates the decline in DOM inertinite is marginally significant (H = 7.98, P = 0.047; SI 5.5) but only between 350 and 340 Ma; this is likely due to the large spread of data at 330 Ma (standard error = 8.25%).

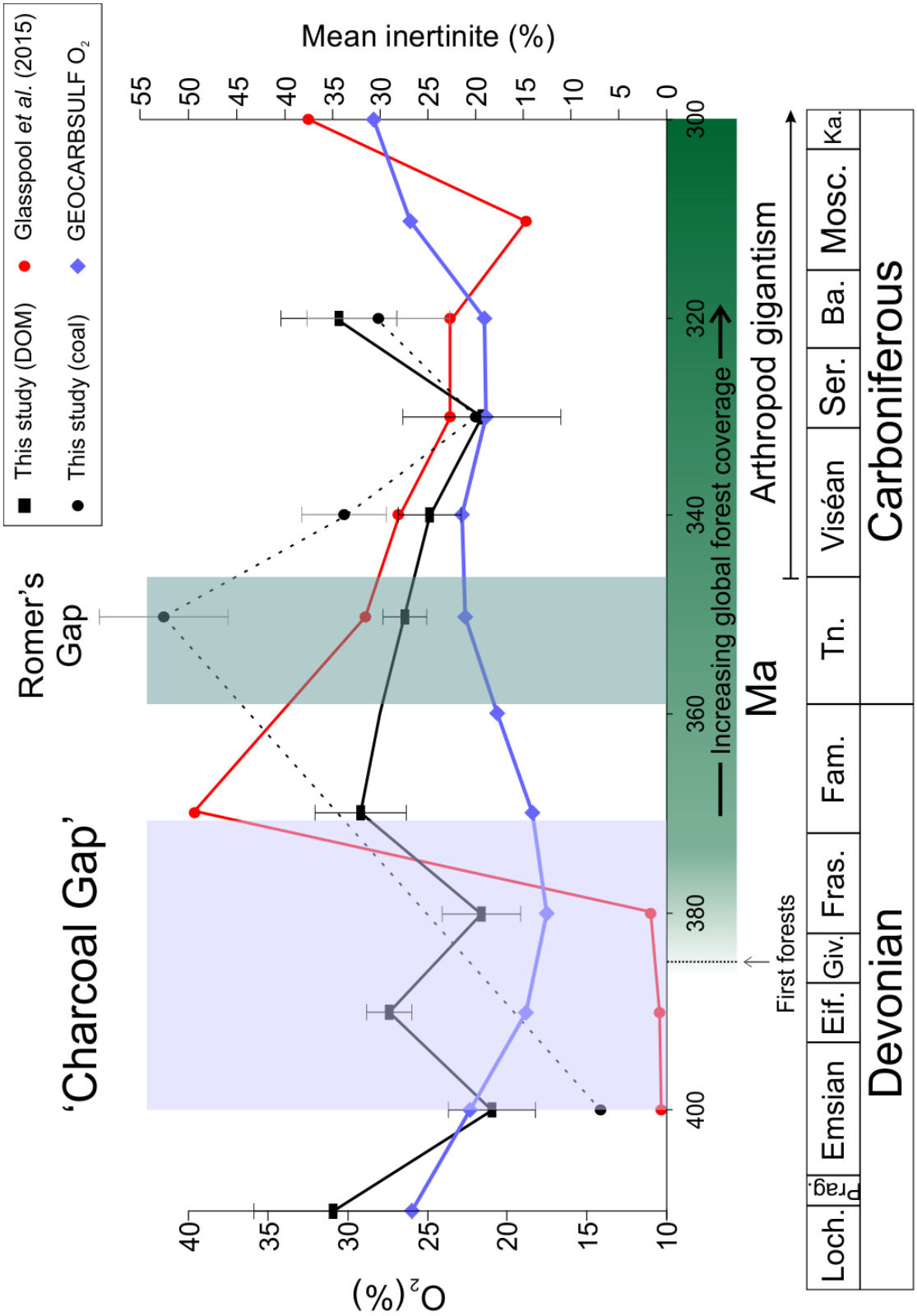

Figure 5.10: Combined data, showing Lochkovian–Bashkirian coal and DOM-inertinite abundance binned to 10Ma (this study) compared with Emsian–Kasimovian coal data of Glasspool *et al*. (2015), and output of GEOCARBSULF O_2 model (Berner 2009). Error bars represent standard error.

5.3 Discussion

The inertinite data on which the present study is based represent a wide range of environmental, climatic, and ecological settings spread across two palaeocontinents, over a span of c. 110 million years. As discussed in section 2.6, organic matter carried by rivers is largely soil-derived (albeit with an undefined contribution from re-worked fossil material), and may be transported great distances before deposition. Hence, inertinite abundance in dispersed organic matter represents a time-averaged signal typically on the scale of 0.1–10 kyr (but potentially much longer), sourced from a wide geographic region (i.e. an entire drainage basin), which has been relatively enriched by differential decay. In comparison, coal-inertinite data such as that used by Glasspool *et al*. (2015) are subject to good environmental and climatic control because coal-forming environments are, by definition, permanently wet (Taylor *et al*. 1998) but represent a more local fire signal because coals are predominantly formed in-situ. Taken at face value, the fact that the two datasets are so closely matched during the Mississippian suggests that the observed reduction in fire activity was occurring worldwide, and cannot be attributed to local climatic or environmental changes. Unfortunately the perennial problem of limited datapoints with a large σ means that, despite a high correlation coefficient ($r = 0.84$), the two datasets cannot be said to display a statistically significant correlation ($P = 0.16$); similarly, only the 6% reduction from 350 to 340 Ma can be considered statistically valid. Nevertheless, the convergence of DOM-inertinite, two separate sets of coal-inertinite data, and the GEOCARBSULF O_2 model at 330 Ma is quite striking, and even the most conservative interpretation (that there is little statistically significant change in fire frequency) is inconsistent with increasing pO_2 during the Mississippian, as predicted by the majority of models (Figs 1.3, 5.1). The apparent fall in inertinite abundance fits well with the GEOCARBSULF model of Berner (2009), however, which indicates a small reduction in pO_2 at this time, followed by a rapid increase from the Bashkirian. It is also notable that GEOCARBSULF is the only model which does not indicate $O_2 \leq 16.5\%$ vol. at any time during the studied interval, which is in accord with the continued presence of charcoal in the fossil record. If correct, this has implications for several of the debates surrounding the late Palaeozoic oxygen pulse, as well as the relationship between afforestation and atmospheric pO_2 generally.

Arthropod gigantism

The radiation of winged insects during the late Palaeozoic produced the greatest diversity, and some of the best-known, examples of arthropod gigantism (Shear and Kukalová-Peck 1990; Carpenter 1992); as a result, many examinations of the phenomenon are, in fact, primarily studies of *insect* gigantism rather than arthropod gigantism *per se* (e. g. Harlé and Harlé 1911; Weis-Fogh 1964; Rutten 1966; Dudley 1998; Harrison *et al*. 2010; Clapham and Carr 2012). This is an important distinction, because while giant arthropods such as *Arthropleura* first appeared during the Viséan (Pearson 1992; Schneider *et al*. 2010), winged insects (of any size) do not appear in the fossil record until the Serpukhovian (Wolfe *et al*. 2016). In concluding that, in the absence of aerial predation from birds and bats, pO_2 is the main limiting factor on large body size Clapham and Carr (2012) make the implicit assumption that pO_2 had already increased substantially by the Viséan. This is not supported by the palaeofire record as recorded by DOM or coal inertinite, suggesting that other selective pressures were at work as argued by Dorrington (2012). For now, the obvious question of why the level of gigantism seen during the Permo-Carboniferous has never been repeated remains open.

Atmospheric pO_2 and the evolution of wood

Genetic and fossil evidence suggests that lignin first evolved during the latest Silurian (c. 420 Mya; Robinson 1990; Nelsen *et al*. 2016), but was present only at low levels (10–15%) in early vascular plants (Raven 1977; Niklas 1982). The rise of arborescent forms during the Mid-Devonian, with their greater need for structural support, introduced groups such as the Progymnospermopsida and Cladoxylopsida in which secondary xylem (wood) was a significant component (Meyer-Berthaud *et al*. 1999; Stein *et al*. 2007); however, phylogenetic and molecular clock estimates place the evolution of lignin-degrading basidiomycete 'white rot' fungi in the early Permian (c. 295 Mya) representing a lag of some 100 Ma (Floudas *et al*. 2012; Kohler *et al*. 2015). It has been suggested (Robinson 1990; Berner 2001; Berner *et al*. 2003; Floudas 2012) that this delay led to greatly increased burial of C_{org} in the form of un-degraded wood, particularly during the Pennsylvanian and early Permian, contributing significantly to the progressive rise in atmospheric pO_2 which culminated in the late Palaeozoic oxygen pulse. In opposition to

this hypothesis, Nelsen *et al*. (2016) argued that mass-balance calculations indicate the absence of lignin-decay would result in unfeasibly large rates of carbon deposition, such that atmospheric CO_2 would be completely removed in < 1 million years; that this demonstrably did not occur indicates that even if lignin-degrading fungi were absent, other modes of decay must have been in operation. Furthermore, the authors noted that coal accumulation rates (as measured by bed thickness and geographical distribution) show no correspondence to changes in the composition of plant communities as regards their lignin content; for example, the widespread replacement of arborescent lycopsids by non-woody ferns in Euramerica during the latest Pennsylvanian/earliest Permian was not matched by a decrease in coal accumulation rates. Stable or declining atmospheric pO_2 through much of the Mississippian is a strong argument in favour of this position.

Calculation of O_2 from inertinite abundance

Aside from the upper and lower limits imposed by the fire window, this study has largely considered DOM and coal inertinite in terms of *relative* changes in atmospheric pO_2. Model predictions of hyper- or hypoxic intervals imply a corresponding change in wildfire activity; examining the inertinite record allows us to test these, without necessarily providing any insight into the absolute pO_2 values involved. However, Glasspool and Scott (2010) and Glasspool *et al*. (2015) did present a reconstruction of Phanerozoic pO_2 in absolute terms, calculated from the relative abundance of coal inertinite through time. Calculation was by means of a calibration curve, which assumed coals would contain 0% inertinite at 15% vol. O_2, 4.2% mean inertinite at PAL (as observed in recent peats), and 100% inertinite at 35% vol. O_2. As shown in Fig. 5.1, this reconstruction indicates > 25% vol. O_2 during the Tournaisian and Viséan, which is higher than any model prediction. Although this does not negate the main conclusion of this chapter that pO_2 did not track afforestation during the Mississippian, it does have implications for the record of arthropod gigantism in the Viséan. In this alternative interpretation, pO_2 had already increased enough to permit giant forms by the Famennian, and remained high enough to support them, despite the Mississippian decline, through to the end-Permian.

There are several reasons to treat this pO_2 reconstruction cautiously. First, as discussed in section 1.4, it is possible that charcoal abundance has been routinely underestimated in

recent peats; if so, the inertinite calibration point used by Glasspool *et al*. (2015) for modern pO_2 would also be too low, resulting in a systematic overestimate in their O_2 curve. Second, their calibration curve assumes 35% vol. to be the maximum permissible level of O_2 in the atmosphere. If the upper limit of the fire window is closer to 25%, as suggested by e.g. Lenton (2001), this would also contribute to a systematic overestimate. Finally, the very high O_2 (27.7% vol.) indicated by their reconstruction for the Famennian is based on 18 samples from a single locality, raising the possibility of distortion by local fire activity.

Afforestation and the late Palaeozoic oxygen pulse

It is widely accepted that the late Palaeozoic peak in atmospheric pO_2 predicted by palaeoatmosphere models is linked to the rise and spread of vascular plants from the Mid-Devonian, via the increased burial of organic carbon (e.g. Berner 1989, 2006; Berner and Canfield 1989; Lenton 2001; Bergman *et al*. 2004). There is no consensus, however, on the precise mechanism by which this occurred; an increase in primary productivity at constant burial rate, or increased burial at constant primary productivity (or a combination thereof) would have an equivalent effect. For example, Berner (1989) and Berner and Canfield (1989) attributed the O_2 pulse to enhanced coal formation in the massive equatorial wetland basins that formed during the Pennsylvanian as Pangea was assembled. Obviously this could not have occurred prior to widespread afforestation, but was driven by tectonic factors rather than the rise of forests *per se*. Conversely, Lenton (2001) proposed that enhanced chemical weathering by deep-rooting arborescent groups increased the supply of phosphates to the oceans, fuelling primary productivity and a corresponding increase in C_{org} burial. In this case, the chief driver of increasing O_2 was biological.

Because no Mid-Pennsylvanian–Permian material was available for analysis, the results of this study neither confirm nor refute hyperoxia during the late Palaeozoic, though the increase in DOM inertinite seen during the Early Pennsylvanian is certainly not inconsistent with a subsequent rapid rise in pO_2. However, the data do provide some constraints on the possible timing of the event, which could not have been initiated prior to the late Serpukhovian, following a period of stable or declining fire activity through the

Early and Mid-Mississippian. If correct, this record of fire history indicates a significant hiatus (c. 50 Ma) between the spread of forests and an increase in pO_2; this in turn suggests that, while a combination of factors is likely, the main causes for the oxygen pulse were tectonic rather than directly biological.

5.4 Summary

Most palaeoatmosphere models consistently predict a near-continuous increase in atmospheric pO_2 from the Famennian onwards, reaching a peak during the latest Carboniferous or early to mid-Permian; this is often referred to as the late Palaeozoic oxygen pulse, and is usually attributed to a massive increase in C_{org} burial resulting from the rise and spread of the first forests. The exact mechanism is disputed, however; increased Corg burial may have been the direct result of increased coal formation, or have been indirectly triggered by enhanced nutrient supply to the marine realm.

The combined Lochkovian to Bashkirian DOM inertinite record, in close agreement with the coal-inertinite data of Glasspool *et al*. (2015) and this study (Fig. 5.10), suggests a progressive, moderate decrease in fire activity during the Mississippian. The consistency of datasets compiled from disparate sources with varying levels of environmental, climatic and ecological control strongly suggests a mild reduction of atmospheric pO_2 as the cause; this is uniquely in accord with predictions of the GEOCARBSULF palaeoatmosphere model, and constrains the timing of the Late Palaeozoic oxygen pulse to no earlier than the Mid-Pennsylvanian. If correct, this indicates that hypoxia is not a requirement for arthropod gigantism, and that other evolutionary factors drove arthropods to attain very large sizes at this time. The c. 50 Ma lag between widespread afforestation and any significant increase in global fire activity suggests that the lack of lignin-degrading fungi was not a serious impediment to C_{org} decay during the Late Devonian and Carboniferous; had this been the case, pO_2 increase would be expected to increase progressively from the Givetian onwards. By the same reasoning, it also suggests that it was the onset of extremely widespread coal-forming environments, driven by tectonic activity, rather than a progressive increase in nutrient supply to the oceans which increased C_{org} burial during the Permo-Carboniferous and ultimately led to the late Palaeozoic oxygen pulse.

6. Conclusions

Efforts to unravel Phanerozoic variations in atmospheric pO_2 have been hampered by a lack of direct geochemical proxies, and uncertainty over how best to model pO_2 indirectly. The wildfire-based O_2 reconstruction of Glasspool *et al*. (2015), while a significant contribution, is based on inertinite abundance in coals and so provides limited information for periods when coals were rare, such as the Devonian and Early Mississippian. In particular, the following hypotheses remain untested or lack independent verification:

1) *That a 'charcoal gap' exists from the late Emsian to the early Famennian, indicating that wildfire activity was significantly supressed by a reduction of atmospheric* pO_2.

2) *That 'Romer's Gap' represents a genuine bottleneck in tetrapod diversity caused by global hypoxia following the End Devonian Mass Extinction (EDME), resulting in a significant reduction in wildfire activity during the Tournaisian.*

3) *That there was a progressive increase in* pO_2 *during the Carboniferous which is reflected by a corresponding increase in wildfire activity and is associated with arthropod gigantism.*

4) *That the spread of forests significantly increased the production and retention of atmospheric oxygen by fuelling increasing organic carbon burial to fundamentally alter biotic regulation of Earth's* O_2 *concentration and that this is recorded in the abundance of fossil charcoal.*

By assembling a new Devonian–Carboniferous inertinite dataset based on dispersed organic matter in clastic sedimentary rocks, it has been possible to investigate these issues. However, the quantification of DOM inertinite in the fossil record is problematic, regardless of the method chosen; this situation is in part due to the inadequacy of current definitions for inertinite-group macerals favoured by the ICCP, but also stems from the fact that approaches based on incident light microscopy were originally intended for use with coals rather than DOM. The use of reflectograms to quantify DOM inertinite is found to be unreliable, and although restricting the analysis to fusinite alone yields greater

success, this maceral is a poor predictor of total inertinite. Thus, a new inertinite quantification method was developed, in which mixture models are applied to interpretation of maceral reflectance distributions. While based on probabilistic statistical arguments, this approach provides results which are consistent with empirically derived maceral abundance and reflectance data.

The effects of natural oxidation on maceral reflectance appear to have been overstated; past reports of reflectance increase due to oxidation can be more simply explained as the result of exposure to high temperatures, casting doubt on claims that inertinite can form via oxidative decay. The effects of artificial oxidation during palynological processing (e.g. during pyrite removal) are less certain, and appear to be quite variable depending on the method used; treatment of organic residue with nitric acid at room temperature caused no consistent change in the maceral reflectance profile, but nevertheless resulted in a significant increase in relative inertinite abundance after only 5 minutes of exposure. This is attributed to the preferential destruction of macerals other than inertinite, which are more vulnerable to oxidation; it is therefore recommended that the use of oxidising agents during palynological processing should be avoided in studies involving inertinite.

Also investigated was the possibility of taphonomic bias, due to the different physical and chemical properties of charcoal compared to other plant material, and the potential introduction of re-worked lithogenic material. Size distribution analysis indicates that differential fragmentation could significantly skew results; whether this occurs in practice is currently unknown, but where time permits it is advisable to adopt area estimation rather than particle counts. Lithogenic contributions are at present impossible to quantify, and remain a concern.

The Devonian Charcoal gap

Analysis of Lochkovian–Famennian shale samples revealed no statistically significant trend in inertinite content through the Devonian, relative to total organic matter; the apparent scarcity of Emsian–Frasnian charcoal reported in previous studies (Scott and Glasspool 2006; Glasspool and Scott 2010; Glasspool *et al*. 2015) is here considered to be an artefact of limited data. This assessment is supported by the discovery of macroscopic charcoal of Givetian age in the Mid-Devonian successions of the Catskill Front, New York

State. Thus, fire activity is judged to have been relatively stable through the supposed 'charcoal gap'. When examined separately, no significant correlation is seen between Gondwanan and Euramerican inertinite levels through time, suggesting that variations in fire activity were not driven by changes in atmospheric pO_2. This record of fire activity is inconsistent with models predicting a profound fall in pO_2 during the Early or Mid-Devonian followed by a rapid rise during the late Famennian, and as such *do not support the existence of a 'charcoal gap'*.

Romer's Gap, and Tournaisian hypoxia

Fire activity appears to have remained stable from the Famennian–Viséan, with neither DOM or coal inertinite levels showing any statistically significant trend, in agreement with previously published coal data for this interval (Diessel 2010; Glasspool *et al*. 2015). These results suggest that palaeoatmosphere models predicting a sudden decrease in pO_2 immediately after the D/C boundary are incorrect, and that the disappearance of *Archaeopteris*-dominated forests at this time (representing a reduction in fuel-laden, possibly fire-prone ecosystems) did not significantly affect fire activity. Interestingly, and in contrast to results for the Devonian, a clear positive correlation is seen between inertinite and palaeolatitude, suggesting climate (i.e. aridity) was an important control on fire frequency at this time. Thus, the wildfire record *does not support the hypothesis of Ward et al. (2006) that the Tournaisian tetrapod diversity crisis (Romer's Gap) can be attributed to global hypoxia.*

Afforestation, gigantism, and the late Palaeozoic oxygen pulse

When binned to 10 Ma intervals, the combined Lochkovian to Bashkirian DOM inertinite record, in close agreement with the coal inertinite data of Glasspool *et al*. (2015) and this study, suggests a progressive, moderate decrease in fire activity during the Mississippian. The consistency of datasets compiled from disparate sources with varying levels of environmental, climatic and ecological control (Fig. 5.10) strongly suggests a mild reduction of atmospheric pO_2 as the cause; this is uniquely in accord with predictions of the GEOCARBSULF palaeoatmosphere model, and constrains the timing of any late Palaeozoic oxygen pulse to no earlier than the Mid-Pennsylvanian. If correct, this indicates *that hyperoxia is not a requirement for arthropod gigantism and that other*

evolutionary factors drove arthropods to attain very large sizes at this time. The c. 50 million year lag between widespread afforestation and any significant increase in global fire activity suggests that the lack of lignin-degrading fungi was not a serious impediment to C_{org} decay during the Late Devonian and Carboniferous; had this been the case, pO_2 increase would be expected to increase progressively from the Givetian onwards. By the same reasoning, it also suggests that it was the onset of extremely widespread coal-forming environments, driven by tectonic activity, rather than a progressive increase in nutrient supply to the oceans which increased C_{org} burial during the Permo-Carboniferous. Thus, *the spread of forests did not directly drive increased net photosynthesis and a corresponding rise in atmospheric* pO_2.

Future work

This study establishes that DOM inertinite can provide useful insights into wildfire activity through geological time, and addresses several critical gaps in our understanding of atmospheric pO_2 evolution during the mid- to late Palaeozoic. Nevertheless, there are a number of areas in which further investigation is required. The contribution of reworked lithogenic material to total sedimentary inertinite is unclear, and should be explored more fully; future work should focus on methods by which it might be distinguished from biogenic and pedogenic contributions. The behaviour of DOM inertinite at very high pO_2 is also uncertain, and should be examined for the Mid-Pennsylvanian–Permian; this would permit further comparisons between the coal and DOM inertinite record, and may provide further insights into the late Palaeozoic oxygen pulse.

These issues notwithstanding, and given that the principal advantage of DOM over coal inertinite is that it can be examined through coal-poor intervals, an obvious next step is to apply this method to Ordovician–Silurian wildfire activity. Palynological evidence suggests that land-plants arose no later than the Mid-Ordovician (Rubinstein et al. 2010), and yet the earliest confirmed charcoal in the fossil record is of late Silurian age. Model predictions for Ordovician–Silurian pO_2 diverge widely (Figs. 1.3, 5.1), from c. 5% vol. (COPSE model; Bergman *et al*. 2004) to c. 20% vol. (GEOCARBSULF; Berner 2009). The logic of the 'fire window' implies that, if fuel is present, the absence of fire suggests

atmospheric O_2 < 16.5% vol.; however, since no systematic search for inertinite (as opposed to macroscopic charcoal) has been conducted, the question remains open.

Another important extension to this work would be the use of DOM inertinite data to reconstruct pO_2 in absolute terms, following the calibration curve approach of Glasspool et al. (2015). This will be challenging, because establishing a calibration point for DOM inertinite under PAL O_2 would require a detailed study of relative charcoal abundance in a range of recent sediments, such that a plausible average figure could be obtained; uncertainties over the sensitivity of charcoal production to high pO_2 (see above) would also first need to be resolved. Nevertheless, it would be instructive to see if the persistent high pO_2 inferred by Glasspool *et al*. (2015) for the Carboniferous is also indicated by DOM inertinite.

Finally, that so many palaeoatmosphere models violate the constraints of the fire window is testament to the fact that most predate the confirmation of the 16.5% vol. O_2 lower boundary (Belcher *et al*. 2010). It is critical that new models at least incorporate this basic constraint into their calculations, and it is to be hoped that, as the major role that fire plays in maintaining a balanced Earth-system becomes more widely recognised, studies such as this one can be drawn upon as a source of raw data and guidance going forward.

7. Appendix 1: high-vitrinite samples

7.1 Tynemouth (DOM)

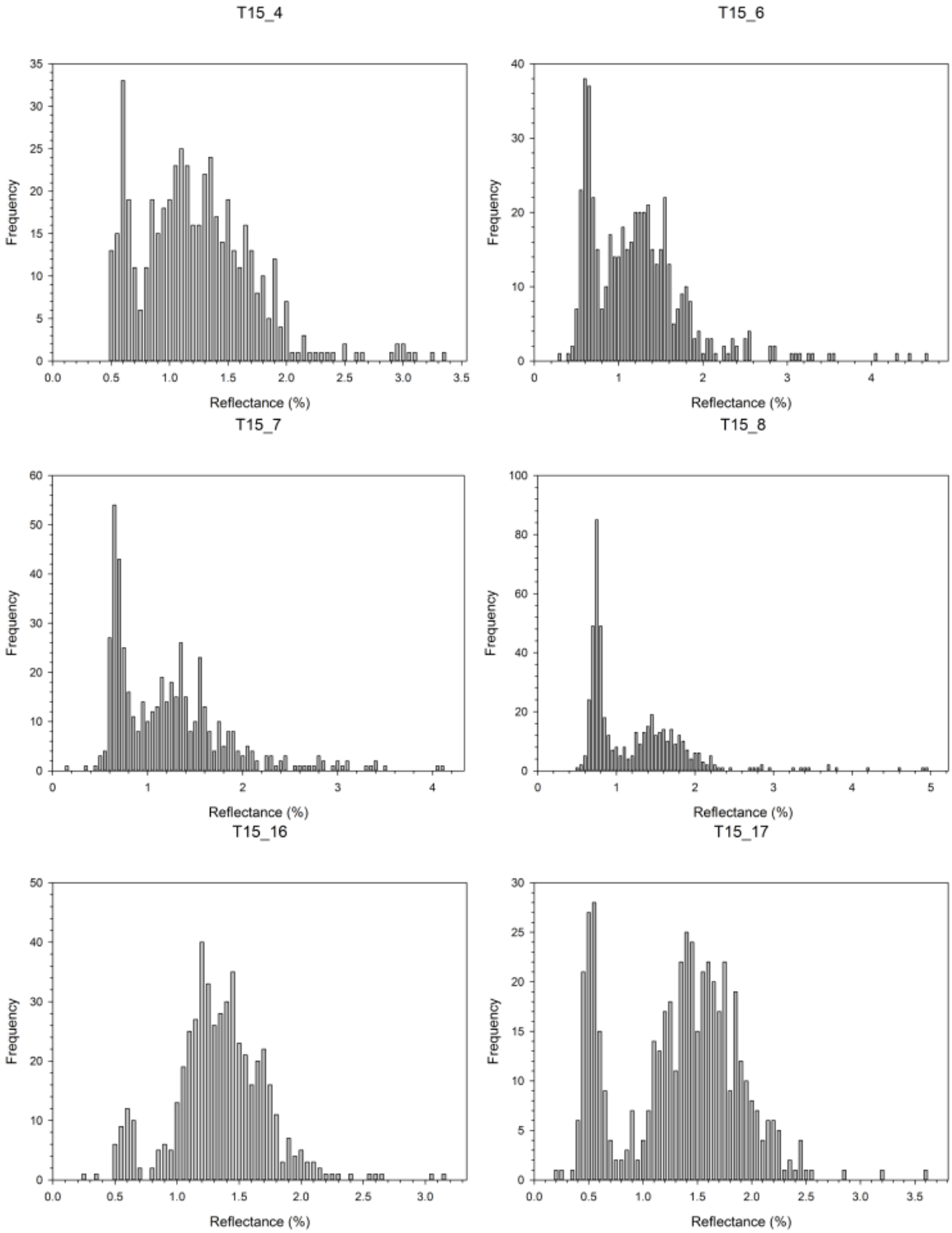

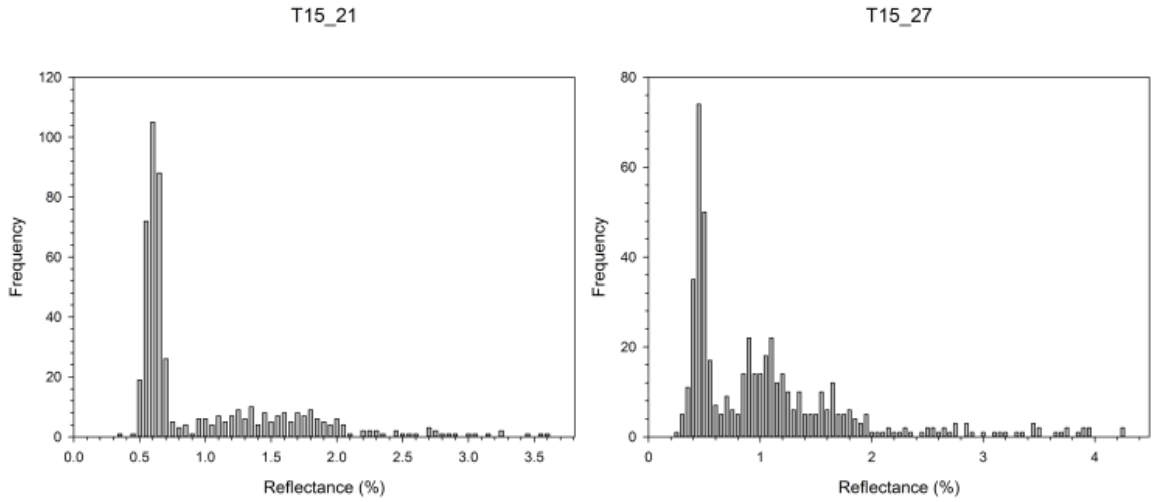
T15_21
Frequency
Reflectance (%)
T15_27
Frequency
Reflectance (%)

7.2 Tynemouth (coals)

T15_1

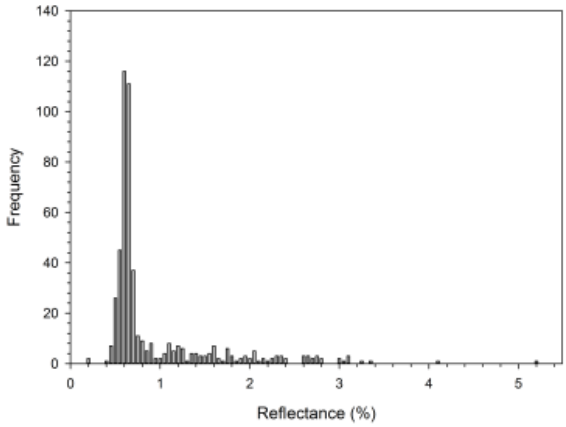

T15_13

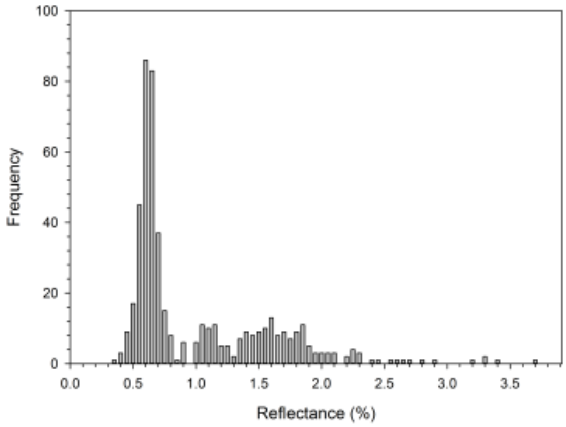

T15_15

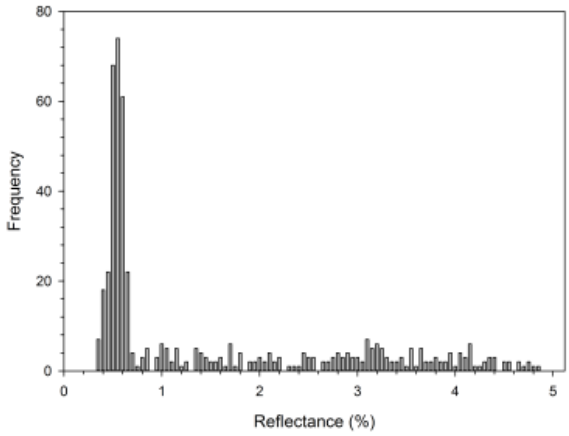

T15_16

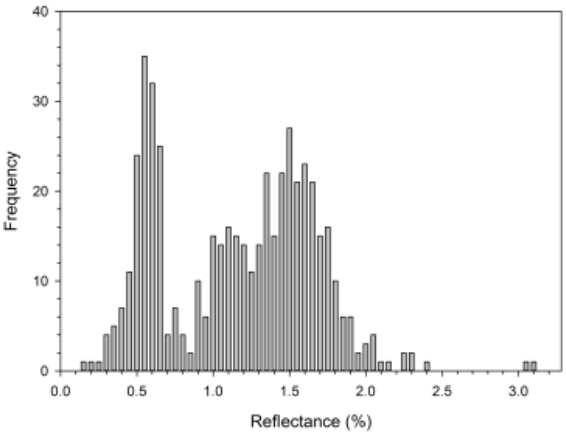

T15_18

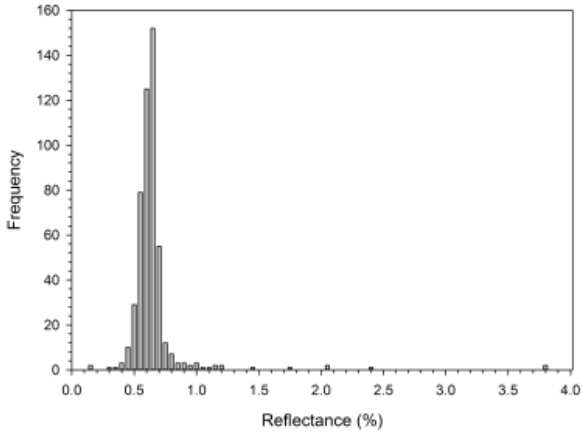

T15_22

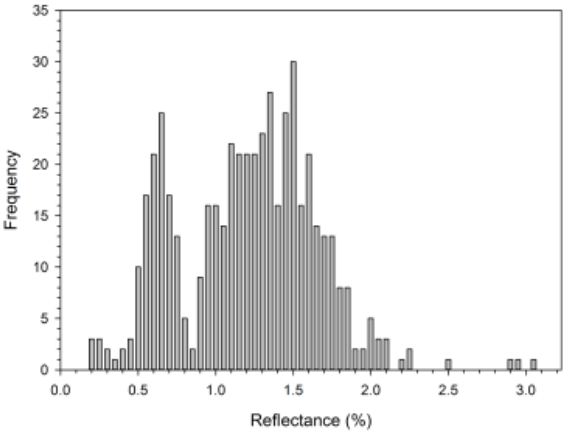

T15_23

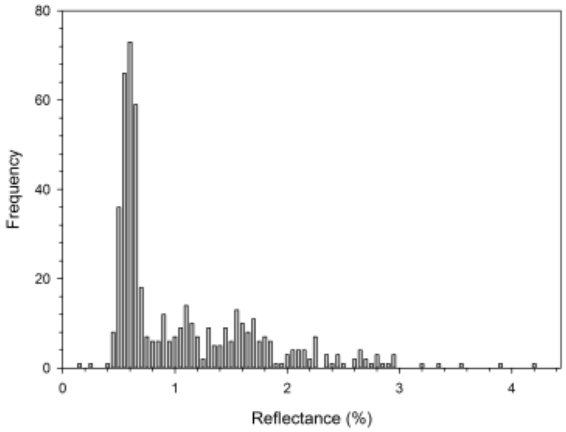

T15_31

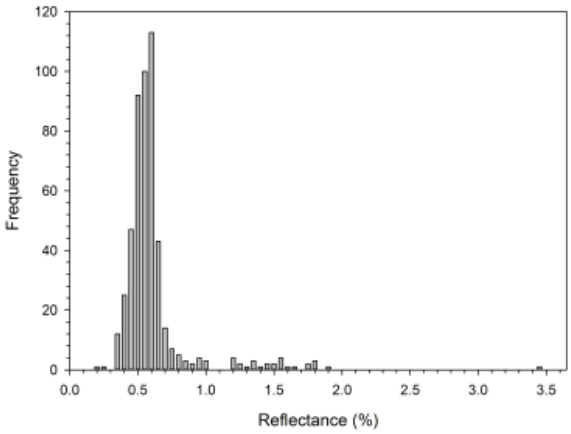

T15_33

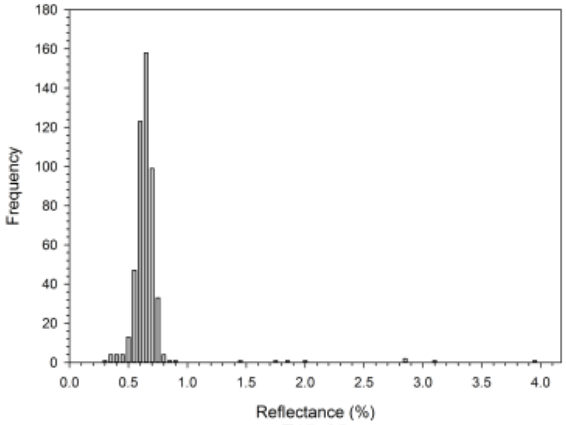

T15_34

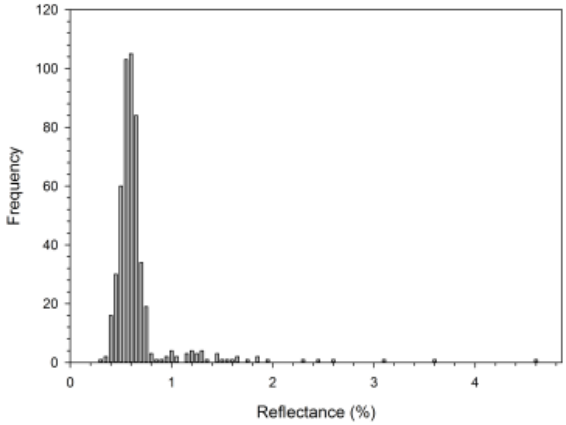

T15_35

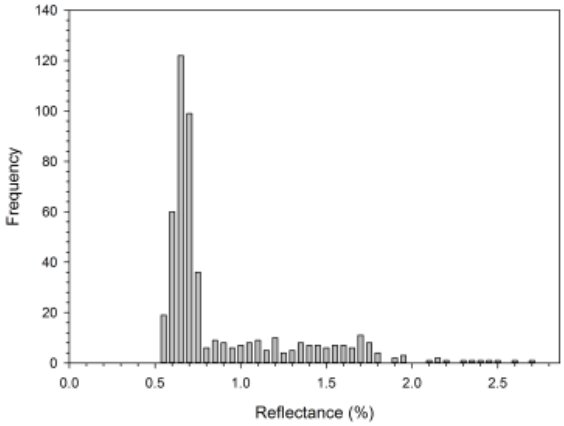

7.3 Willie's Hole (DOM)

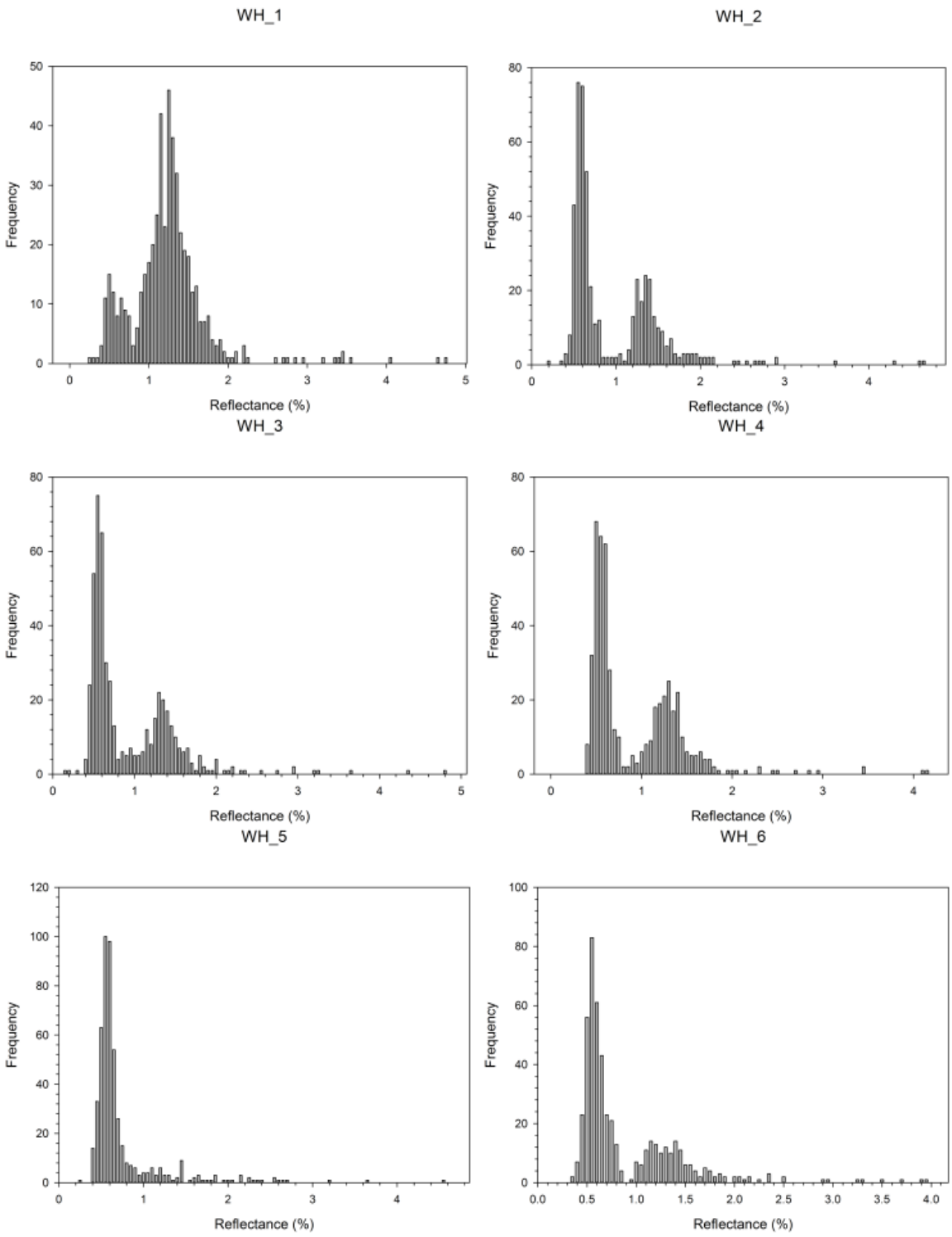

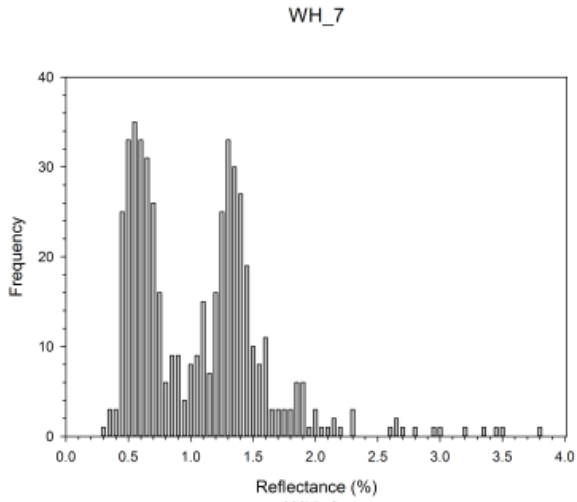
WH_7
Frequency
Reflectance (%)

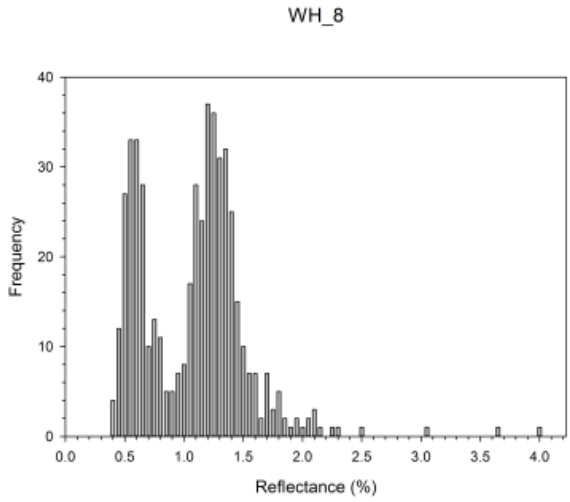
WH_8
Frequency
Reflectance (%)

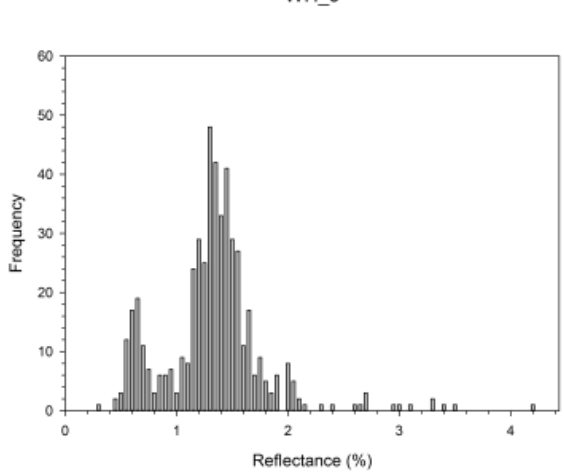
WH_9
Frequency
Reflectance (%)

7.4 Fife (DOM)

F14_19

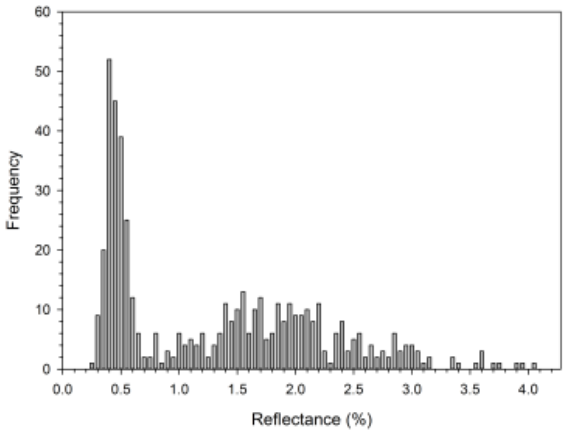

F14_32

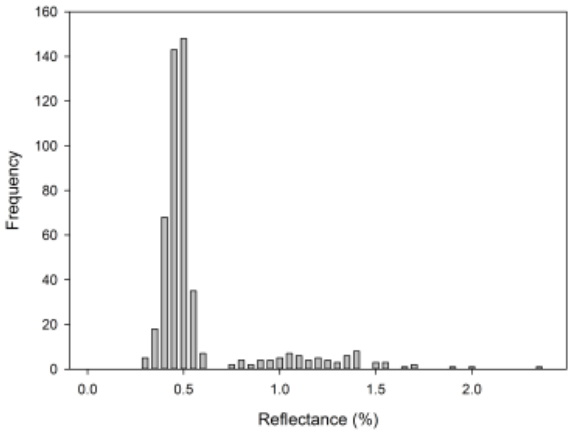

F14_36

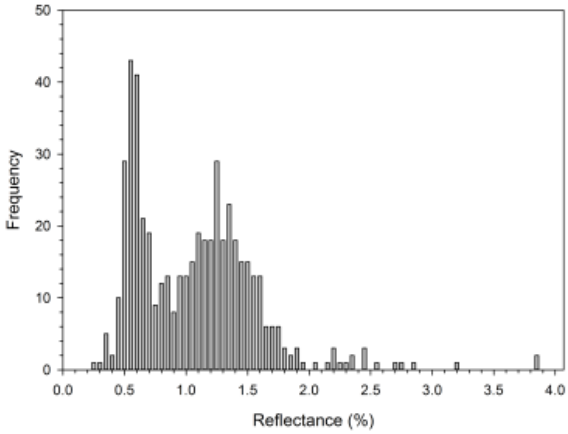

F14_38

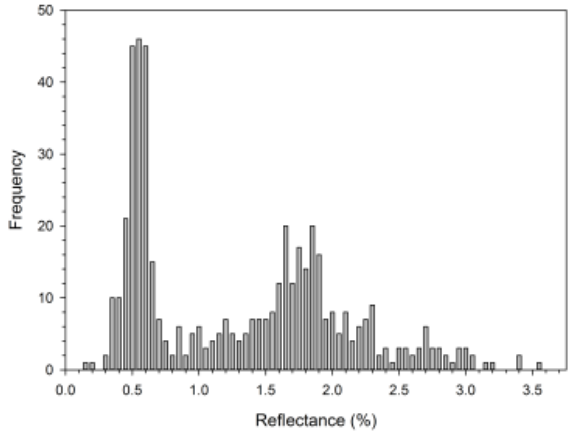

F14_41

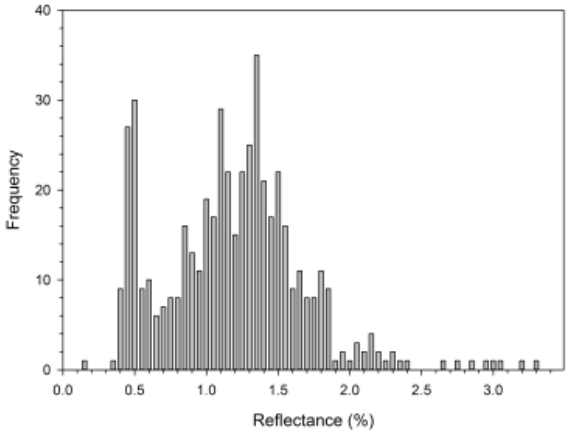

F14_43

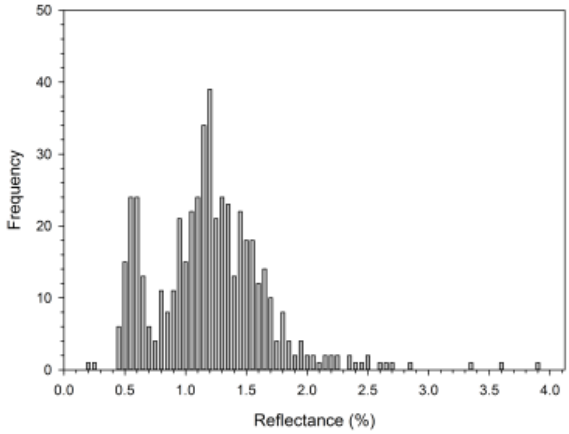

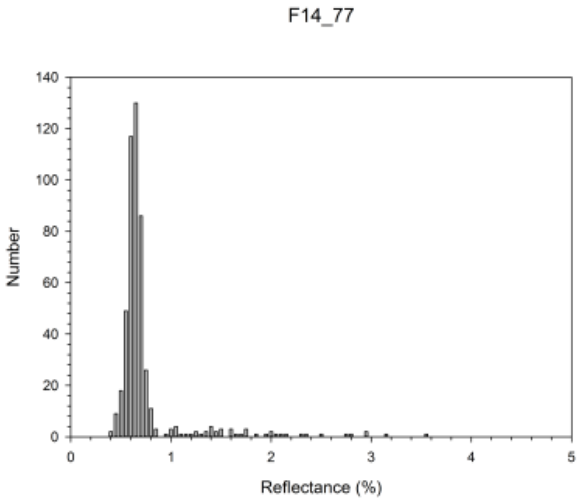
F14_77
Number
Reflectance (%)
0
20
40
60
80
100
120
140
0
1
2
3
4
5

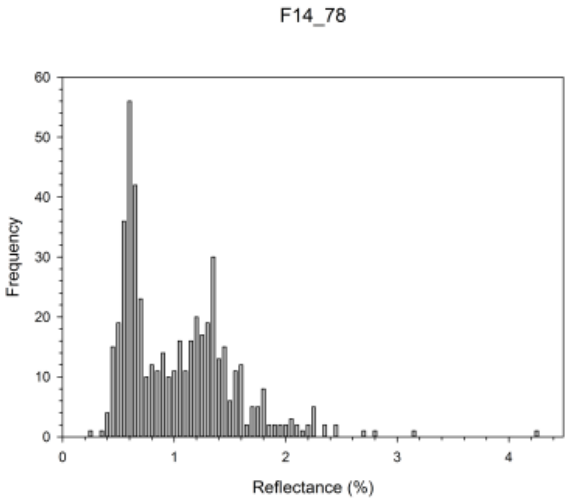
F14_78
Frequency
Reflectance (%)
0
10
20
30
40
50
60
0
1
2
3
4

7.5 Fife (coals)

F14_3

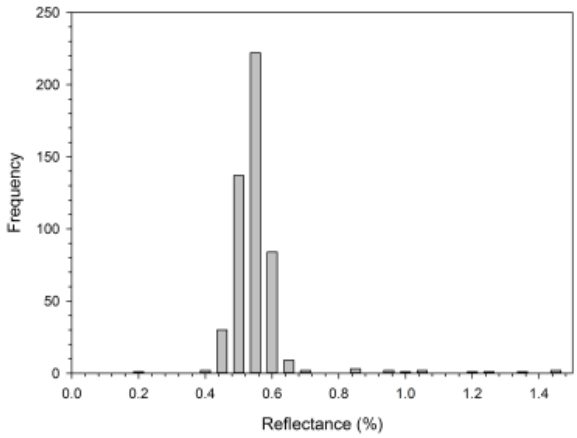

F14_12

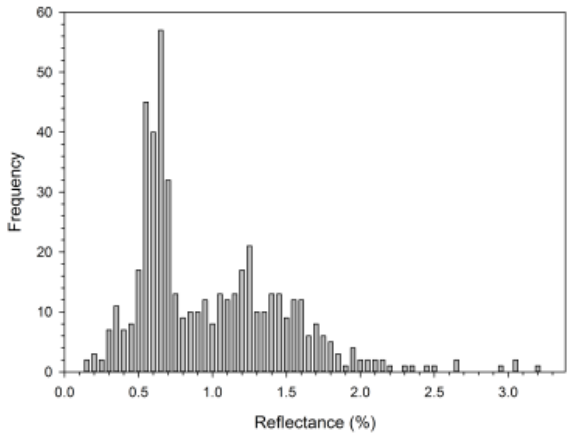

F14_17

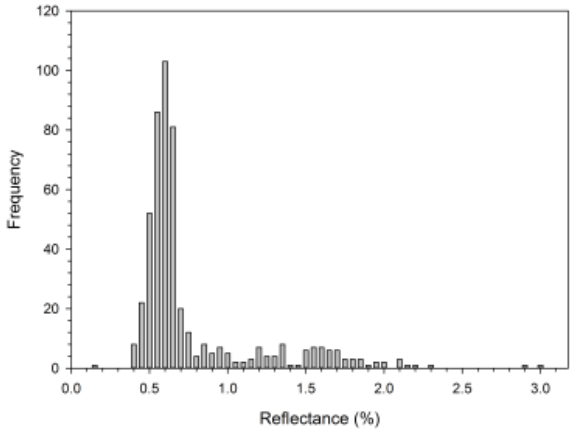

F14_18

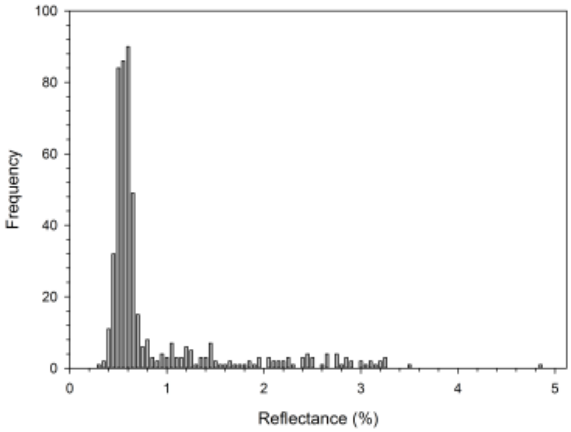

F14_21

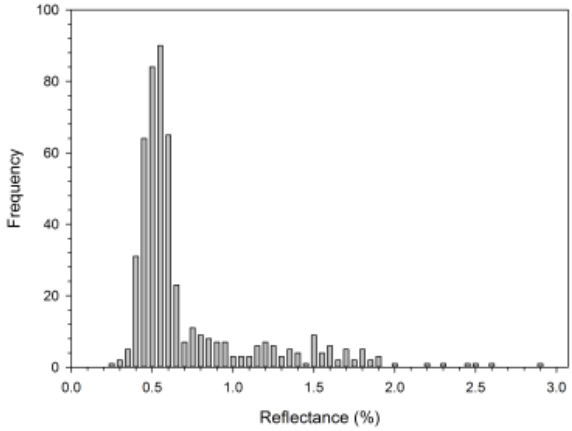

F14_30

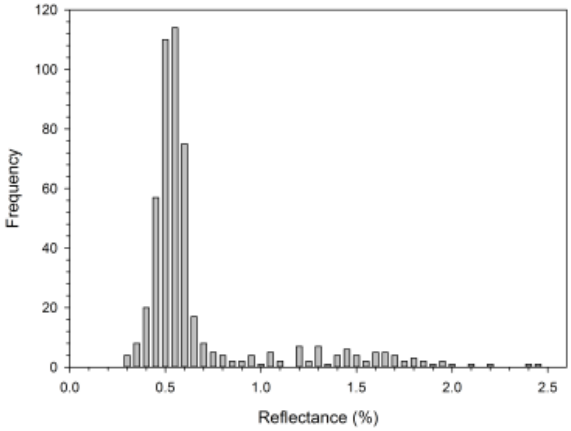

F14_37

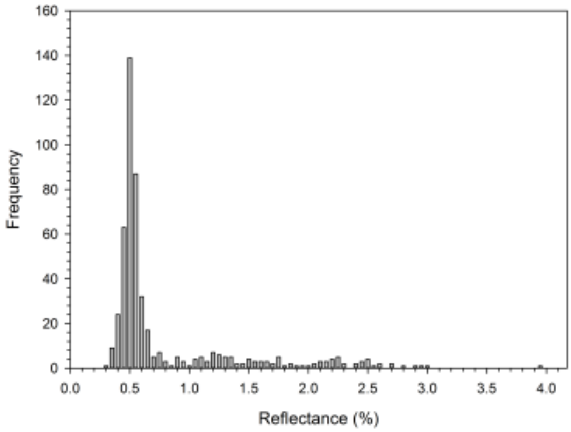

F14_50

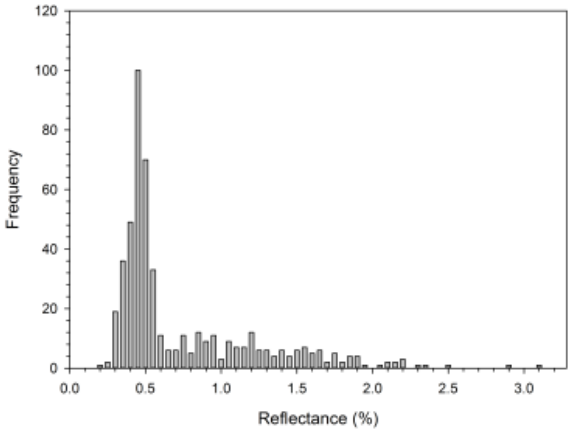

F14_61

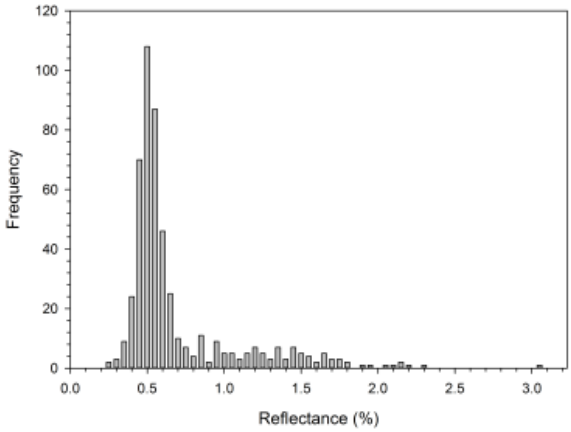

F14_62

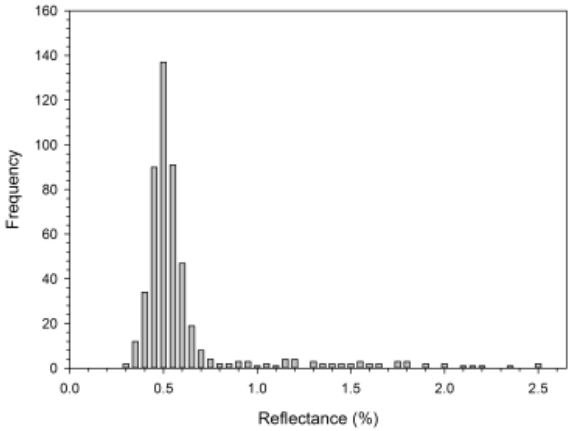

F14_63

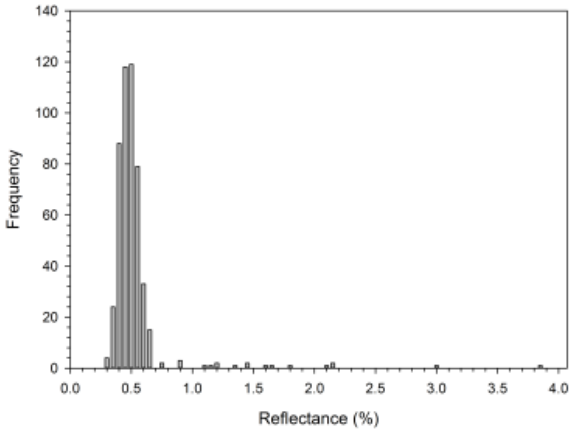

F14_83

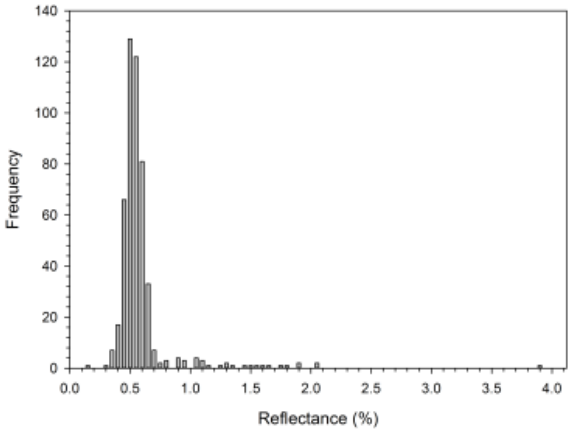

7.6 Fife (Carbonaceous shales)

F14_4

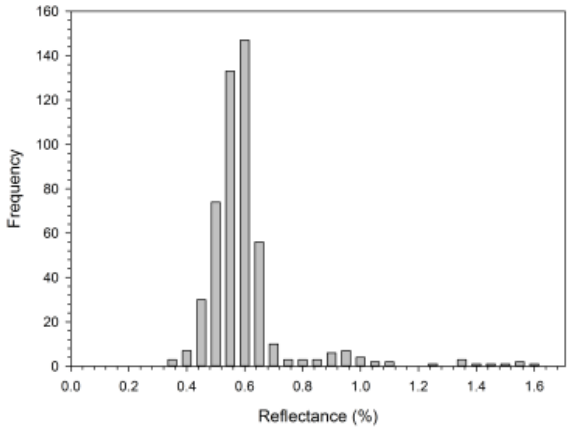

F14_11

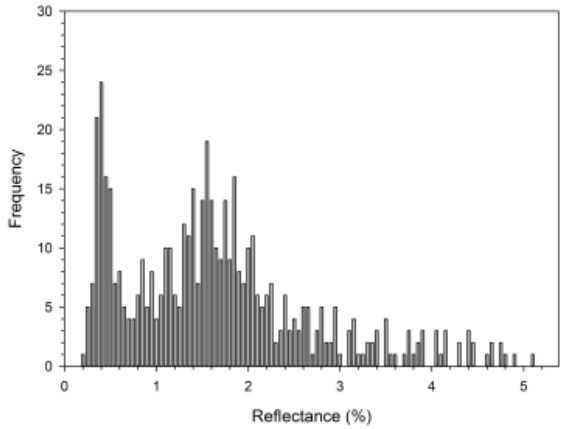

F14_14

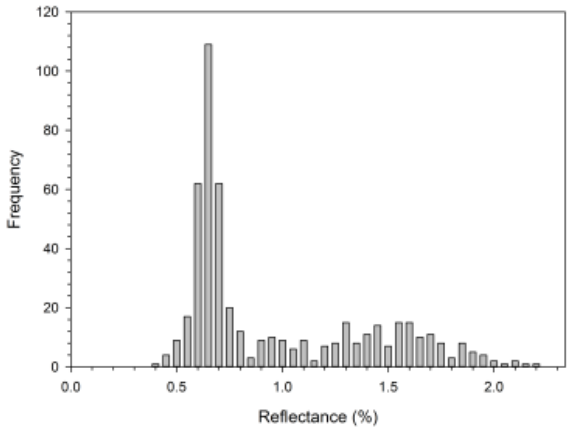

F14_25

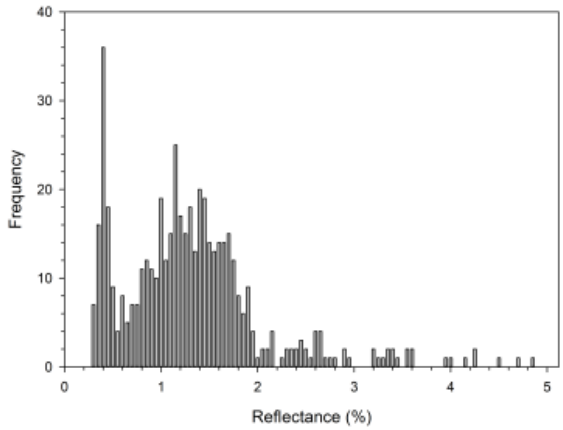

F14_26

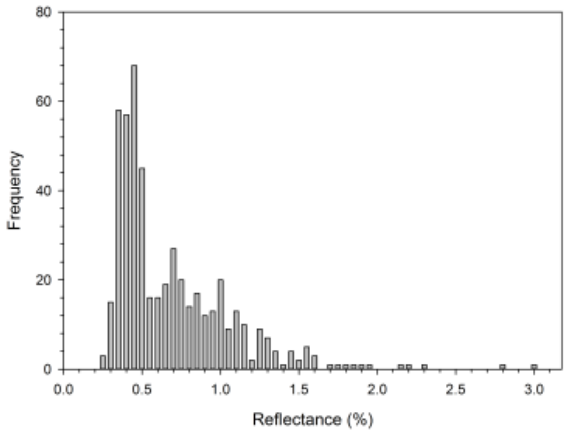

F14_28

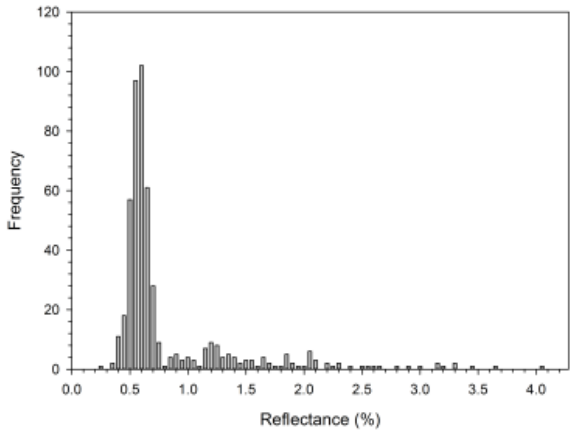

8. Appendix 2: keys for sedimentary logs

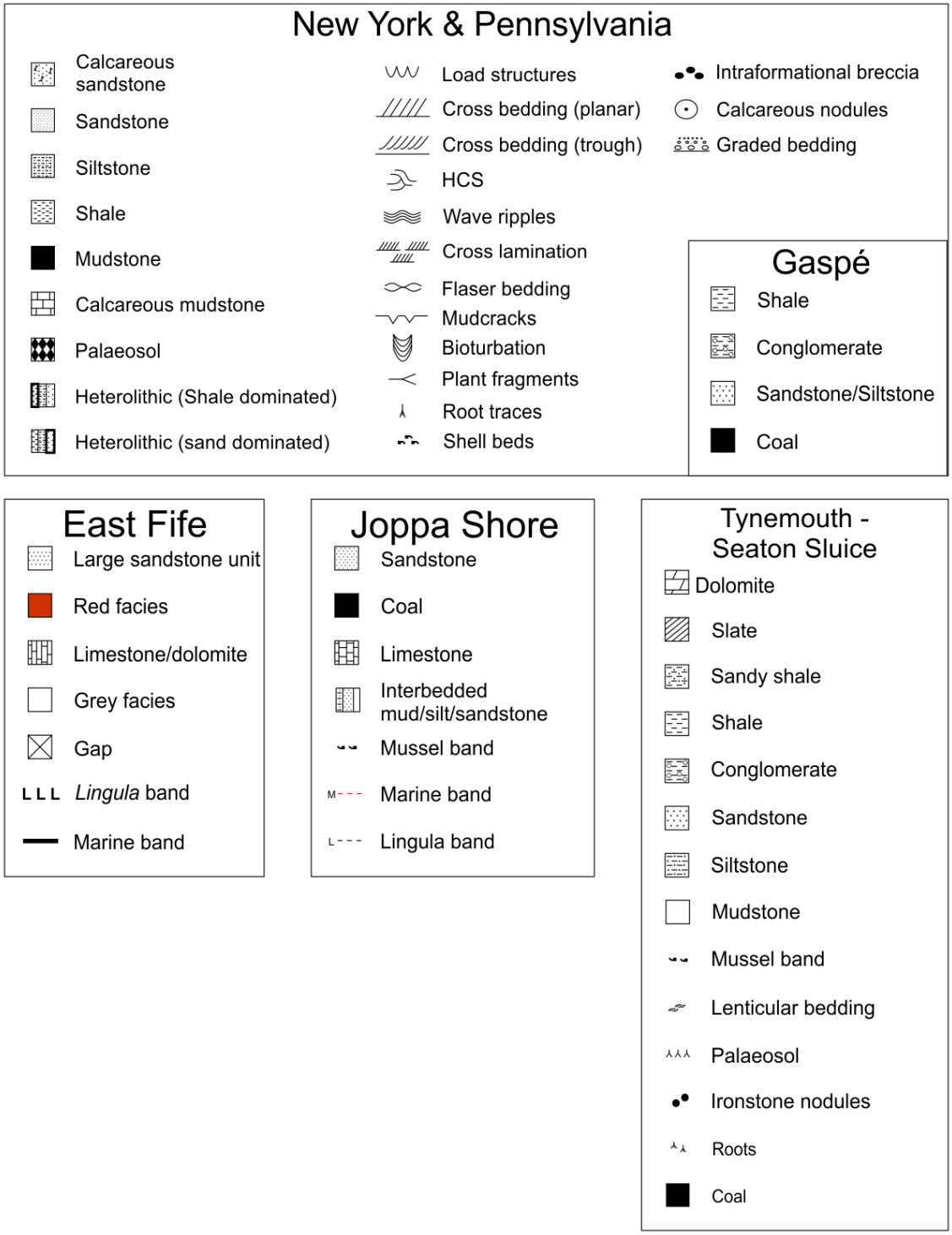

9. References

Abdullah, W. H., Murchison, D, Jones, J. M. Telnaes, N. and Gjelberg, J. 1987. Lower Carboniferous coal depositional environments on Spitsbergen, Svalbard. *Organic Geochemistry*, **13**, 953–964.

Absalom, R. G. and Hopkins, W. 1926. The geological relations of the coast section between Tynemouth and Seaton Sluice. *Proceedings of the University of Durham Philosophical Society*, **7**, 142–157.

Aldiss, D. T. and Edwards, E. J. 1999. The geology of the Falkland Islands. *British Geological Survey Technical Report WC/99110,* 135 pp.

Algeo, T. J. and Ingall, E. 2007. Sedimentary C_{org}:P ratios, paleocean ventilation, and Phanerozoic atmospheric pO_2. *Palaeogeography, Palaeoclimatology, Palaeoecology*, **256**, 130–155.

Ali, A. A., Higuera, P. E., Bergeron, Y. and Carcaillet, C. 2009. Comparing fire-history interpretations based on area, number, and estimated volume of macroscopic charcoal in lake sediments. *Quaternary Research*, **72**, 462–468.

Alpern, B. and Lemos de Susa, M. J. 1970. Sur le pouvoir réflecteur de la vitrinite et de la fusinite des houilles. *Comptes Rendus de l'Académie des Sciences, Paris, Série D*, **271**, 956–959.

American Society for Testing and Materials (ASTM), 2014. D7708 - 14. Standard test method for microscopical determination of the reflectance of vitrinite dispersed in sedimentary rocks. 823–830 in: *Annual book of ASTM standards section 5 – Petroleum products, lubricants, and their fossil fuels. Volume 05.06 Gaseous Fuels; Coal and Coke; Bioenergy and Industrial Chemicals from Biomass*. ASTM International, West Conshohocken, PA, OI: 10.1520/D7708-11, http://www.astm.org/Standards/D7708.htm

Anderson, J. S., Smithson, T., Mansky, C. F., Meyer, T. and Clack, J. 2015. A diverse tetrapod fauna at the base of Romer's Gap. *PLOS One*, **10**, 1–27.

Anderton, R., 1985. Sedimentology of the Dinantian of Foulden, Berwickshire, Scotland. *Transactions of the Royal Society of Edinburgh, Earth Sciences*, **76**, 7–12.

Andrews, J. E., Turner, M. S., Nabi, G. and Spiro, B. 1991. The anatomy of an early Dinantian terraced floodplain: palaeo-environment and early diagenesis. *Sedimentology,* **38**, 271–287.

Arvidson, R. S., Mackenzie, F. T. and Guidry, M. 2006. MAGic: A Phanerozoic model for the geochemical cycling of major rock-forming components. *American Journal of Science*, **306**, 135–190.

Astin, T. R., Marshall, J. E. A., Blom, H. and Berry, C. M. 2010. The sedimentary environment of the Late Devonian East Greenland tetrapods. 93–109 in: Vecoli, M., Clement, G. and Meyer-Berthaud, B. (*eds*.). *The terrestrialization process: modelling complex interactions at the biosphere-geosphere interface*. *Geological Society, London, Special Publications, 339.* Geological Society Publishing House, Bath, 192 pp.

Austen, D. E. G., Ingram, D. J. B., Given, P. H., Binder, C. R. and Hill, L. W. 1966. Electron spin resonance study of pure macerals. 344–362 in: Given, P. H. (*ed*). *Coal Science. Advances in Chemistry Series, 55*. American Chemical Society, Washington, D.C., 743 pp.

Baird, G. C. and Brett, C. E. 2008. Late Givetian Taghanic bioevents in New York State: new discoveries and questions. *Bulletin of Geosciences*, **83**, 357–370.

Banks, H. P. 1966. Devonian flora of New York State. *Empire State Geogram*, **4**, 10–24.

Banks, H. P. and Davis, M. R. 1969. Crenaticaulis, a new genus of Devonian plants allied to Zosterophyllum, and its bearing on the classification of early land plants. *American Journal of Botany*, **56**, 436–449.

Banks, H. P., Bonamo, P. M. and Grierson, J. D. 1972. *Leclercqia complexa* gen. et sp. nov., a new lycopod from the late Middle Devonian of eastern New York. *Review of Palaeobotany and Palynology,* **14**, 19–40.

Banks, H. P., Grierson, J. D. and Bonamo, P. M. 1985. The flora of the Catskill Clastic Wedge. 125–141 in: Woodrow, D. L. and Sevon, W. D. (*eds*.). *The Catskill Delta. Geological*

Society of America Special Paper 201. Geological Society of America, Boulder, Colorado, 246 pp.

Barrell, J. 1916. Influence of Silurian-Devonian climates on the rise of air-breathing vertebrates. *Bulletin of the Geological Society of America*, **27**, 387–436.

Bartholomew, A., Schramm, T, Ver Straeten, C. and Over, J. 2009. Refining the Timing of Faunal Turnover in the Middle Devonian Appalachian Basin: Paleoecological Analysis of the Earliest Hamilton Fauna and a Revision of the Base of the Givetian Stage in Eastern North America. 10.1–10.20 in: Vollmer, F. W. (*ed*.). *New York Geological Association 81st annual meeting field trip guidebook*. New York State Geological Association, New York, 256 pp.

Batten, D. J. 1981. Palynofacies, organic maturation and source potential for petroleum. 201–223 in: Brooks, J. (*ed*.). *Organic maturation studies and fossil fuel exploration*. Academic Press, London, 441 pp.

Batten, D. J. 1996. Palynofacies and palaeoenvironmental interpretation. 1011–1064 in: Jansonius, J. and McGregor, D. C. (*eds*.). *Palynology: principles and applications, volume 3.* American Association of Stratigraphic Palynologists Foundation, Dallas, 1330 pp.

Batten, D. J. 2002. Palynofacies and palaeoenvironmental interpretation. 1011–1084 in: Jansonius, J. and McGregor, D. C. (*eds*.). *Palynology: principles and applications, volume 3 (2nd ed.).* American Association of Stratigraphic Palynologists Foundation, Dallas, 1330 pp.

Beck, C. W. 1988. In reply: is air in amber ancient? *Science*, **241**, 718–719.

Beck, J. H. and Strother, P. K. 2008. Miospores and cryptospores from the Silurian section at Allenport, Pennsylvania, USA. *Journal of Paleontology*, **82**, 857–883.

Becker, R. T., Königshof, P. and Brett, C. E. 2016. Devonian climate, sea level and evolutionary events: an introduction. 1–10 in: Becker, R. T., Königshof, P. and Brett, C. E. (*eds*.). *Devonian climate, sea level and evolutionary events. Geological Society special publication 423*. Geological Society Publishing House, Bath, 481 pp.

Beerling, D. J. and Berner, R. A. 2005. Feedbacks and the coevolution of plants and atmospheric CO_2. *Proceedings of the National Academy of Sciences*, **102**, 1302–1305.

Beerling, D. J., Osbourne, C. P. and Chaloner, W. G. 2001. Evolution of leaf-form in land plants linked to atmospheric CO_2 decline in the Late Palaeozoic era. *Nature*, **410**, 352–354.

Belcher, C. M., Collinson, M. E., Sweet, A. R., Hildebrand, A. R. and Scott, A. C. 2003. Fireball passes and nothing burns – the role of thermal radiation in the Cretaceous-Tertiary event: evidence from the charcoal record of North America. *Geology*, **31**, 1061–1064.

Belcher, C. M. and McElwain, J. C. 2008. Limits for combustion in low O2 redefine paleoatmospheric predictions for the Mesozoic. *Science*, **321**, 1197–1200.

Belcher, C. M., Yearsley, J. M., Hadden, R. M., McElwain, J. C. and Guillermo, R. 2010. Baseline intrinsic flammability of Earth's ecosystems estimated from paleoatmospheric oxygen over the past 350 million years. *Proceedings of the National Academy of Sciences*, **107**, 22448–22453.

Belcher, C. M., Mander, L., Rein, G., Jervis, F. X., Haworth, M., Hesselbo, S. P., Glasspool, I. J. and McElwain, J. C. 2010b. Increased fire activity at the Triassic/Jurassic boundary in Greenland due to climate-driven floral change. *Nature Geoscience*, **3**, 426–429.

Belcher, C. M., Collinson, M. E. and Scott, A. C. 2013. A 450-million-year history of fire. 229–249 in: Belcher, C. M. (*ed*.). *Fire phenomena and the Earth system. An interdisciplinary guide to fire science*. Wiley-Blackwell, Chichester, 333 pp.

Belkin, H. E., Tewalt, S. J., Hower, J. C., Stucker, J. D. and O'Keefe, J. M. K. 2009. Geochemistry and petrology of selected coal samples from Sumatra, Kalimantan, Sulawesi, and Papua, Indonesia. *International Journal of Coal Geology*, **77**, 260–268.

Benaglia, T., Chauveau, D., Hunter, D. R. and Young, D. 2009. Mixtools: an R package for analyzing finite mixture models. *Journal of Statistical Software*, **32**, 1–29.

Bend, S. L. and Kosloski, D. M. 1993. A petrographic examination of coal oxidation. *International Journal of Coal Geology,* **24**, 233–243.

Benedict, L. G. and Berry, W. F. 1964. *Recognition and measurement of coal oxidation*. Bituminous Coal Research Inc., Monroeville, 41 pp.

Benedict, L. G. and Berry, W. F. 1966. Further applications of coal petrography. 577 – 601 in: Given, P. H. (ed.). *Coal Science. Advances in Chemistry series, 55*. American Chemical Society, Washington DC, 743 pp.

Bennett, C. E, Kearsey, T. I., Davies, S. J., Millward, D., Clack, J. A., Smithson, T. R. and Marshall, J. E. A. 2016. Early Mississippian sandy siltstones preserve rare vertebrate fossils in seasonal flooding episodes. *Sedimentology*, **63**, 1677–1700.

Bennett, C. E, Kearsey, T. I., Davies, S. J., Leng, M. J., Millward, D., Smithson, T. R., Brand, P. J., Browne, M. A. E., Carpenter, D. K. and Marshall, J. E. A. 2017. Mississippian coastal lakes and marshes provide habitat for emerging life on land. *Geological Society of America Bulletin*, in press.

Berg, T. M. and Edmunds, W. E. 1979. *Pennsylvania Geological Survey Circular 83, The Huntley Mountain Formation Catskill-to-Burgoon transition in north-central Pennsylvania*. Commonwealth of Pennsylvania Department of Environmental Resources, Bureau of Topographic and Geologic survey, Harrisburg, 80 pp.

Bergman, N. M., Lenton, T. M. and Watson, A. J. 2004. COPSE: A new model of biogeochemical cycling over Phanerozoic time. *American Journal of Science*, **304**, 397–437.

Berna, F., Goldberg, P., Horwitz, L. K., Brink, J., Holt, S., Bamford, M. and Chazan, M. 2012. Microstratigraphic evidence of in situ fire in the Archeulean strata of Wonderwerk Cave, Northern Cape province, South Africa. *Proceedings of the National Academy of Sciences,* **109**(20), E1215–E1220.

Berner, R. A. 1987. Models for carbon and sulfur cycles and atmospheric oxygen: applications to Paleozoic geologic history. *American Journal of Science*, **287**, 177–196.

Berner, R. A. 1989. Biogeochemical cycles of carbon and sulfur and their effect on atmospheric oxygen over Phanerozoic time. *Palaeogeography, Palaeoclimatology, Palaeoecology*, **75**, 87–122.

Berner, R. A. 1992. Weathering, plants and the long-term carbon cycle. *Geochimica et Cosmochimica Acta*, **56**, 3225–3231.

Berner, R. A. 1997. The rise of plants and their effect on weathering and atmospheric CO_2. *Science*, **276**, 544–546.

Berner, R. A. 1999. Atmospheric oxygen over Phanerozoic time. *Proceedings of the National Academy of Sciences*, **96**, 10955–10957.

Berner, R. A. 2001. Modeling atmospheric O_2 over Phanerozoic time. *Geochimica et Cosmochimica Acta*, **65**, 685–694.

Berner, R. A. 2004. The Phanerozoic Carbon Cycle: CO_2 and O_2. Oxford University Press, Oxford, 160 pp.

Berner, R. A. 2006. GEOCARBSULF: A combined model for Phanerozoic atmospheric O_2 and CO_2. *Geochimica et Cosmochimica Acta*, **70**, 5653–5664.

Berner, R. A. 2009. Phanerozoic atmospheric oxygen: new results using the GEOCARBSULF model. *American Journal of Science*, **309**, 603–606,

Berner, R. A. and Landis, G. P. 1988. Gas bubbles in fossil amber as possible indicators of the major gas composition of ancient air. *Science*, **239**, 1406.

Berner, R. A. and Canfield, D. E. 1989. A new model for atmospheric oxygen over Phanerozoic time. *American Journal of Science*, **289**, 333–361.

Berner, R. A., Beerling, D. J., Dudley, R., Robinson, J. M. and Wildman, R. A. Jr. 2003. Phanerozoic atmospheric oxygen. *Annual Review of Earth and Planetary Sciences*, **31**, 105–134.

Berkner, L. V. and Marshall, L. C. 1965. On the origin and rise of oxygen concentration in the Earth's atmosphere. *Journal of the Atmospheric Sciences*, **22**, 225–261.

Bischoff, G. and Ziegler, W. 1957. Die Conodonten-cronologie des Mittledevons und des tiefsten Oberdevons. *Abhandlungn des Hessischen Landesamtes für Bodenforschung*, **22**, 136.

Bishuk, D., Applebaum, R. & Ebert, J. E. 1991. Storm-dominated shelf and tidally-influenced foreshore sedimentation, Upper Devonian Sonyea Group, Bainbridge to Sidney Center, New York. 413–462 in: Ebert, J. R. (*ed*.). *New York State Geological Association 63rd annual meeting field trip guidebook*. New York State Geological Association, Albany, 488 pp.

Bishuk, D., Hairabedian, J. and Ebert, J. R. 2003. Trip A-2. Coastal margin interfluve paleosols and their stratigraphic relationships with tidally-influenced deltaic deposits in the Sonyea Group (Frasnian) of northwestern Delaware County, New York. 55–101 in: Johnson, E. L. (*ed*.). *New York State Geological Association 75th annual meeting field trip guidebook*. New York State Geological Association, Albany, 321 pp.

Bisat, W. S. 1924. The Carboniferous goniatites of the north of England and their zones. *Proceedings of the Yorkshire Geological Society,* **20**, 40.

Blair, N. E. and Aller, R. C. 2012. The fate of terrestrial organic carbon in the marine environment. *Annual Review of Marine Science*, **4**, 401–423.

Blair, N. E., Leithold, E. L., Ford, S. T., Peeler, K. A., Holmes, J. C. and Perkey, D. W. 2003. The persistence of memory: the fate of ancient sedimentary organic carbon in a modern sedimentary system. *Geochimica et Cosmochimica Acta*, **67**, 63–73.

Blair, N. E., Leithold, E. L., Brackley, H. Trustrum, N., Page, M. and Childress, L. 2010. Terrestrial sources and export of particulate organic carbon in the Waipaoa sedimentary system: problems, progress and processes. *Marine Geology*, **270**, 108–118.

Blokker, P., Yeloff, D., Boelen, P., Brockman, R. A. and Rozema, J. 2005. Development of a proxy for past surface UV-B irradiation: a thermally assisted hydrolysis and methylation py-GC/MS method for the analysis of pollen and spores. *Analytical Chemistry*, **77**, 6026–6031.

Bojesen-Koefoed, J. A., Petersen, H. I., Surlyk, F. and Vosgerau, H. 1997. Organic petrography and geochemistry of inertinite-rich mudstones, Jakobsstigen Formation, Upper Jurassic, northeast Greenland: Indications of forest fires and variations in relative sea-level. *International Journal of Coal Geology*, **34**, 345–370.

Boucot, A. J., 1975. *Evolution rates and extinction rate controls*. Elsevier, New York, 413 pp.

Bridge, J. S. and Willis, B. J. 1991. Middle Devonian near-shore marine, coastal and alluvial deposits, Schoharie Valley, central New York State. 131–160 in: Ebert, J. R. (*ed*.). *New York State Geological Association 63rd annual meeting field trip guidebook*. New York State Geological Association, Oneonta, New York, 488 pp.

Bridge, J. S. and Willis, B. J. 1994. Marine transgressions and regressions recorded in middle Devonian shore-zone deposits of the Catskills clastic wedge. *Geological Society of America Bulletin*, **11**, 1440–1458.

Bridge, J. S., Gordon, E. A. and Titus, R. C. 1986. Non-marine bivalves and associated burrows in the Catskill magnafacies (Upper Devonian) of New York State. *Palaeogeography, Palaeoclimatology, Palaeoecology*, **55**, 65–77.

Briggs, D. E. G. 1985. Gigantism in Palaeozoic arthropods. *Special Papers in Palaeontology*, **33**, 157.

Brongniart, C. 1884. Sur un gigantesque Neurorthoptère, provenant des terrains houillers de Commentry (Allier). *Comptes Rendus Hebdomadaires des Séances de l'Académie des Sciences*, **98**, 832–833.

Browne, M. A. E., Dean, M. T., Hall, I. H. S., McAdam, A. D., Monro, S. K. and Chisholme, J. I. 1999. A lithostratigraphical framework for the Carboniferous rocks of the Midland Valley of Scotland, Version 2. *British Geological Survey Research Report RR/99/07*, 30 pp.

Bultynck, P., 1987. Pelagic and neritic conodont successions from the Givetian of Pre-Sahara Morocco and the Ardennes. *Bulletin Institut Royal des Sciences Naturelles de Belgique. Sciences de la Terre*, **57**, 149–181.

Bustin, R. M., Cameron, A., Grieve, D. and Kalkreuth, W. 1985. *Geological Association of Canada short course notes volume 3: Coal Petrology, its Principles, Methods and Applications (2nd ed.)*. Geological Association of Canada, St. John's, 230 pp.

Calemma, V., Del Piero, G., Rausa, R. and Girardi, E. 1995. Changes in optical properties of coals during air oxidation at moderate temperature. *Fuel*, **74**, 383–388.

Canfield, D. E. 2005. The early history of atmospheric oxygen: homage to Robert M. Garrels. *Annual Review of Earth and Planetary Sciences,* **33**, 1–36.

Canfield, D. E., Poulton S. W. and Narbonne, G. M. 2007. Late-Neoproterozoic deep-ocean oxygenation and the rise of animal life. *Science*, **315**, 92–95.

Carpenter, F. M. 1992. *Treatise on Invertebrate Paleontology, Part R, Arthropoda 4*, *volume 3 and 4, superclass Hexapoda.* University of Kansas Press, Lawrence, Kansas, 655 pp.

Cater J. M. L., Briggs D. E. G. and Clarkson, E. N. K. Shrimp-bearing sedimentary successions in the Lower Carboniferous (Dinantian) Cementstone and Oil Shale Groups of northern Britain. *Transactions of the Royal Society of Edinburgh, Earth Sciences*, **80**, 5–15.

Chandra, D. 1958. Reflectance of oxidized coals. *Economic Geology*, **53**, 102–108.

Chandra, D. 1962. Reflectance and microstructure of weathered coals. *Fuel*, **41**, 185–193.

Chandra, D. 1966. Effect of storage of coals on reflectance and petrological composition. *Economic Geology*, **61**, 754–759.

Chave, K. E. and Smith, S. V. 1988. In reply: is air in amber ancient? *Science*, **241**, 719–720.

Chayes, F. 1956. *Petrographic modal analysis: an elementary statistical appraisal*. John Wiley & Sons, New York, 113 pp.

Chen, H., Zhao, W. and Liu, N. 2011. Thermal analysis and decomposition kinetics of Chinese forest peat under nitrogen and air atmospheres. *Energy Fuels*, **25**, 797–803.

Chen, Y., Mastalerz, M. and Schimmelmann, A. 2012. Characterization of chemical functional groups in macerals across different coal ranks via micro-FTIR spectroscopy. *International Journal of Coal Geology*, **104**, 22–33.

Chen, Y., Caro, L. D., Mastalerz, M., Schimmelmann, A. and Blandon, A. 2013. Mapping the chemistry of resinite, funginite and associated vitrinite in coal with micro-FTIR. *Journal of Microscopy*, **249**, 69–81.

Chen, Y., Mastalerz, M. and Schimmelmann, A. 2014. Heterogeneity of shale documented by micro-FTIR and image analysis. *Journal of Microscopy*, **256**, 177–189.

Chen, Y., Zou, C., Mastalerz, M., Hu, S., Gasaway, C. and Tao, X. 2015. Applications of Micro-Fourier Transform Infrared Spectroscopy (FTIR) in the geological sciences – a review. *International Journal of Molecular Sciences*, **16**, 30223–30250.

Christian, H. J., Blakeslee, R. J., Boccippio, D. J., Boeck, W. L., Buechler, D. E., Driscoll, K. T., *et al*., 2003. Global frequency and distribution of lightning as observed from space by the Optical Transient Detector. *Journal of Geophysical Research: Atmosphere*, **108**, ACL4-1–ACL4-15.

Christy, A. A., Hopland, A. L., Barth, T. and Kvalheim, O. M. 1989. Quantitative determination of thermal maturity in sedimentary organic matter by diffuse reflectance infrared spectroscopy of asphaitenes. *Organic Geochemistry*, **14**, 77–81.

Clack, J. A. 2002. An early tetrapod from 'Romer's Gap'. *Nature*, **418**, 72–76.

Clack, J. A. 2007. Devonian climate change, breathing, and the origin of the tetrapod stem group. *Integrative and comparative biology*, **4**, 510–523.

Clack, J. A. 2011. *Gaining ground: the origin and evolution of tetrapods (2nd edition)*. Indiana University Press, Bloomington and Indianapolis, 557 pp.

Clack, J. A., Bennett, C. E., Carpenter, D., Davies, S. J., Fraser, N. C., Kearsey, T. I., Marshall, J. E. A., Millward, D., Otoo, B. K. A., Reeves, E. J., Ross, A. J., Ruta, M., Smithson, K. Z., Smithson, T. R. and Walsh, S. A. 2016. Phylogenetic and environmental context of a Tournaisian tetrapod fauna. *Nature Ecology and Evolution*, **1**, 0002.

Clapham, M. E. and Carr, J. A. 2012. Environmental and biotic controls on the evolutionary history of insect body size. *Proceedings of the National Academy of Sciences*, **109**, 10927–10930.

Clark, R. L. 1982. Point count estimation of charcoal in pollen preparations and thin sections of sediments. *Pollen et Spores*, **24**, 523–535.

Clark, R. I. 1985. Effects on charcoal of pollen preparation procedures. *Pollen et spores*, **26**, 559–76.

Clark, J. S. 1988. Stratigraphic charcoal analysis on petrographic thin sections: application to fire history in northwestern Minnesota. *Quaternary Research*, **30**, 81–91.

Clayton, G., Coquel, R., Doubinger, J., Gueinn, K.J., Loboziak, S., Owens, B. and Streel, M., 1977. Carboniferous miospores of western Europe: illustration and zonation. *Mededelingen Rijks Geologische Dienst*, **29**, 1–71.

Cleal, C. J. and Thomas, B. A. 1996. *British Upper Carboniferous Stratigraphy*. Chapman and Hall, London, 339 pp.

Cloud, P. E. Jr. 1968. Atmospheric and hydrospheric evolution on the primitive earth. Both secular accretion and biological and geochemical processes have affected earth's volatile envelope. *Science*, **160**, 729–736.

Coates, M. I. and Clack, J. C. 1991. Fish-like gills and breathing in the earliest known tetrapod. *Nature*, **352**, 234–236.

Coates, M. I. and Clack, J. A. 1995. Romer's Gap: tetrapod origins and terrestriality. *Bulletin du Muséum Nationale d'Histoire Naturelle, Paris*, **17**, 373–388.

Cochran, W. G. 1977. *Sampling techniques 3rd edition*. New York, Wiley, 448 pp.

Cohen-Ofri, I., Weiner, L., Boaretto, E., Mintz, G. and Weiner, S. 2006. Modern and fossil charcoal: aspects of structure and diagenesis. *Journal of Archaeological Science*, **33**, 428–439.

Collins, A. 1990. The 1–10 spore colour index (SCI) scale: a universally applicable colour maturation scale, based on graded, picked palynomorphs. *Mededelingen Rijks Geologisce Dienst*, **45**, 39–47.

Cook, A. C. and Taylor, G. 1963. The petrography of some Triassic Ipswich coals. *The Australasian Institute of Mining and Metallurgy*, **205**, 33–35.

Copard, Y., Disnar, J-R., Becq-Giraudon, J-F. and Laggoun-Défarge, F. 2004. Erroneous coal maturity assessment caused by low temperature oxidation. *International Journal of Coal Geology*, **58**, 171–180.

Cope, M. J. and Chaloner, W. G. 1980. Fossil charcoal as evidence of past atmospheric composition. *Nature*, **283**, 647–649.

Corlett, R. T. 1979. Human impact on the subalpine vegetation of Mt. Wilhelm, Papua New Guinea. *Unpublished PhD thesis*, Australian National University, Canberra.

Cotter, E. 1990. Storm effects on siliciclastic and carbonate shelf sediments in the medial Silurian succession of Pennsylvania. *Sedimentary Geology*, **69**, 245–258.

Cotter, E. and Link, J. E. 1993. Deposition and diagenesis of Clinton ironstones (Silurian) in the Appalachian Foreland Basin of Pennsylvania. *Geological Society of America Bulletin*, **105**, 911–922.

Coward, H. F. and Jones, G. W. 1953. Limits of flammability of gases and vapours. *United States Department of the Interior Bureau of Mines Bulletin*, **503**, 155 pp.

Crawford, A. J. and Belcher, C. M. 2014. Charcoal Morphometry for Paleoecological Analysis: The Effects of Fuel Type and Transportation on Morphological Parameters. *Applications in plant sciences*, **2**, 1400004.

Crawford, A. J. and Belcher, C. M. 2016. Area–volume relationships for fossil charcoal and their relevance for fire history reconstruction. *The Holocene*, **26**, 822–826.

Cressler III, W. L. 2001. Evidence of earliest known wildfires. *Palaios*, **16**, 171–174.

Cressler III, W. L. 2006. Plant paleoecology of the Late Devonian Red Hill locality, north-central Pennsylvania, an Archaeopteris-dominated wetland plant community and early

tetrapod site. 79–102 in: Greb, F. and DiMichele, W. A. (*eds*.). *Wetlands through time. Geological Society of America special publication 399*. Geological Society of America, Boulder, Colorado, 332 pp.

Cressler III, W. L., Daeschler, E. B., Slingerland R. and Peterson, D. A. 2010. Terrestrialization in the Late Devonian: A palaeoecological overview of the Red Hill site, Pennsylvania, USA. 111–128 in: Vecoli, M., Clement, G. and Meyer-Berthaud, B. (*eds*.). *The terrestrialization process: modelling complex interactions at the biosphere-geosphere interface. Geological Society Special Publication 339*. Geological Society Publishing House, Bath, 192 pp.

Currie, E. D. 1954. Scottish Carboniferous Goniatites. *Transactions of the Royal Society of Edinburgh*, **62**, 527–602.

Cutbill, J. L. and Challinor, A. 1965. Revision of the Stratigraphical Scheme for the Carboniferous and Permian Rocks of Spitsbergen and Bjameya. *Geological Magazine*, **102**, 418–439.

Daber, R. 1960. *Eogaspesiea gracilis* n. g. n. sp. *Geologie*, **9**, 418–425.

Daeschler, E. B. 2000. An early actinopterygian fish from the Catskill Formation (Late Devonian, Famennian) in Pennsylvania, U.S.A. *Proceedings of the Academy of Natural Sciences of Philadelphia*, **150**, 181–192.

Daeschler, T. and Cressler, W. 2006. *Paleontology and paleoenvironments of the upper Devonian Catskill Formation in north-central Pennsylvania. Geological Society of America post-meeting fieldtrip, 26–27 October 2006*. Academy of Natural Sciences, Pennsylvania State University, 48 pp.

Daeschler, E. B. and Cressler, W. L. III. 2011. Late Devonian paleontology and paleoenvironments at Red Hill and other fossil sites in the Catskill Formation of north-central Pennsylvania. 1–16 in: Ruffolo, R. M. and Ciampaglio, C. N. (*eds*.). *From the Shield to the Sea: Geological Trips from the 2011 Joint Meeting of the GSA Northeastern and North-Central Sections*. *Geological Society of America Field Guide 20*. Geological Society of America, Boulder, Colorado, 186 pp.

Daeschler, E. B., Shubin, N. H., Thomson, K. S. and Amaral, W. W. 1994. A Devonian tetrapod from North America. *Science*, **265**, 639.

Dallmann, W. K. (*ed*.) 1999. *Lithostratigraphic Lexicon of Svalbard: review and recommendations for nomenclature use. Upper Palaeozoic Quaternary Bedrock*. Norwegian Polar Institute, Tromsø, 318 pp.

Davies, N. S. and Gibling, M. R. 2010. Cambrian to Devonian evolution of alluvial systems: The sedimentological impact of the earliest land plants. *Earth-Science Reviews*, **98**, 171–200.

Davis, A. 1975. Developments in the techniques of coal microscopy. *Microstructural Science*, **3**, 973–990.

Dawson, J. W. 1859. On fossil plants from the Devonian rocks of Canada. *Quarterly Journal of the Geological Society, London,* **15**, 477-488.

Dempster, A. P., Laird, N. M. and Rubin, D. B. 1977. Maximum likelihood from incomplete data via the EM algorithm. *Journal of the Royal Statistical Society. Series B (methodological)*, **39**, 1–38.

Desantis, M. K., Brett, C. E. and Ver Straeten, C. A. 2007. Persistent depositional sequences and bioevents in the Eifelian (early Middle Devonian) of eastern Laurentia: North American evidence of the Kačák events? 83–104 in: Becker, R. T. and Kirchgasser, W. T. (*eds*.). *Devonian events and correlations. Geological Society Special Publication 278*. Geological Society Publishing House, Bath, 280 pp.

Diessel, C. F. 2010. The stratigraphic distribution of inertinite. *International Journal of Coal Geology*, **81**, 251–268.

Dobel, P., Cameron, A. R. and Kalkreuth, W. D. 1984. Petrographic examination of low-rank coals from Saskatchewan and British Columbia, Canada, including reflected and fluorescent light microscopy, SEM, and laboratory oxidation procedures. *Canadian Journal of Earth Sciences*, **21**, 1209–1228.

Domagal-Goldman, S. D., Kasting, J. F., Johnston, D. T. and Farquhar, J. 2008. Organic haze, glaciations and multiple sulfur isotopes in the Mid-Archean Era. *Earth and Planetary Science Letters*, **269**, 29–40.

Dorrington, G. E. 2012. On flying insect size and Phanerozoic atmospheric oxygen. *Proceedings of the National Academy of Sciences*, **109**, E3393.

Dow, W. G. 1977. Kerogen studies and geological applications. *Journal of Geochemical Exploration*, **7**, 79–99.

Downs, J. P. and Daeschler, E. B. 2001. Variation within a large sample of *Ageleodus pectinatus* teeth (Chondrichthyes) from the Late Devonian of Pennsylvania, U.S.A. *Journal of Vertebrate Paleontology*, **21**, 811–814.

Dudley, R. 1998. Atmospheric oxygen, giant Paleozoic insects and the evolution of aerial locomotor performance. *The Journal of Experimental Biology*, **201**, 1043–1050.

Ebelmen, J. J. Sur les produits de la decomposition des especes minérales de la famille des silicates. *Annales des Mines*, **7**, 3–66.

Edney, P. A., Kershaw, A. P. and De Deckker, P. 1990. A late Pleistocene and Holocene vegetation and environmental record from Lake Wangoom, Western Plains of Victoria, Australia. *Palaeogeography, Palaeoclimatology, Palaeoecology*, **80**, 325–43.

Edwards, W. N. 1924. On the cuticular structure of the Devonian plant Psilophyton. *Journal of the Linnean Society (Botany)*, **46**, 377–385.

Edwards, D. and Axe, L. 2004. Anatomical Evidence in the Detection of the Earliest Wildfires. *Palaios*, **19**, 113–128.

Edwards, D., Morris, J. L., Richardson, J. B. and Kenricks, P. 2014. Cryptospores and cryptophytes reveal hidden diversity in early land floras. *New Phytologist*, **202**, 50–78.

Elick, J. M., Driese, S. G. and Mora, C. I. 1998. Very large plant and root traces from the Early to Middle Devonian: Implications for early terrestrial ecosystems and atmospheric pCO_2. *Geology*, **26**, 143–146.

Enache, M. D. and Cumming, B. F. 2005. Tracking recorded fires using charcoal morphology from the sedimentary sequence of Prosser Lake, British Columbia (Canada). *Quaternary Research*, **65**, 282–292.

Everitt, B. S. and Hand, D. J. 1981. *Monography on applied probability and statistics. Finite mixture distributions*. Chapman and Hall, London, 143 pp.

Faill, R. T. 1985. The Acadian Orogeny and the Catskill Delta. 15–37 in: Woodrow, D. L. and Sevon, W. D. (*eds*.). *The Catskill Delta. Geological Society of America special paper 201*. Geological Society of America, Boulder, Colorado, 246 pp.

Faill, R. T. 1997. A geologic history of the north-central Appalachians. Part 1: Orogenesis from the Mesoproterozoic through the Taconic Orogeny. *American Journal of Science*, **297**, 551–629.

Fairon-Demaret, M. and Hartkopf-Fröder, C. 2004. Late Famennian plant mesofossils from the Refrath 1 Borehole (Bergisch Gladbach–Paffrath Syncline; Ardennes–Rhenish Massif, Germany). *Courier Forschungsinstitut Senckenberg*, **251**, 89–121.

Falcon, R. M. S. and Snyman, C. P. 1986. *Introduction to coal petrography: Atlas of petrographic constituents in the bituminous coals from South Africa. Review Paper Number 2*. The Geological Society of South Africa, Johannesburg, 17pp.

Falcon-Lang, H. J. 1999. The Early Carboniferous (Courceyan–Arundian) monsoonal climate of the British Isles: evidence from growth rings in fossil woods. *Geological Magazine*, **136**, 177–187.

Falcon-Lang, H. J. 2000. Fire ecology of the Carboniferous tropical zone. *Palaeogeography, Palaeoclimatology, Palaeoecology*, **164**, 339–355.

Farquhar, J., Bao, H. and Thiemens, M. 2000. Atmospheric influence of Earth's earliest sulfur cycle. *Science*, **289**, 756–758.

Feist, M. and Hernick, L. V. 2014. *Monoecious Sycidium*, and other charophytes, from the Middle Devonian of eastern New York State, USA, with an update on the oldest bisexual plant. *Review of palaeobotany and palynology*, **200**, 188–195.

Finkelstein, D. B., Pratt, L. M., Curtin, T. M., and Brassell, S. C. 2005. Wildfires and seasonal aridity recorded in Late Cretaceous strata from south-eastern Arizona, USA. *Sedimentology*, **52**, 587–599.

Floudas, D., Binder, M., Riley, R., Barry, K., Blanchette, R. A., Henrissat, B., Martínez, A. T., Otillar, R., Spatafora, J. W., Yadav, J. S. and Aerts, A. 2012. The Paleozoic origin of enzymatic lignin decomposition reconstructed from 31 fungal genomes. *Science*, **336**, 1715–1719.

Forsythe, J. H. and Chisholm, M. A. 1977. *The geology of east Fife (Explanation of the Fife portion of 'one-inch' geological sheet 41 and part of sheet 49)*. HM Stationery Office, Edinburgh, 284 pp.

Fraley, C. and Raftery, A. E. 2006. MCLUST Version 3: an R package for normal mixture modelling and model-based clustering. Technical report no. 504, Dept. of Statistics, University of Washington. University of Washington, Seattle, 50 pp.

Franklin, R. E. 1951. Crystallite growth in graphitizing and non-graphitizing carbons. *Proceedings of the Royal Society A*, **209**, 196–218.

Ganz, H. and Kalkreuth, W. 1987. Application of infrared spectroscopy to the classification of kerogen types and the evaluation of source rock and oil shale potentials. *Fuel*, **66**, 708–711.

Garrels, R. M. and Perry, E. A. 1974. Cycling of carbon, sulfur, and oxygen through geologic time. 303-316 in: Goldberg, E. D. (*ed*.). *The Sea, Volume 5*. Wiley, New York, 914 pp.

Garrels, R. M. and Lerman, A. 1984. Coupling of the sedimentary sulfur and carbon cycles - an improved model. *American Journal of Science*, **284**, 989–1007.

George, A. M., 1975. *Brown coal lithotypes in the Latrobe Valley deposits*. Exploration and Geological Division, Planning and Investigation Department, State Electricity Commission of Victoria, Australia, Melbourne, 36 pp.

Gibling, M. R. and Davies, N. S. 2012. Palaeozoic landscapes shaped by plant evolution. *Nature Geoscience*, **5**, 99–105.

Glasspool, I. J. 2000. A major fire event recorded in the mesofossils and petrology of the Late Permian, Lower Whybrow coal seam, Sydney Basin, Australia. *Palaeogeogeography, Palaeoclimatology, Palaeoecology*, **164**, 357–380.

Glasspool, I. J. and Scott, A. C. 2010. Phanerozoic concentrations of atmospheric oxygen reconstructed from sedimentary charcoal. *Nature Geoscience*, **3**, 627–630.

Glasspool, I. J., and Scott, A. C. 2013. Identifying past fire events. 179–205 in: Belcher, C. M. (ed). *Fire phenomena and the Earth System: An Interdisciplinary Guide to Fire Science*. John Wiley and Sons Ltd., Oxford, 333pp.

Glasspool, I. J., Edwards, D. and Axe, L. 2004. Charcoal in the Silurian as evidence for the earliest wildfire. *Geology*, **32**, 381–383.

Glasspool, I. J., Scott, A. C., Waltham, D., Pronina, N. and Shao, L. 2015. The impact of fire on the Late Paleozoic Earth system. *Frontiers in Plant Science*, **6**, 1–13.

Goodarzi, F. 1985. Organic petrology of Hat Creek coal deposit No. 1, British Columbia. *International Journal of Coal Geology*, **5**, 377–396.

Goodarzi, F., and Murchison, D. G. 1973. Oxidized vitrinites—their aromaticity, optical properties and possible detection. *Fuel*, **52**, 90–92.

Gomez, B., Brackley, H. L., Hicks, D. M., Neff, H. and Rogers, K. M. 2004. Organic carbon in floodplain alluvium: Signature of historic variations in erosion processes associated with deforestation, Waipaoa River basin, New Zealand. *Journal of Geophysical Research*, **109**, F04011.

Goni, M. A., Ruttenberg, K. C. and Eglinton, T. I. 1997. Sources and contribution of terrigenous organic carbon to surface sediments in the Gulf of Mexico. *Nature*, **389**, 275–278.

Goni, M. A., Ruttenberg, K. C. Eglinton, T. I. 1998. A reassessment of the sources and importance of land-derived organic matter in surface sediments from the Gulf of Mexico. *Geochimica et Cosmochimica Acta*, **62**, 3055–3075.

Goni, M. A., Yunker, M. B., Macdonald, R. W. and Eglinton, T. I. 2005. The supply and preservation of ancient and modern components of organic carbon in the Canadian Beaufort Shelf of the Arctic Ocean. *Marine Chemistry*, **93**, 53–73.

Gordon, E. A. and Bridge, J. S. 1987. Evolution of Catskill (Upper Devonian) river systems: intra- and extrabasinal controls. *Journal of Sedimentary Petrology*, **57**, 234–249.

Gradstein, F., Ogg, J., Schmitz, M. and Ogg, G. 2012. *The geologic timescale 2012*. Elsevier, Amsterdam, 1176 pp.

Grahn, Y. 2005. Devonian Chitinozoan biozones of western Gondwana. *Acta Geologica Polonica,* **55**, 211–227.

Graham, J. B. 1988. Ecological and evolutionary aspects of integumentary respiration: body size, diffusion, and the Invertebrata. *American Zoologist*, **28**, 1031–1045.

Graham, J. B. 1990. Ecological, evolutionary, and physical factors influencing aquatic animal respiration. *American Zoologist*, **30**, 137–146.

Graham, J. B., Dudley, R., Aguilar, N. M. and Gans, C. 1995. Implications of the late Palaeozoic oxygen pulse for physiology and evolution. *Nature*, **375**, 117–120.

Grahn, Y., Mendlowicz Mauller, P., Bergamaschi, S. & Bosetti, E. P. 2013. Palynology and sequence stratigraphy of three Devonian rock units in the Apucarana Sub-basin (Parana´ Basin, south Brazil): additional data and correlation. *Review of Palaeobotany and Palynology*, **198**, 27–44.

Greb, S. F., DiMichele, W. A. and Gastaldo, R. A. 2006. Evolution and importance of wetlands in earth history. 1–40 in: Greb, S. F., DiMichele, W. A. (*eds*.). *Wetlands through Time*. *Geological Society of America Special Paper 399.* Geological Society of America, Boulder, Colorado, 332 pp.

Griffing, D. H. and Ver Straeten, C. A. 1991. Stratigraphy and depositional environments of the lower part of the Marcellus Formation (Middle Devonian) in eastern New York State. 205–249 in: Ebert, J. R. (*ed*.). *New York State Geological Association 63rd annual meeting field trip guidebook*. New York State Geological Association, Plattsburgh, New York, 488 pp.

Griffing, D. H., Bridge, J. S. and Hotton, C. L. 2000. Coastal-fluvial palaeoenvironments and plant palaeoecology of the Lower Devonian (Emsian), Gaspé Bay, Quebec, Canada. 61–84 in: Friend, P. F. and Williams, B. P. J. (*eds*.). *New perspectives on the Old Red Sandstone*. *Geological Society of London Special Publication 180.* Geological Society Publishing House, Bath*,* 623 pp.

Guo, Y. and Bustin, R. M. 1998. FTIR spectroscopy and reflectance of modern charcoals and fungal decayed woods: implications for studies of inertinite in coals. *International Journal of Coal Geology*, **37**, 29–53.

Guo, L. and Macdonald. R. W. 2006. Source and transport of terrigenous organic matter in the upper Yukon River: evidence from isotope ($\delta^{13}C$, $\Delta^{14}C$, and $\delta^{15}N$) composition of dissolved, colloidal, and particulate phases. *Global Biogeochemical Cycles*, **20**, 1–12.

Hansen, K. W. and Wallmann, K. 2003. Cretaceous and Cenozoic evolution of seawater composition, atmospheric O_2 and CO_2: a model perspective. *American Journal of Science*, **303**, 94–148.

Harland, W. B. and Geddes, I. 1997. Carboniferous–Permian history of Svalbard. *Geological Society of London, Memoirs*, **17**, 310–339.

Harlé, É. and Harlé, A. 1911. Le vol de grands reptiles et insects disparus semble indiquer une pression atmosphérique levée. *Bulletin de la Société Géologique de France, 4 Serie,* **11**, 118–121.

Harrison, J. F., Kaiser, A. and VandenBrooks, J. M. 2010. Atmospheric oxygen level and the evolution of insect body size. *Proceedings of the Royal Society of London B: Biological Sciences*, **277**, 1937–1946.

Hartley, H. 0. 1958. Maximum likelihood estimation from incomplete data. *Biometrics*, **14**, 174–194.

Hedges, J. I., Clark, W. A., Quay, P. D., Richey, J. E., Devol, A. H. and Santos, U. de M. 1986. Compositions and fluxes of particulate organic material in the Amazon River. *Limnology and Oceanography*, **31**, 717–738.

Hedges, J. I., Keil, R. G. and Benner, R. 1997. What happens to terrestrial organic matter in the ocean? *Organic Geochemistry*, **27**, 195–212.

Helfrich, C. T. 1980. Late Llandovery-early Wenlock conodonts from the upper part of the Rose Hill and the basal part of the Mifflintown formations, Virginia, West Virginia, and Maryland. *Journal of Paleontology*, **54**, 557–569.

Hemsley, A. R., Scott, A. C., Barrie, P. J. and Chaloner, W. G. 1996. Studies of Fossil and Modern Spore Wall Biomacromolecules using ^{13}C Solid State NMR. *Annals of Botany*, **78**, 83–94.

Hernick, L. V., Landing, E. and Bartowski, K. E. 2008. Earth's oldest liverworts—*Metzgeriothallus sharonae* sp. nov. from the Middle Devonian (Givetian) of eastern New York, USA. *Review of palaeobotany and palynology*, **148**, 154–162.

Herring, J. R. 1985. Charcoal fluxes into sediments of the North Pacific Ocean: the Cenozoic record of burning. 419–442 in: Sundquist, E. T. and Broecker, W. S. (*eds*.). *The Carbon cycle and atmospheric CO_2: natural variations, Archean to present. Volume 32 of the geophysical monograph series.* American Geophysical Union, Washington D.C., 627 pp.

Higgs, K., Clayton, G. and Keegan, J. B. 1988. *The Geological Survey of Ireland special paper number 7. Stratigraphic and systematic palynology of the Tournaisian rocks of Ireland*. Geological Survey of Ireland, Dublin, 93 pp.

Hillier, S. and Marshall, J. 1988. A rapid technique to make polished thin sections of sedimentary organic matter concentrates. *Journal of Sedimentary Petrology*, **58**, 754–755.

Hilton, R. G., Galy, A. and Hovius, N. 2008. Riverine particulate organic carbon from an active mountain belt: importance of landslides. *Global Biogeochemical Cycles*, **22**, GB1017.

Holland, H. D. 1973. Systematics of the isotopic composition of sulfur in the oceans during the Phanerozoic and its implications for atmospheric oxygen. *Geochimica et Cosmochimica Acta*, **37**, 2605–2616.

Holland, H. D. 1978. *The chemistry of the atmosphere and oceans*. Wiley, New York, 369 pp.

Holland, H. D. 1984. *The chemical evolution of the atmosphere and oceans*. Princeton University Press, Princeton, 598 pp.

Hoover, D. S. and Davis, A. 1979. The role of automated reflectance microscopy in coal petrographic characterisation. *9th International Congress on Carboniferous Stratigraphy and Geology, Abstracts of Papers*, 91–92.

Hoover, D. S., Kuehn, K. W., Davis, A. and Vastola, F. J. 1976. Characterisation of coals by automated reflectance microscopy. *Geological Society of America Abstracts with Programs*, **8**, 925–926.

Hoover, D. S. and Davis, A. 1980. *The development and evaluation of an automated reflectance microscope system for the petrographic characterisation of bituminous coals*. Penn. State University, US Dept. of Energy Technical Report FE-2030-TR23, 261 pp.

Hopfenberg, H. B., Witchey, L. C. and Poinar, G. O., Jr. 1988. ls air in amber ancient? *Science*, **241**, 717–718.

Horibe, Y. and Craig, H. 1988. In reply: is air in amber ancient? *Science*, **241**, 720–721.

Hotton, C. L., Hueber, F. M., Griffing, D. H. and Bridge, J. S. 2001. Early terrestrial plant environments: an example from the Emsian of Gaspé, Canada. 179–212 in: Gensel, P. G. and Edwards, D. (*eds*.). *Plants invade the land: evolutionary and environmental perspectives*. University Press, New York, 304 pp.

Hower, J. C., Stanton, R. W., Gammidge, L. C. and Hutton, A. C. 1999. Atlas of coal geology volume II: coal petrology. American Association of Petroleum Geologists, Tulsa, 385 pp.

Hower, J. C., O'Keefe, J. M. K., Watt, M. A., Pratt, T. J., Eble, C. F., Stucker, J. D., Richardson, A. R. and Kostova, I. J. 2009. Notes on the origin of inertinite macerals in

coals: observations on the importance of fungi in the origin of macrinite. *International Journal of Coal Geology*, **80**, 135–143.

Hower, J. C., O'Keefe, J. M. K., Eble, C. F. , Raymond, A., Valentim, B., Volk, T. J., Richardson, A. R., Satterwhite, A. B., Hatch, R.S., Stucker, J.D. and Watt, M.A. 2011. Notes on the origin of inertinite macerals in coal: Evidence for fungal and arthropod transformations of degraded macerals. *International Journal of Coal Geology*, **86**, 231–240.

Huddle, J. F. and Repetski, J. E. 1981. Conodonts from the Genesee Formation in Western New York. *Geological Survey Professional Paper* **1032 – B**, 1–63.

Hudspith, V. A., Belcher, C. M. and Yearsley, J. M. 2014. Charring temperatures are driven by the fuel types burned in a peatland wildfire. *Frontiers in Plant Science*, **5**, 1–12.

Hueber, F. M. and Banks, H. P. 1979. *Serrulacaulis furcatus* gen. et sp. nov., a new zosterophyll from the lower Upper Devonian of New York State. *Review of Palaeobotany and Palynology*, **28**, 169–189.

Hünicken, M., Kullmann, J., Suarez Riglos, M., 1980. Consideraciones sobre el Devonico boliviano en base a un nuevo goniatites de la Formacion Huamampampa en Campo Redondo, Departamento Chuquisaca, Bolivia. *Boletín de la Academia Nacional de Ciencias,* **53**, 237–253.

Hunter, D. R., Wang, S. and Hettmansperger, T. P. 2007. Inference for mixtures of symmetric distribution. *The Annals of Statistics*, **35**, 224–251.

Hunter, M. A. and Lomas, S. A. 2003. Reconstructing the Siluro-Devonian coastline of Gondwana: insights from the sedimentology of the Port Stephens Formation, Falkland Islands. *Journal of the Geological Society, London*, **160**, 459–476.

Iglesias, M. J., Jiménez, A., Laggoun-Défarge, F., Suárez-Ruiz, I. 1995. FTIR study of pure vitrains and associated coals. *Energy and Fuels*, **9**, 458–466.

International Committee for Coal and Organic Petrology (ICCP). 1998. The new vitrinite classification (1998). *Fuel*, **77**, 349–358.

International Committee for Coal and Organic Petrology (ICCP). 2001. The new inertinite classification (ICCP System 1994). *Fuel*, **80**, 459–471.

Ittekot, V. 1988. Global trends in the nature of organic matter in river suspension. *Nature*, **332**, 436–438.

Jardine, P. E., Fraser, W. T., Lomax, B. and Gosling, W. D. 2015. The impact of oxidation on spore and pollen chemistry. *Journal of Micropalaeontology*, **34**, 239–249.

Jarvik, E. 1952. On the fish-like tail in the ichthyostegid stegocephalians with descriptions of a new stegocephalian and a new crossopterygian from the Upper Devonian of East Greenland. *Meddelelser om Grønland*, **114**, 1–90.

Jarvik, E. 1996. The Devonian tetrapod Ichthyostega. *Fossils and Strata*, **40**, 1–206.

Jiang, C., Alexander, R., Kagi, R. I. and Murray, A. P. 1998. Polycyclic aromatic hydrocarbons in ancient sediments and their relationships to palaeoclimate. *Organic Geochemistry*, **29**, 1721–1735.

Johnson, J. G. 1970. The Taghanic onlap and the end of North American Devonian provinciality. *Geological Society of America Bulletin,* **81**, 2077–2106.

Johnson, J. H. 1972. Evidence for tidal origin of Late Devonian clastics in eastern New York State, U.S.A. 285–293 in: McLaren, D. J. and Middleton, G. V. (*eds*.). *Proceedings of the 24th International Geological Congress, Montreal, Section 6, Stratigraphy and Sedimentology*. 24th International Geological Congress, Ottawa, 446 pp.

Johnson, J. H. and Friedman, G. M. 1969. The Tully clastic correlatives (Upper Devonian) of New York State: a model for recognition of alluvial, dune(?), tidal, nearshore (bar and lagoon), and offshore sedimentary environments in a tectonic delta complex. *Journal of Sedimentary Research*, **39**, 451–485.

Jones, J. M. 1967. Geology of the coast section from Tynemouth to Seaton Sluice. *Transactions of the Natural History Society of Northumberland, Durham and Newcastle upon Tyne*, **16**, 153–192.

Jones, V. J., Stevenson, A. C. and Battarbee, R. W. 1987. A palaeolimnological evaluation of peatland erosion. Report to NCC, Palaeoecological Research Unit, Department of Geography, University College London.

Jones, T. P., Scott, A. C. and Cope, M. J., 1991. Reflectance measurements and the temperature of formation of modern charcoals and implications for studies of fusain. *Bulletin de la Société Géologique de France*, **162**, 193–200.

Jones, T. P., Scott, A. C. and Mattey, D. P. 1993. Investigations of "fusain transition fossils" from the Lower Carboniferous: comparisons with modem partially charred wood. *International Journal of Coal Geology*, **22**, 37–59.

Jordan, H. and Meyer, H. V. 1854. Ueber die Crustaceen der Steinkohlenformation von Saarbrücken. *Palaeontographica,* **1846-1933**, 1–16.

Junge, C. E., Schidlowski, M., Eichmann, R. and Pietrek, H. 1975. Model Calculations for the Terrestrial Carbon Cycle: Carbon Isotope Geochemistry and Evolution of Photosynthetic Oxygen. *Journal of Geophysical Research*, **80**, 4542–4552.

Kaiser, S. I., Aretz, M. and Becker, R. T. 2015. The global Hangenberg Crisis (Devonian–Carboniferous transition): review of a first-order mass extinction. Becker, R. T., Königshof, P. and Brett, C. E. (*eds*). *Devonian Climate, Sea Level and Evolutionary Events. Geological Society of London Special Publication 423*. Geological Society Publishing House, Bath, 481 pp.

Kao, S. J. and Liu, K. K. 1996. *Limnology and Oceanography*, **41**, 1749–1757.

Kasting, J. F. 1993. Earth's early atmosphere. *Science*, **259**, 920–926.

Kasting, J. F. and Walker, J. C. 1981. Limits on oxygen concentration in the prebiological atmosphere and the rate of abiotic fixation of nitrogen. *Journal of Geophysical Research: Oceans*, **86**, 1147–1158.

Kasting, J. F. and Catling, D. 2003. Evolution of a habitable planet. *Annual Review of Astronomy and Astrophysics*, **41**, 429–463.

Kearsey, T. I., Bennett, C. E., Millward, D., Davies, S. J., Gowing , C. J. B., Kemp, S. J., Leng, M. J., Marshall, J. E. A., Michael, A.E. and Browne, M. A. E. 2016. The terrestrial landscapes of tetrapod evolution in earliest Carboniferous seasonal wetlands of SE Scotland. *Palaeogeography, Palaeoclimatology, Palaeoecology*, **457**, 52–69.

Keeley, J. E. 2009. Fire intensity, fire severity and burn severity: a brief review and suggested usage. *International Journal of Wildland Fire*, **18**, 116–126.

Keeley, J. E., Pausas, J. G., Rundel, P. W., Bond, W. J. and Bradstock, R. A. 2011. Fire as an evolutionary pressure shaping plant traits. *Trends in Plant Science,* **16**, 406–411.

Kennedy, K. L., Gibling, M. R., Eble, C. F., Gastaldo, R. A., Gensel, P. G., Werner-Zwanziger, U. and Wilson, R. A. 2013. Lower Devonian coaly shales of northern New Brunswick, Canada: plant accumulations in the early stages of Terrestrial colonization. *Journal of Sedimentary Research*, **83**, 1202–1215.

Kenrick, P. and Crane, P. R. 1997. The origin and early evolution of plants on land. *Nature*, **389**, 33–39.

Kermandji, A. M. H., Kowalski W. M. and Touhami, F. K. 2008. Miospore stratigraphy of Lower and early Middle Devonian deposits from Tidikelt, Central Sahara, Algeria. *Geobios*, **41**, 227–251.

Killops, S. D. and Massoud, M. S. 1992. Polycyclic aromatic hydrocarbons of pyrolytic origin in ancient sediments: evidence for Jurassic vegetation fires. *Organic Geochemistry*, **18**, 1–7.

Knoll, A. H. 1996. Breathing room for early animals. *Nature*, **382**(6587), 111–112.

Knoll, A. H. 2003. The geological consequences of evolution. *Geobiology*, **1**, 3–14.

Knoll, A. H. and Carroll, S. B. 1999. Early animal evolution: emerging views from comparative biology and geology. *Science*, **284**, 2129–2137.

Koch, J., 1969. Mikropetrographische Untersuchungen an einigen organischen Komponenten jungpleistozäner und holozäner Torfe Stiddeutschlands und der Schweiz. *Geologisches Jahrbuch*, **87**, 333–360.

Koch, W. F. and Day, J. E. 1996. Late Eifelian-early Givetian (Middle Devonian) brachiopod paleobiogeography of eastern and central North America. 135–143 in: Copper, P. and Jin, Y. (*eds*.). *Proceedings of the third International Brachiopod Congress, Sudbury, Ontario*. Balkema, Rotterdam, 372 pp.

Koch, L. G. and Britton, S. L. 2008. Aerobic metabolism underlies complexity and capacity. *Journal of Physiology*, **586**, 83–95.

van Koeverden, J. H., Karlsen, D. A. and Backer-Owe, K. 2011. Carboniferous non-marine source rocks from Spitsbergen and Bjørnøya: comparison with the western arctic. *Journal of Petroleum Geology*, **34**, 53–66.

Kohler, A., Kuo, A., Nagy, L. G., Morin, E., Barry, K. W., Buscot, F., Canbäck, B., Choi, C., Cichocki, N., Clum, A. and Colpaert, J. 2015. Convergent losses of decay mechanisms and rapid turnover of symbiosis genes in mycorrhizal mutualists. *Nature genetics*, **47**(4), 410–415.

Kojima, K., Sakurai, Y., Suzai, T. and Motogi, M. 1974. An automation of coal petrographic analysis: presented in the 11th Coal Science Congress, October 1st, Hokkaido, Japan [in Japanese].

Konhauser, K. O., Hamade, T., Raiswell, R., Morris, R. C., Ferris, F. G., Southam, G. and Canfield, D. E. 2002. Could bacteria have formed the Precambrian banded iron formations? *Geology*, **30**, 1079–1082.

Kopp, R. E., Kirschvink, J. L., Hilburn, I. A. and Nash, C. Z. 2005. The paleoproterozoic snowball Earth: a climate disaster triggered by the evolution of oxygenic photosynthesis. *Proceedings of the National Academy of Sciences*, **102**, 11131–11136.

Kosanke, R. M., Harrison, J. A., 1957. Microscopy of the resin rodlets of Illinois coal. *Circular of the Illinois State Geological Survey*, **234**, 1–14.

Kruge, M. A., Stankiewicz, B. A., Crelling, J. C., Montanari, A. and Bensley, D. F. 1994. Fossil charcoal in Cretaceous-Tertiary boundary strata: evidence for catastrophic firestorm and megawave. *Geochimica et Cosmochimica Acta*, **58**, 1393–1397.

Kruszewska, K. J. and du Cann, M. 1996. Detection of the incipient oxidation of coal by petrographic techniques. *Fuel*, **75**, 769–774.

Kukalová-Peck, J. 1987. New Carboniferous Diplura, Monura and Thysanura, the hexapod ground plan and the role of thoracic lobes in the origin of wings (Insecta). *Canadian Journal of Zoology*, **65**, 2327–2345.

Kump, L. R. and Garrels, R. M. 1986. Modeling atmospheric O_2 in the global sedimentary redox cycle. *American Journal of Science*, **286**, 337–360.

Kump, L. R. 2008. The rise of atmospheric oxygen. *Nature*, **451**, 277–278.

Labandeira, C. C., Tremblay, S. L., Bartowski, K. E. and Hernick, L. V. 2014. Middle Devonian liverwort herbivory and antiherbivore defence. *New Phytologist*, **202**, 247–258.

Landis, G. P. and Berner, R. A. 1988. In reply: is air in amber ancient? *Science*, **241**, 721–724.

Landis, G. P. and Snee, L. W. 1991. $^{40}Ar/^{39}Ar$ systematics and argon diffusion in amber: implications for ancient earth atmospheres. *Palaeogeography, Palaeoclimatology, Palaeoecology (Global and Planetary Change Section),* **97,** 63–67.

Lawrence, D. A. and Rust, B. R. 1988. The Devonian Clastic Wedge of eastern Gaspé and the Acadian Orogeny. 53–64 in: McMillan, N. J., Embry, A. F. and Glass, D. J. (*eds*.). *Devonian of the World: proceedings of the Second International Symposium on the Devonian System, Calgary, Canada*. Canadian Society of Petroleum Geologists, Calgary, 795 pp.

Le Bayon, R., Brey, G. P., Ernst, W. G. and Mählmann, R. F. 2011. Experimental kinetic study of organic matter maturation: Time and pressure effects on vitrinite reflectance at 400 °C. *Organic Geochemistry*, **42**, 340–355.

Le Bayon, R., Buhre, S., Schmidt, B. C. and Mählmann, R. F. 2012. Experimental organic matter maturation at 2kbar: Heat-up effect to low temperatures on vitrinite reflectance. *International Journal of Coal Geology*, **92**, 45–53.

Le Hir, G., Donnadieu, Y., Goddéris, Y., Meyer-Berthaud, B., Ramstein, G. and Blakey, R. C. 2011. The climate change caused by the land plant invasion in the Devonian. *Earth and Planetary Science Letters*, **310**, 203–212.

Lehmann, J., Czimczik, C., Laird, D. and Sohi, S. 2009. Stability of biochar in soil. 183–198 in: Lehmann, J. and Joseph, S. (*eds*.). *Biochar for environmental management science and technology*. Earthscan, London, 416 pp.

Leithold, E. L. and Blair, N. E. 2001. Watershed control on the carbon loading of marine sedimentary particles. *Geochimica et Cosmochimica Acta*, **65**, 2231–2240.

Leithold, E. L., Blair, N. E. and Perkey, D. W. 2006. Geomorphologic controls on the age of particulate organic carbon from small mountainous and upland rivers, *Global Biogeochemical Cycles*, **20**, GB3022.

Lenton, T. M. 2001. The role of land plants, phosphorus weathering and fire in the rise and regulation of atmospheric oxygen. *Global Change Biology*, **7**, 613–629.

Lenton, T. M. and Watson, A. J. 2000. Redfield revisited: what regulates the oxygen content of the atmosphere. *Global Biogeochemical Cycles*, **14**, 249–268.

Lenton, T. M. 2013. Fire feedbacks on atmospheric oxygen. 289–308 in: Belcher, C. M. (*ed*.). *Fire phenomena and the Earth system. An interdisciplinary guide to fire science*. Wiley-Blackwell, Chichester, 333 pp.

Lenton, T. M., Dahl, T. W., Daines, S. J., Mills, B. J. W., Ozaki, K., Saltzman, M. R. and Porada, P. 2016. Earliest land plants created modern levels of atmospheric oxygen. *Proceedings of the National Academy of Science*, **113**, 9704–9709.

Leys, B., Carcaillet, C. Dezileau, L., Ali, A. A. and Bradshaw, R. H. W. 2013. A comparison of charcoal measurements for reconstruction of Mediterranean paleo-fire frequency in the mountains of Corsica. *Quaternary research*, **79**, 337–349.

Lin, R. and Ritz, G. P. 1993. Studying individual macerals using i.r. microspectrometry, and implications on oil versus gas/condensate proneness and “low-rank” generation. *Organic Geochemistry*, **20**, 695–706.

Lindemann, F-J., Volohonsky, E. and Marshall, J. E. A. 2013. A bonebed in the Hørbyebreen Formation (Famennian–Viséan) on Spitsbergen. *NGF Abstracts and Proceedings*, **1**, 81–82.

Little, C. 1983. *The colonisation of land. Origins and adaptations of terrestrial animals*. Cambridge University Press, Cambridge, 290 pp.

Lo, H. B., & Cardott, B. J. (1995). Detection of natural weathering of Upper McAlester coal and Woodford Shale, Oklahoma, USA. *Organic Geochemistry*, **22**, 73–83.

Lovelock, J. E. 1972. Gaia as seen through the atmosphere. *Atmospheric Environment*, **6**, 579–780.

Lovelock, J. E. 1979. *Gaia – a new look at life on Earth (1st edition)*. Oxford University Press, Oxford, 157 pp.

Lovelock, J. E. 1988. *The ages of Gaia – a biography of our living Earth*. W. W. Norton and Co., New York, 252 pp.

Lüthi, D., LeFloch, M., Bereiter, B., Blunier, T., Barnola, J-M., Siegenthaler, U., Raynaud, D., Jouzel, J., Fischer, H., Kawamura, K. and Stocker, T. F. 2008. High-resolution carbon dioxide concentration record 650,000–800,000 years before present. *Nature*, **453**, 379–382.

Lyons, P. C. 2000. Funginite and secretinite – two new macerals of the inertinite group. *International Journal of Coal Geology*, **44**, 95–98.

Lyons, P. C., Finkelman, R. B., Thompson, C. L., Brown, F. W. and Hatcher, P. G. 1982. Properties, origin and nomenclature of rodlets of the inertinite maceral group. *International Journal of Coal Geology*, **1**, 313–346.

Lyons, P. C., Hatcher, P. G. and Brown, F. W. 1986. Secretinite — a proposed new maceral of the inertinite maceral group. *Fuel*, **65**, 1094–1098.

Lyons, T. W., Reinhard, C. T. and Planavsky, N. J. 2014. The rise of oxygen in Earth's early ocean and atmosphere. *Nature*, **506**, 307–315.

MacDonald, G. M., Larsen, C. P. S., Szeicsz, J. M. and Moser, K. A. 1991. The reconstruction of boreal forest fire history from lake sediments: a comparison of charcoal pollen, sedimentological, and geochemical indices. *Quaternary Science Reviews*, **10**, 53–71.

MacGregor, A. R. 1996. *Fife and Angus field geology. An excursion guide, third edition*. The Pentland Press, Durham, 291 pp.

Malkowski, K. and Racki, G. 2009. A global biogeochemical perturbation across the Silurian–Devonian boundary: Ocean–continent–biosphere feedbacks. *Palaeogeography, Palaeoclimatology, Palaeoecology*, **276**, 244–254.

Mansky, C. F. and Lucas, S. G. 2013. Romer's Gap revisited: continental assemblages and ichno-assemblages from the basal Carboniferous of Blue Beach, Nova Scotia, Canada. 244–273 in: Lucas, S. G., DiMichele, W. A., Barrick, J. E., Schneider, J. W. and Spielmann, J. A. (*eds*). *The Carboniferous-Permian transition*. Bulletin of the New Mexico Museum of Natural History & Science, **60**, 465 pp.

Marchioni, D. L. The detection of weathering in coal by petrographic, rheologic and chemical methods. *International Journal of Coal Geology*, **2**, 231–259.

Marlon, J. R., Bartlein, P. J., Carcaillet, C., Gavin, D. G., Harrison, S. P., Higuera, P. E., Joos, F., Power, M. J. and Prentice, I. C. 2008. Climate and human influences on global biomass burning over the past two millennia. *Nature Geoscience*, **1**, 697–702.

Marshall, J. E. A. 1994. Vitrinite reflectivity and the structure and burial history of the Old Red Sandstone of the Midland Valley of Scotland. *Journal of the Geological Society, London*, **151**, 425–438.

Marshall, J. E. A. 2015. An early Carboniferous palaeoclimate record from East Greenland. *Strata*, **15**, 92–93.

Marshall, J. E. A. 2016. Palynological calibration of Devonian events at near-polar palaeolatitudes in the Falkland Islands, South Atlantic. 25–44 in: Becker, R. T., Königshof, P. and Brett, C. E. (*eds*.). *Devonian Climate, Sea Level and Evolutionary Events*. *Geological Society, London, Special Publications, 423*. The Geological Society, Bath, 481 pp.

Marshall, J. E. A. and Yule, B. L. 1999. Spore colour measurement. 165–168 in: Jones, T. P. and Rowe, N. P. (*eds*.). *Fossil plants and spores: modern techniques*. Geological Society, London, 396 pp.

Marshall, J. E. A, Haughton, P. D. W. and Hillier, S. J. 1994. Vitrinite reflectivity and the structure and burial history of the Old Red Sandstone of the Midland Valley of Scotland. *Journal of the Geological Society, London*, **151**, 425–438.

Marshall, J. E. A., Astin, T. R. and Clack, J. A. 1999. East Greenland tetrapods are Devonian in age. *Geology*, **27**, 637–640.

Marshall, J. E. A., Astin, T. R., Brown, J. F., Mark-Kurik, E. and Lazauskiene, J. 2007. Recognising the Kačák event in the Devonian terrestrial environment and its implications for understanding land-sea interactions. 133–156 in: Becker, R. T. and Kirchgasser, W. T. (*eds*.). *Devonian events and correlations. Geological Society Special Publication 278*. The Geological Society, Bath, 280 pp.

Märss, T. and Männik, P. 2013. Revision of Silurian vertebrate biozones and their correlation with the conodont succession. *Estonian Journal of Earth Sciences*, **62**, 181–204.

Marynowski, L. and Simoneit, B. R. 2009. Widespread Upper Triassic to Lower Jurassic wildfire records from Poland: evidence from charcoal and pyrolytic polycyclic aromatic hydrocarbons. *Palaios*, **24**, 785–798.

Marynowski, L., Szełęg, E., Jędrysek, M. O. and Simoneit, B. R. T. 2011. Effects of weathering on organic matter Part II: Fossil wood weathering and implications for organic geochemical and petrographic studies. *Organic Geochemistry*, **42**, 1076–1088.

Marynowski, L., Smolarek, J. and Hautevelle, Y. 2015. Perylene degradation during gradual onset of organic matter maturation. *International Journal of Coal Geology*, **139**, 17–25.

Matten, I. C. and Banks, H. P. 1969. *Stenokoleos bifidus* sp. n. in the Upper Devonian of New York State. *American Journal of Botany*, **56**, 880–891.

Matten, L. C. 1973. The Cairo flora (Givetian) from eastern New York. I. *Reimannia*, terete axes, and *Cairoa lamanekii* gen. et sp. n. *American Journal of Botany*, **60**, 619–630.

Matten, L. C., 1974. The Givetian flora from Cairo, New York: *Rhacophyton*, *Triboxylon*, and *Cladoxylon*. *Botanical Journal of the Linnean Society*, **68**, 303–318.

Matten, L. C., 1975. Additions to the Givetian Cairo flora from eastern New York. *Bulletin of the Torrey Botany Club*, **102**, 45–52.

McCartney, J. T., O'Donnel, H. J. and Ergun, S. 1971. Determination of proportion of coal components by automated microscopic reflectance scanning. *Fuel*, **50**, 226–235.

McGhee Jr, G. R. 2013. *When the invasion of land failed: the legacy of the Devonian extinctions*. Columbia University Press, New York, 317 pp.

McGregor, D. C. 1973. Lower and Middle Devonian spores of eastern Gaspé, Canada. I. Systematics. *Palaeontographica Abteilung B*, **142**, 1–77.

McGregor, D. C. 1977. Lower and Middle Devonian spores of eastern Gaspé, Canada. II. Biostratigraphy. *Palaeontographica Abteilung B*, **163**, 111–142.

McGregor, D. C. and Camfield, M. 1976. Upper Silurian (?) to Middle Devonian spores of the Moose River Basin, Ontario. *Geological Survey of Canada Bulletin*, **263**, 1–63.

McLean, D., Owens, B., Pendleton, J. L. and Bodman, D. 2013. Pennsylvanian (Namurian and Westphalian) miospore assemblages from the west coast of Scotland. *Review of Palaeobotany and Palynology*, **190**, 1–14.

Melo, J. H. G. and Loboziak, S. 2003. Devonian-Early Carboniferous miospore biostratigraphy of the Amazon Basin, northern Brazil. *Review of Palaeobotany and Palynology*, **124**, 131–202.

Meyer-Berthaud, B., Scheckler, S. E. and Wendt, J. 1999. Archaeopteris is the earliest known modern tree. *Nature*, **398**, 700–701.

Meyers, P. A., Leenheer, M. J., Kawka, O. E. and Trull, T. W. 1984. Enhanced preservation of marine-derived organic matter in Cenomanian black shales from the southern Angola Basin. *Nature*, **312**, 356–359.

Midgley, J. L. and Bond, W. J. 2013. Plant adaptations to fire: an evolutionary perspective. 125–134 in: Belcher, C. M. (*ed*). *Fire phenomena and the Earth system. An interdisciplinary guide to fire science*. Wiley-Blackwell, Chichester, 333 pp.

Miller, M. F. and Woodrow, D. L. 1991. Shoreline deposits of the Catskill deltaic complex, Schoharie Valley, New York. 153–177 in: Landing, E. and Brett, C. E. (*eds*.). *Dynamic stratigraphy and depositional environments of the Hamilton Group (Middle Devonian) in New York State, Part II*. *Bulletin 469 of the New York State Museum/Geological Survey*. State Education Department, Albany, 177 pp.

Mills, D. B., Ward, L. M., Jones, C., Sweeten, B., Forth, M., Treusch, A. H. and Canfield, D. E. 2014. Oxygen requirements of the earliest animals. *Proceedings of the National Academy of Sciences*, **111**, 4168–4172.

Mintz, J. S, Driese, S. G. and White, J. D. 2010. Environmental and ecological variability of Middle Devonian (Givetian) forests in appalachian basin paleosols, New York, United States. *Palaios*, **25**, 85–96.

Mitchell, G. H., Tulloch, W. and Wilson, R. B. 1962. *The geology of the neighbourhood of Edinburgh. Third edition. Memoirs of the Geological Survey, Scotland*. HM Stationery Office, Edinburgh, 159 pp.

Mooney, S. D. and Tinner, D. 2011. The analysis of charcoal in peats and modern sediments. *Mires and Peat*, **7**, 1–18.

Mora, C. I. and Colarusso, L. A. 1996. Middle to late Paleozoic atmospheric CO_2 levels from soil carbonate and organic matter. *Science*, **271**, 1105–1107.

Moran, M. A., Sheldon Jr., W. M. and Sheldon, J. E. 1999. Biodegradation of riverine dissolved organic carbon in five estuaries of the southeastern United States. *Estuaries*, **22**, 55–64.

Morris, J. L., Leake, J. R., Stein, W. E., Berry, C. M., Marshall, J. E. A., Wellman, C. H., Milton, A., Hillier, S., Mannolini, F., Quirk, J. and Beerling, D. J. 2015. Investigating Devonian trees as geo-engineers of past climates: linking palaeosols to palaeobotany and experimental geobiology. *Palaeontology*, **58**, 787–801.

Naiman, R. J. 1982. Characteristics of sediment and organic carbon export from pristine boreal forest watersheds. *Canadian Journal of fisheries and aquatic sciences*, **39**, 1699–1718.

Nelsen, M. P., DiMichele, W. A., Peters, S. E. and Boyce, C. K. 2016. Delayed fungal evolution did not cause the Paleozoic peak in coal production. *Proceedings of the National Academy of Sciences*, **113**, 2442–2447.

Neves, R., Gueinn, K. J., Clayton, G., Ioannides, N. S., Neville, R. S. W. and Kruszewska, K. 1973. Palynological correlations within the Lower Carboniferous of Scotland and Northern England. *Transactions of the Royal Society of Edinburgh,* **69**, 4–70.

Nichols, G., Cripps, J. A., Collinson, M. E. and Scott, A. C. 2000. Experiments in waterlogging and sedimentology of charcoal: results and implications. *Palaeogeography, Palaeoclimatology, Palaeoecology*, **164**, 43–56.

Nickelsen, R. P. and Cotter, E. 1983. Silurian depositional history and Alleghanian deformation in the Pennsylvania valley and ridge. *Guidebook for the 48th annual field conference of Pennsylvania Geologists*. Bureau of Topographic and Geologic Survey, Harrisburg, 192 pp.

Niklas, K. J. 1982. Chemical diversification and evolution of plants as inferred from paleobiochemical studies. 29–91 *in*: Nitecki, M. H. (*ed*.). *Biochemical aspects of evolutionary biology*. University of Chicago Press, Chicago, 256 pp.

O'Mara, P. T., 1995. *Correlation, facies distribution and sequence stratigraphic analysis of the Westphalian B Coal Measures in Quadrant 44 of the southern North Sea*. Unpublished MSc Thesis, University of Durham.

O'Mara, P. T. and Turner, B. R. 1999. Sequence stratigraphy of coastal alluvial plain Westphalian B Coal Measures in Northumberland and the southern North Sea. *International Journal of Coal Geology*, **42**, 33–62.

Onstad, G. D., Canfield, D. E., Quay, P. D., Hedges, J. I. 2000. Sources of particulate organic matter in rivers from the continental USA: lignin phenol and stable carbon isotope compositions. *Geochimica et Cosmochimica Acta*, **64**, 3539–3546.

Organ, C., Nunn, C. L., Machanda, Z. and Wrangham, R. W. 2011. Phylogenetic rate shifts in feeding time during the evolution of Homo. *Proceedings of the National Academy of Sciences*, **108**, 14555–14559.

Owens, B., Neves, R., Gueinn, K. J., Mishell, D. R. F., Sabry, H. S. M. Z. and Williams, J. E. 1977. Palynological division of the Namurian of northern England and Scotland. *Proceedings of the Yorkshire Geological Society*, **41**, 381–398.

Owens, B., McLean, D., Simpson, K. R. M., Shell, P. M. J. and Robinson, R. 2005. Reappraisal of the Mississippian palynostratigraphy of the east fife coast, Scotland, United Kingdom. *Palynology*, **29**, 23–47.

Painter, P., Starsinic, M. and Coleman, M. 1985. Determination of functional groups in coal by Fourier transform interferometry. 169–241 in: Ferraro, J. R. and Basile, L. J. (*eds*.). *Fourier transform infrared spectroscopy: applications to chemical systems. Vol. 4.* Academic Press, London, 406 pp.

Paton, R. L., Smithson, T. R. and Clack, J. A. 1999. An amniote-like skeleton from the Early Carboniferous of Scotland. *Nature*, **398**, 508–513.

Patterson, W. A. III, Edwards, K. J. and Maguire, D. J. 1987. Microscopic charcoal as a fossil indicator of fire. *Quaternary Science Reviews*, **6**, 3–23.

Pavlov, A. A., Kasting, J. F., Brown, L. L., Rages, K. A. and Freedman, R., 2000. Greenhouse warming by CH_4 in the atmosphere of early Earth. *Journal of Geophysical Research*, **105**, 981–11.

Pavlov, A. A., Kasting, J. F., Eigenbrode, J. L. and Freeman, K. H. 2001. Organic haze in Earth's early atmosphere: source of low -^{13}C Late Archean kerogens? *Geology*, **29**, 1003–1006.

Pavlov, A. A. and Kasting, J. F. 2002. Mass-independent fractionation of sulfur isotopes in Archean sediments: strong evidence for an anoxic Archean atmosphere. *Astrobiology*, **2**, 27–41.

Partin, C. A., Bekker, A., Planavsky, N. J., Scott, C. T., Gill, B. C., Li, C., Podkovyrov, V., Maslov, A., Konhauser, K. O., Lalonde, S. V. and Love, G. D. 2013. Large-scale fluctuations in Precambrian atmospheric and oceanic oxygen levels from the record of U in shales. *Earth and Planetary Science Letters*, **369**, 284–293.

Peach, B. N. and Flett, J. S. 1910. *The Geology of the neighbourhood of Edinburgh. Second edition. Memoirs of the Geological Survey, Scotland*. HM Stationery Office, Edinburgh, 507 pp.

Pearson, P. N., 1992. Walking traces of the giant myriapod Arthropleura from the Strathclyde Group (Lower Carboniferous) of Fife. *Scottish Journal of Geology*, **28**, 127–133.

Peel, M. C., Finlayson, B. L., McMahon, T. A., 2007. Updated world map of the Köppen–Geiger climate classification. *Hydrology and Earth System Science Discussions*, **11**, 1633–1644.

Pessenda, L. C. R., Boulet, R., Aravena, R., Rosolen, V., Gouveia, S. E. M., Ribeiro, A. S. and Lamotte, M. 2001. Origin and dynamics of soil organic matter and vegetation changes during the Holocene in a forest-savanna transition zone, Brazilian Amazon region. *The Holocene*, **11**, 250–254.

Pederson, K., Sichko Jr., M. and Wolff, M. P. 1976. Trip B-4. Stratigraphy and structure of Silurian and Devonian rocks in the vicinity of Kingston, N.Y. 56–82 in: Johnson, J. H. (*ed*.). *New York State Geological Association, 48th annual meeting field trip guidebook.* New York State Geological Association, Ploughkeepsie, 340 pp.

Pflug, H. D. and Prössl, K. F. 1989. Palynology in Gneiss - Results from the Continental Deep Drilling Program. *Naturwissenschaften*, **76**, 565–567.

Pflug, H. D. and Prössl, K. F. 1991. Palynostratigraphical and paleobotanical studies in the pilot hole of the German continental deep drilling program: results and implications. *Scientific Drilling*, **2**, 13–33.

Piasecki, S. and Stemmerik, L. 1991. Late Permian anoxia in east Greenland. 275–290 in: Tyson, R. V. and Pearson, T. H. (eds.). *Modern and ancient continental shelf anoxia.*

Geological Society of London Special Publication, 58. Geological Society Publishing House, Bath, 470 pp.

Piepjohn, K., Brinkmann, L., Grewing, A. and Kerp, H. 2000. New data on the age of the uppermost ORS and the lowermost post-ORS strata in Dickson Land (Spitsbergen) and implications for the age of the Svalbardian deformation. 603–609 in: Friend, P. F. and Williams, B. P. J. (*eds*.). *New perspectives on the Old Red Sandstone. Geological Society, London, Special Publications 180*. Geological Society Publishing House, Bath, 440 pp.

Piepjohn, K. and Dalmann, W. K. 2014. Stratigraphy of the uppermost Old Red Sandstone of Svalbard (Mimerdalen Subgroup). *Polar Research*, **33**, 19998.

Pires, N. D. and Dolan, L. 2012. Morphological evolution in land plants: new designs with old genes. *Philosophical Transactions of the Royal Society B*, **367**, 508–518.

Playford, G. 1962. Lower Carboniferous microfloras of Spitsbergen. *Palaeontology*, **5**, 550–618.

Potvin-Leduc, D., Cloutier, R., Landing, E., Hernick, L. V. and Mannolini, F. 2015. Givetian (Middle Devonian) sharks from Cairo, New York (USA): Evidence of early cosmopolitanism. *Acta Palaeontologica Polonica*, **60**, 183–200.

Power, M. J., Marlon, J., Ortiz, N. *and 72 others*. 2008. Changes in fire activity since the Last Glacial Maximum: an assessment based on a global synthesis and analysis of charcoal data. *Climate Dynamics*, **30**, 887–907.

Power, M. J. 2013. A 21 000-year history of fire. 207–227 in: Belcher, C. M. (*ed*.). *Fire phenomena and the Earth system. An interdisciplinary guide to fire science*. Wiley-Blackwell, Chichester, 333 pp.

Prestianni, C., Deconbeix, A-L., Thorez, J., Fokan, D., and Gerrienne, P. 2010. Famennian charcoal of Belgium. *Palaeogeography, Palaeoclimatology, Palaeoecology*, **291**, 60–71.

Preston, C. M. and Schmidt, M. W. I. 2006. Black (pyrogenic) carbon: a synthesis of current knowledge and uncertainties with special consideration of boreal regions. *Biogeosciences*, **3**, 397–420.

Pyne, S. J., Andrews, P. L. and Laven, R. D. 1996. *Introduction to wildland fire*. John Wiley and sons, New York, 808 pp.

Ransom, B., Kim, D., Kastner, M. and Wainright, S. 1996. Organic matter preservation on continental slopes: importance of mineralogy and surface area. *Geochimica et Cosmochimica Acta*, **62**, 1329–1345.

Raven, J. A. 1977. The evolution of vascular land plants in relation to supracellular transport processes. *Advances in Botanical Research*, **5**, 153–219.

Ravindra, K., Sokhi, R. and Van Grieken, R. 2008. Atmospheric polycyclic aromatic hydrocarbons: source attribution, emission factors and regulation. *Atmospheric Environment*, **42**, 2895–2921.

Raymond, P. A. and Bauer, J. E. 2001. Riverine export of aged terrestrial matter to the North Atlantic Ocean. *Nature*, **409**, 497–500.

Reed, J. W. 1986. The acanthodian genera *Machaeracanthus* and *Persacanthus*from the Devonian of Red Hill, Nevada. *Geobios* **19**, 409–419.

Reed, J. C., Wheeler, J. O. and Tucholke, B. E. 2005. *Decade of North American Geology continent-scale map 001. Geologic map of North America with explanatory notes*. Geological Society of America, Boulder, Colorado, 28 pp.

Rein, G. 2013. Smouldering fires and natural fuels. 15–33 in: Belcher, C. M. (*ed*.). *Fire phenomena and the Earth system. An interdisciplinary guide to fire science*. Wiley-Blackwell, Chichester, 333 pp.

Retallack, G. J. 1997. Early forest soils and their role in Devonian global change. *Science*, **276**, 583–585.

Retallack, G. J. 2015. Silurian vegetation stature and density inferred from fossil soils and plants in Pennsylvania, USA. *Journal of the Geological Society*, **172**, 693–709.

Retallack, G. J., Catt, J. A. and Chaloner, W. G. 1985. Fossil soils as grounds for interpreting the advent of large plants and animals on land [and discussion]. *Philosophical Transactions of the Royal Society of London, Series B, Biological Sciences*, **309**, 105–142.

Rhoads, D. C. and Morse, J. W. 1971. Evolutionary and ecologic significance of oxygen deficient marine basins. *Lethaia*, **4**, 413–428.

Rhodes, A. N. 1998. A method for the preparation and quantification of microscopic charcoal from terrestrial and lacustrine sediment cores. *The Holocene*, **8**, 113–117.

Richardson, J. B. and McGregor, D. C., 1986. Silurian and Devonian spore zones of the Old Red Sandstone region. *Geological Survey of Canada Bulletin*, **364**, 1–79.

Richardson, J. B., Bonamo, P. M. and McGregor, D. C. 1993. The spores of *Leclerqia* and the dispersed spore morphon *Acinosporites lindlarensis* Riegel: a case of gradualistic evolution. *Bulletin of the Natural History Museum London (Geology)*, **49**, 121–155.

Rickard, L. V. 1975. Correlation of the Silurian and Devonian rocks in New York State. *New York State museum map and chart series*, **24**.

Rickard, L. V. 1989. *Stratigraphy of the subsurface Lower and Middle Devonian of New York, Pennsylvania, Ohio and Ontario*. *New York State Museum map and chart series number 39*, State Education Department, Albany, 59 pp.

Rimmer, S. M., Hawkins, S. J., Scott, A. C. and Cressler (III), W. L. 2015. The rise of fire: fossil charcoal in late Devonian marine shales as an indicator of expanding terrestrial ecosystems, fire, and atmospheric change. *American Journal of Science*, **315**, 713–733.

Robinson, D. 1984. The estimation of the charcoal content of sediments: a comparison of methods on peat sections from the Island of Arran. *Circaea,* **2**, 121–128.

Robinson, J. M. 1989. Phanerozoic O_2 variation, fire, and terrestrial ecology. *Palaeogeography, Palaeoclimatology, Palaeoecology*, **75**, 223–240.

Robinson, J. M. 1990. Lignin, land plants, and fungi: Biological evolution affecting Phanerozoic oxygen balance. *Geology*, **15**, 607–610.

Robinson, J. M. 1991. Phanerozoic atmospheric reconstructions: a terrestrial perspective. *Palaeogeography, Palaeoecology, Palaeoclimatology (Global and Planetary Change Section*), **97**, 51–62.

Rode, A. L. S. and Lieberman, B. S. 2005. Using environmental niche modeling to study the Late Devonian biodiversity crisis. 93–179 in: Over, D. J., Morrow, J. R. and Wignall, P. B. (*eds*.). *Developments in palaeontology and stratigraphy 20. Understanding Late Devonian and Permian-Triassic Biotic and Climatic Events: Towards an Integrated Approach*. Elsevier, Amsterdam, 337 pp.

Romer, A. S. 1956. The early evolution of land vertebrates. *Proceedings of the American Philosophical Society*, **100**, 157–167.

Rosing, M. T. and Frei, R. 2004. U-rich Archaean sea-floor sediments from Greenland—indications of 3700 Ma oxygenic photosynthesis. *Earth and Planetary Science Letters*, **217**, 237–244.

Rothermal, R. C. 1972. A mathematical model for predicting fire spread in wildland fuels. *USDA Forest Service, Intermountain Forest and Range Experiment Station, Research Paper INT-115*.

Rouxhet, P. G. and Robin, P. L. 1978. Infrared study of the evolution of kerogens of different origins during catagenesis and pyrolysis. *Fuel*, **57**, 533–540.

Rowe, N. P. and Jones, T. P., 2000. Devonian charcoal. *Palaeogeography, Palaeoclimatology, Palaeoecology*, **164**, 331–338.

Rubinstein, C. V., Gerrienne, P., de la Puente, G. S., Astini, R. A. and Steemans, P. 2010. Early Middle Ordovician evidence for land plants in Argentina (eastern Gondwana). *New Phytologist*, **188**, 365–369.

Runnegar, B. 1991. Precambrian oxygen levels estimated from the biochemistry and physiology of early eukaryotes. *Palaeogeography, Palaeoclimatology and Palaeoecology*, **97**, 97–111.

Rust, B. R. 1984. Proximal braidplain deposits in the Middle Devonian Malbaie Formation of Eastern Gaspé, Quebec, Canada. *Sedimentology*, **31**, 675–695.

Rust, B. R., Lawrence, D. A. and Zaitlin, B. A. 1989. The sedimentology and tectonic significance of Devonian and Carboniferous terrestrial successions in Gaspe, Quebec. *Atlantic Geology*, **25**, 1–13.

Rutten, M. G. 1966. Geologic data on atmospheric history. *Palaeogeography, Palaeoclimatology, Palaeoecology,* **2**, 47–57.

Sahoo, S. K., Planavsky, N. J., Kendall, B., Wang, X., Shi, X., Scott, C., Anbar, A. D., Lyons, T. W. and Jiang, G. 2012. Ocean oxygenation in the wake of the Marinoan glaciation. *Nature*, **489**, 546–549.

Sallan, L. C. and Coates, M. I. 2010. End-Devonian extinction and a bottleneck in the early evolution of modern jawed vertebrates. *Proceedings of the National Academy of Sciences*, **107**, 10131–10135.

Sandberg, C. A. and Ziegler, W. 1996. Devonian conodont biochronology in geologic time calibration. *Senckenbergiana Lethaea*, **76**, 259–265.

Sarwar, G. and Friedman, G. M. 1995. Post-Devonian sediment cover over New York State: Evidence from fluid-inclusion, organic maturation, clay diagenesis and stable isotope studies. *Lecture Notes in Earth Sciences*, **58**, 113.

Säve-Söderbergh, G. 1932. Preliminary note on Devonian stegocephalians from East Greenland. *Meddelelser om Grønland*, **94**, 1–211.

Schaefer, L. and Fegley, B. 2007. Outgassing of ordinary chondritic material and some of its implications for the chemistry of asteroids, planets, and satellites. *Icarus*, **186**, 462–483.

Scheckler, S. E. 1986. Geology, floristics and paleoecology of Late Devonian coal swamps from Appalachian Laurentia (U.S.A.). *Annales de la Société Géologique de Belgique*, **109**, 209–222.

Scheckler, S. E. 2001. Afforestation - the first forests. 67–71 in: Briggs, D. E. G. and Crowther, P. R. (*eds*.). *Palaeobiology II*. John Wiley and Sons, Oxford, 600 pp.

Schieber, J. 1999. Distribution and deposition of mudstone facies in the Upper Devonian Sonyea Group of New York. *Journal of Sedimentary Research*, **69**, 1–23.

Schidlowski, M., Junge, C. E. and Pietrek, H. 1977. Sulfur isotope variations in marine sulfate evaporites and the Phanerozoic oxygen budget. *Journal of Geophysical Research*, **82**, 2557–2565.

Schidlowski, M. and Junge, C. E. 1981. Coupling among the terrestrial sulfur, carbon and oxygen cycles: numerical modeling based on revised Phanerozoic carbon isotope record. *Geochimica et Cosmochimica Acta*, **45**, 589–594.

Schlünze, B. and Schneider, R. R. 2000. Transport of terrestrial organic carbon to the oceans by rivers: re-estimating flux- and burial rates. *International Journal of Earth Sciences*, **88**, 599–606.

Schneider, J. W., Lucas, S. G., Werneburg, R. and Rößler, R. 2010. Euramerican Late Pennsylvanian/early Permian arthropleurid/tetrapod associations: Implications for the habitat and paleobiology of the largest terrestrial arthropod. 49–70 in: Lucas, S. G., Schneider, J. W. and Spielmann, J. A. (*eds*.). *Carboniferous–Permian transition in Cañon del Cobre, northern New Mexico. Bulletin 49, New Mexico Museum of Natural History*. New Mexico Museum of Natural History and Science, Albuquerque, 229 pp.

Schuyler, A. and Traverse, A. 1990. Sedimentology of miospores in the Middle to Upper Devonian Oneonta Formation, Catskill Magnafacies, New York. *Review of Palaeobotany and Palynology,* **64**, 305–313.

Scotese, C. R. and McKerrow, W. S. 1990. Revised world maps and introduction. 1–21 *in:* McKerrow, W. S. and Scotese, C. R. (*eds*). *Palaeozoic Palaeogeography and Biogeography. Geological Society of London Memoir 12*. Geological Society, Bath, 442 pp.

Scotese, C. R., 2001. Digital Paleogeographic Map Archive on CD-ROM. PALEOMAP Project, Arlington, Texas.

Scott, A. C. 1989. Observations on the nature and origin of fusain. *International Journal of Coal Geology*, **12**, 443–475.

Scott, A. C. 2000. The pre-Quaternary history of fire. *Palaeogeography, Palaeoclimatology, Palaeoecology*, **164**, 281–329.

Scott, A. C. 2010. Charcoal recognition, taphonomy, and uses in palaeoenvironmental analysis. *Palaeogeography, Palaeoclimatology, Palaeoecology*, **291**, 11–39.

Scott, A. C. and Jones, T. P. 1991. Fossil charcoal: a plant fossil record preserved by fire. *Geology Today*, **7**, 214–216.

Scott, A. C. and Glasspool, I. J. 2005. Charcoal reflectance as a proxy for the emplacement temperature of pyroclastic flow deposits. *Geology*, **33**, 589–592.

Scott, A. C. and Glasspool, I. J. 2006. The diversification of Palaeozoic fire systems and fluctuations in atmospheric oxygen concentration. *Proceedings of the National Academy of Sciences*, **103**, 10861–10865.

Scott, A. C. and Glasspool, I. J. 2007. Observations and experiments on the origin and formation of inertinite group macerals. *International Journal of Coal Geology*, **70**, 53–66.

Scott, A. C., Cripps, J. A., Collinson, M. E. and Nichols, G. J. 2000. The taphonomy of charcoal following a recent heathland fire and some implications for the interpretation of fossil charcoal deposits. *Palaeogeography, Palaeoclimatology, Palaeoecology*, **164**, 1–31.

Scott, A. C., Bowman, D. M. J. S., Bond, W. J., Pyne, S. J. and Alexander, M. E. 2014. *Fire on Earth. An introduction*. Wiley-Blackwell, Chichester, 413 pp.

Sevon, W. D. 1985. Nonmarine facies of the Middle and Late Devonian Catskill coastal alluvial plain. 79–90 in: Woodrow, D. L. and Sevon, W. D. (*eds*.). *The Catskill delta. Geological Society of America special paper 201*. Geological Society of America, Boulder, Colorado, 246 pp.

Shear, W. A. and Kukalová-Peck, J. 1990. The ecology of Paleozoic terrestrial arthropods: the fossil evidence. *Canadian journal of zoology*, **68**, 1807–1834.

Shear, W. A., Selden, P. A., Rolfe, W. D. I., Bonamo, P. M. and Grierson, J. D. 1987. New Terrestrial Arachnids from the Devonian of Gilboa, New York (Arachnida, Trigonotarbida). *American Museum Novitates*, **2901**, 1–74.

Shubin, N. H., Daeschler, E. B. and Coates, M. I. 2004. The early evolution of the tetrapod humerus. *Science*, **304**, 90–93.

Singh, G., Kershaw, A.P. and Clark. R. 1981. Quaternary vegetation and fire history in Australia. 23–54 in: Gill, A.M., Groves, R.H. and Noble, IR. (*eds*). *Fire and the Australian Biota.* Australian Academy of Science, Canberra, 582 pp.

Smith, A. H. V. and Butterworth, M. A. 1967. Miospores in the coal seams of the Carboniferous of Great Britain. *Special Papers in Palaeontology*, **1**, 1–324.

Smith, G. C. and Cook, A. C., 1980. Coalification paths of exinite, vitrinite and inertinite. *Fuel*, **59**, 641–647.

Smithson, T. R., Wood, S. P., Marshall, J. E. A. and Clack, J. A. 2012. Earliest Carboniferous tetrapod and arthropod faunas from Scotland populate Romer's Gap. *Proceedings of the National Academy of Sciences*, **109**, 4532–4537.

Smyth, M., 1980. Coal encounters of the third kind: Triassic. *Journal of the Coal Geology Group, Geological Society of Australia*, **2**, 161–177.

Solomon, P. R., Hanblen, D. G. and Carangelo, R. M. 1982. Applications of Fourier transform IR spectroscopy in fuel science. 77–131 in: Fuller, E. L. (*ed*.). *Coal and coal products: analytical characterisation techniques*. American Chemical Society, Washington D.C., 326 pp.

Spackman, W., Vastola, F. J., and Ford, R. H. 1973. Advances in the automation of microscopy for coal petrographic analysis. *Geological Society of America Abstracts with Programs*, **5**, 221.

Sperling, E. A., Halverson, G. P., Knoll, A. H., MacDonald, F. A. and Johnston, D. T. 2013a. A basin redox transect at the dawn of animal life. *Earth and Planetary Science Letters*, **371**, 143–155.

Sperling, E. A., Frieder, C. A., Raman, A. V., Girguis, P. R., Levin, L. A. and Knoll, A. H. 2013b. Oxygen, ecology, and the Cambrian radiation of animals. *Proceedings of the National Academy of Sciences*, **110**, 13446–13451.

Sperling, E. A., Wolock, C. J., Morgan, A. S., Gill, B. C., Kunzmann, M., Halverson, G. P., Macdonald, F. A., Knoll, A. H. and Johnston, D. T. 2015. Statistical analysis of iron geochemical data suggests limited late Proterozoic oxygenation. *Nature*, **523**, 451–454.

Stach, E. and Teichmüller, M. 1953. Zur Chemie und Petrographie der Ionen-Austauscher aus Braun- und Steinkohlen. *Brennst. Chemie*, **34**, 275–281, 333–338.

Stach, E., Mackowsky, M. Th., Teichmüller, M., Taylor, G. H., Chandra, D. and Teichmüller, R. 1982. *Stach's textbook of coal petrology, third edition*. Gebrüder Borntraeger, Berlin, 535 pp.

Stein, W. E., Mannolini, F., Van A-H, L., Landing, E. and Berry, C. 2007. Giant cladoxylopsid trees resolve the enigma of the Earth's earliest forest stumps at Gilboa. *Nature*, **446**, 904–907.

Stein, W. E., Berry, C. M., Hernick, L. V. and Mannolini, F. 2012. Surprisingly complex community discovered in the mid-Devonian fossil forest at Gilboa. *Nature*, **483**, 78–82.

Stemmerik, L. 2000. Late Palaeozoic evolution of the north Atlantic margin of Pangea. *Palaeogeography, Palaeoclimatology, Palaeoecology*, **161**, 95–126.

Stephenson, M. H., Williams, M., Monghan, A. A., Arkley, S., Smith, R. A. Dean, M., Browne, M. A. E. and Leng, M. 2004. Palynomorph and ostracod biostratigraphy of the Ballagan Formation, Midland Valley of Scotland, and elucidation of intra-Dinantian unconformities. *Proceedings of the Yorkshire Geological Society*, **55**, 131–143.

Stopes, M. C. 1919. On the four visible ingredients in banded bituminous coal: studies in the composition of coal No. 1. *Proceedings of the Royal Society, London, Series B*, **90**, 480–487.

Stopes, M. C. 1935. On the petrology of banded bituminous coals. *Fuel*, **14**, 4–13.

Streel, M., Higgs, K., Loboziak, S., Riegel, W. and Steemans, P. 1987. Spore stratigraphy and correlation with faunas and floras in the type marine Devonian of the Ardenne-Rhenish regions. *Review of Palaeobotany and Palynology*, **50**, 211–229.

Sutton, R. G. and McGhee, R. 1985. The evolution of Frasnian marine “community-types” of south-central New York. 211–224 in: Woodrow, D. L. and Sevon, W. D. (*eds*.). *The Catskill Delta. Geological Society of America special paper 201*. Geological Society of America, Boulder, Colorado, 246 pp.

Sutton, R. G., Bowden, Z. P. and McAlester, A. L. 1970. Marine shelf environments of the Upper Devonian Sonyea Group of New York. *Geological Society of America Bulletin*, **81**, 2975–2992.

Swain, A. M. 1973. A history of fire and vegetation in northeastern Minnesota as recorded in lake sediments. *Quaternary Research*, **3**, 383–96.

Taylor, W. A. 2003. Ultrastructure of selected Silurian trilete spores and the putative Ordovician trilete spore *Virgatasporites*. *Review of Palaeobotany and Palynology*, **126**, 211–223.

Taylor, G. H. and Liu, S. Y. 1989. Micrinite – its nature, origin and significance. *International Journal of Coal Geology*, **14**, 29–46.

Taylor, G. H., Teichmüller, M., Davis, A., Diessel, C. F. K., Littke, R. and Robert, P. 1998. *Organic Petrology*. Gebrüder Borntraeger, Berlin, 704pp.

Teichmüller, M. 1987a. Organic material and very low-grade metamorphism. 115–161 in: Frey, M. (*ed*.). *Low temperature metamorphism*. Glasgow, Blackie, 351 pp.

Teichmüller, M. 1987b. Recent advances in coalification studies and their application to geology. 127–169 in: Scott, A. C. (*ed*). *Coal and coal-bearing strata: recent advances*. *Geological Society Special Publication 32*. Blackwell Scientific Publications, Oxford, 332pp.

Teichmüller, M. 1989. The genesis of coal from the viewpoint of coal petrology. *International Journal of Coal Geology*, **12**, 1–87.

Teichmüller, M. and Teichmüller, S. 1981. The significance of coalification studies to geology – a review. *Bulletin des Centres de Recherches Exploration-Production Elf-Aquitaine,* **5**, 491–534.

Thomas, A. L. R. 1997. The breath of life – did increased oxygen levels trigger the Cambrian explosion? *Trends in Ecology and Evolution*, **12**, 44–45.

Thomson, K. S. 1968. A new Devonian fish (Crossopterygii: Rhipidistia) considered in relation to the origin of the Amphibia. *Postilla*, **124**, 1–13.

Timofeev, P. P. and Bogliubova, I. I. 1964. Die stoffliche Zusammensetzung der Kohlen der JuraKohlenbildung in der UdSSR. *Fortschritt Geologie Reinland und Westfalen*, **12**, 357–376.

Tinner, W. and Hu, F. S. 2003. Size parameters, size-class distribution and area-number relationship of microscopic charcoal: relevance for fire reconstruction. *The Holocene*, **13**, 291–296.

Tinner, W., Conedera, M., Ammann, B., Heinz W. Gaggeler, H. W., Gedye, S., Jones, R. and Sagesser, B. 1998. Pollen and charcoal in lake sediments compared with historically documented forest fires in southern Switzerland since AD 1920. *The Holocene*, **8**, 31–42.

Trainer, M. G., Pavlov, A. A., DeWitt, H. L., Jimenez, J. L., McKay, C. P., Toon, O. B. and Tolbert, M. A. 2006. Organic haze on Titan and the early Earth. *Proceedings of the National Academy of Sciences*, **103**, 18035–18042.

Traverse, A. 2003. Dating the earliest tetrapods: a Catskill Palynological problem in Pennsylvania. *Courier Forschungs-Institut Senckenberg*, **241**, 19–29.

Traverse, A. and Schuyler, A. 1994. Palynostratigraphy of the Catskill and part of the Chemung magnafacies, southern New York State, USA. *Courier Forschungsinstitut Senckenberg*, **169**, 261–274.

Troth, I. 2006. *The applications of palynostratigraphy to the Devonian of Bolivia*. Unpublished PhD thesis, University of Southampton, 203 pp.

Troth, I., Marshall, J. E. A., Racey, A. and Becker, R. T. 2011. Devonian sea-level change in Bolivia: A high palaeolatitude biostratigraphical calibration of the global sea-level curve. *Palaeogeography, Palaeoclimatology, Palaeoecology*, **304**, 3–20.

Tucker, M. 2001. Sedimentary petrology: an introduction to sedimentary rocks, 3rd ed. Blackwell, Oxford, 272 pp.

Tulloch, W. and Walton, H. S. 1958. *The geology of the Midlothian Coalfield*. Memoirs of the Geological Survey Scotland. HM Stationery Office, Edinburgh, 157 pp.

Turner, B. and Smith, D. 1995. The Carboniferous and Permian rocks between Tynemouth and Seaton Sluice. 92–104 in: Scrutton, C. (*ed*). *Northumbrian rocks and landscape – a field guide*. Ellenbank Press, Cumbria, 216 pp.

Tyson, R. V. 1995. *Sedimentary organic matter*. Chapman and Hall, London, 615 pp.

Ueno, Y., Yamada, K., Yoshida, N., Maruyama, S. and Isozaki, Y. 2006. Evidence from fluid inclusions for microbial methanogenesis in the early Archaean era. *Nature*, **440**, 516–519.

Urey, H. C. 1952. On the early chemical history of the Earth and the origin of life. *Proceedings of the National Academy of Sciences*, **38**, 351–363.

Vaughan, A. and Nichols, G. 1995. Controls on the deposition of charcoal: implications for sedimentary accumulations of fusain. *Journal of Sedimentary Research*, **A65**, 129–135.

Venkatesan, M. I. and Dahl, J., 1989. Organic geochemical evidence for global fires at the Cretaceous/Tertiary boundary. *Nature*, **338**, 57–60.

Ver Straeten, C. A. 1994. Microstratigraphy and depositional environments of a Middle Devonian foreland basin: Berne and Otsego Members, Mount Marion Formation, eastern New York State. 367–380 *in:* Landing, E., (*ed*.). *Studies in Stratigraphy and Paleontology in Honor of Donald W. Fisher*. *New York State Museum Bulletin 481*. New York State Museum, Albany, 380 pp.

Ver Straeten, C. A. 2007. Basinwide stratigraphic synthesis and sequence stratigraphy, upper Pragian, Emsian and Eifelian stages (Lower to Middle Devonian), Appalachian Basin. 39–81 in: Becker, R. T. and Kirchgasser, W. T. (*eds*.). *Devonian events and correlations. Geological Society special publication 278*. Geological Society Publishing House, Bath, 280 pp.

Ver Straeten, C. A. 2009. The Classic Devonian of the Catskill Front: The Foreland Basin Record of Acadia Orogenesis, Volcanism, Depositional Environments, and Sea Level History. 7.1–7.54 in: Vollmer, F. W. (*ed*). *New York State Geological Association 81st annual meeting field trip guidebook*. New York State Geological Society, New York, 256 pp.

Ver Straeten, C. A. 2013. Beneath it all: bedrock geology of the Catskill Mountains and implications of its weathering. *Annals of the New York Academy of Sciences*, **1298**, 1–29.

Ver Straeten, C. A. and Brett, C. 1995. Lower and Middle Devonian foreland basin fill in the Catskill Front: stratigraphic synthesis, sequence stratigraphy, and the Acadian Orogeny. 313–356 in: Garver, J. l. and Smith, J. A. (*eds*.). New York State Geological Association 67th annual meeting field trip guidebook. New York State Geological Society, New York.

Ver Straeten, C. A., Baird, G., Brett, C., Lash, G., Over, J., Karaca, C., Jordan, T. and Blood, R. 2011. Trip A-2. The Marcellus subgroup in its type area, Finger Lakes area of New York, and beyond. 23–86 *in*: Nelson, N. (*ed*.). *New York State Geological Association 83rd annual meeting fieldtrip guidebook*. New York State Geological Society, New York.

Vigran, J. O. 1994. Palynology of Upper Devonian to basal Permian rocks of the Arctic. *IHU report 23.1438.00/18/94*.

Vigran, J. O., Stemmerik, L. and Piasecki, S. 1999. Stratigraphy and depositional evolution of the uppermost Devonian-Carboniferous (Tournaisian-Westphalian) non-marine deposits in North-East Greenland. *Palynology*, **23**, 115–152.

Wallace, J. B., Ross, D. H. and Meyer, J. L. 1983. Seston and dissolved organic carbon dynamics in a southern Appalachian stream. *Ecology*, **63**, 824–838.

Walliser, O. H. 1964. Conodonten des Silurs. *Abhandlungen des Hessischen Landesamtes fur Bodenforschung*, **41**, 1–106.

Ward, P., Labandeira, C., Laurin, M. and Berner, R. A. 2006. Confirmation of Romer's Gap as a low oxygen interval constraining the timing of initial arthropod and vertebrate terrestrialization. *Proceedings of the National Academy of Sciences*, **103**, 16818–16822.

Warg, J. B. and Traverse, A. 1973. A palynological study of shales and “coals” of a Devonian-Mississippian transition zone, central Pennsylvania. *Geoscience and Man*, **7**, 39–46.

Waters, C. N., Browne, M. A. E., Dean, M. T. and Powell, J. H. 2007. Lithostratigraphical framework for Carboniferous successions of Great Britain (Onshore). British Geological Survey Research Report RR/07/01. British Geological Survey, Keyworth, 60 pp.

Watson, A. J., Lovelock, J. E. and Margulis, L. 1978. Methanogenesis, fires and the regulation of atmospheric oxygen. *Biosystems*, **10**, 293–298.

Watson, A. J. and Lovelock, J. E. 2013. The dependence of flame spread and the probability of ignition on atmospheric oxygen: an experimental investigation. 273–287 in: Belcher, C. M. (*ed*.). *Fire phenomena and the Earth system. An interdisciplinary guide to fire science*. Wiley-Blackwell, Chichester, 333 pp.

Webster, J. R., Benfield, E. F., Ehrman, T. P., Schaeffer, M. A., Tank, J. L. Hutchens, J. J. and D'angelo, D. J. 1999. What happens to allochthonous material that falls into streams? A synthesis of new and published information from Coweeta. *Freshwater Biology*, **41**, 687–705.

Weis-Fogh, T. 1964. Diffusion in insect wing muscle, the most active tissue known. *Journal of experimental Biology,* **41**, 229–256.

Wellman, C. H. and Gensel, P. G. 2004. Morphology and wall ultrastructure of the spores of the Lower Devonian plant *Oocampsa catheta* Andrews *et al*., 1975. *Review of Palaeobotany and Palynology*, **130**, 269–295.

Wellman, C. H. 2010. The invasion of the land by plants: when and where? *New Phytologist*, **188**, 306–309.

Wellstead, C. F. 1982. A Lower Carboniferous aistopod amphibian from Scotland. *Palaeontology*, **25**, 193–208.

Weng, C. 2005. An improved method for quantifying sedimentary charcoal via a volume proxy. *The Holocene*, **15**, 298–301.

Wilde, S. A., Valley, J. W., Peck, W. H. and Graham, C. M. 2001. Evidence from detrital zircons for the existence of continental crust and oceans on the Earth 4.4 Gyr ago. *Nature*, **409**, 175–178.

Wildman, R. A., Hickey, L. J., Dickinson, M. B., Berner, R. A., Robinson, J. M. Dietrich, M. Essenhigh, R. H. and Wildman, C. B. 2004. Burning of forest materials under late Paleozoic high atmospheric oxygen levels. *Geology*, **32**, 457–460.

Williams, E. A., Friend, P. F. and Williams, B. P. J. 2000. A review of Devonian timescales: databases, construction, and new data. 1–21 in: Friend, P. F. and Williams, B. P. J. (*eds*.). *New perspectives on the Old Red Sandstone*. *Geological Society of London Special Publication 180***.** Geological Society Publishing House, Bath, 623 pp.

Willis, B. J. and Bridge, J. S. 1988. Evolution of Catskill river sections, New York State. 85–106 in: McMillan, N. J., Embry, A. F. and Glass, D. J. (*eds*.). *Devonian of the world: proceedings of the 2nd International Symposium on the Devonian System — CPSG Memoir 14, Volume II: Sedimentation*. Canadian Society of Petroleum Geologists, Calgary, 674 pp.

Wilson, H. M., Daeschler, E. B. and Desbiens, S. 2005. New flat-backed archipolypodan millipedes from the Upper Devonian of North America. *Journal of Paleontology*, **79**, 738–744.

Winston, R. B. 1993. Reassessment of the evidence for primary fusinite and degradofusinite. *Organic Geochemistry*, **20**, 209–221.

Winkler, M. G. 1985. Charcoal analysis for paleoenvironmental interpretation: a chemical assay. *Quaternary Research*, **23**, 313–326.

Wolfe, J. M., Daley, A. C., Legg, D. A. and Edgecombe, G. D. 2016. Fossil calibrations for the arthropod Tree of Life. *Earth-Science Reviews*, **160**, 43–110.

Wolff, M. P. 1968. Trip 20. The Catskill deltaic complex – deltaic phases and correlations of the Middle Devonian Marcellus Formation in the Albany region. 358–398 in: Bird, J. M. (*ed*.). *New England Intercollegiate Geological Conference 61st Annual Meeting Fieldtrip Guidebook*. State University of New York, Albany, 421 pp.

Wood, S. P., Panchen, A. L. and Smithson, T. R. 1985. A terrestrial fauna from the Scottish Lower Carboniferous. *Nature*, **314**, 355–356.

Wood, G., Gabriel, A. M. and Lawson, J. C. 1996. Palynological techniques – processing and microscopy. 29–50 in: Jansonius, J. and McGregor, D. C. (*eds*.). *Palynology: Principles and Applications. Vol. 1, Principles.* American Association of Stratigraphic Palynologists Foundation, College Station, Texas, 462 pp.

Woodrow, D. L. and Sevon, W. D. 1985. *The Catskill Delta. Geological Society of America special paper 201*. Geological Society of America, Boulder, Colorado, 246 pp.

Woodrow, D. L., Dennison, J. M., Ettensohn, F. R., Sevon, W. T. and Kirchgasser, W. T. 1988. Middle and Upper Devonian stratigraphy and paleogeography of the central and southern Appalachians and eastern Midcontinent, USA. 277–301 in: McMillan, N. J., Embry, A. F. and Glass, D. J. (*eds*.). *Devonian of the World: Proceedings of the 2nd International Symposium on the Devonian System — CPSG Memoir 14, Volume I: Regional Syntheses*. Canadian Society of Petroleum Geologists, Calgary, 795 pp.

Woodrow, D. L., Robinson, R. A. J., Prave, A. R., Traverse, A., Daeschler, E. B., Rowe, N. D. and DeLaney, N. A. 1995. Stratigraphic, sedimentologic, and temporal framework of Red Hill (Upper Devonian Catskill Formation) near Hyner, Clinton County, Pennsylvania: Site of the oldest amphibian known from North America. 1–8 in: Way, J. (*ed*.). *Guidebook, 60th Annual Field Conference of Pennsylvania Geologists*. Lock Haven University, Lock Haven, PA, 16 pp.

Wrangham, R. W. 2009. *Catching fire: how cooking made us human*. Basic Books, New York, 321pp.

Zahnle, K., Schaefer, L. and Fegley, B. 2010. Earth's earliest atmospheres. *Cold Spring Harbor perspectives in biology*, **2**(10), a004895.

Zerkle, A. L., Claire, M. W., Domagal-Goldman, S. D., Farquhar, J. and Poulton, S. W. 2012. A bistable organic-rich atmosphere on the Neoarchaean Earth. *Nature Geoscience*, **5**(5), 359–363.